**UNIVERSIDADE DE LISBOA**

**Faculdade de Farmácia**


# FLUORESCENT-BASED DENDRIMERS AS POTENTIAL DRUG DELIVERY CARRIERS OF CISPLATIN: FROM DESIGN AND SYNTHESIS TO PLATINUM-MEMBRANE INTERACTIONS

**Nuno Filipe Rodrigues Martinho**

Orientadores: Doutora Liana Casquinha da Silva
Prof. Doutor Mire Zloh
Prof. Doutor Steve Brocchini

Tese especialmente elaborada para obtenção do grau de Doutor em Farmácia especialidade em Tecnologia Farmacêutica

**2018**

**UNIVERSIDADE DE LISBOA**

**Faculdade de Farmácia**


# FLUORESCENT-BASED DENDRIMERS AS POTENTIAL DRUG DELIVERY CARRIERS OF CISPLATIN: FROM DESIGN AND SYNTHESIS TO PLATINUM-MEMBRANE INTERACTIONS

**Nuno Filipe Rodrigues Martinho**

**Orientadores:**
Doutora Liana Casquinha da Silva
Prof. Doutor Mire Zloh
Prof. Doutor Steve Brocchini

Tese especialmente elaborada para obtenção do grau de Doutor em Farmácia especialidade em Tecnologia Farmacêutica

**Júri:**

**Presidente:**

- Doutora Matilde da Luz dos Santos Duque da Fonseca e Castro, Professora Catedrática da Faculdade de Farmácia da Universidade de Lisboa

**Vogais:**

- Doutora Maria de La Salette de Freitas Fernandes Hipólito Reis Dias Rodrigues, Professora Associada Faculdade de Farmácia da Universidade do Porto;
- Doutor António Manuel Simões Carrão Albuquerque Baptista, Investigador Principal Instituto de Tecnologia Química e Biológica da Universidade Nova de Lisboa;
- Doutor Nuno Fernando Duarte Cordeiro Correia dos Santos, Professor Associado com Agregação Faculdade de Medicina da Universidade de Lisboa;
- Doutor Vasco Daniel Bigas Bonifácio, Investigador Centro de Química-Física Molecular do Instituto Superior Técnico da Universidade de Lisboa;
- Doutora Rita Alexandra de Nascimento Cardoso Guedes, Professora Auxiliar Faculdade de Farmácia da Universidade de Lisboa;
- Doutora Liana Casquinha da Silva, Investigadora FCT nível inicial com Agregação Faculdade de Farmácia da Universidade de Lisboa, Orientadora;

Trabalho financiado pela Fundação para a Ciência e Tecnologia através da bolsa de doutoramento SFRH/BD/87838/2012

**2018**

**Dedicated to Natália, Lucinda and Henrique**

**“I am afraid the definition of a scientist is a man who can take frustration without end”**

**– Jean-Francois Borel**

**Acknowledgements**

In the end of this incredible journey I want to express my acknowledgment to everyone that helped me.

First I would like to thank my supervisors Dr. Liana Silva, Prof. Dr. Mire Zloh and Prof. Dr. Steve Brocchini for encouraging me to always do my best and contribute to my development as a young scientist. Thank you for your help, support, meaningful and deep conversations about both science and life and for the inspiration that allowed me to enjoy working throughout my PhD. Thank you for providing me this amazing opportunity that culminated in my growth as a person and as a scientist. I learned a lot from you and I will carry this torch of love for research that you have given me.

I also want to express my deeply gratitude for all the laboratories that allowed me do conduct the research that I needed. An acknowledgement is owned to Faculdade de Farmácia da Universidade de Lisboa, School of Pharmacy at University College of London and Hearthfordshire University for allowing me to use their facilities to conduct the research in this thesis. I also want to thank Prof. Dr. Manuel Prieto for receiving me in the Molecular Biophysics Group at Instituto Superior Técnico (IST) and allowing me to perform the biophysical studies with lipid model membranes, for the good science discussions and stories of life. I also want to thank Dr. Rodrigo Almeida for receiving me in the Chemistry and Biochemistry department at Faculdade de Ciências da Universidade de Lisboa and allowing me to sue your lab to perform the release studies. Finally, I also want to thank Dr. Ana Viana for helping me conducting my experiments.

Also, special acknowledgments are due to the people that directly helped me in this journey. First and foremost, thank you Dr. Teresa Barata for helping me starting and for your commitment to uplift me in the hard times. Your creativity was always unmatched and will always remain as a reference to me. Thanks you Prof. Dr. Helena Florindo for all your help every time it was needed and all discussions about nanomedicine. Also, thank you Dr. Sheiliza Carmali and Christina Pickens for the friendship and all laboratory tricks you showed me that no book could ever teach. Honorable mention to Dr. Joaquim Marquês and Tânia Santos for helping me in setting up experiments and interpret the results. A big thank you to Dr. Vasco Bonifácio for all your help, discussions and for providing me new polymers and re-igniting my love for dendrimers.

Last but not least I want to thank my parents for all the motivation, support and security given. To Natália Aniceto, my partner in this entire journey, who I admire most and inspires me every day, for the love in the good and bad times thank you for your understanding and giant support.

To all my dearest friends and colleagues from different groups and countries thank you for the support.

This work was supported by FCT by granting the doctoral fellowship (SFRH/BD/87838/2012) to which I am deeply grateful. I would also like to acknowledge the Engineering & Physical Sciences Research Council (EPSRC) center for their role in this work.

**Preface**

This work was developed under supervision of:
Doutora Liana Silva (supervisor)
Assistant Researcher
Research Institute for Medicines, Faculty of Pharmacy, University of Lisbon, Lisbon, Portugal

Prof. Dr. Mire Zloh
Emeritus Professor,
Department of Medicinal Chemistry, University of Hertfordshire, Hertfordshire, UK

Prof. Dr, Steve Brocchini,
Full Professor
UCL School of Pharmacy, University College of London, London, UK

The work was financially supported by Fundação para a Ciência e Tecnologia, through the doctoral grant (SFRH/BD/87838/2012)

**List of publications**

**Papers in international scientific periodicals with referees:**

Nuno Martinho, Liana C. Silva, Helena F. Florindo, Steve Brocchini, Mire Zloh, Teresa Barata, *Rational Design of novel, fluorescent, tagged glutamic acid dendrimers with different terminal groups and in silico analysis of their properties,* International Journal of Nanomedicine, 2017, (12):7053-7073

Nuno Martinho, Liana C. Silva, Helena F. Florindo, Steve Brocchini, Teresa Barata, Mire Zloh, *Pratical computational toolkits for dendrimers and dendrons structure design,* Journal of Computer-Aided Molecular Design, 2017, 31 (9), 817-827

Nuno Martinho, Helena F. Florindo, Liana C. Silva, Steve Brocchini, Mire Zloh, Teresa Barata, *Molecular Modeling to Study Dendrimers for Biomedical Applications,* Molecules, 2014, 19 (8); 20424-20467

Liane Moura, Nuno Martinho, Liana C. Silva, Teresa Barata, S. Brocchini, Helena Florindo, Mire Zloh, *Poly-glutamic dendrimer-based conjugates for cancer vaccination – a computational design for targeted delivery antigens, Journal of Drug Targeting, 2017, 25(9-10): 1-8*

***Chapters***

João Conniot, Ana Ester Ventura, Tânia Santos, Ana Cláudia Carreira, Nuno Martinho, Ana Varela, Rogério Gaspar, Helena F Florindo, Liana C. Silva, *Drugs, Delivery Systems and Membrane Organization in Model and Cell Membranes* In book: Membrane Organization and Lipid Rafts in the Cell and Artificial Membranes, Chapter: Drugs, Delivery Systems and Membrane Organization in Model and Cell Membranes, Publisher: Nova Science Publishers, Editors: Angel Catalá, pp.53-89

## Abstract

Dendrimers are a class of polymers with high potential as drug delivery systems due to their unique scaffold and properties. Despite their early potential, dendrimer-based therapies have been limited in part due to the considerable lack of understanding of their *in vivo* behavior and in particular, how they interact and cross cellular membranes. Therefore, designing dendrimers with an attached fluorophore would allow their tracking while studying their behavior with lipid bilayers. This work explores the potential of fluorescent dendrimers as carriers for the anti-cancer drug cisplatin, which is known to interact with lipids and induce phase changes in cellular membranes. To this end, fluorescent poly(glutamic acid) (PG) dendrimers were designed *in silico* and suitable candidates were attempted to be synthesized. Furthermore, effects of cisplatin in phase change and integrity of lipid model bilayers was studied to further drive the design of these dendrimers. The choice of PG dendrimers backbone was driven by their ability to fully cover a small fluorophore from the external environment. To quickly generate dendrimers scaffolds a set of computational tools were created to automate this process and facilitate the modeling of any class of dendrimers. Different generations and architecture of PG dendrimers with a fluorophore attached to the core and different terminal groups were created and submitted to all-atom simulations. Data from molecular dynamics showed that generation 4 was necessary to fully cover a low molecular weight fluorophore and partially cover a high molecular weight fluorophore as measured by the solvent accessible surface area. However, the synthesis of these candidates was shown to be difficult due to the amount of side reactions and possible steric hindrance that arises at high generations. Furthermore, the attachment of NBD was required to be carried out at lower generations since its reactivity with higher generations of PG dendrimers was lower. Therefore, analogues of glutamic acid with NBD (nitrobenzoxadiazole) were synthesized to be used as the initial core. Finally, platinum-membrane interactions were characterized by measuring the fluorescence anisotropy of different probes embedded in liposomes composed of different lipid mixtures. Results suggested that both cisplatin and its cationic aquated analogue had low perturbation on the lipid phase and integrity of model membranes. However, cisplatin was able to further reduce the membrane fluidity when a gel phase was present in the membrane. Furthermore, at high concentrations, platinum complexes were shown to compromise the permeability of lipid bilayers without inducing collapse of the membrane. This effect was again dependent on membrane lipid composition. Altogether, these findings were used as a proof-of-concept for designing dendrimers as potential tools to carry and study cisplatin interactions at the lipid membrane.

Keywords: poly(glutamic acid) dendrimers, cisplatin, molecular modeling, lipid membranes, membrane permeability and fluidity

## Resumo

Os dendrímeros são macromoléculas sintéticas com uma estrutura tridimensional regular bem definida e ramificada. Estes são tipicamente descritos por um crescimento radial a partir de um monómero central (geralmente denominado núcleo) ao qual são incorporados de forma sucessiva e iterativa camadas (geralmente referidas como geração) de monómeros até à última camada, designada de grupos terminais. Devido às suas características estruturais, os dendrímeros têm demonstrado potencial em várias áreas e em particular no transporte de moléculas terapêuticas e de imagiologia sendo que também podem demonstrar actividade biológica. Apesar de extensamente estudados, o mecanismo de interacção dos dendrímeros com componentes biológicos, e em particular com as membranas lipídicas, é relativamente pouco conhecido. Vários estudos com dendrímeros de poli(amido aminas) (PAMAM) demonstraram que para dendrímeros de maiores gerações estes interagem fortemente com camadas lipídicas causando poros na membrana e que estes efeitos estão correlacionados com os efeitos de toxicidade observados em células. Uma vez que a maioria dos dendrímeros têm tamanhos na escala de outros componentes biológicos tais como as proteínas, existe uma dificuldade acrescida de os estudar nas células. Uma maneira de contornar este problema é pela incorporação de sondas fluorescentes na estrutura dos dendrímeros. Contudo, adicionar as sondas à superfície pode não só alterar as propriedades de superfície, que por sua vez podem contribuir por si só para a interacção destes com a membrana, como também a adição é feita de maneira estatística e por isso existe um controlo menor da estrutura. Assim sendo, a incorporação de sondas fluorescentes no interior central do dendrímero é vantajoso. No entanto, isto requer que o monómero central tenha capacidade de ligação a um fluoróforo. Por outro lado, dependendo do tamanho do fluoróforo em relação ao tamanho e estrutura do dendrímero existirá uma geração mínima capaz de incorporar totalmente o fluoróforo no seu interior. Os modelos computacionais da estrutura de dendrímeros são assim úteis para definir estruturas promissoras para a incorporação do fluoróforo no seu interior anteriormente à sua síntese. Assim sendo, o ácido glutâmico foi escolhido para constituir a base estrutural dos dendrímeros a serem construídos *in silico*. O uso de aminoácidos como monómeros oferece vantagens em aplicações biológicas uma vez que os produtos de degradação têm grande probabilidade de serem biocompatíveis. Por outro lado, o ácido glutâmico é assimétrico e apresenta 3 grupos funcionais (2 ácidos carboxílicos e 1 amina) que permitem explorar variadas estruturas dendríticas deixando sempre um grupo do monómero central para reagir com o fluoróforo.

Um dos problemas na criação de modelos computacionais de dendrímeros ocorre a grandes gerações onde a adição manual de ligações entre monómeros facilmente pode criar erros na estrutura por erro humano. Para isso, várias metodologias têm sido descritas na literatura para a construção de dendrímeros mas requerem sempre um nível elevado de construção manual. Com o objectivo de colmatar este problema foram desenvolvidas ferramentas computacionais para automatizar este processo. Este método foi então posteriormente testado com os dendrímeros de ácido poli-glutâmico ligados a um fluoróforo com a construção de vários modelos de diferentes gerações e com diferentes grupos terminais. A ferramenta desenvolvida gerou a descrição do dendrímero como uma sequência linear de monómeros e uma tabela de conectividade que indica ao programa de software XPLOR-NIH como “montar” o

dendrímero na sua forma tridimensional. Após construção dos vários modelos de dendrímeros estes foram submetidos a simulação com o uso da parametrização CHARMM. Os resultados das simulações demonstraram que estruturalmente apenas a partir da geração 4 foi possível a capacidade de evitar o contacto de um fluoróforo pequeno com o meio exterior, sendo que este efeito seria apenas parcial no caso de um fluoróforo de dimensões maiores. Os efeitos da alteração dos monómeros terminais com triptofano e lisina revelaram ainda que no caso do triptofano este aumentou o tamanho do dendrímero e reduziu a flexibilidade com evidência de interacções do tipo $\pi$-$\pi$.

Os candidatos gerados pelas simulações computacionais foram de seguida sintetizados por métodos divergentes e convergentes pelo uso de reagentes comumente utilizados na síntese peptídica. Em geral os vários reagentes demonstraram elevados rendimentos para as gerações pequenas de dendrímeros. No entanto, para dendrímeros de geração 2 e superiores, várias reacções incompletas dos grupos terminais foram verificadas. Isto foi atribuído ao espaçamento curto entre os grupos carboxílicos na molécula de ácido glutâmico que restringe a reacção de ambos os lados quando a superfície começa a ficar congestionada pelos vários monómeros ao redor. Por outro lado, os resultados indicaram que o fluoróforo teria de ser incorporado nas primeiras gerações do dendrímero uma vez que para dendrímeros de geração superior o rendimento da reacção foi baixo. Assim sendo, o fluoróforo foi introduzido no monómero central. No entanto, nestas condições a amina secundária formada teve capacidade de reacção pelo que outras alternativas de transformação da amina do monómero central foram testadas. Contudo, estas reacções apresentaram um rendimento baixo pelo que outras alternativas devem ser exploradas. Por outro lado, diferentes grupos terminais foram sintetizados com os mesmos protocolos usados para a estrutura central do dendrímero, sendo obtidos em rendimento elevado. No entanto, foi verificado que para monómeros com grupos de protecção de elevado caracter hidrofóbico, que o produto recuperado apresentou solubilidade limitada nos solventes testados pelo que dificultaria a sua acoplagem à estrutura central. Outros grupos de protecção deverão portanto ser explorados.

Uma das aplicações para este tipo de dendrímeros é o transporte de fármacos. Em particular os dendrímeros aniónicos de ácido glutâmico oferecem vantagens para a incorporação de cisplatina. A cisplatina em solução aquosa com baixa concentração de cloro forma espécies carregadas positivamente que poderiam complexar com o dendrímero de ácido glutâmico. A cisplatina é um anticancerígeno muito utilizado no tratamento de vários tumores sólidos mas cujo uso é limitado pelos efeitos secundários geralmente observados. Apesar de ser estruturalmente simples a cisplatina demonstra um comportamento complexo nas células. Como anticancerígeno a cisplatina atua primariamente no ADN genómico por reacção com as bases e formação de complexos. No entanto, o contributo dos lípidos da membrana plasmática tem sido reportado tanto para os efeitos no mecanismo de acção da cisplatina por indução da apoptose através da oligomerização de receptores à superfície da membrana, bem como nas diferenças lipídicas da composição das membranas celulares que levam a mecanismos de resistência por menor acumulação de platina no interior da célula. Contudo, o efeito da cisplatina na alteração de fase verificada nas células não é completamente compreendida. Assim sendo, os efeitos na fluidez da

membrana pela cisplatina e da sua forma catiónica foram testadas em modelos lípidos na forma de lipossomas pela medição da anisotropia e tempos de vida de fluorescência de várias sondas com localização em diferentes regiões da bicamada lipídica e com partição distinta para diferentes fases lipídicas. A formação das espécies de carga positiva em tampões sem cloro foi verificada em misturas de lípido com carga negativa onde se observou uma redução da carga negativa à superfície dos lipossomas que foi atribuída à neutralização de cargas. O efeito da redução de cargas foi proporcional à concentração e transitório sendo que após 24 horas os valores retornaram a valores semelhantes ao controlo. O mesmo efeito transitório foi observado na fluidez de membranas de POPC onde entre os 60-100 minutos se verificou um ligeiro aumento da ordem tendo posteriormente retornado a valores semelhantes ao controlo. Por outro lado, os complexos de platina não demonstraram alterações significativas da fluidez, excepto para os sistemas de fase gel onde uma diminuição significativa da fluidez foi observada com o aumento de concentração dos complexos de platina(II) em lipossomas de DPPC. Por outro lado, os complexos de platina aumentaram a permeabilidade das camadas lipídicas a concentrações mais altas e este efeito foi dependente da composição lipídica.

Em suma, os efeitos dos complexos de platina nas alterações de fase e propriedades biofísicas das membranas parecem ser limitados, sugerindo que as alterações de fluidez reportadas nas células pela cisplatina que levam a uma fluidificação da membrana não parecem ser devido ao aumento da ceramida mas sim a outros factores. Estes resultados constituíram importantes avanços na perspectiva de desenvolvimento de dendrímeros e a sua possível utilização no estudo das interacções de cisplatina com membranas lipídicas e para o desenvolvimento de novas abordagens como terapias anticancerígenas. Neste contexto os dendrímeros oferecem uma vantagem porque não só podem ser concomitantemente complexados com cisplatina e moléculas sinergísticas à sua acção como também podem ser usados para evadir os mecanismos de resistência que geralmente surgem em tratamentos prolongados.

Keywords: cisplatin, dendrimer modeling, peptide dendrimers, membrane fluidity, membrane permeability

## List of abbreviations

**AqCis**: Aquated cisplatin species

**Boc**: tert-butoxycarbonyl

**Boc**: tert-butoxycarbonyl

**CDI**: carbonyldiimidazole

**Chol**: cholesterol

**DCC**: dicyclohexylcarbodiimide

**DCM**: Dichloromethane

**DDS**: Drug delivery systems

**DIPC**: N,N'-diisopropylcarbodiimide

**DLS**: dynamic light scattering

**DMAP**: 4-(dimethylamino)pyridine

**DMF**: dimethylformamide

**DMSO**: dimethylsulfoxide

**DMPC**: 1,2-dimyristoyl-sn-glycero-3-phosphocholine

**DPH**: Dihenylhexatriene

**DPPC**: 1,2-dipalmitoyl-sn-glycero-3-phosphocholine

**DPPG**: 1,2-dipalmitoyl-sn-glycero-3-phosphorylglycerol

**EDC**: 1-ethyl-3(3'-(dimethylamino)propyl)carbodiimide

**Et**: Ethyl

**Fmoc**: fluorenylmethyloxycarbonyl

**G#:** Generation [#number]

**GLU**: glutamic acid

**HATU**: [(dimethylamino)-1*H*-1,2,3-triazolo[4,5-b]pyridin-1-ylmethylene)-*N*-methyl-methanaminium hexafluorophosphate *N*-oxide

**HOAt**: 1-hydroxy-7-azabenzotriazole

**HOBt**: 1-hydroxybenzotriazole

**IR**: infrared

**MC**: Monte Carlo

**MD**: Molecular dynamics

**Me**: Methyl

**MS**: mass spectrometry

**NBD**-Cl: 7-chloride-4-nitrobenz-2-oxa-1,3-diazole

**NHS**: N-hydroxysuccinimide

**NMR**: nuclear magnetic resonance

**PAMAM**: poly(amidoamine)

**PG**: poly(glutamic acid)

**PLL**: poly(L-lysine)

**PPI**: poly(propylene imine)

**POPC**: 1-palmitoyl-2-oleoyl-sn-glycero-3-phosphocholine.

**PURE** dendrimers: poly(urea) dendrimers

**SANS**: Small angle neutron scattering

**tBu**: *tert*-butyl

**TFA**: trifluoroacetate

**THF**: tetrahydrofuran

**TMA**-**DPH**; trimethylammonium diphenylhexatriene

**t-PnA**: trans-parinaric acid

# List of Figures

## Chapter I

.



## Chapter III

## Chapter V

# List of Tables

## Chapter III

## Aims and outline of the thesis

The main goal of this thesis is to evaluate the potential use of fluorescent dendrimers as drug delivery systems (DDS) for the anti-cancer drug cisplatin and study the interactions of platinum(II) complexes with lipid model membranes. For this approach, different methodologies from molecular modeling to biophysical properties changes induced by cisplatin were tested. Due to the multidisciplinary approach taken in this work, this thesis is divided into three distinct (and almost independent) chapters that outline the common goal of designing a DDS based on dendrimers. Therefore, a brief introduction outlining the general fields related to this thesis is described in chapter 1 followed by specific and more detailed introductions concerning each subject at the beginning of each chapter. Moreover, for chapter 2 and 4, introductions are given in the form of review papers as these have directly been devised from the work described herein. Finally, the final remarks concerning all chapters is provided in chapter 5.

Chapter 1 outlines a brief summary of the state-of-the-art regarding the development and properties of dendrimers as potential drug carriers and their interaction with biomembranes. It also describes computational tools that have been employed in the design of dendrimers and general strategies to synthetize these branched polymers. Finally, it outlines the importance of the lipid bilayer to both anti-cancer drugs and dendrimers.

In chapter 2, peptide dendrimers composed of GLU backbone were designed by molecular modelling to carry a single fluorophore attached to the core, protected from the external environment. Furthermore, different terminal groups were tested to display different surface properties (charge and hydrophobic characteristics) and their contribution the overall conformation of PG dendrimers. Because one of the current problems with modeling of dendrimers is the quick generation of their molecular structure, a set of tools were developed to increase the automation process of generating the 3D structure of dendrimers. PG dendrimers with a fluorophore attached to the core were then submitted to molecular dynamic simulations to generate candidate structures to be synthesized.

Chapter 3 describes attempts to synthesize the PG dendrimer candidates generated by molecular modelling in chapter 2. Both divergent and convergent approaches were tested to achieve the PG generation 4 in the lowest amount of reactions. Moreover, the attachment of the fluorophore to the core at different generations was tested as well as

different modification to the GLU of the core. Finally, attempts to synthesize the terminal groups were carried.

In chapter 4, cisplatin influence on the fluidity and integrity of lipid model bilayers of different composition were tested with the aim to further elucidate its mechanism of interaction with biological membranes, and help resolving conflicting data in the literature regarding cisplatin effects in membrane properties. Furthermore, cisplatin and its aquated analogues were tested on their ability to modulate permeability of lipid bilayers.

Chapter 5 outlines the final remarks of all individual chapters and describes ongoing research of this thesis. Furthermore, the overall conclusions and future work from this thesis are provided.

Overall, this thesis exemplifies a proof-of-concept workflow that could typically be employed in the design of novel DDS as it covers both the design of carrier as well as the mechanisms of interaction of the drug at the membrane interface and how these DDS could improve it. This issue is further discussed in chapter 5, where a critical analysis is presented in the form of future perspectives.

# Table of contents

# CHAPTER I
# GENERAL INTRODUCTION

## Chapter I – General Introduction

### 1.1. Drug development and nanomedicine

The drug development pipeline is a complex, time consuming and costly program with a high attrition rate (Figure 1.1). It generally starts with the characterization of a medical problem, identification of potential targets and its targeting compounds. However, at this point there are no guarantees about their efficacy and safety *in vivo*. Common problems that molecules face are related to them failing to reach their primary target, interacting in off-target receptors or tissues (causing side effects) or simply not having the right biophysical properties. These problems can however be minimized with the use of different drug delivery systems (DDS)[1–4]. In effect, the repertoire of drugs available could probably be greatly extended with the use of new DDS. The premise is that they are theoretically able to overcome the physiological barriers, avoid rapid clearance and mask the problems related to physicochemical properties of drugs. This includes the three most predominant ones: solubility, stability and bioavailability. Furthermore, the possibility of combining targeting moieties to re-direct the drug onto specific tissues where it is required is of utmost importance as it makes the development of drugs focused solely on their pharmacological effects while minimizing off-target toxicity.

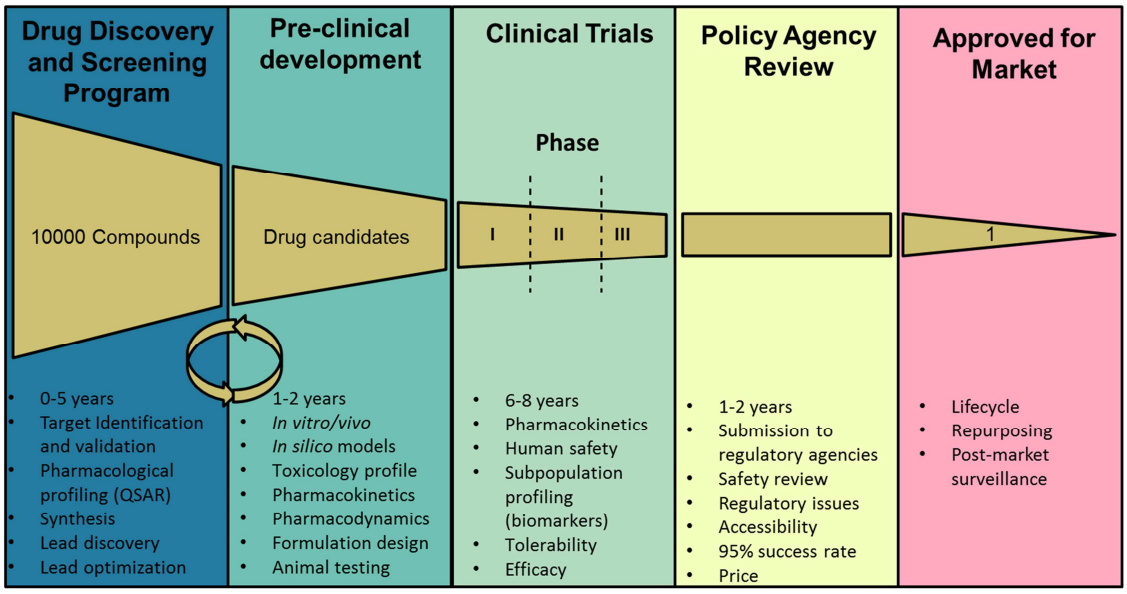


**Figure 1.1 – Typical theoretical drug development program.** Over the course of the development program the number of potential candidates that reaches the clinical setting is relatively low due to the inherent problems of most drugs. Specifically designed DDS introduced at the pre-clinical development stage or as a repurposing strategy could potential improve the number of drugs

A particular area within drug delivery that has raised increased attention is the use of synthetic polymers in nanomedicine. The key feature for their success is their multivalence and their structure that can be modified to have suitable biological properties. However, despite all the successes associated with polymeric nanomedicines, there has been an increased concern over the balance between efficacy and potential biological risks[1]. This mainly results from a lack of knowledge of their biological interactions, particularly at biological interfaces, as well as the impact of their long term use. Consequently, the development of the next generation of polymeric drug delivery systems should be carried concomitantly with the understanding of their interactions with the major components of the biological milieu. In this regard, dendrimers are viewed as suitable DDS due to their precise structure that can be further tuned to have desired biophysical properties. This allows the study of specific modification to the backbone and how these interact at the interface of biological membranes, which can provide value insights that may unravel ways to improve targeting. Furthermore, dendrimers can also be made of biocompatible and biodegradable building blocks such as amino acids which facilitate their degradation process for long term use.

### 1.2. Dendrimer definition and applications

Dendrimers belong to a subclass of synthetic macromolecular hyper-branched polymers that include random-hyperbranched polymers, hypergraft and dendrigraft polymers as well as dendrons (Figure 1.2). One of the main distinctions compared to other polymers has been the precise substitution from a multifunctional core that can be achieved. With the exception of hyperbranched-based dendrimers, this type of polymers also generally demonstrates a well-defined radial branching architecture. Notably, a key factor for their advantage over conventional polymers that rely on statistical characterization of their molecular structure is that dendrimers can be synthesized with no batch differences[5]. This unmatched topology control is highly desired since high homogeneous populations of very narrow molecular weight distribution can be achieved[6,7]. Modification of the surface functional groups also allows a control over the physicochemical properties of dendrimers. In fact, the degree of substitution at the surface can be studied for their contribution to activity as well as interactions with other biological components.

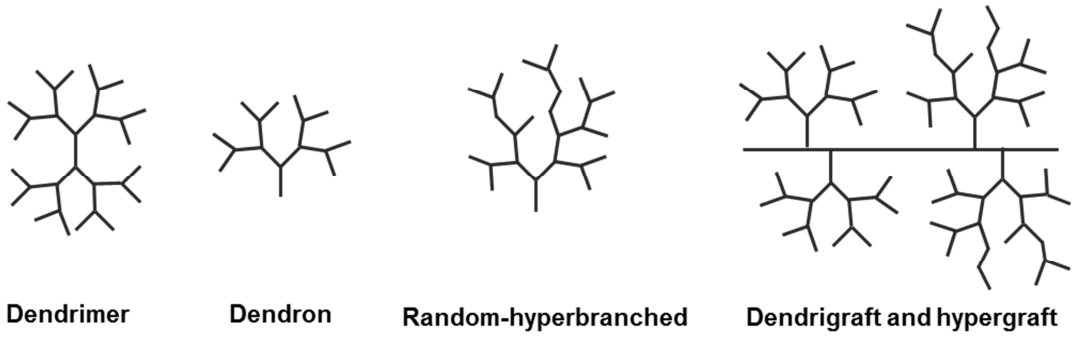


**Figure 1.2 – Schematic topology representation of different types of hyperbranched polymers.** Dendrimers can be generated by attaching dendrons to a multifunctional core and are generally differentiated from other hyperbranched polymers where the growth is more random.

The concept of dendrimers was first introduced in 1978 by Vögtle[8] referring to the description of "cascade molecules" due to the repetitive branching of the "arms" in the polymer in an analogy to a water cascade of a fountain[9]. Mono- or diamines were used as starting units to which subsequent addition of branching monomers resulted in the growth of the polymer. The word "dendrimer" was then first introduced by Tomalia et al. in 1986[10], which was derived from the Greek words "*dendros*", meaning tree or branch, and "*meros*", meaning part. Historically, other names have also been suggested for this type of macromolecules including arborols, "cauliflower polymers", shell topological compounds or starburst polymers but have been rarely used. Initially, a number of patents describing the synthesis of poly(lysine) (PLL)[11–13] dendrimers via divergent synthesis (outward from the core) were registered. Later, polyamidoamine (PAMAM) dendrimers were introduced to study host-guest interactions (similar to interactions between proteins and small ligands) and have since been used in a wide variety of other applications[10]. In particular, dendrimers have received an increased amount of attention over the past decades as materials in nanomedicine (e.g. DDS or as therapeutics) due to their unique vast array of properties that can be optimized for a variety of fields.

The application of dendrimers in the biomedical field has been extensive and includes catalysis (or synthetic enzymes)[14], metal-binding[15], biosensors and contrast agents for imaging[16], drug delivery agents and solubilizing agents[17], transfection agents[18] and as therapeutics[19,20]. In particular, as DDS these molecules have shown the ability to: (i) enhance aqueous solubility; (ii) provide controlled release; (iii) protect drugs from enzymatic degradation; (iv) improve drugs' pharmacokinetics; (v) enhance permeation of drugs through biological barriers and (vi) improve the toxicity profile of drugs[21].

Moreover, their ability to form polyvalent and cooperative binding combined with the possibility for specific attachment of functional moieties[22] has been shown to be useful for targeting specific molecular pathways[20,23–25] and avoid non-specific distribution[26]. Overall, this substantially increases the repertoire of drugs that can theoretically be used in human administration by minimizing their negative intrinsic properties. In fact, docetaxel- and cabazitaxel- conjugated to PEGylated PLL dendrimers are currently in phase 2 and phase 1/2 clinical trials respectively[27]. In animals studies these have shown enhancement of the anti-cancer activity, prevented side-effects and preferentially accumulated in the cancer tissues. Furthermore, VivaGel® a PLL-based dendrimer with mucoadhesive properties has also been approved against bacterial vaginosis[28,29]. These results increase the confidence of the potential of dendrimers as DDS or imaging agents and serve as a platform to further explore their clinical use.

### 1.3. Dendrimers topology and nomenclature

Structurally, dendrimers are characterized by a repetitive radial growth of branched monomers connected to a central core, and are defined by the following: (i) core; (ii) internal monomers or backbone; (iii) terminal groups; and (iv) void space or cavities/pockets (Figure 1.3). The core defines the 3D topology through its size and branching multiplicity, while the terminal groups define mostly the physicochemical properties and which can be further modified with active functional moieties[30,31]. On the other hand, the internal structural backbone defines the density of dendrimers and can result in free space cavities for “guest” molecules. Also, an interesting property of the interior chemistry is that the selected monomers can be sensitive to triggers (pH, solvent, light) resulting in controlled release or other necessary functionality (e.g. catalysis)[32].

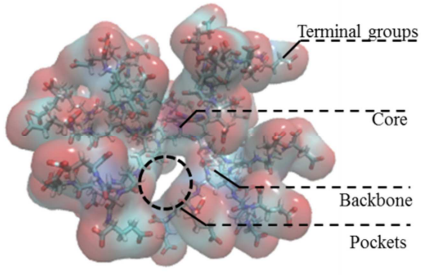


**Figure 1.3 – Topology description of a typical dendrimer.** The backbone is grown from the central core unit and the terminal groups define the overall charge displayed at the surface (red spots). At this generation, void space (pockets) created by the backbone or the terminal branches allow space for small molecules to be incorporated.

Due to their iterative nature, dendrimers are often described by their generation number which describes the number of layers added from the core, i.e. counting the number of branching points from core to the periphery. What constitutes a layer or a generation is however not completely agreed upon throughout the literature, tending to be specific to individual work and by authors' preferences. This is partly due to the complex chemistry nature that can be used to generate a dendrimer and the further modifications that can be carried to the main backbone and core. Similarly, the exact definition of what constitutes a generation 0 (G0) is not fully agreed upon, with some authors defining the G0 essentially as the core, while others defining it as the core together with the first layer. In this work G0 is defined by the first layer added to the core (e.g. glutamic acid (GLU)), as it allows the same naming regardless of the modifications of the core (Figure 1.4). It is also common to describe certain modifications to the terminal groups as half-generation. For example, when terminal groups are altered from an amine-terminated to a carboxyl-terminated group it is common to find this described as G1.5 or G1.5-COOH. This informs that the functionality of the terminal groups has been altered. In the framework of this dissertation, this nomenclature will however not be used since the terminal groups are not modified but rather de-protection modifications will be described.

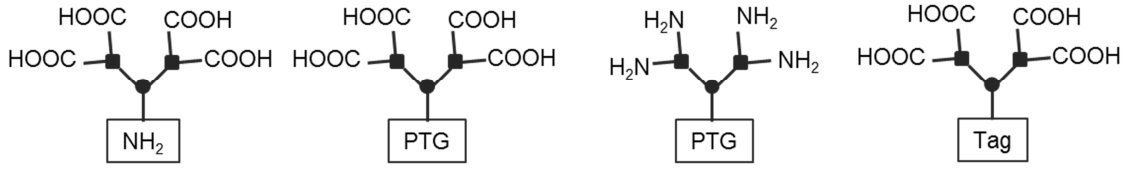


**Figure 1.4 – Types of G0 for a series of different dendrimers with the same core (●) and branches (■) but with different terminal groups and core modifications.** The scaffold of dendrimers is flexible to modification which can be valuable to display different surface properties. PTG: protecting group; Tag: Tag molecule

Finally, naming and describing the 2D structure of these molecules is also still debated[33]. The IUPAC nomenclature is the accepted way of naming small molecules that enable their reconstruction and identification. Even though the IUPAC nomenclature can be applied to small dendrimers and dendrons, it is clear that with the higher generations, the naming of dendrimers becomes complex and leads to difficulties in understanding all the structural features. Similarly, the nodal nomenclature, which is based on graph theory, struggles to describe at higher generations and more complex dendrimers[34,35]. For this reason, Newkome-

nomenclature, cascadane and dotted cap notation (see references[35–37] for more details) have been specifically adapted to describe dendrimers. These nomenclatures are capable of representing the hyper-branched and repetitive nature of dendrimers to some degree and offer clear advantages representing the core, monomers and capping groups. However, this nomenclature can still be complex and therefore have not been fully adopted. As a result, in order to facilitate the description of dendrimers in this work, poly(glutamic acid) (PG) dendrimers will be named according to the amine-modification of the core and the carboxyl-modification of the terminal monomers, as well as the generation. Therefore, different dendrimers and generations will be named as follow: [N-coupled group]-[name of the backbone]-[Carboxyl-protecting group] [Generation number] (Figure 1.4). For example, one dendrimer would be named Fmoc-PG-Methyl ester G1 for denoting Fmoc-capped to the amine of the core, GLU modified as a backbone for 2 layers, and methyl ester protecting the carboxyl groups for the terminal groups.

### 1.4. General considerations for synthesis of dendrimers

The synthesis of dendrimers is commonly carried out by cyclic repetitive addition of layers of monomers to branches connected to a multifunctional core, where each new layer forms new generations. The precise nature of monomer additions during synthesis is what differentiates from other hyperbranched polymers and results in ideally monodisperse populations. However, both the synthesis and characterization of dendrimers are still presenting a challenge. Dendrimers' synthesis strategies involve either growing a molecule from the core by addition of layers of branches (divergent synthesis) or growing the branches and attaching them onto the core in the final step (convergent synthesis). Alternatively, a mix of both strategies can be used to minimize the number of reactions that need to occur where the pre-formed branches generated using a convergent manner are then attached to a product of a partial divergent synthesis from the core.

The chemical reaction routes that can be used in the synthesis of dendrimers depend on the type of chemistry of the monomers. Since dendrimers can be generated as long as the monomers have branching functional groups (branching units) there is a wide variety of scaffolds that can be synthesized (Figure 1.5). However, despite the numerous possibilities of scaffolds, PAMAM and poly(propylene imine) (PPI) dendrimers have been by far the most studied dendrimers and for which high generations were obtained.

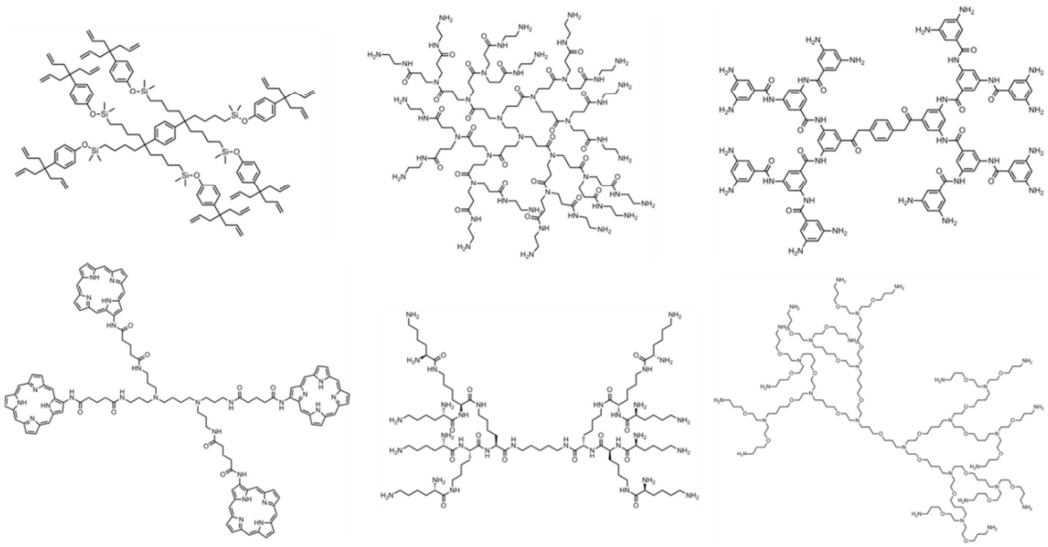

**Figure 1.5 – Examples of dendrimers synthesized from different starting cores and different branching monomers.** Since the limiting factor for synthesis is based on the reactivity of the active groups used, a wide diversity of scaffolds can be generated.

Albeit lower generation dendrimers can be easily obtained and purified, minor defects in the branches can arise at higher generations due to a plethora of chemical constraints. This produces defective, but structurally very similar dendrimers that are difficult to separate, thus not being able to obtain a pure final product. Therefore, highly selective reactions with high yields are necessary for growing dendrimers and to minimize the occurrence of defective branches. As an example, using divergent synthesis (from the core to the terminal groups), assuming a core of multiplicity 4, branch monomers with multiplicity of 2 and a reaction for growth of 99% selectivity, this results in the following statistical amount of pure dendrimers: 96% (G0), 92% (G1), 85% (G2), 72% (G3), 52% (G4), 27% (G5) and 7% (G6). In this theoretical example, the defects arising from de-protecting reactions that are usually necessary are not accounted for. Therefore, even for highly selective reactions the yield for high generations drops considerable.

Finally, the structural characterization of dendrimers is complex and limited due partly to their flexible and symmetrical nature[38,39] that result in multiple and broad identical signal peaks for structure based characterization. As a result, multiple analytical methods, such as, nuclear magnetic resonance (NMR), mass spectrometry (MS), infrared (IR) and X-Ray as well as computational methods are generally employed to correctly assign the structure and dynamics of these macromolecules. In particular, these techniques have provided quantitative analysis of chemical transformations as well as quantification of side reactions and defective branching. Moreover, these have

been used to evaluate the degree of substitution, as well as, the mobility and backfolding of the terminal groups and their effect on the hydrodynamic volume[7,40,41]. Finally, precise structural characterization has been carried in dendrimers where the molecular arrangement and the density distribution of monomers within the backbone have been determined[40].

### 1.5. Dendrimers biological interactions and drug delivery

Drug delivery is an area of continuous research and development towards avoiding the possible problematic pharmacokinetics properties shown by a variety of drugs. However, designing functional dendrimers is still challenging since both the core and surface groups determine not only the topology but also the physicochemical nature and ultimately the biological activity of dendrimers[42]. In fact, the safety and precision has to be adequate even for nanocarriers, which has been the major impediment encountered during translation into a clinical setting[43,44]. In this regard, dendrimers as a type of branched polymers offers advantages over conventional polymers since they are a monodisperse population of structures and both their size, shape and surface properties can be controlled. Moreover, whereas linear polymers usually adopt random-coil structures, the architecture of dendrimers has a defined 3D shape despite their intrinsic flexibility. This unique feature predisposes them to be good candidates as nanocarriers for delivery of drugs or as imaging agents.

Dendrimers have been used as DDS for a variety of biological routes (e.g. oral, pulmonary, transdermal and ocular) for small molecules, peptides and nucleic acids[45–50]. Comprehensive understanding of their molecular mechanisms of action should allow the design of these carriers to have specific tissue accumulation profiles, and optimized drug release rates and elimination rates. Furthermore, dendrimers have the possibility to be designed to established specific dendrimer-drug (host-guest) interactions and therefore minimize the solubility problems of these drugs[51,52]. In fact, drugs can establish interactions with the dendrimers by complexation in the interior branches (also known as dendrimer acting as an endo-receptor) or at the dendrimers' surface (also known as an exo-receptors), which typically occurs through hydrophobic or electrostatic interactions. The electrostatic forces can then be controlled to release drugs as a function of gradients of pH (e.g. acidic environment in the endosome) or by using counter-charged groups[53,54]. Although the number of guest molecules incorporated into a dendrimer will depend to some extent on the architecture and the size of a dendrimer, the loading capacity may be dramatically increased through complexation with the large number of groups on the dendrimer surface. Alternatively,

therapeutics can be conjugated to the scaffold backbone. This is necessary in cases where the drug may not complex with the dendrimer or when the release of the drug needs to be precise and limited to a certain reaction, such as an acid-labile cleavage in the matured endosome[23]. In general, both these strategies result in prolonged circulation half-time of a drug by reducing clearance from the bloodstream, as well as preventing hepatic clearance and rapid filtration through the glomerular membrane[55–57]. Finally, dendrimers have multiple terminal groups that can produce multivalent coordination with biological motifs (peptides, proteins, sugars). Generally this can enhance the avidity and selectivity in a similar way to multivalent mechanisms that exist in nature[58,59]. This constitutes a versatile approach to drug delivery as it improves their ability to overcome physiological barriers, while enabling preferential accumulation in specific cells or intracellular compartments. Even though increasing functionalization can be used as a strategy to enhance tissue targeting, these factors might not always follow a linear relationship. For example, while arginylglycylaspartic acid (RGD) functionalization increases affinity of the dendrimers to the receptor, a higher number of RGD peptides can create steric hindrance of their binding surface and thus reducing the overall affinity[23].

One of the most attractive applications for dendrimers is the targeted delivery of cytotoxic drugs for cancer therapy. The aim of this approach is to have a high partition of drug molecules into the cancer tissue, while having low amounts in other (healthy) tissues. Dendrimers are particularly suited for this since multiple molecules of the drug or combination of drugs with synergistic effects can be complexed to a single scaffold[60,61]. Moreover, these carriers usually exhibit enhanced permeation and retention into the pathogenic tissue and bypass the efflux transporters commonly overexpressed in cancer cells[62]. As a result, it may be possible to reduce the dosage of drug necessary while increasing the effectiveness of these drugs at the same time[60,61]. To illustrate this point, cisplatin is a widely used anti-cancer drug that acts through interaction with DNA[63], but it is very promiscuous and binds to a large number of other targets, which will typically result in side effects[64] (further discussed in topic 1.11). Moreover, cells develop resistance mechanisms in long term. Therefore, using anionic dendrimers or complexing cisplatin directly at the DDS surface could allow controlled and targeted delivery and bypass resistance mechanisms. In fact, cisplatin-complexed dendrimers have shown reduced off-target toxicity while maintaining significant anti-proliferative activity[65]. Furthermore, cisplatin-terminated dendrimers accumulated 50 fold more in solid tumors but showed less undesired off-target toxicity than free cisplatin, which was attributed to suboptimal release[65]. In another example, cisplatin

was complexed to the surface groups of a carboxylate-terminated PAMAM dendrimer which led to a 10 fold increase in the solubility of cisplatin compared to the free drug[65].

### 1.6. Peptide Dendrimers

Amino acid-based dendrimers (also known as peptide dendrimers) are an interesting polymeric system to be developed as biomaterials due to their inherent protein-like nature. In fact, they are expected to have an acceptable biocompatibility and biodegradability[66] since upon partial decomposition or degradation they are broken down to low molecular weight fragments that are expected to be non-toxic. Also, due to their similarity to biomolecules they have shown to be able to mimic proteins activities (e.g. enzymatic activity, synthetic vaccines and ion-channels), as well as having therapeutic activity of their own[67] while maintaining water solubility.

The synthesis of peptide dendrimers depends on the type of amino acids used (including non-natural amino acids), as well as in which step they are used. In terms of synthetic approaches these can be differentiated into: (i) backbone amino acids that have two branching points for dendrimers growth (i.e. trifunctional amino acids); (ii) backbone amino acids with one branching point that are connected to branching unit monomers; (iii) backbone of a mixture of amino acids with both single and double branching unit points; (iv) grafting of amino acids or peptides on the periphery of a conventional/classical dendrimers[68].This results in a diverse variety of peptide classes that can be used in a variety of applications.

In fact, PLL have been extensively used as the backbone for many scaffolds with success. These have shown anti-angiogenic activity with retardation of tumor growth[40] and PLL with the arginine conjugated to the terminal groups (8 and 16 groups) showed ability to bind to heparin[69]. Similarly, different PLL generations (with 4, 8 and 16 terminal groups) were modified terminally with shikimic and quinic acid to bind to lectin[70]. PLL has also been modified with PEG chains that self-assembled with DNA to form complexes with 50-150 nm in size[71]. Other interesting modification has been the use of PLL dendrimer with naphthalene sulfonic acid terminal groups (SPL7013, VivaGel®), which has shown antiviral activity against Herpes Simplex Virus (HSV) and human immunodeficiency virus (HIV) *in vitro*[29] and *in vivo*[72]. Furthermore, dendrimers terminated with tryptophan have shown to inhibit early steps of the viral infections namely the entry into its target cell[73]. Finally, cyclic multiple antigenic peptides (MAPs) dendrimers have been synthesized by attachment of antigenic peptides to a dendritic lysine dendrimer scaffold with different amounts of terminal groups as a mean of producing an immune response[74].

As a monomer, glutamic acid (GLU) is also interesting to be used as a building block of a dendrimer scaffold. This is because GLU is anionic and negatively charged species have been associated with enhanced circulation *in vivo* and superior biocompatibility[75]. Thus anionic dendrimers are expected to have enhanced passive accumulation in target tissues instead. Indeed, other anionic dendrimers with encapsulated drugs have shown enhanced uptake in different human cell lines[76,77]. PG dendrimers with different cores and surface modification have also been shown to be good candidates as drug delivery systems and in particular for anti-cancer drugs such as doxorubicin[78–82]. GLU is also a suitable monomer for synthesis of dendrimers since it has a trifunctional structure, presenting two carboxyl groups and one amine group that can be further modified. This is advantageous since PG dendrimers can be grown from both carboxylic acid groups and the amine in a variety of ways. To achieve this, the groups that are not used for branching must be protected to be compatible with the coupling reagents and to avoid racemization. This is usually carried by using ester forms of the carboxyl group  or using protecting groups such as fluorenylmethyloxycarbonyl (Fmoc-), *tert*-Butyloxycarbonyl (Boc)-, carboxybenzyl (Cbz) for the amine[83]. Those protecting groups have advantageous properties over other alternatives due to their superiority in terms of cleavage[83] and ability to withstand common peptide coupling chemistry reagents. Moreover, the use of alkyl esters are better suited for protection since aromatic esters can hydrolyze (due to its electrophilicity)[84]. Other property that makes PG dendrimer desirable is that GLU has several protonation states depending on the pH (Figure 1.6). This can be an interesting property to modulate in DDS making them pH-sensitive. In fact, this was previously explored by attaching a sequence of glutamic acids to a dendrimer G3 backbone which adopted a helical conformation or random coil in water depending of the pH[85]. Similarly, dendrimers have also been created with amphiphilic L-glutamic acid analogues that can self-assemble and form gels at specific conditions[86,87].

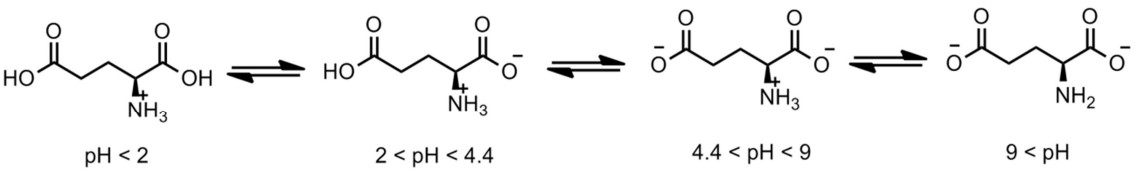


**Figure 1.6 – Glutamic acid protonation at different pH.** The variation of pH results in different protonation of the amine and carboxyl groups which modulated the effective final charge of the monomer. In fact, at low pH glutamic acid is positively charged whereas at high pH it is negatively charged.

## 1.7. Dendrimers and fluorescence tagging

For any drug delivery application, knowledge of the fundamental mechanisms of cellular uptake is essential for improving their design and efficacy[23]. Having a way to track macromolecules in the biological milieu could aid elucidation of relevant mechanisms and inform the design of delivery systems. In particular, tracking a single macromolecule should allow selective and non-invasive monitoring of cellular fate. Because many dendrimers do not present inherent fluorescence properties, fluorescence tagging is a technique commonly used and in rapid expansion in the biomedical field. The addition of a fluorophore allows the observation of dynamic processes within a useful space and time resolution. Conjugation of fluorophores to the dendrimer also allows to probing their topological and biochemical features[88], which is valuable to track during their intracellular trafficking[89]. This also includes determining if the dendrimer crossed biological barrier and entered the cells instead of remaining bound to the cell membrane. Contrary to most of other polymers, dendrimers can be modified to contain one single probe per dendrimer, and thus reducing undesired effects, such as self-quenching, while enabling precise monitoring of mobility and rotation of the attached molecule[90]. In fact, the number and type of fluorescence probes has to be taken into account when designing the dendrimers. Fluorescence intensities can decrease with the increasing number of coupled fluorophores. This has been attributed to the self-quenching that can arise from their proximity in the polymer backbone[90]. Furthermore this type of attachment is carried by a so called statistical loading that can increase the variability of the dendrimers' signals. On the other hand, having a significant amount of fluorophores attached to the surface of the dendrimer can result in alterations of surface properties that can affect the biological interaction, stability and solubility. In fact, it was recently reported that the transfection of luciferase was enhanced by the incorporation of different amounts of Oregon green 488 at the surface of a PAMAM dendrimer in a concentration dependent manner[91], showing the importance in terminal group substitution for their efficacy. In addition, since probes can have charge or have a lipophilic character, these features may influence the interaction with membranes for small dendrimers. Therefore, the "encapsulation" of the fluorophore and isolation from the exterior environment could be a way to avoid such type of problems. In fact, these potential disadvantages can be addressed by loading the fluorophore into the core. However, this raises problems in the early stages of the dendrimer design since modifications have to be carried in a rational design approach to account for the incorporation of the fluorophore. This means that the core and the generation at which the fluorophore has minimal interactions with the external

environment have to be chosen accordingly. Computational rational design using molecular modeling is suitable for this kind of approach since it can ideally study the topological features of using different building blocks before attempt bench experimental studies.

### 1.8. Molecular modelling

Computational methods to investigate complex biological systems have been an important tool in the discovery of new drugs and unveiling the biological mechanisms that govern cell function. Molecular simulations can also enable the understanding of dynamic processes in biological systems within the atomic scale resolution[33]. Moreover, the combination between bench experiments and simulation data has reinforced many areas of drug development where results are not accessible through bench experiments.

A number of theoretical approaches have been developed to describe molecules. As with any computational approach, the central question is the quality of the model and the level of complexity to be achieved, as well as how much information needs to be predicted. Although the laws governing atoms' motion are described by quantum mechanics, it was the realization that simpler models built using classical mechanics principles could predict some molecular properties that has enabled the revolution of computer simulations applied to drug discovery. In summary, more detailed theoretical models can describe more complex systems with higher accuracy, but less detailed ones allow simulations of larger systems.

Quantum mechanics (QM) is so far the most accurate theory to describe the geometry and energetics associated with the probability of a position of a wave with a mass and charge in the interaction of electrons and nuclei. The key equation in quantum mechanics is the time-independent form of Schrödinger equation (equation 1), which should predict the properties of any molecule and the energetics associated with it.

$$\hat{H}\,\Psi = E\Psi \qquad \textbf{(Eq. 1)}$$

The wavefunction, $\Psi$, describes the shape of the electron distribution, $\hat{H}$ is the Hamiltonian operator (composed of kinetics and potential energy) and E is the energy[92,93]. The Hamiltonian is very important in QM, and is the first term to be solved. Only then the equation is solved by finding a wavefunction that satisfies it[94]. The solutions from the Schrödinger equation belong to the area of *ab initio* quantum calculations and are able to describe the orbitals of the electron[92,93]. However, the Schrödinger equations cannot be solved for molecules bigger than $H_2^+$. Therefore,

simplifications of these equations were introduced, and one of the most important contributions was the Born-Oppenheimer approximation. This model treats the motion of electrons decoupled from the motion of the nuclei, since electrons are much faster and thus the motion of electrons becomes a constant. When many electrons are involved other approximations can be made which require the use of a basis set of Gaussian functions (mathematical functions that when combined are able to represent orbitals) such as the Hartree-Fock (HF) method. In its essence, the HF method solves the many-electron problem by replacing it by one-electron calculations. The atomic basis sets are first used to estimate the initial guest at the orbital, and then the electron motion is treated as in an average electron distribution, and the energy is calculated until it reaches a minimum[95]. However, even with the simplifications above, it still requires a lot of computational resources to solve these equations, especially for larger molecules. As a result, QM calculations are used mostly for small molecules to calculate geometries and equilibrium constants, which provide a reference value for simpler models. In an effort to compute larger sets of molecules, empirical methods were introduced by using a classical view of atoms by fitting them into a potential energy function.

Molecular mechanics is an approach used to calculate the structure and energy of molecules based on nuclear motions only. In this method electrons are not considered explicitly, meaning that quantum effects are ignored, and the motion of “hard spheres” that interact to each other through “springs” is treated with Newton’s equations of motion. Simulations can be performed by different methods including (i) Brownian Dynamics; (ii) Monte Carlo (MC); or (iii) Molecular Dynamics (MD). In Brownian simulations, macromolecules are treated as a Brownian particle and evaluated for its friction in the surrounding solvent[96]. For MC simulations, macromolecules are simulated to find a low-energy conformation by iterative random atomic displacements which are evaluated for their energetics and accepted or rejected within a probability Boltzmann statistics function[96–98]. Finally, in MD simulations atoms are allowed to move and interact over time through integration of classical mechanics. During MD simulations the atoms (the “spheres”) will interact with other atoms through mathematical harmonic functions (“springs”) that keep bonds and angles within an equilibrium. This is a useful way of representing the motion as it requires energy to pull atoms apart or push them closer[92]. In order to calculate the energy associated with it, the whole mathematical function will be populated by these various terms related to each atom and their interactions with other atoms. These terms are parametrized and validated using experimental data, and stored into a data set named the force field.

Various mathematical models have been devised to calculate a potential energy of a system, and choosing one is a compromise between simplicity *vs.* accuracy. In general, these functions calculate energy based on the atom positions and are composed by terms representing the bonded and non-bonded interactions. Extensions to the main functions of the energy function can be added but these may not yield significant accuracy gain[99,100] and in general Class I force fields (e.g. used by CHARMM and AMBER where the harmonic terms are restricted) have been adequate to treat intermolecular distances and their energetics[100]. In this work NAMD software was used for MD simulation, which employs a common potential energy function that contains the following terms (equation 2 and figure 1.7):

$$U_{total} = U_{bond} + U_{angle} + U_{dihedral} + U_{vdW} + U_{Coulomb}$$

$$U_{bond} = \sum_{bonds\ i} K_i^{bond} (r_i - r_{0i})^2$$

$$U_{angle} = \sum_{angles\ i} K_i^{angle} (\theta_i - \theta_{0i})^2$$

$$U_{dihedral} = \sum_{dihedral\ i} K_i^{dihe} [1 + \cos(n_i \phi_i - \gamma_i)]$$

$$U_{vdW} = \sum_i \sum_{j>i} 4\varepsilon_{ij} \left[ \left( \frac{\sigma_{ij}}{r_{ij}} \right)^{12} - \left( \frac{\sigma_{ij}}{r_{ij}} \right)^{6} \right]$$

$$U_{Coulomb} = \sum_i \sum_{j>i} \frac{q_i q_j}{4\pi\varepsilon_0 r_{ij}}$$

(**Eq. 2**)

The first two terms ($U_{bond}$ and $U_{angle}$) describe the stretching (1-2 interaction, i.e. two adjacent atoms) and the bending (1-3 interaction, i.e. between 3 atoms) between molecules through their respective constants ($K^{bond}$ and $K^{angle}$) from an equilibrium length ($r_{0i}$ and $\theta_0$)[101,102]. The third term, the dihedral angle, describes the 1-4 interaction. Dihedral terms are described in terms of multiplicity (n) and phase (φ) that characterize the height of energy barrier to rotation (e.g. larger for double bounds than for single bond) and the maximum and minima of such rotations between two planes to atoms[101,103]. Finally, the last two terms describe the non-bonded interactions. These are of paramount importance for modeling macromolecules since they govern much of their structure and properties, and therefore should be properly parameterized[100]. These are

the forces that govern for example the base pairing of the DNA, as well as protein-protein interactions. In the van der Waals term, the Lennard-Jones potential is commonly used to describe the attractive London dispersion forces that arise from neighbor dipoles. There are various ways of describing this potential but commonly the 12-6 potential is used. Finally, the electrostatic interactions are treated through the Coulombic terms by using static partial charges. The method by which charges are calculated are a matter of great debate since this is not experimentally observable and therefore various methods of calculations have been proposed. For example, CHARMM charge assignment makes use of supramolecular structures of water-molecules interactions at idealized distances between the polar groups[104]. The charge calculation should be consistent and should be representative of the environment for which they will be used (most charge calculations are performed in vacuum)[101]. For dendrimers, this is very important as simulations are carried out in the condensed phase. Since the force field employed by NAMD does not account for explicit treatment of polarization terms, it is necessary to reproduce this electrostatic interaction by other means[100]. Luckily, it was observed that HF in conjunction with a 6-31G* basis set include an overestimation that cancels underestimation error, and as such suitable for describing charges in force fields.

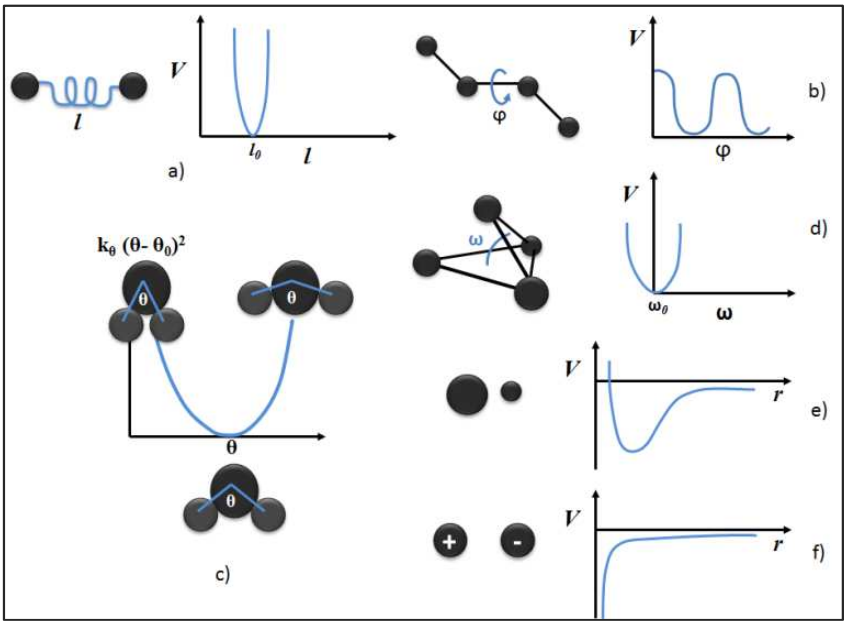


**Figure 1.7 – Schematic representation of "spheres" and "springs" and their contribution to the potential energy function;** a) bond length term; b) dihedral angle term; c) bond angle term; d) improper angle term; e) van der Waals term; f) coulomb term

The potential energy is then calculated iteratively to find a low-energy region within a thermal equilibrium[105]. These energy calculations are a function of the position of the

atoms and hence treated by classical mechanics of Newton's law. These simulations allow probing the motions and distribution of the different atoms of the structure in a biologically relevant system as well as predicting potential bonding networks with the surrounding environment.

### 1.9. Molecular modeling and dynamics of dendrimers

When designing a dendrimer, computational simulations offer a major advantage since one can perform several MD simulations before empirical decision on the overall structure to be synthesized. These simulations can provide detailed insights at atomic resolutions, including size and shape, which can then be corroborated by experimental data. To date, computational studies have been applied to study dendrimers with two main focuses: (i) dendrimers' conformation in solution; and (ii) dendrimers interaction with molecules. As an example, efforts have been made in order to correctly predict the structure of PAMAM dendrimers in different solvent conditions. This arises from the evidence that due to its flexible nature, dendrimers have a vast range of conformations with similar potential energy making it difficult to probe the spatial and geometrical configuration by experimental techniques[106–111]. For PAMAM dendrimers it was recently reported that MD simulations could explain experimental data obtained by small-angle neutron scattering (SANS)[112]. Using the Dreiding FF with accurate QM calculations for hydrogen interactions, it was observed that various conformational changes occur in PAMAM dendrimers with alteration in pH, without changing the overall size[113]. MD simulations were able to reveal that some groups reorganize internally, ending up in a different distribution that can be more extended ("dense-shell") or more compacted ("dense-core")[7].

Another interesting approach of molecular simulations is the interaction with other biomolecules and applies to many fields of research. These have included MD simulations studies on the interaction of dendrimers with peptides[114], drugs[109], small molecules (for catalysis)[110], polymers[115], nucleic acids[116] and membranes[117]. In all cases, MD simulations were able to elucidate the network of interactions at the atomic resolution and corroborate bench experimental data, serving as a guide for further improvements.

However, there is still not a consistent way to prepare *in silico* models of dendrimers. Different studies use different ways to construct dendrimers (i.e. software), select force field parameters and finally setup different simulation conditions (water model type, use of ions, etc…). To construct a dendrimer, any molecular drawing software may be suffice and only depends on the level of automation intended. However, in the case of

selecting parameters, these should be carefully chosen and there is not enough data to appropriately select one. Furthermore, details about selection, optimization and validations of parameters are not always provided in the literature therefore making it difficult to evaluate and compare. Often dendrimers have been parameterized with force fields that have been developed for proteins and small molecules including CHARMM[118], AMBER[119], CVFF[120], Dreiding[113], GROMOS[108] and OPLS[121]. In general, this type of parameterization has shown to give enough details to corroborate bench experimental data and study the different forces involved (electrostatic, hydrogen, van der Waals and hydrophobic). In particular, simulations of PAMAM dendrimers with lipid membranes have provided insights into the mechanisms of toxicity of these dendrimers[33,111,122]. In this regard, studying the dendrimer-lipid interactions with the use of both computational and bench experiments could provide interesting insights on how to overcome the lipid membrane barrier to better deliver drugs.

### 1.10. Biophysical properties of cell lipid bilayers with anti-cancer drugs

More than acting as a barrier that compartmentalizes organelles there has been growing evidence that cellular membranes have a direct role in cell function, regulating uptake mechanisms, signaling pathways and determining cellular response to stress signals. Cellular membranes are heterogeneous and dynamic, presenting asymmetric distribution of lipids between membrane leaflets. In addition, it is now recognized that biological membranes are compartmentalized into functionally distinct domains[123–125]. At these domains specific lipid-lipid and lipid-protein interactions take place and result in distinct lateral organization and composition. In particular, some of these domains composed of sphingolipids, cholesterol and distinct proteins, named lipid rafts, have shown to actively modulate signaling pathways involved in cellular proliferation and growth, but also in trafficking and clustering of cell death receptors[126–131]. Furthermore, lipids might directly bind to proteins (e.g. ADP/ATP carriers, cytochrome C oxidase)[132] or act as protein co-factors (e.g. $Na^+/K^+$ ATPase and protein kinases). In addition, some proteins require specific lipids in their vicinity to regulate their conformation and "solubility" in the membrane (annular lipids)[133], and some proteins have shown greater affinity for their substrate in specific lipid phases, including in lipid gel phases compared to fluid phases[134]. It is therefore not surprising that de-regulation of lipid metabolism and consequently the membrane lateral organization is also associated with several diseases including cancer[135–138]. In certain cancer cells, alterations in the lipid metabolism results in changes of the biophysical properties of the plasma membrane, which in turn can affect how drugs interact with the cell [139,140]. In fact, alterations in membrane fluidity have been implicated in resistance of cancer cells to drugs[141–147],

which can result in reduced accumulation compared to sensitive cells[148]. This is however a complex process and not fully understood. On the other hand, differences in lipid composition can also be beneficial for treatment and specific targeting. For example, anionic lipids, such as, phosphatidylserines (PS) are normally present in the inner leaflet of the plasma membrane of normal cells. This lipid is crucial for many cellular events as it anchors proteins to the inner monolayer of the plasma membrane[149]. It also influences the activity of enzymes including $Na^+/K^+$-ATPase[150], which has been reported to be involved in the uptake of drugs, such as cisplatin[151,152]. However, in cancer cells there is an increased level of PS in the external leaflet[153,154], which can directly interact with drugs[155–159]. In fact, drugs, such as, cisplatin and daunorubicin have shown to specifically bind to PS[155–159].

On the other hand, drugs can also alter lipid metabolism and cause alterations of plasma membrane biophysical properties, such as fluidity, permeability and lateral organization that can result in a cascade of cellular events. For example, formation of ceramide-enriched domains induced by drugs have shown to be important in inducing apoptosis[160,161]. Therefore, targeting lipid metabolism and/or membrane biophysical properties might be an effective strategy to overcome resistance mechanisms[137,162–170]. In addition, since anti-cancer drugs activity starts at the plasma membrane, this biological barrier is nowadays regarded as a good target to develop new therapies or improve old ones. However, to attain this stage it is necessary to study drug-membrane interactions to understand (i) how membrane lipid composition and biophysical properties affect the mechanisms of drugs action; and (ii) how the interaction of the drug with the membrane influences membrane organization, properties and lipid composition. This should provide further information on how new molecules and/or DDS can be designed to improve their uptake and evade resistance mechanisms in cell membranes. On the other hand, it may also enable the identification of membrane targets. In this regard, cisplatin is a good model candidate to study due to its multitude of interactions at cellular milieu, including membrane lipids. Moreover, several mechanisms of resistance have been described for this chemotherapeutic, some of which associated with membrane lipid composition and/or membrane properties[171–173].

### 1.11. Cisplatin interactions with lipid membranes

Cisplatin is an anti-cancer drug used to treat a variety of cancers. However, it displays severe adverse effects and cancer cells are prone to develop cross-resistance against platinum(II) compounds after long term treatment[174]. Inside the cell, cisplatin exerts its primary action by targeting the genomic DNA with which it forms cross-links that

prevent further DNA replication[175]. As a response, cells develop resistance by (i) triggering responses to the effects of DNA damage; (ii) directly remove the formed adducts; or (iii) preventing the steps preceding the DNA binding related to off-targets[175]. In this regard, lipids have shown to play an important role in both the toxicity associated with platinum(II) compounds, as well as, in the resistance mechanisms.

In solution cisplatin exists in a state of multiple species in equilibrium known as "aquated" species. Particularly, at low chloride concentration and/or pH, this equilibrium favors the formation of positively charge species[176,177]. The latter have different properties and therefore are expected to behave differently with other biomolecules including lipids. Indeed, the diffusion of cisplatin in phosphocholine membranes was shown to be much slower for the charged species in comparison to neutral cisplatin species[178]. On the other hand, these positively charged species were shown to have preferential binding to negatively charged lipids, such as, DOPS (1,2-dioleoyl-sn-glycero-3-phospho-3-L-serine)[155,176], by directly binding to the serine headgroup and complexing with the carboxyl and amine groups[155,157,179]. This mode of binding is different for zwitterionic lipids, such as DPPC (1,2-dipalmitoyl-sn-glycero-3-phosphocholine), where cisplatin binds to the phosphate groups and forms a 2:1 complex (lipid:platinum)[63,180,181]. Studies have shown that in cells, cisplatin is able to accumulate at the surface and bind to cell membranes, ultimately crossing the membrane through passive diffusion[152,182]. This is likely to be due to interactions with membrane lipids[183–187]. Furthermore, detailed analysis of the mode of cisplatin binding in erythrocytes suggested that cisplatin-membrane interactions were mainly attributed to electrostatic forces, followed by hydrogen bonding and coordination to the phosphate polar head as a Pt-O-P complex[187] which further corroborates the *in vitro* binding observed for cisplatin with specific lipids.

Platinum(II) complexes have also shown to cause changes in the phase properties of certain lipid membranes. In particular, cisplatin-induced changes in the phase properties of the membranes are dependent on membrane lipid composition since alterations found in lipid extracts[187,188] were not evidenced in model membranes[189]. Moreover, the binding to specific lipids may also contribute to the observed effect. In fact, reorganization of lipid bilayers by induction of several lamellar phases were observed for charged species[156], but the same effects were not observed for zwitterionic lipids[179]. Furthermore, cisplatin was also shown to cause weak and transient alterations in lipid order in erythrocyte membranes that were transmitted inwards from the headgroup to the core of the bilayer, whereas in DPPC membranes it caused a rearrangement of the headgroups but did not affect the lipid chains[180].

Overall, these results suggest that cisplatin interacts with lipid bilayers but its effects are complex and dependent on a variety of extrinsic factors including, pH and chloride concentration, as well as, membrane composition and other unknown factors.

Similarly, the importance of the physical state of lipid membranes as a mechanism of resistance of cells to cisplatin is controversial and remains to be determined. Accumulating evidence suggests that membrane composition determines membrane structure and fluidity, which modulate membrane permeability to cisplatin[143,190,191]. Indeed, platinum accumulation is generally higher in sensitive cells and this accumulation occurs as early as 10 minutes after exposure, suggesting an active role on membrane composition to the permeation[143,190,191]. Furthermore, cisplatin caused alterations in the membrane miscibility in models of cisplatin-sensitive cells but not on models cisplatin-resistant cells[192]. Analogously, cisplatin was able to increase the membrane fluidity of sensitive-cells whereas in resistant-cells caused increased microviscosity[193]. On the other hand, modulating the fluidity of membranes of both sensitive- and resistance-cells models, resulted in different toxicity of cisplatin on those cells[143,192,194]. Even though the molecular details underlying the contribution of membrane lipid composition and fluidity to the mechanisms of resistance are yet not fully known, evidence suggests that resistant cells are less fluid than their sensitive counterparts[173,195,196].

Understanding drug-membrane interactions may thus create new opportunities to target membrane lipid composition and biophysical properties to develop innovative strategies to optimize drug efficacy and bypass the mechanisms of drug resistance originated by efflux of the drug or the DNA repair mechanisms. It might also guide the design of improved cisplatin derivatives and/or other chemotherapeutics and DDS..

### 1.12. Dendrimers and lipid membrane interactions

Dendrimers are in the same size scale of other common biomolecules, such as, proteins and nucleic acids, as well as, the thickness of the membrane (Figure 1.8). As a result, membranes can accommodate dendrimers in a similar manner to membrane proteins or the dendrimer can create holes in the membrane[197]. These effects have shown to be dependent on the dendrimer composition and terminal groups, size and concentration, as well as, the properties of the membrane (phase and lipid composition). In fact, studies on PAMAM dendrimers evidenced high deleterious effects both in model membranes[198,199] and cells[200,201], including pore formation, membrane disruption, destruction of microvilli and hemolysis, particularly when large generations of positively charged PAMAM dendrimers were used. To better understand

the molecular mechanism underlying the interaction of dendrimers with membranes both bench[198,199,202] and computational experiments[111,117,203] have been performed. Results suggest that increasing the generation and concentration of PAMAM dendrimers resulted in deleterious effects for the membrane. In DPPC (1,2-Dimyristoyl-*sn*-glycero-3-phosphocholine) bilayer stabilized in a mica layer[198,199], PAMAM G7 dendrimers with different terminal groups (amine, carboxylic and acetamide) were able to form holes ranging from 15-40 nm in the membrane, but the extent of hole formation was smaller for acetamide-terminated dendrimers, which suggests that these groups are better accommodated in the membrane. Contrary to G7, amine-terminated PAMAM G5 dendrimers did not show the ability to form holes but rather were able to enlarge existing defects in the bilayer[199]. However, substituting the terminal amines with acetamide groups abolished these effects, and the dendrimers were intercalated within the lipid bilayer instead[199]. Similarly, amine-terminated PAMAM G3 and G4 showed a concentration-dependent incorporation within the lipid membranes with preferential absorption at defective edges and lacked the ability to expand defective parts of the membrane[199,202,204].

In addition, the simulations showed that an initial strong interaction with the headgroups[117] is followed by the flattening of the dendrimer to cover a greater area and enhance interactions[203]. However, the flattening process is dependent on the size of the dendrimer, as it is energetically unfavorable for higher generations[205], and also dependent on the fluidity of the membrane, since it was not observed for the gel phase lipid bilayer[117]. This effect was attributed to the capacity of fluid membranes to create a pocket to accommodate the dendrimers, promoting a higher number of interactions[117]. However, upon dendrimer-membrane interaction the ordering of the lipid bilayer increases comparable to gel conditions due to tilting of the chains[206] promoted by the hydrophobic parts of the dendrimer[117,207]. Therefore, in the case of PAMAM G7 these have limited flexibility. Thus the mechanism by which they promote pore formation is due to extraction of lipids from the bilayer forming lipid vesicles encasing these dendrimers [198,199,208]. On the other hand, at small generations, PAMAM dendrimers lack the ability to form and stabilize these vesicles which may explain the pore formation in supported bilayers[205,209].

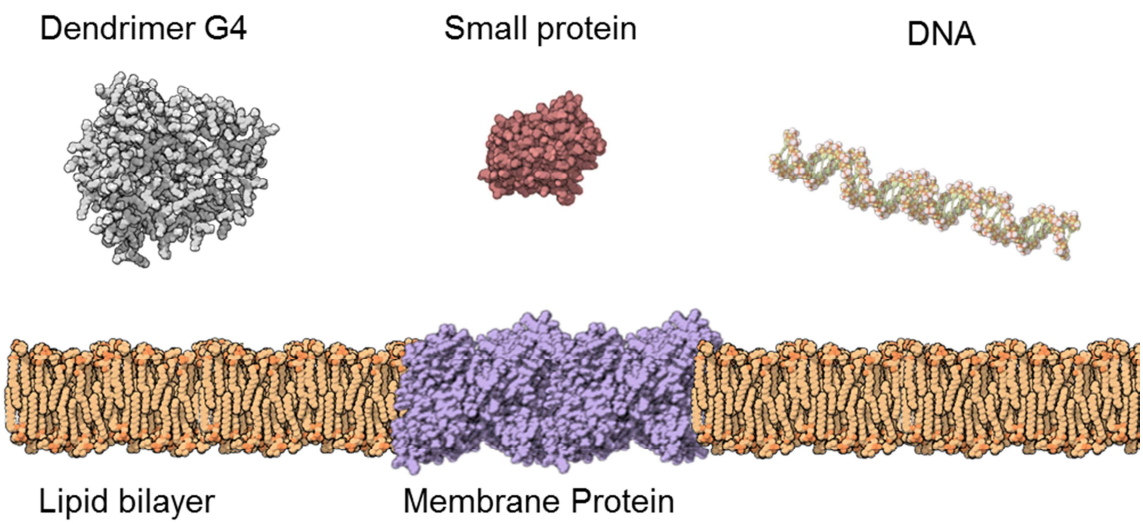


**Figure 1.8 – Dendrimers size scale in comparison to other biological molecules.** Dendrimers have the approximate size of small proteins, DNA as well as the lipid bilayer.

The results observed for model membranes correlate well with the toxicity observed in cells. In a similar way to what was observed in model membranes, PAMAM dendrimers were found to cause toxicity in a concentration, terminal charge- and generation-dependent manner[210]. The mechanistic effect of dendrimers as observed for model membranes may also explain the leakage observed for PAMAM dendrimers upon interaction with the cell as measured by LDH assay[211]. The correlation between *in vitro* and *in vivo* may however not be straightforward and extrapolations should be done conservatively. One particular factor is the difference between *in vivo* and *in vitro* environments, which may have a key role in the difference of efficacy of the dendrimers in the two types of experiments. Indeed, when PAMAM G5 dendrimers were added to a cell culture in serum not only did their transfection decrease but also their toxicity, as compared to serum free media[91]. This was attributed to a shielding effect caused by proteins which is also expected to occur *in vivo*. Further studies are therefore required to understand the interactions of dendrimers with biological systems so that new drug delivery systems can be rationally designed to better meet a desired therapeutic profile.

## 1.13. Overview and contextualization of the thesis

The task of developing new drug delivery systems for anti-cancer drugs requires a multidisciplinary approach. Anti-cancer therapies generally suffer from severe side effects as a result of non-specific binding to cells. Furthermore, platinum(II) compounds, such as, cisplatin have demonstrated limiting therapeutic effects on long term treatment due to the arise of resistance mechanism, particularly at cell lipid membranes, that are still poorly understood. Consequently, the development of new

DDS that address these limitations are of utmost importance. In this regard, this thesis describes a proof-of-concept approach starting from the design of fluorescent dendrimers as tools to investigate how these behave with lipid membranes and how they can impact the delivery of cisplatin. Concomitantly, the interaction of cisplatin with lipid model membranes should be used as a guide to further improve the design of these dendrimers. The use of computational modelling approaches is therefore critical to understand the structure of these dendrimers at the molecular level and how these relate to the interactions with both cisplatin and different lipid models. The synthesis of these candidates from a bottom up approach also allows a higher control over the structure and understanding of the physicochemical properties of these dendrimers, which in turn are valuable to validate the computational models. Particularly, it allows the creation of a modular synthetic approach where the fluorophore can be easily exchangeable so that probes with different properties can be tested. As a result, the combined knowledge of each approach should converge to improve the design of future DDS.

**References**


(1) Juliano, R. Nanomedicine: Is the Wave Cresting? *Nat. Rev. Drug Discov.* **2013**, *12*, 171–172.

(2) Duncan, R.; Gaspar, R. Nanomedicine(s) under the Microscope. *Mol. Pharm.* **2011**, *8*, 2101–2141.

(3) Venditto, V.; Szoka Jr, F. Cancer Nanomedicines: So Many Papers and So Few Drugs. *Adv Drug Deliv Rev* **2014**, *65*, 80–88.

(4) Maurer-Jones, M.; Bantz, K.; Love, S.; Marquis, B.; Haynes, C. Toxicity of Therapeutic Nanoparticles. *Nanomedicine (Lond)* **2009**, *4*, 219–241.

(5) Ali, M.; Brocchini, S. Synthetic Approaches to Uniform Polymers. *Adv. Drug Deliv. Rev.* **2006**, *58*, 1671–1687.

(6) Jackson, C. L.; Chanzy, H. D.; Booy, F. P.; Drake, B. J.; Tomalia, D. A.; Bauer, B. J.; Amis, E. J. Visualization of Dendrimer Molecules by Transmission Electron Microscopy ( TEM ): Staining Methods and Cryo-TEM of Vitrified Solutions. *Macromolecules* **1998**, *31*, 6259–6265.

(7) Maiti, P. K.; Çağın, T.; Wang, G.; Goddard, W. a. Structure of PAMAM Dendrimers: Generations 1 through 11. *Macromolecules* **2004**, *37*, 6236–6254.

(8) Buhleier, E.; W, W.; Vogtle, F. “Cascade”-and “Nonskid-Chain-like” Syntheses of Molecular Cavity Topologies. *Synthesis (Stuttg).* **1978**, *02*, 155–158.

(9) Vogtle, F.; Richardt, G.; Werner, N. *Dendrimer Chemistry: Concepts, Syntheses, Properties, Applications*; Wiley VCH, 2009.

(10) Tomalia, D. A.; Baker, H.; Dewald, J.; Hall, M.; Kallos, G.; Martin, S.; Roeck, J.; Ryder, J.; Smith, P. Dendritic Macromolecules: Synthesis of Starburst

Dendrimers. *Macromolecules* **1986**, *19*, 2466–2468.

(11) Denkewalter, R. G.; Kolc, J.; J, L. W. Macromolecular Highly Branched Homogeneous Compound Based on Lysine Units. 4,289,872, 1981.

(12) Denkewalter, R. G.; Kolc, J.; Lukasavage, W. J. Preparation of Lysine Based Macromolecular Highly Branched Homogeneous Compound. 4,360,646, 1982.

(13) Denkewalter, R. G.; Kolc, J. F.; Lukasavage, N. J. Macromolecular Highly Branched Homogeneous Compound. 4,410,688, 1983.

(14) Twyman, L. J.; King, A. S. H.; Martin, I. K. Catalysis inside Dendrimers. *Chem. Soc. Rev.* **2002**, *31*, 69–82.

(15) Yamamoto, K. Dendrimer Complexes: Fine Control of Metal Assembly in Macromolecules. *J. Polym. Sci. Part A Polym. Chem.* **2005**, *43*, 3719–3727.

(16) Satija, J.; Sai, V. V. R.; Mukherji, S. Dendrimers in Biosensors: Concept and Applications. *J. Mater. Chem.* **2011**, *21*, 14367.

(17) Shaunak, S.; Brocchini, S. Dendrimer-Based Drugs as Macromolecular Medicines. *Biotechnol Genet Eng Rev* **2006**, *23*, 309–315.

(18) Shcharbin, D. G.; Klajnert, B.; Bryszewska, M. Dendrimers in Gene Transfection. *Biochem.* **2009**, *74*, 1070–1079.

(19) Tyssen, D.; Henderson, S. A.; Johnson, A.; Sterjovski, J.; Moore, K.; La, J.; Zanin, M.; Sonza, S.; Karellas, P.; Giannis, M. P.; *et al.* Structure Activity Relationship of Dendrimer Microbicides with Dual Action Antiviral Activity. *PLoS One* **2010**, *5*, e12309.

(20) Darbre, T.; Reymond, J.-L. Peptide Dendrimers as Artificial Enzymes, Receptors, and Drug-Delivery Agents. *Acc. Chem. Res.* **2006**, *39*, 925–934.

(21) Cloninger, M. J. Biological Applications of Dendrimers. *Curr. Opin. Chem. Biol.* **2002**, *6*, 742–748.

(22) Mammen, M.; Choi, S.-K.; Whitesides, G. M. Polyvalent Interactions in Biological Systems: Implications for Design and Use of Multivalent Ligands and Inhibitors. *Angew Chem Int Ed Engl.* **1998**, *37*, 2754–2794.

(23) Liu, J.; Gray, W. D.; Davis, M. E.; Luo, Y. Peptide- and Saccharide-Conjugated Dendrimers for Targeted Drug Delivery: A Concise Review. *Interface Focus* **2012**, *2*, 307–324.

(24) Reymond, J.-L.; Darbre, T. Peptide and Glycopeptide Dendrimer Apple Trees as Enzyme Models and for Biomedical Applications. *Org. Biomol. Chem.* **2012**, *10*, 1483–1492.

(25) Esfand, R.; Tomalia, D. A. Poly(Amidoamine) (PAMAM) Dendrimers: From Biomimicry to Drug Delivery and Biomedical Applications. *Drug Discov. Today* **2001**, *6*, 427–436.

(26) Shaunak, S.; Thomas, S.; Gianasi, E.; Godwin, A.; Jones, E.; Teo, I.; Mireskandari, K.; Luthert, P.; Duncan, R.; Patterson, S.; *et al.* Polyvalent Dendrimer Glucosamine Conjugates Prevent Scar Tissue Formation. *Nat Biotechnol.* **2004**, *22*, 977–984.

(27) [accessed on 1 july 2018] StarPharma. StarPharma clinical trials available online: https://starpharma.com/about_us/clinical_trials.

(28) [accessed on 1 July 2018] Starpharma. Starpharma Vivagel available online: https://starpharma.com/vivagel_bv.

(29) Rupp, R.; Rosenthal, S. L.; Stanberry, L. R. VivaGel (SPL7013 Gel): A Candidate Dendrimer-Microbicide for the Prevention of HIV and HSV Infection. *Int. J. Nanomedicine* **2007**, *2*, 561–566.

(30) Duncan, R.; Izzo, L. Dendrimer Biocompatibility and Toxicity. *Adv. Drug Deliv. Rev.* **2005**, *57*, 2215–2237.

(31) Tian, W.; Ma, Y. Theoretical and Computational Studies of Dendrimers as Delivery Vectors. *Chem. Soc. Rev.* **2013**, *42*, 705–727.

(32) Tanis, I.; Karatasos, K. Association of a Weakly Acidic Anti-Inflammatory Drug (Ibuprofen) with a Poly(Amidoamine) Dendrimer as Studied by Molecular Dynamics Simulations. *J. Phys. Chem. B* **2009**, *113*, 10984–10993.

(33) Martinho, N.; Florindo, H.; Silva, L.; Brocchini, S.; Zloh, M.; Barata, T. Molecular Modeling to Study Dendrimers for Biomedical Applications. *Molecules* **2014**, *19*, 20424–20467.

(34) Lozac'h, N.; Goodson, A. L.; Powell, H. Nobel Nomenclature - General Principles. *Angew. Chemie* **1979**, *18*, 887–899.

(35) Roberts, B. P.; Scanlon, M. J.; Krippner, G. Y.; Chalmers, D. K. The Dotted Cap Notation: A Concise Notation for Describing Variegated Dendrimers. *New J. Chem.* **2008**, *32*, 1543.

(36) Newkome, G. R.; Baker, G. R.; Young, J. K.; Traynham, J. G. Systematic Nomenclature for Cascade Polymers. *J. Polym. Sci. Part A Polym. Chem.* **1993**, *31*, 641–651.

(37) Friedhofen, J. H.; Vögtle, F. Detailed Nomenclature for Dendritic Molecules. *New J. Chem.* **2006**, *30*, 32.

(38) Markelov, D. a.; Falkovich, S. G.; Neelov, I. M.; Ilyash, M. Y.; Matveev, V. V.; Lähderanta, E.; Ingman, P.; Darinskii, A. a. Molecular Dynamics Simulation of Spin–lattice NMR Relaxation in Poly-L-Lysine Dendrimers: Manifestation of the Semiflexibility Effect. *Phys. Chem. Chem. Phys.* **2015**, *17*, 3214–3226.

(39) Ranganathan, D.; Kurur, S.; Gilardi, R.; Karle, I. L. Design and Synthesis of AB3-Type (A = 1,3,5-Benzenetricarbonyl Unit; B = Glu DiOMe or GLU7 Octa OMe) Peptide Dendrimers: Crystal Structure of the First Generation*. *Biopolymers* **2000**, *54*, 289–295.

(40) Caminade, A.; Majoral, J. Characterization of Dendrimers. *Adv. Drug Deliv. Rev.* **2005**, *57*, 2130–2146.

(41) Maiti, P. K.; Çağin, T.; Lin, S. T.; Goddard, W. A. Effect of Solvent and PH on the Structure of PAMAM Dendrimers. *Macromolecules* **2005**, *38*, 979–991.

(42) Poupot, M.; Ouali, A.; Caminade, A. The Key Role of the Scaffold on the Efficiency of Dendrimer Nanodrugs. *Nat. Commun.* **2015**, *6*, 1–11.

(43) Desai, N. Challenges in Development of Nanoparticle-Based Therapeutics.

*AAPS J.* **2012**, *14*, 282–295.

(44) De Jong, W. H.; Borm, P. J. a. Drug Delivery and Nanoparticles:Applications and Hazards. *Int. J. Nanomedicine* **2008**, *3*, 133–149.

(45) Kulhari, H.; Kulhari, D. P.; Prajapati, S. K.; Chauhan, A. S. Pharmacokinetic and Pharmacodynamic Studies of Poly(Amidoamine) Dendrimer Based Simvastatin Oral Formulations for the Treatment of Hypercholesterolemia. *Mol. Pharm.* **2013**, *10*, 2528–2533.

(46) Chauhan, A. S.; Jain, N. K.; Diwan, P. V.; Khopade, A. J. Solubility Enhancement of Indomethacin with Poly(Amidoamine) Dendrimers and Targeting to Inflammatory Regions of Arthritic Rats. *J. Drug Target.* **2004**, *12*, 575–583.

(47) Morris, C. J.; Aljayyoussi, G.; Mansour, O.; Griffiths, P.; Gumbleton, M. Endocytic Uptake, Transport and Macromolecular Interactions of Anionic PAMAM Dendrimers within Lung Tissue. *Pharm. Res.* **2017**, *34*, 2517–2531.

(48) Palmerston Mendes, L.; Pan, J.; Torchilin, V. Dendrimers as Nanocarriers for Nucleic Acid and Drug Delivery in Cancer Therapy. *Molecules* **2017**, *22*, 1401.

(49) Singh, A. K.; Sharma, A. K.; Khan, I.; Gothwal, A.; Gupta, L.; Gupta, U. *Oral Drug Delivery Potential of Dendrimers*; 2017.

(50) Yellepeddi, V. K.; Ghandehari, H. Poly(Amido Amine) Dendrimers in Oral Delivery. *Tissue Barriers* **2016**, *4*, 1–12.

(51) Choudhary, S.; Gupta, L.; Rani, S.; Dave, K.; Gupta, U. Impact of Dendrimers on Solubility of Hydrophobic Drug Molecules. *Front. Pharmacol.* **2017**, *8*, 1–23.

(52) Twyman, L. J.; Beezer, A. E.; Esfand, R.; Hardy, M. J.; Mitchell, J. C. The Synthesis of Water Soluble Dendrimers, and Their Application as Possible Drug Delivery Systems. *Tetrahedron Lett.* **1999**, *40*, 1743–1746.

(53) Liu, D.; Hu, H.; Zhang, J.; Zhao, X.; Tang, X.; Chen, D. Drug PH-Sensitive Release in Vitro and Targeting Ability of Polyamidoamine Dendrimer Complexes for Tumor Cells. *Chem. Pharm. Bull. (Tokyo).* **2011**, *59*, 63–71.

(54) Tekade, R. K.; Dutta, T.; Gajbhiye, V.; Jain, N. K. Exploring Dendrimer towards Dual Drug Delivery: PH Responsive Simultaneous Drug-Release Kinetics. *J. Microencapsul.* **2009**, *26*, 287–296.

(55) Kaminskas, L. M.; McLeod, V. M.; Ascher, D. B.; Ryan, G. M.; Jones, S.; Haynes, J. M.; Trevaskis, N. L.; Chan, L. J.; Sloan, E. K.; Finnin, B. A.; *et al.* Methotrexate-Conjugated PEGylated Dendrimers Show Differential Patterns of Deposition and Activity in Tumor-Burdened Lymph Nodes after Intravenous and Subcutaneous Administration in Rats. *Mol. Pharm.* **2015**, *12*, 432–443.

(56) Kojima, C.; Turkbey, B.; Ogawa, M.; Bernardo, M.; Kobayashi, H. Dendrimer-Based MRI Contrast Agents: The Effects of PEGylation on Relaxivity and Pharmacokinetics. *Nanomedicine* **2011**, *7*, 1001–1008.

(57) Aulenta, F.; Hayes, W.; Rannard, S. Dendrimers: A New Class of Nanoscopic Containers and Delivery Devices. *Eur. Polym. J.* **2003**, *39*, 1741–1771.

(58) Hong, S.; Leroueil, P. R.; Majoros, I. J.; Orr, B. G.; Baker, J. R.; Banaszak Holl, M. M. The Binding Avidity of a Nanoparticle-Based Multivalent Targeted Drug

Delivery Platform. *Chem. Biol.* **2007**, *14*, 107–115.

(59) Silpe, J. E.; Sumit, M.; Thomas, T. P.; Huang, B.; Dongen, M. A. Van; Holl, M. M. B.; Orr, B. G.; Choi, S. K. Avidity Modulation of Folate-Targeted Multivalent Dendrimers for Evaluating Biophysical Models of Cancer Targeting Nanoparticules. *ACS Chem Biol* **2013**, *8*, 2063–2071.

(60) Kydd, J.; Jadia, R.; Velpurisiva, P.; Gad, A.; Paliwal, S.; Rai, P. Targeting Strategies for the Combination Treatment of Cancer Using Drug Delivery Systems. *Pharmaceutics* **2017**, *9*, 1–26.

(61) Yan, G.; Li, A.; Zhang, A.; Sun, Y.; Liu, J. Polymer-Based Nanocarriers for Co-Delivery and Combination of Diverse Therapies against Cancers. *Nanomaterials* **2018**, *8*, 1–27.

(62) Yabbarov, N. G.; Posypanova, G. A.; Vorontsov, E. A.; Obydenny, S. I.; Severin, E. S. A New System for Targeted Delivery of Doxorubicin into Tumor Cells. *J. Control. Release* **2013**, *168*, 135–141.

(63) Wang, K.; Lu, J.; Li, R. The Events That Occur When Cisplatin Encounters Cells. *Coord. Chem. Rev.* **1996**, *151*, 53–88.

(64) Mezencev, R. Interactions of Cisplatin with Non-DNA Targets and Their Influence on Anticancer Activity and Drug Toxicity: The Complex World of the Platinum Complex. *Curr. Cancer Drug Targets* **2015**, *14*, 794–816.

(65) Malik, N.; Evagorou, E.; Duncan, R. Dendrimer-Platinate: A Novel Approach to Cancer Chemotherapy. *Anticancer Drugs* **1999**, *10*, 767–776.

(66) Filipe, L. C. S.; Machuqueiro, M.; Darbre, T.; Baptista, A. M. Unraveling the Conformational Determinants of Peptide Dendrimers Using Molecular Dynamics Simulations. *Macromolecules* **2013**, *46*, 9427–9436.

(67) Sadler, K.; Tam, J. P. Peptide Dendrimers: Applications and Synthesis. *Rev. Mol. Biotechnol.* **2002**, *90*, 195–229.

(68) Lin, X.; Weis, C. D.; Newkome, G. R. Polytryptophane Terminated Dendritic Macromolecules. *Tetrahedron: Asymmetry* **1991**, *2*, 957–960.

(69) Kasai, S.; Nagasawa, H.; Shimamura, M.; Uto, Y.; Hori, H. Design and Synthesis of Antiangiogenic/Heparin-Binding Arginine Dendrimer Mimicking the Surface of Endostatin. *Bioorg. Med. Chem. Lett.* **2002**, *12*, 951–954.

(70) Grandjean, C.; Rommens, C.; Gras-Masse, H.; Melnyk, O. Convergent Synthesis of D-(-)-Quinic and Shikimic Acid-Containing Dendrimers as Potential C-lectin Ligands by Sulfide Ligation of Unprotected Fragments. *J. Chem. Soc. - Perkin Trans. 1* **1999**, *0*, 2967–2975.

(71) Choi, J. S.; Joo, D. K.; Kim, C. H.; Kim, K.; Park, J. S. Synthesis of a Barbell-like Triblock Copolymer, Poly( l -Lysine) Dendrimer- *Block* -Poly(Ethylene Glycol)- *Block* -Poly( l -Lysine) Dendrimer, and Its Self-Assembly with Plasmid DNA. *J. Am. Chem. Soc.* **2000**, *122*, 474–480.

(72) Jiang, Y.; Emau, P.; Cairns, J. S.; Flanary, L.; Morton, W. R.; Mccarthy, T. O. M. D.; Tsai, C. SPL7013 Gel as a Topical Microbicide for Prevention of Vaginal Transmission of SHIV. *AIDS Res. Hum. Retroviruses* **2005**, *21*, 207–213.

(73) Rivero-Buceta, E.; Doyagüez, E. G.; Colomer, I.; Quesada, E.; María-jesús, P.

Tryptophan Dendrimers That Inhibit HIV Replication , Prevent Virus Entry and Bind to the HIV Envelope Glycoproteins Gp120 and Gp41. *Eur. J. Med. Chem.* **2015**, *106*, 34–43.

(74) Tam, J. P. Synthetic Peptide Vaccine Design : Synthesis and Properties of a High-Density Multiple Antigenic Peptide System. *Proc. Natl. Acad. Sci. U. S. A.* **1988**, *85*, 5409–5413.

(75) Malik, N.; Wiwattanapatapee, R.; Klopsch, R.; Lorenz, K.; Frey, H.; Weener, J. W.; Meijer, E. W.; Paulus, W.; Duncan, R. Dendrimers: Relationship between Structure and Biocompatibility in Vitro, and Preliminary Studies on the Biodistribution Of125I-Labelled Polyamidoamine Dendrimers in Vivo. *J. Control. Release* **2000**, *65*, 133–148.

(76) Morgan, M. T.; Nakanishi, Y.; Kroll, D. J.; Griset, A. P.; Carnahan, M. A.; Wathier, M.; Oberlies, N. H.; Manikumar, G.; Wani, M. C.; Grinstaff, M. W. Dendrimer-Encapsulated Camptothecins: Increased Solubility, Cellular Uptake, and Cellular Retention Affords Enhanced Anticancer Activity in Vitro. *Cancer Res.* **2006**, *66*, 11913–11921.

(77) Haririan, I.; Shafiee, M.; Reza, M.; Ardestani, M. S.; Ghane, Z. Z.; Namazi, H. Anionic Linear-Globular Dendrimer-Cis-Platinum (II) Conjugates Promote Cytotoxicity in Vitro against Different Cancer Cell Lines. *Int. J. Nanomedicine* **2010**, *5*, 63–75.

(78) Zeng, X.; Pan, S.; Li, J.; Wang, C.; Wen, Y. A Novel Dendrimer Based on Poly ( L -Glutamic Acid ) Derivatives as an Efficient and Biocompatible Gene Delivery Vector. *Nanotechnology* **2011**, *22*, 375102.

(79) Uehara, T.; Ishii, D.; Uemura, T.; Suzuki, H.; Kanei, T.; Takagi, K.; Takama, M.; Murakami, M.; Akizawa, H.; Arano, Y. Gamma-Glutamyl PAMAM Dendrimer as Versatile Precursor for Dendrimer-Based Targeting Devices. *Bioconjug. Chem.* **2010**, *21*, 175–181.

(80) Yuan, H.; Luo, K.; Lai, Y.; Pu, Y.; He, B.; Wang, G.; Wu, Y.; Gu, Z. A Novel Poly ( L -Glutamic Acid ) Dendrimer Based Drug Delivery System with Both PH-Sensitive and Targeting Functions. *Mol. Pharm.* **2010**, *7*, 953–962.

(81) Pu, Y.; Chang, S.; Yuan, H.; Wang, G.; He, B.; Gu, Z. The Anti-Tumor Efficiency of Poly ( L-Glutamic Acid ) Dendrimers with Polyhedral Oligomeric Silsesquioxane Cores. *Biomaterials* **2013**, *34*, 3658–3666.

(82) Tansey, W.; Ke, S.; Cao, X.; Pasuelo, M. J.; Wallace, S.; Li, C. Synthesis and Characterization of Branched Poly ( L -Glutamic Acid ) as a Biodegradable Drug Carrier. *J. Control. release* **2004**, *94*, 39–51.

(83) Golkowski, M.; Ziegler, T. The 2-(Triphenylsilyl)Ethoxycarbonyl-("Tpseoc"-) Group: A New Silicon-Based, Fluoride Cleavable Oxycarbonyl Protecting Group Highly Orthogonal to the Boc-, Fmoc- and Cbz-Groups. *Molecules* **2011**, *16*, 4695–4718.

(84) Morpurgo, M.; Bayer, E. A.; Wilchek, M. N-Hydroxysuccinimide Carbonates and Carbamates Are Useful Reactive Reagents for Coupling Ligands to Lysines on Proteins. *J. Biochem. Biophys. Methods* **1999**, *38*, 17–28.

(85) Higashi, N.; Koga, T.; Niwa, M. Enantioselective Binding and Stable Encapsulation of a -Amino Acids in a Helical Poly (L-Glutamic Acid)-Shelled

Dendrimer in Aqueous Solutions. *ChemBioChem* **2002**, *3*, 448–454.

(86) Duan, P.; Qin, L.; Zhu, X.; Liu, M. Hierarchical Self-Assembly of Amphiphilic Peptide Dendrons : Evolution of Diverse Chiral Nanostructures Through Hydrogel Formation Over a Wide PH Range. *Chem. Eur. J.* **2011**, *17*, 6389–6395.

(87) Qin, L.; Duan, P.; Xie, F.; Zhang, L.; Liu, M. A Metal Ion Triggered Shrinkable Supramolecular Hydrogel and Controlled Release by an Amphiphilic Peptide Dendron. *Chem. Commun.* **2013**, *49*, 10823–10825.

(88) Balzani, V.; Ceroni, P.; Gestermann, S.; Gorka, M.; Vo, F. Fluorescent Guests Hosted in Fuorescent Dendrimers. *Tetrahedron* **2002**, *58*, 629–637.

(89) Lin, Y.-L.; Khanafer, K.; El-Sayed, M. E. H. Quantitative Evaluation of the Effect of Poly(Amidoamine) Dendrimers on the Porosity of Epithelial Monolayers. *Nanoscale* **2010**, *2*, 755–762.

(90) Wängler, C.; Moldenhauer, G.; Saffrich, R.; Knapp, E.-M.; Beijer, B.; Schnölzer, M.; Wängler, B.; Eisenhut, M.; Haberkorn, U.; Mier, W. PAMAM Structure-Based Multifunctional Fluorescent Conjugates for Improved Fluorescent Labelling of Biomacromolecules. *Chemistry (Easton).* **2008**, *14*, 8116–8130.

(91) Yoo, H.; Juliano, R. L. Enhanced Delivery of Antisense Oligonucleotides with Fluorophore-Conjugated PAMAM Dendrimers. *Nucleic Acids Res.* **2000**, *28*, 4225–4231.

(92) Moore, E. *Molecular Modelling and Bonding*; Moore, E., Ed.; 2nd ed.; RSC Publishing, 2007.

(93) Lewars, E. G. *Computational Chemistry: Introduction to the Theory and Applications of Molecular and Quantum Mechanics*; 2011.

(94) Jensen, J. H. *Molecular Modeling Basics*; CRC Press, 2009.

(95) Leach, A. R. *Molecular Modeling: Principles and Applications*; Prentice Hall, 2001.

(96) Ballauff, M.; Likos, C. N. Dendrimers in Solution: Insight from Theory and Simulation. *Angew. Chem. Int. Ed. Engl.* **2004**, *43*, 2998–3020.

(97) Notman, R.; Anwar, J. Breaching the Skin Barrier-Insights from Molecular Simulation of Model Membranes. *Adv. Drug Deliv. Rev.* **2013**, *65*, 237–250.

(98) Fleharty, M. Molecular Simulations of Dendritic Molecules : A Study of PAMAM and Phenyl-Acetylene Dendrimers, The University of New Mexico, 2010.

(99) Becker, O. M.; MacKerell Jr, A. D.; Roux, B.; Watanabe, M. *Computational Biochemistry and Biophysics*; 2001.

(100) Mackerell, A. D. Empirical Force Fields for Biological Macromolecules: Overview and Issues. *J Comput Chem.* **2004**, *25*, 1584–1604.

(101) Wang, J.; Wolf, R. M.; Caldwell, J. W.; Kollman, P. A.; Case, D. A. Development and Testing of a General Amber Force Field. *J. Comput. Chem.* **2004**, *25*, 1157–1174.

(102) Guha, R. Force Fields in Molecular Mechanics.

(103) MacKerell Jr, A. D. Atomistic Models and Force Fields. In *Computational Biochemistry and Biophysics*; 2001; pp. 1–32.

(104) Ponder, J. W.; Case, D. A. FORCE FIELDS FOR PROTEIN SIMULATIONS I. *Adv. Protein Chem.* **2003**, *66*, 27–85.

(105) Vanommeslaeghe, K.; Hatcher, E.; Acharya, C.; Kundu, S.; Zhong, S.; Shim, J.; Darian, E. CHARMM General Force Field : A Force Field for Drug-Like Molecules Compatible with the CHARMM All-Atom Additive Biological Force Fields. *J. Comput. Chem.* **2010**, *31*, 671–690.

(106) Wiesler, U.; Mu, K.; Spiess, H. W. Solid-State NMR Investigations of Molecular Dynamics in Polyphenylene Dendrimers : Evidence of Dense-Shell Packing. *Macromolecules* **2002**, *35*, 10071–10086.

(107) Cagin, T.; Wang, G.; Martin, R.; Iii, W. A. G. Molecular Modeling of Dendrimers for Nanoscale Applications. *Nanotechnology* **2013**, *11*, 1–20.

(108) Javor, S.; Reymond, J.-L. Molecular Dynamics and Docking Studies of Single Site Esterase Peptide Dendrimers. *J. Org. Chem.* **2009**, *74*, 3665–3674.

(109) Avilla-Salas, F.; Sandoval, C.; Caballero, J.; Guinez-Molinos, S.; Santos, L. S.; Cachau, R. E.; González-Nilo, F. D. Study of Interaction Energies between the PAMAM Dendrimer and Nonsteroidal Anti-Inflammatory Drug Using a Distributed Computational Strategy and Experimental Analysis by ESI-MS. *J Phys Chem B* **2012**, *116*, 2031–2039.

(110) Filipe, L. C. S.; Machuqueiro, M.; Baptista, A. M. Unfolding the Conformational Behavior of Peptide Dendrimers: Insights from Molecular Dynamics Simulations. *J. Am. Chem. Soc.* **2011**, *133*, 5042–5052.

(111) Lee, H.; Larson, R. G. Multiscale Modeling of Dendrimers and Their Interactions with Bilayers and Polyelectrolytes. *Molecules* **2009**, *14*, 423–438.

(112) Nisato, G.; Ivkov, R.; Amis, E. J. Size Invariance of Polyelectrolyte Dendrimers. *Macromolecules* **2000**, *33*, 4172–4176.

(113) Liu, Y.; Bryantsev, V. S.; Diallo, M. S.; Goddard, W. a. PAMAM Dendrimers Undergo PH Responsive Conformational Changes without Swelling. *J. Am. Chem. Soc.* **2009**, *131*, 2798–2799.

(114) Isea, R.; Hoebeke, J.; Mayo-García, R. Designing a Peptide-Dendrimer for Use as a Synthetic Vaccine Against Plasmodium Falciparum. *Am. J. Bioinforma. Comput. Biol.* **2013**, 1–8.

(115) Jusufi, A.; Konieczny, M.; Likos, C. N. Complexation of Charged Colloids with Polyelectrolyte Stars. *Zeitschrift für Phys. Chemie* **2012**, *226*, 585–596.

(116) Pavan, G. M.; Mintzer, M. a; Simanek, E. E.; Merkel, O. M.; Kissel, T.; Danani, A. Computational Insights into the Interactions between DNA and SiRNA with “Rigid” and “Flexible” Triazine Dendrimers. *Biomacromolecules* **2010**, *11*, 721–730.

(117) Kelly, C. V; Leroueil, P. R.; Orr, B. G.; Banaszak Holl, M. M.; Andricioaei, I. Poly(Amidoamine) Dendrimers on Lipid Bilayers II: Effects of Bilayer Phase and Dendrimer Termination. *J. Phys. Chem. B* **2008**, *112*, 9346–9353.

(118) Barata, T. S.; Shaunak, S.; Teo, I.; Zloh, M.; Brocchini, S. Structural Studies of

Biologically Active Glycosylated Polyamidoamine (PAMAM) Dendrimers. *J. Mol. Model.* **2011**, *17*, 2051–2060.

(119) Maingi, V.; Jain, V.; Bharatam, P. V.; Maiti, P. K. Dendrimer Building Toolkit: Model Building and Characterization of Various Dendrimer Architectures. *J. Comput. Chem.* **2012**, *33*, 1997–2011.

(120) Quintana, A.; Raczka, E.; Piehler, L.; Lee, I.; Myc, A.; Majoros, I.; Patri, A. K.; Thomas, T.; Mulé, J.; Baker, J. R. Design and Function of a Dendrimer-Based Therapeutic Nanodevice Targeted to Tumor Cells through the Folate Receptor. *Pharm. Res.* **2002**, *19*, 1310–1316.

(121) Roberts, B. P.; Krippner, G. Y.; Scanlon, M. J.; Chalmers, D. K. Molecular Dynamics of Variegated Polyamide Dendrimers. *Macromolecules* **2009**, *42*, 2784–2794.

(122) Lee, H.; Larson, R. G. Molecular Dynamics Simulations of PAMAM Dendrimer-Induced Pore Formation in DPPC Bilayers with a Coarse-Grained Model. *J. Phys. Chem. B* **2006**, *110*, 18204–18211.

(123) Silva, L. C.; Almeida, R. F. M. De; Castro, B. M.; Fedorov, A.; Prieto, M. Ceramide-Domain Formation and Collapse in Lipid Rafts : Membrane Reorganization by an Apoptotic Lipid. *Biophys. J.* **2007**, *92*, 502–516.

(124) Murai, T. The Role of Lipid Rafts in Cancer Cell Adhesion and Migration. *Int. J. Cell Biol.* **2012**, *2012*, 1–6.

(125) Rajendran, L. Lipid Rafts and Membrane Dynamics. *J. Cell Sci.* **2005**, *118*, 1099–1102.

(126) C. Peetla, A. Stine, V. L. Biophysical Interactions with Model Lipid Membranes: Applications in Drug Discovery and Drug Delivery. *Mol Pharm.* **2009**, *6*, 1264–1276.

(127) Ponnusamy, S.; Meyers-needham, M.; Senkal, C. E.; Sahar, A.; Ogretmen, B. Sphingolipids and Cancer: Ceramide and Sphingosine-1-Phosphate in the Regulation of Cell Death and Drug Resistance. *Futur. Oncol.* **2011**, *6*, 1603–1624.

(128) Carreira, A. C.; Ventura, A. E.; Varela, A. R. P.; Silva, L. C. Tackling the Biophysical Properties of Sphingolipids to Decipher Their Biological Roles. *Biol. Chem.* **2015**, *396*, 597–609.

(129) Lahiri, S.; Futerman, A. H. The Metabolism and Function of Sphingolipids and Glycosphingolipids. *Cell. Mol. Life Sci.* **2007**, *64*, 2270–2284.

(130) Futerman, A. H.; Hannun, Y. A. The Complex Life of Simple Sphingolipids. *EMBO Rep.* **2004**, *5*, 777–782.

(131) Grassme, H.; Jekle, A.; Riehle, A.; Schwarz, H.; Berger, J.; Sandhoff, K.; Kolesnick, R.; Gulbins, E. CD95 Signaling via Ceramide-Rich Membrane Rafts. *J. Biol. Chem.* **2001**, *276*, 20589–20596.

(132) Yeagle, P. L. Non-Covalent Binding of Membrane Lipids to Membrane Proteins. *Biochim. Biophys. Acta* **2014**, *1838*, 1548–1559.

(133) Lee, A. G. How Lipids Affect the Activities of Integral Membrane Proteins. *Biochim. Biophys. Acta* **2004**, *1666*, 62–87.

(134) Clay, A. T.; Sharom, F. J. Lipid Bilayer Properties Control Membrane Partitioning, Binding, and Transport of p-Glycoprotein Substrates. *Biochemistry* **2013**, *52*, 343–354.

(135) Gulbins, E.; Petrache, I. *Sphingolipids in Disease*; Springer, 2013.

(136) Don, A.; Lim, X.; Couttas, T. Re-Configuration of Sphingolipid Metabolism by Oncogenic Transformation. *Biomolecules* **2014**, *4*, 315–353.

(137) Roh, J.-L. L.; Park, J. Y.; Kim, E. H.; Jang, H. J. Targeting Acid Ceramidase Sensitises Head and Neck Cancer to Cisplatin. *Eur. J. Cancer* **2016**, *52*, 163–172.

(138) Giussani, P.; Tringali, C.; Riboni, L.; Viani, P.; Venerando, B. Sphingolipids: Key Regulators of Apoptosis and Pivotal Players in Cancer Drug Resistance. *Int. J. Mol. Sci.* **2014**, *15*, 4356–4392.

(139) Lúcio, M.; Lima, J. L. F. C.; Reis, S. Drug-Membrane Interactions : Significance for Medicinal Chemistry. *Curr. Med. Chem.* **2010**, *17*, 1795–1809.

(140) Alves, A. C.; Ribeiro, D.; Nunes, C.; Reis, S. Biophysics in Cancer: The Relevance of Drug-Membrane Interaction Studies. *Biochim. Biophys. Acta - Biomembr.* **2016**, *1858*, 2231–2244.

(141) Dobrzyńska, I.; Szachowicz-petelska, B.; Sulkowski, S.; Figaszewski, Z. Changes in Electric Charge and Phospholipids Composition in Human Colorectal Cancer Cells. *Mol Cell Biochem* **2005**, *276*, 113–114.

(142) Szachowicz-Petelska, B.; Dobrzyńska, I.; Skrodzka, M.; Figaszewski, Z. A.; Kudelski, J. Phospholipid Composition and Electric Charge in Healthy and Cancerous Parts of Human Kidneys. *J Membr Biol* **2013**, *246*, 421–425.

(143) Liang, X.; Huang, Y. Physical State Changes of Membrane Lipids in Human Lung Adenocarcinoma A 549 Cells and Their Resistance to Cisplatin. *Int. J. Biochem. Cell Biol.* **2002**, *34*, 1248–1255.

(144) Jekunen, A. P.; Shalinsky, D. R.; Hom, D. K.; Albright, K. D.; Heath, D.; Howell, S. B. Modulation of Cisplatin Cytotoxicity by Permeabilization of the Plasma Membrane by Digitonin in Vitro. *Biochem. Pharmacol.* **1993**, *45*, 2079–2085.

(145) Todor, I. N.; Lukyanova, N. Y.; Chekhun, V. F. The Lipid Content of Cisplatin- and Doxorubicin-Resistant MCF-7 Human Breast Cancer Cells. *Exp. Oncol.* **2012**, *34*, 97–100.

(146) Zoellner, H.; Paknejad, N.; Manova, K.; Moore, M. A. S. A Novel Cell-Stiffness-Fingerprinting Analysis by Scanning Atomic Force Microscopy: Comparison of Fibroblasts and Diverse Cancer Cell Lines. *Histochem. Cell Biol.* **2015**, *144*, 533–542.

(147) Deliconstantinos, G. Physiological Aspects of Membrane Lipid Fluidity in Malignancy. *Anticancer Res.* **1987**, *7*, 1011–1021.

(148) Marverti, G.; Andrews, A. Stimulation Modulation Response of Cis-Diamminedichloroplatinum ( II ) of Passive Permeability with Genistein : In Accumulation-Defective Resistant Accumulation An Altered By. *Clin. Cancer Res.* **1996**, *2*, 991–999.

(149) Buckland, A. G.; Wilton, D. C. Anionic Phospholipids, Interfacial Binding and the

Regulation of Cell Functions. *Biochim. Biophys. Acta* **2000**, *1483*, 199–216.

(150) Schuurmans Stekhoven, FM Tesser, G.; Ramsteyn, G.; Swarts, H.; De Pont, J. Binding of Ethylenediamine to Phosphatidylserine Is Inhibitory to Na+/K(+)-ATPase. *Biochim Biophys Acta* **1992**, *1109*, 17–32.

(151) Andrews, P. A.; Mann, S. C.; Huynh, H. H.; Albright, K. D. Role of the Na + , K + -Adenosine Triphosphatase in the Accumulation of Cis-Diamminedichloroplatinum (II) in Human Ovarian Carcinoma Cells. *Cancer Res.* **1991**, *51*, 3677–3682.

(152) Gately, D. P.; Howell, S. B. Cellular Accumulation of the Anticancer Agent Cisplatin : A Review. *Br. J. Cancer* **1993**, *67*, 1171–1176.

(153) Manjarika; Ghosh, S.; Sen, T.; Shadab, M.; Banerjee, I.; Basu, S.; Ali, N. A Novel Therapeutic Strategy for Cancer Using Phosphatidylserine Targeting Stearylamine-Bearing Cationic Liposomes. *Mol. Ther. - Nucleic Acids* **2018**, *10*, 9–27.

(154) Sharma, B.; Kanwar, S. S. Phosphatidylserine: A Cancer Cell Targeting Biomarker. *Semin. Cancer Biol.* **2017**, *52*, 17–25.

(155) Speelmans, G.; Staffhorst, R. W. H. M.; Versluis, K.; Reedijk, J.; Kruijff, B. De. Cisplatin Complexes with Phosphatidylserine in Membranes. *Biochemistry* **1997**, *36*, 10545–10550.

(156) Jensen, M.; Bjerring, M.; Nielsen, N. C.; Nerdal, W. Cisplatin Interaction with Phosphatidylserine Bilayer Studied by Solid-State NMR Spectroscopy. *J Biol Inorg Chem* **2010**, *15*, 213–223.

(157) Burger, K. N. J.; Sta, R. W. H. M.; Kruij, B. De. Interaction of the Anti-Cancer Drug Cisplatin with Phosphatidylserine in Intact and Semi-Intact Cells. *Biochim. Biophys. Acta* **1999**, *1419*, 43–54.

(158) Zwaal, R. F. A.; Comfurius, P.; Bevers, E. M. Surface Exposure of Phosphatidylserine in Pathological Cells. *Cell. Mol. Life Sci* **2005**, *62*, 971–988.

(159) Peetla, C.; Bhave, R.; Vijayaraghavalu, S.; Stine, A.; Kooijman, E.; Labhasetwar, V. Drug Resistance in Breast Cancer Cells : Biophysical Characterization of and Doxorubicin Interactions with Membrane Lipids. *Mol. Pharm.* **2010**, *7*, 2334–2348.

(160) Saddoughi, S. A.; Ogretmen, B. Diverse Functions of Ceramide in Cancer Cell Death and Proliferation. *Adv. Cancer Res.* **2013**, *117*, 37–58.

(161) Hannun, Y. A.; Obeid, L. M. Principles of Bioactive Lipid Signalling: Lessons from Sphingolipids. *Nat. Rev. Mol. Cell Biol.* **2008**, *9*, 139–150.

(162) Min, J.; Van Veldhoven, P. P.; Zhang, L.; Hanigan, M. H.; Alexander, H.; Alexander, S. Sphingosine-1-Phosphate Lyase Regulates Sensitivity of Human Cells to Select Chemotherapy Drugs in a P38-Dependent Manner. *Mol. Cancer Res.* **2005**, *3*, 287–296.

(163) Sassa, T.; Suto, S.; Okayasu, Y.; Kihara, A. A Shift in Sphingolipid Composition from C24 to C16 Increases Susceptibility to Apoptosis in HeLa Cells. *Biochim. Biophys. Acta - Mol. Cell Biol. Lipids* **2012**, *1821*, 1031–1037.

(164) Roh, J.-L.; Kim, E. H.; Park, J. Y.; Kim, J. W. Inhibition of Glucosylceramide

Synthase Sensitizes Head and Neck Cancer to Cisplatin. *Mol. Cancer Ther.* **2015**, *14*, 1907–1915.

(165) Min, J.; Mesika, A.; Sivaguru, M.; Veldhoven, P. P. Van; Alexander, H.; Futerman, A. H.; Alexander, S. (Dihydro)Ceramide Synthase 1 – Regulated Sensitivity to Cisplatin Is Associated with the Activation of P38 Mitogen-Activated Protein Kinase and Is Abrogated by Sphingosine Kinase 1. *Mol Cancer Res* **2007**, *5*, 801–813.

(166) Chalfant, C. E.; Rathman, K.; Pinkerman, R. L.; Wood, R. E.; Obeid, L. M.; Ogretmen, B.; Hannun, Y. A. De Novo Ceramide Regulates the Alternative Splicing of Caspase 9 and Bcl-x in A549 Lung Adenocarcinoma Cells. Dependence on Protein Phosphatase-1. *J. Biol. Chem.* **2002**, *277*, 12587–12595.

(167) Martínez, R.; Navarro, R.; Lacort, M.; Ruiz-Sanz, J. I.; Ruiz-Larrea, M. B. Doxorubicin Induces Ceramide and Diacylglycerol Accumulation in Rat Hepatocytes through Independent Routes. *Toxicol. Lett.* **2009**, *190*, 86–90.

(168) Charles, A. G.; Han, T. Y.; Liu, Y. Y.; Hansen, N.; Giuliano, A. E.; Cabot, M. C. Taxol-Induced Ceramide Generation and Apoptosis in Human Breast Cancer Cells. *Cancer Chemother. Pharmacol.* **2001**, *47*, 444–450.

(169) Dumitru, C. A.; Sandalcioglu, I. E.; Wagner, M.; Weller, M.; Gulbins, E. Lysosomal Ceramide Mediates Gemcitabine-Induced Death of Glioma Cells. *J. Mol. Med. (Berl).* **2009**, *87*, 1123–1132.

(170) Peetla, C.; Raghavan, V.; Vijayaraghavalu, S.; Yamada, M.; Morisada, M.; Labhasetwar, V. Sustained Epigenetic Drug Delivery Depletes Cholesterol / Sphingomyelin Rafts from Resistant Breast Cancer Cells , Influencing Biophysical Characteristics of Membrane Lipids Sustained Epigenetic Drug Delivery Depletes Cholesterol-Sphingomyelin Rafts From. *Langmuir* **2015**, *31*, 11564–11573.

(171) Lacour, S.; Hammann, A.; Lagadic-gossmann, D.; Athias, A.; Sergent, O.; Laurent, G.; Gambert, P.; Solary, E. Cisplatin-Induced CD95 Redistribution into Membrane Lipid Rafts of HT29 Human Colon Cancer Cells. *Cancer Res.* **2004**, *64*, 3593–3598.

(172) Maurmann, L.; Belkacemi, L.; Adams, N. R.; Majmudar, P. M.; Moghaddas, S.; Bose, R. N. A Novel Cisplatin Mediated Apoptosis Pathway Is Associated with Acid Sphingomyelinase and FAS Proapoptotic Protein Activation in Ovarian Cancer. *Apoptosis* **2015**, *20*, 960–974.

(173) Liang, X.; Huang, Y. Alteration of Membrane Lipid Biophysical Properties and Resistance of Human Lung Adenocarcinoma A549 Cells to Cisplatin. *Sci. China Ser. C Life Sci.* **2001**, *44*, 25–32.

(174) Shen, D.; Pouliot, L. M.; Hall, M. D.; Gottesman, M. M. Cisplatin Resistance : A Cellular Self-Defense Mechanism Resulting from Multiple Epigenetic and Genetic Changes. *Pharmacol. Rev.* **2012**, *64*, 706–721.

(175) Dasari, S.; Tchounwou, P. B. Cisplatin in Cancer Therapy : Molecular Mechanisms of Action. *Eur J Pharmacol* **2014**, *0*, 364–378.

(176) Speelmans, G.; Sips, W. H. H. .; Grisel, R. J. H.; Staffhorst, R. W. H. M.; Fichtinger-Schepman, A. M. J.; Reedijk, J.; Kruijff, B. de. The Interaction of the

Anti-Cancer Drug Cisplatin with Phospholipids Is Specific for Negatively Charged Phospholipids and Takes Place at Low Chloride Ion Concentration. *Biochim. Biophys. Acta* **1996**, *1283*, 60–66.

(177) Maheswari, K. U.; Ramachandran, T.; Rajaji, D. Interaction of Cisplatin with Planar Model Membranes - Dose Dependent Change in Electrical Characteristics. *Biochim. Biophys. Acta* **2000**, *1463*, 230–240.

(178) Eljack, N. D.; Ma, H. M.; Drucker, J.; Shen, C.; Hambley, T. W.; New, E. J.; Clarke, R. J. Mechanisms of Cell Uptake and Toxicity of the Anticancer Drug Cisplatin. *Metallomics* **2014**, 2126–2133.

(179) Suwalsky, M.; Hernández, P.; Villenab, F.; Sotomayorc, C. P. The Anticancer Drug Cisplatin Interacts with the Human Erythrocyte Membrane. *Z Naturforsch C.* **2000**, *55*, 461–466.

(180) Shen, Z.-W.; Sun, Z.-P.; Zhao, N.-M. Study of the Effects of the Antitumor Drug Cis-DPP on the Phase Behavior of DPPC Liposomes and Molecular Mechanism of the Interaction. *Chinese Sci. Bull.* **1991**, *36*, 149–153.

(181) Wang, K.; Liu, D.; Zhuo, Z. C. A NMR Study of the Reaction Between Cis-Diaquodiammine-Platinum(Ⅱ) and Biomembranic Phospholipids. *Chem. J. Chinese Univ.* **1991**, *12*, 1382–1385.

(182) Hromas, R.; North, J.; Burns, C. Decreased Cisplatin Uptake by Resistant L1210 Leukemia Cells. *Cancer Lett.* **1987**, *36*, 197–201.

(183) Beretta, G. L.; Righetti, S. C.; Lombardi, L. Electron Microscopy Analysis of Early Localization of Cisplatin in Ovarian Carcinoma Cells. *Ultrastruct. Pathol.* **2002**, *26*, 331–335.

(184) Baowei, C.; Kui, W. Interaction of Cisplatin with Membranes of Rat Ehrlich Ascites Tumor Cell. *Chinese J. Cancer Res.* **1995**, *7*, 1–4.

(185) Carvalho, A. L. M. B. De; Pilling, M.; Gardner, P.; Doherty, J. Chemotherapeutic Response to Cisplatin- like Drugs in Human Breast Cancer Cells Probed by Vibrational Microspectroscopy. *Faraday Discuss.* **2016**, *187*, 273–298.

(186) Marques, M. P. .; Batista de Carvalho, A. L. M.; Garcia Sakai, V.; Hatter, L.; Batista de Carvalho, L. A. E. Intracellular Water - an Overlooked Drug Target? Cisplatin Impact in Cancer Cells Probed By. *Phys. Chem. Chem. Phys.* **2017**, *19*, 2702–2713.

(187) Lu, J.-F.; Xia, W.-S.; Wang, K.; Zhai, C.; Liu, Q.-L. A Study of Interaction of Cisplatin and Its Analogues WithPhospholipid of Erythrocyte Membrane. *J. Chinese Pharm. Sci.* **1995**, *4*, 136–143.

(188) Fang, A.; Wang, S.-H.; Zou, J.; Chen, B. The Kinetic Studies of Across-Erythrocyte Membrane Transport of 1,2-Cyclohexanediamine Platinum(Ⅱ) Complexes. *Chinese J. Inorg. Chem.* **2000**, *4*, 680–682.

(189) Peleg-shulman, T.; Gibson, D.; Cohen, R.; Abra, R. Characterization of Sterically Stabilized Cisplatin Liposomes by Nuclear Magnetic Resonance. *Biochim. Biophys. Acta* **2001**, *1510*, 278–291.

(190) Mann, S. C.; Andrews, P. A.; Howell, S. B. Short-Term Cis-Diamminedichloroplatinum ( II ) Accumulation in Sensitive and Resistant Human Ovarian Carcinoma Cells. *Cancer Chemother Pharmacol* **1990**, 236–240.

(191) Lu, J.-F.; Wang, K.; Sun, X.-Z.; Xing, F.; An, P.-D.; Yang, Z.-H.; Yin, J.-J. Effects of Cisplatin and Its Analogues on the Permability of Humam Membrane Erythrocyte Membrane. *Met. Based Drugs* **1995**, *2*, 73–80.

(192) Raghunathan, K.; Ahsan, A.; Ray, D.; Nyati, M. K. Membrane Transition Temperature Determines Cisplatin Response. *PLoS One* **2015**, 1–15.

(193) Huang, Z.; Tong, Y.; Wang, J.; Huang, Y. NMR Studies of the Relationship between the Changes of Membrane Lipids and the Cisplatin-Resistance of A549/DDP Cells. *Cancer Cell Int.* **2003**, *8*, 1–8.

(194) Liang, X.; Yin, J.; Zhou, J.; Wang, P. C.; Taylor, B.; Cardarelli, C.; Kozar, M.; Forte, R.; Aszalos, A.; Gottesman, M. M. Changes in Biophysical Parameters of Plasma Membranes Influence Cisplatin Resistance of Sensitive and Resistant Epidermal Carcinoma Cells. *Exp. Cell Res.* **2004**, *293*, 283–291.

(195) Todor, I. N.; Lukyanova, N. Y.; Chekhun, V. F. The Lipid Content of Cisplatin- and Doxorubicin-Resistant MCF-7 Human Breast Cancer Cells. *Exp. Oncol.* **2012**, *34*, 97–100.

(196) Shen, D. W.; Akiyama, S.; Schoenlein, P.; Pastan, I.; Gottesman, M. M. Characterisation of High-Level Cisplatin-Resistant Cell Lines Established from a Human Hepatoma Cell Line and Human KB Adenocarcinoma Cells: Cross-Resistance and Protein Changes. *Br. J. Cancer* **1995**, *71*, 676–683.

(197) Hong, S.; Bielinska, A. U.; Mecke, A.; Keszler, B.; Beals, J. L.; Shi, X.; Balogh, L.; Orr, B. G.; Baker, J. R.; Banaszak Holl, M. M. Interaction of Poly(Amidoamine) Dendrimers with Supported Lipid Bilayers and Cells: Hole Formation and the Relation to Transport. *Bioconjug. Chem.* **2004**, *15*, 774–782.

(198) Mecke, A.; Uppuluri, S.; Sassanella, T. M.; Lee, D.-K.; Ramamoorthy, a; Baker, J. R.; Orr, B. G.; Banaszak Holl, M. M. Direct Observation of Lipid Bilayer Disruption by Poly(Amidoamine) Dendrimers. *Chem. Phys. Lipids* **2004**, *132*, 3–14.

(199) Mecke, A.; Majoros, I. J.; Patri, A. K.; Baker, J. R.; Holl, M. M. B.; Orr, B. G. Lipid Bilayer Disruption by Polycationic Polymers: The Roles of Size and Chemical Functional Group. *Langmuir* **2005**, *21*, 10348–10354.

(200) Domański, D. M.; Klajnert, B.; Bryszewska, M. Influence of PAMAM Dendrimers on Human Red Blood Cells. *Bioelectrochemistry* **2004**, *63*, 189–191.

(201) Kitchens, K. M.; Foraker, A. B.; Kolhatkar, R. B.; Swaan, P. W.; Ghandehari, H. Endocytosis and Interaction of Poly (Amidoamine) Dendrimers with Caco-2 Cells. *Pharm. Res.* **2007**, *24*, 2138–2145.

(202) Gardikis, K.; Hatziantoniou, S.; Viras, K.; Wagner, M.; Demetzos, C. A DSC and Raman Spectroscopy Study on the Effect of PAMAM Dendrimer on DPPC Model Lipid Membranes. *Int. J. Pharm.* **2006**, *318*, 118–123.

(203) Kelly, C. V; Leroueil, P. R.; Nett, E. K.; Wereszczynski, J. M.; Baker, J. R.; Orr, B. G.; Banaszak Holl, M. M.; Andricioaei, I. Poly(Amidoamine) Dendrimers on Lipid Bilayers I: Free Energy and Conformation of Binding. *J. Phys. Chem. B* **2008**, *112*, 9337–9345.

(204) Ionov, M.; Gardikis, K.; Wróbel, D.; Hatziantoniou, S.; Mourelatou, H.; Majoral, J.-P.; Klajnert, B.; Bryszewska, M.; Demetzos, C. Interaction of Cationic Phosphorus Dendrimers (CPD) with Charged and Neutral Lipid Membranes.

*Colloids Surf. B. Biointerfaces* **2011**, *82*, 8–12.

(205) Lipid, D.; Kelly, C. V; Liroff, M. G.; Triplett, Ḱ. L. D.; Leroueil, P. R.; Mullen, Ḱ. D. G.; Wallace, J. M.; Meshinchi, Ḱ. S.; Baker, J. R.; Orr, B. G.; *et al.* Stoichiometry and Structure of Poly(Amidoamine) Dendrimer-Lipid Complexes. *ACS Nano* **2009**, *3*, 1886–1896.

(206) Ottaviani, M. F.; Daddi, R.; Brustolon, M.; Turro, N. J.; Tomalia, D. A. Structural Modifications of DMPC Vesicles upon Interaction with Poly ( Amidoamine ) Dendrimers Studied by CW-Electron Paramagnetic Resonance and Electron Spin - Echo Techniques. *Langmuir* **1999**, *62*, 1973–1980.

(207) Yan, L.-T.; Yu, X. Complexes Comprised of a Dendrimer and a Vesicle: Role of Vesicle Size and the Surface Tension of the Vesicle Membrane. *Nanoscale* **2011**, *3*, 3812–3818.

(208) Taylor, P.; Lee, H. Self-Assembly of Mixtures of a Dendrimer and Lipids : Effects of Hydrophobicity and Electrostatics. *Mol. Simul.* **2012**, *38*, 534–539.

(209) Ottaviani, M. F.; Matteini, P.; Brustolon, M.; Turro, N. J.; Jockusch, S. Characterization of Starburst Dendrimers and Vesicle Solutions and Their Interactions by CW- and Pulsed-EPR , TEM , and Dynamic Light Scattering. *J Phys Chem B* **1998**, *5647*, 6029–6039.

(210) Kitchens, K. M.; El-Sayed, M. E. H.; Ghandehari, H. Transepithelial and Endothelial Transport of Poly (Amidoamine) Dendrimers. *Adv. Drug Deliv. Rev.* **2005**, *57*, 2163–2176.

(211) El-Sayed, M. E. H.; Ghandehari, H.; Ginski, M.; Rhodes, C. a. Influence of Surface Chemistry of Poly ( Amidoamine ) Dendrimers on Caco-2 Cell Monolayers. *J. Bioact. Compat. Polym.* **2003**, *18*, 7–22.

# CHAPTER II
# MOLECULAR MODELING AND DYNAMICS OF FLUORESCENCE PG DENDRIMERS

# Chapter II – Molecular modeling and dynamics of fluorescence PG dendrimers

The introduction of this chapter is presented as a published review paper that originated from this work and is relevant for the discussions in this chapter.

# PAPER 1 (Introduction) – Molecular modeling to study dendrimers for biomedical applications

*Molecules* **2014**, *19*, 20424-20467; doi:10.3390/molecules191220424

OPEN ACCESS

*molecules*

**ISSN 1420-3049**

www.mdpi.com/journal/molecules

*Review*

## Molecular Modeling to Study Dendrimers for Biomedical Applications

**Nuno Martinho [1,2,3], Helena Florindo [1], Liana Silva [1], Steve Brocchini [2], Mire Zloh [3,*] and Teresa Barata [2,*]**

[1] Research Institute for Medicines (iMed.ULisboa), Faculty of Pharmacy, Universidade de Lisboa, Av. Professor Gama Pinto, Lisbon 1649-003, Portugal

[2] Department of Pharmaceutics, The School of Pharmacy, University of London, 29/39 Brunswick Square, London WC1N 1AX, UK

[3] Department of Pharmacy, University of Hertfordshire, College Lane, Hatfield AL10 9AB, UK

* Authors to whom correspondence should be addressed; E-Mails: m.zloh@herts.ac.uk (M.Z.); t.barata@ucl.ac.uk (T.B.); Tel.: +44-1707-284-540 (M.Z.); +44-020-7753-5805 (T.B.).

External Editor: Zofia Urbanczyk-Lipkowska

*Received: 2 October 2014; in revised form: 12 November 2014 / Accepted: 17 November 2014 / Published: 8 December 2014*

---

**Abstract:** Molecular modeling techniques provide a powerful tool to study the properties of molecules and their interactions at the molecular level. The use of computational techniques to predict interaction patterns and molecular properties can inform the design of drug delivery systems and therapeutic agents. Dendrimers are hyperbranched macromolecular structures that comprise repetitive building blocks and have defined architecture and functionality. Their unique structural features can be exploited to design novel carriers for both therapeutic and diagnostic agents. Many studies have been performed to iteratively optimise the properties of dendrimers in solution as well as their interaction with drugs, nucleic acids, proteins and lipid membranes. Key features including dendrimer size and surface have been revealed that can be modified to increase their performance as drug carriers. Computational studies have supported experimental work by providing valuable insights about dendrimer structure and possible molecular interactions at the molecular level. The progress in computational simulation techniques and models provides a basis to improve our ability to better predict and understand the biological activities and interactions of dendrimers. This review will focus on the use of molecular modeling tools for the study and design of dendrimers, with particular emphasis on the

efforts that have been made to improve the efficacy of this class of molecules in biomedical applications.

**Keywords:** dendrimers; molecular dynamics; molecular docking; biological interactions; drug encapsulation; dendrimer-drug interaction; biomaterials; hyperbranched polymer design; molecular recognition; nanomedicine

## 1. Introduction

Dendrimer is a name derived from the Greek word *dendros* (tree or branch) and *meros* (part of) [1] to describe a class of macromolecular hyperbranched polymers with a well-defined radial branching architecture. Contrary to most other polymers—*i.e.*, linear and branched polymers—dendrimers often do not rely on statistical description of average structure and molecular weight characteristics [2]. Dendrimers can be synthesised by iterative stepwise reactions of monomers. The synthetic route is often characterized as either divergent (from the centre outwards) or convergent (from the outside towards the centre) [3].

Of these two methods, divergent strategies appear to be better suited for large-scale production. The synthesis starts from the core where consecutive generations or layers, of what is often a tri-functional monomer are added. Moreover, often two functional groups of this monomer are masked (*i.e.*, protected from reaction). Each monomer then undergoes reaction at the one available functional moiety leaving the two masked moieties available for repeat reaction after deprotection. Hence each iterative reaction sequence or generation doubles the number of end groups as the dendrimer grows (Figure 1A). This method, however, has some drawbacks since incomplete or side reactions results in structural heterogeneity, especially as the number of generations increases. This is often thought to be due to increased steric interactions as the number of end groups increase. There are, however, purification challenges (see [4,5]) with this strategy, when trying to separate dendrimers that differ by small differences in monomer incorporation. To overcome these hurdles, at small scale, convergent methods of synthesis were developed [6]. In these methods the structure is built from the ends of the branches towards the dendrimer core. The monomers undergo reactions to form the arms that are then covalently linked to the core (Figure 1B). Convergent methods, though solving the purification and side reaction problems of the divergent methods do not allow the synthesis of high generation dendrimers due to steric effects that are encountered when trying to bring the dendrimer fragments (called dendrons) together to react with a reagent that forms the core [5].

Generally, dendrimer structure can be described by the: (i) core; (ii) branches; (iii) terminal groups and (iv) void space. Due to the iterative chemistry underlying dendrimer synthesis, these macromolecules are usually described by their generation number, for example generation 0 (G0), 1 (G1), 2 (G2) and so on. It is also common to describe the dendrimers as half-generation when the terminal groups of the last monomer are altered (e.g., G1.5 or G1.5-COOH) to change chemical functionality of the end groups.

**Figure 1.** Structural properties of dendrimers; (**A**) Divergent synthesis; (**B**) Convergent synthesis; (**C**) Different topological structures that can be obtained from synthesis.

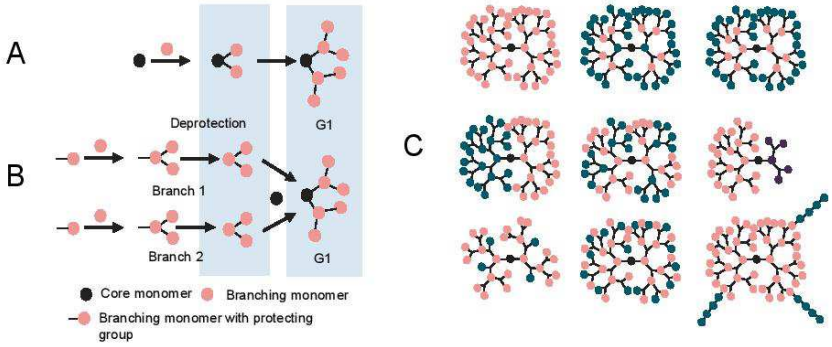


As with all molecules, dendrimer structure correlates with properties and applications. There are key intrinsic features that include the potential for the precise control of molecular weight, branching and interior chemistry. Interestingly, since dendrimers are hyperbranched they tend to have much lower viscosity properties compared to linear polymers of comparable molecular weight. For some dendrimers, the intrinsic viscosity reaches a maximum with the increase in molecular weight and then decreases with further increase of molecular weight (see [7,8]). Synthetic versatility can usually be achieved to give multivalent terminal groups and a wide variety of cores (see [9,10] and as reviewed elsewhere [1,11–13]). A vast array of dendrimer structures have been prepared since dendrimers were first described [14] and the potential number of structures of these molecules is almost limitless (Figure 1C).

In principle, dendrimers can be composed of any type of monomer and hence different physicochemical behaviours can be expected based on the kind of monomers used. A widely described example is the poly(amidoamine) (PAMAM) dendrimers. These are the most extensively studied dendrimers in the biomedical field. Other commonly studied dendrimers include poly(propylene imine) (PPI or DAB) [15], polypeptides [16], poly(ester) [17], triazines [18] and phosphorus-containing [19] dendrimers. The final end groups can be further modified with other chemical moieties including recognition moieties (e.g., folate, glutathione, RGD, immunoglobulins (Ig)), lipids and bioresponsive elements or polymers (e.g., PEG (polyethyleneglycol)) to optimise the biological properties [20–22].

Dendrimers can also act as materials, excipients or active molecules and can be applied as catalysts, in the preparation of hydrogels, biosensors (molecular recognition), tissue engineering, drug delivery systems, transfection agents and even as therapeutic agents or biomimetics. Hence the recurrent need is to develop a better understanding to aid the design and increase the performance of these macromolecules (for further reading see [23–30]).

Computer simulation techniques are a valuable tool to predict the properties of dendrimers at the molecular level. By gaining insight into the key biomedical factors that correlate with dendrimer structure one can design and optimize their properties for various applications. Nevertheless there is still a great challenge to develop novel dendrimers as any modification (e.g., terminal groups) in the dendrimer structure is likely to alter its morphological properties and hence its biological activity and

toxicity (reviewed elsewhere [31–33]). Therefore a better understanding how these macromolecules interact with the biological systems is required to develop safer therapeutics.

Although the use of molecular modeling techniques for dendrimers can be a powerful tool, there is a lack of dedicated software for these macromolecules. In particular, force field development still presents a significant challenge to model dendrimer properties. Herein we review the current strategies used to computationally model dendrimers and describe how these models have been applied to develop dendrimers for use in drug delivery and as therapeutic agents.

## 2. Molecular Modeling of Dendrimers

Several parameters impact on the architecture of dendrimers in aqueous medium. These include generation number (size), type of monomer (e.g., spacer length, density groups, void space and branching units) and surface terminal groups (charge and hydrophobicity) (see Figure 2). Valence of counter-ions in the solution and presence of other molecules, pH or ion salt concentration, also play a role. Several experimental techniques are used to probe dendrimer structure, including nuclear magnetic resonance (NMR), mass spectroscopy, infrared and Raman spectroscopy, fluorescence and small angle neutron scattering (SANS) (as reviewed in [34]). Although these techniques provide valuable information about the size and molecular constituents they have some limitations. For example, the determination of spatial configuration and geometric characterization [35] can be challenging. Since dendrimers are essentially a repetitive sequence of monomers, probing configurations is limited due to the low differentiation of the signal. Furthermore, flexible dendrimers can have a number of permissible configurations in solution with a rapid interchange between them [35–38]. Nevertheless, sometimes, specific chemical groups can be used to probe their local environment if they are different enough. As an example, amide protons in a poly(L-glutamic acid) dendrimers had separate NMR chemical shifts and those were used to probe their exposure to solvent in two different generations by changing the temperature [39], as well as to obtain information about flexibility and the association of lipidic peptide G3 dendrons [40].

Computational techniques can offer valuable insight into the study and exploration of the properties of complex systems such as dendrimers. Properties such as conformational analysis, molecular interaction (biological and drugs) and validation of experimental data can be determined by molecular modeling strategies. Ultimately, molecular modeling strategies have the potential to provide valuable data, which can help to minimize often laborious and expensive laboratory experiments. We believe that experimentation can be made much more efficient when guided by rational design.

Using only theoretical models or even experimental data, simulations can render mechanisms of biological interactions at atomic-level resolution. From the initial theoretical models to complex molecular simulations [41] there has been a great investment in understanding how these macromolecules behave (Section 3). A major benefit from molecular modeling is that allows the user to control every key parameter (e.g., ions, pH, dendrimers' structure) that might be involved in their biological activity [42–45]. This comprises simulations in conditions that would be too difficult to study experimentally. Examples of such value could be the study of dendrimers with lack of one dendron or defective parts of the branches. This opens a promising avenue for interpretation and validation of experimental data [46] as well as the design and characterization of many biological interactions.

**Figure 2.** Topological structures obtained with different core and branching monomers; From top to bottom: monomeric units, 2D structure of a G2 dendrimer, 3D structure of G2 dendrimer.

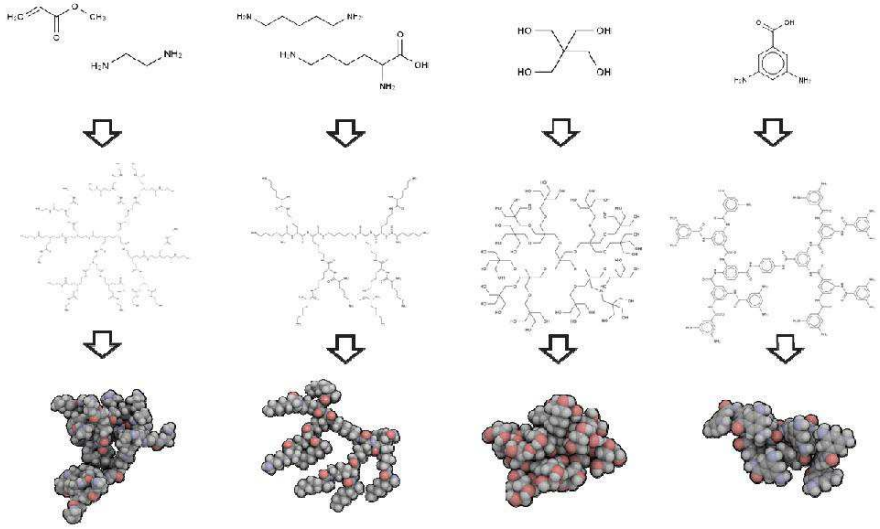

Understanding molecular interactions is fundamental to improve biological activity. Based on the energy potential function, molecular dynamic simulations of dendrimers have focused on their behaviour in aqueous solutions (Section 3.1) as well as in interacting with drugs (Section 3.4) and biomolecules including lipid membranes (Section 3.3), nucleic acids and proteins [47–53] (see Figure 3 and Section 3). Moreover, dendrimers can be seen as protein-like, a sequence of monomers in a three dimensional assembly. Therefore not only their structure can be generated in similar fashion as proteins but modeling techniques such as molecular docking studies can be applied [38,54]. Docking studies allow greater insight on interaction of dendrimers with drugs and biological target. In this regard, docking of several hydrophobic molecules (resveratrol, curcumin and genistein) was able to show that the interaction was mainly in the hydrophobic parts of the dendrimer with some hydrophilic interaction via the hydroxyl groups [55]. Docking studies also contribute to improve dendrimer design, allowing the selection of potential groups that will increase affinity [56,57]. In a recent study, PAMAM dendrimers partially glycosylated were found to dock with MD-2 protein in such a way that was able to prevent its interaction with LPS (Lipopolysaccharide) [52].

The crucial step when using molecular simulations techniques is to establish the main questions and goals for the intended study. With current access to computational power it is possible to perform more and more complex simulations, despite the yet great challenge to accurately describe complex systems, in a reasonable time scale [58]. The prediction of dendrimer properties can be studied under different ensemble configurations (temperature, pressure and volume), which can sometimes be challenging due to the high molecular density and conformations that need to be defined. Depending on the time-scale and properties to be evaluated, there is no single method available that will provide all the different

types of information desired. Dendrimers can be simulated alone or in a certain concentration in the solvent, in the presence of small drugs, proteins and nucleic acids or even in the presence of a lipid bilayer. These involve different scales of the number of atoms necessary to simulate and hence the computational cost differs. Ideally, these simulations would be carried with all atoms taken into account (all-atom simulations) to get a finer description of the interactions involved (e.g., hydrogen bonds). However, due to the resources available and the time scale necessary to study certain events (e.g., incorporation of a drug inside the dendrimer), it is sometimes required the use of simplified models. In this regard, coarse-grained simulations have been a valuable tool in particular to study the interactions with lipid bilayers [53,59–61].

**Figure 3.** Biomedical applications where MD has been important to probe biological interactions.

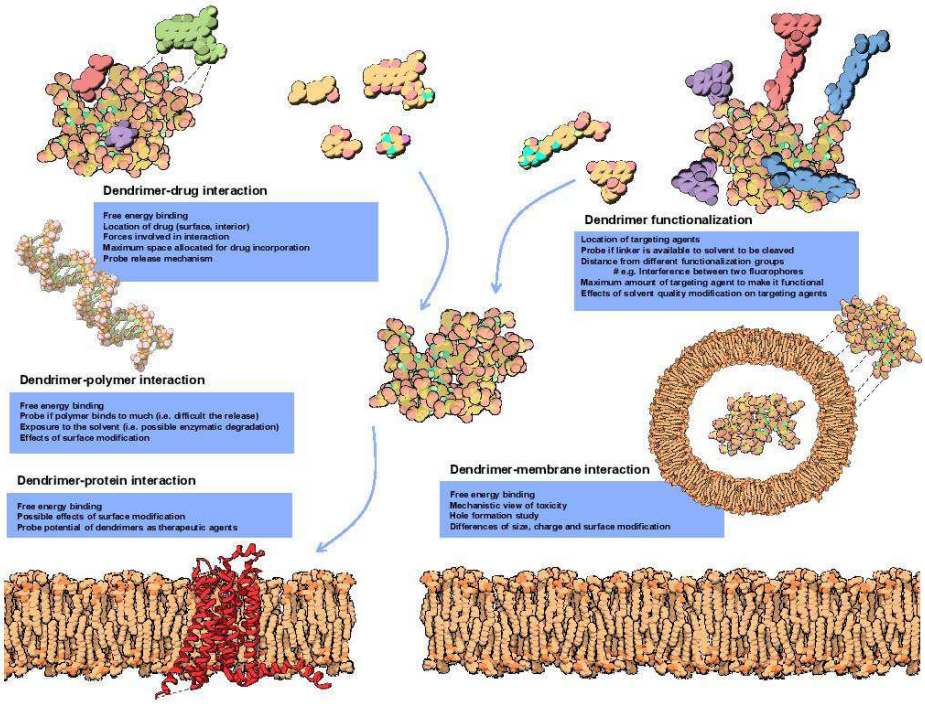


*2.1. 3D Structure Generation*

To provide a more general modeling procedure to study dendrimers there is a need for an appropriate nomenclature capable of accurately describing their topology and structure. To start with, the naming and description of the 2D structure (topology) of these molecules is still not universally accepted. IUPAC nomenclature is generally an acceptable way of naming molecules and should enable the exact description of any type of a molecule. Though this nomenclature can be applied to dendrimer-like molecules, it becomes less clear with the increase of dendrimers' size and does not

capture all the necessary structural features (e.g., distribution of residues). Nodal nomenclature based on graph theory is also able to describe dendrimers but has not been widely used [62,63].

Other two nomenclatures for dendrimeric structures are the Newkome-nomenclature [64] and cascadane [65]. Both of these nomenclatures are capable of representing the hyper-branched nature of dendrimers. Both systems make use of the repetitive units that constitute dendrimers to simplify their notation [64,65]. However, as the dendrimers increase in size, the notation becomes complex and difficult to interpret. Further simplification on dendrimer nomenclature, taking advantage of their repetitive topology and symmetry has been proposed with a dotted cap notation [63]. This notation represents dendrimers as building blocks, with a core unit, monomers and capping groups. The core is bound to the monomers which forms the dendrimer framework where the caps are attached [63]. The dotted cap notation then represents the surface of the dendrimer by means of sequential caps (Figure 4). Figure 4 shows an example of how the dotted cap notation would be used to interpret a poly(lysine) dendrimer.

**Figure 4.** Example of the dotted cap notation for a poly(aspartic acid) dendrimer; The dendrimer is represented by the core, branches and capping groups; This type of notation is useful since several capping groups with different branching points can be easily compared.

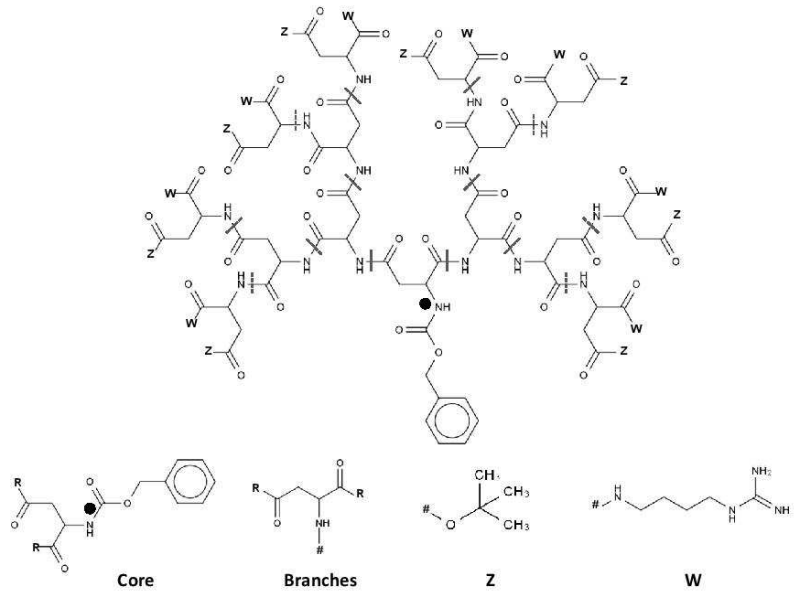


In this case the final notation would be WZ●●WZ●●●WZ●●WZ●●●WZ●●WZ●●●WZ●●WZ or $(WZ)_8$ in condensed notation [63]. Here the ● represents the topology distance between the capping groups from the primary atom represented in the core. However, as seen in the example, no information regarding the core or branching units is given, restricting the value of this nomenclature to comparison purposes between complex structures, with variable surface topology. Despite the importance of nomenclature and its contribution to the description of dendrimer topology, it does not provide information

on the 3D structure arrangement. Different strategies had to be developed to quickly and effectively generate 3D structures and describe topology. In principle, any chemical drawing software should be sufficient to construct a representation of the dendrimer. Unfortunately the manual assembly of these macromolecules is tedious and highly prone to mistakes, especially with higher generation dendrimers.

To ease this task there are four main packages dedicated to sequential assembly of molecules namely Gromacs [66] and XPLOR [67,68], Starmaker (part of Silico) [69] and Dendrimer Building Toolkit (utilizing AMBERTOOLS) [70]. The first has primarily been used for the dynamic simulation of proteins. XPLOR is used for structure generation based on NMR and X-ray experimental data while the last two packages are dedicated to dendrimer assembly. Regardless of the software package, the topology and parameters of initial monomers have to be defined for the force field that is to be used. All of the information regarding each individual atom and how they are brought together first in monomers and further along as a molecule then needs to be described. It is important to note that the topology and parameter files are specific to each force field. These files often limit the ability to inter-convert between these four molecular assembly packages.

**Figure 5.** Strategy employed for building dendrimers of different types and generations using XPLOR [71].

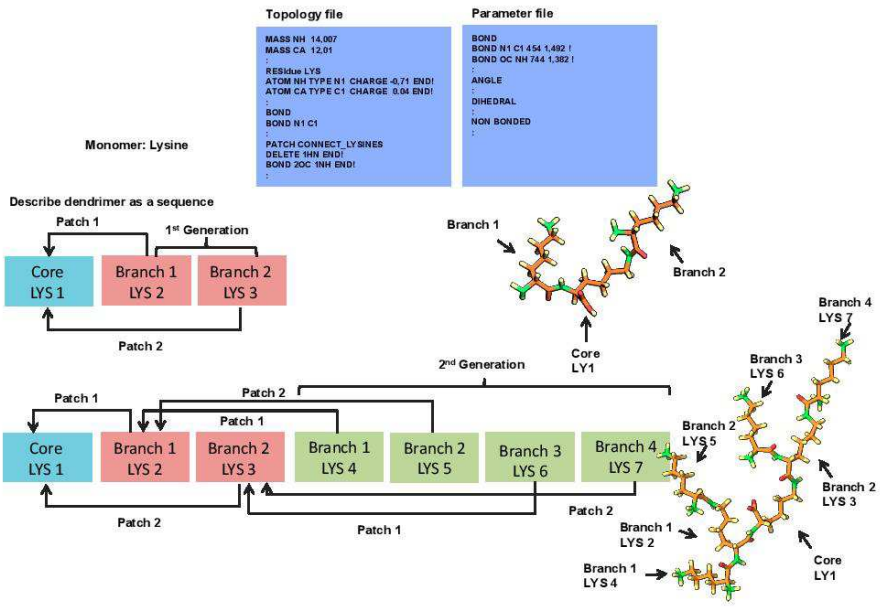


Recently, a protocol has been described that facilitates dendrimer construction by describing the dendrimer and the connection between monomers in a sequence [71] using the XPLOR-NIH program (see Figure 5). This requires that the monomers are constructed in the initial stages, which can be achieved by common programs for molecular drawing. These monomers have to be defined within both the topology and parameter files in the XPLOR format. All the information regarding each

individual atom and how they are brought together first in monomers and further along as a bigger molecule is described for use in standard molecular dynamics methods. The software then takes the sequence and its connectivity, and assembles each monomer through a simulated annealing protocol so that it can minimize clashes in the structure.

### *2.2. Simulation of Dendrimers*

After obtaining the Cartesian (x, y, z) or internal coordinates of either the whole dendrimer or the monomers, the structures are then minimized. Since dendrimers have a large number of atoms, establishing the initial conditions to perform the simulations is a laborious task due to steric overlaps and biased local minima. Moreover, appropriate stereochemistry should be checked as this can lead to erroneous initial structures that are not corrected during the simulation.

Currently there are various approaches to perform molecular simulations. They are based on quantum and molecular mechanics and molecular dynamics. However, in the case of dendrimers, molecular mechanics and dynamics are mostly used due to the high computational cost of quantum calculations. The quantum mechanics or *ab-initio* approach is limited to the lowest generation dendrimers or to defined monomers in an initial conformation. To overcome issues with the size of dendrimers, strategies similar to those used for modeling of proteins such as molecular mechanics methods with reliable parameterization, semi-empirical methods and hybrid quantum/molecular mechanics may give reliable results [50].

The force field (FF) establishes the forces that will be applied to simulate the behaviour of atoms within the dendrimer structure as a function of time [42]. The force fields represent the potential energy and define the forces applied to the system (ensemble of N atoms), which includes the sum of bonded (bond-length, bond-angle, torsion terms) and non-bonded (electrostatic and van der Waals interactions). Commonly force fields that have been used for dendrimers include the AMBER [43,72], CHARMM [73–75], GROMOS [38,76], MARTINI [77–79] CVFF [80,81], OPLS [29,82,83] and DREIDING Force [84,85]. An overview of the different force fields applied to dendrimers can be seen in Table 1. Force fields use different methods for parameterization and can refer to general atom types or to specific classes of molecules. It is, therefore, extremely important to make sure that the parameters are suitable for the system, when choosing the FF to use, as its choice can lead to different outcomes.

All-atom simulations were conducted with PAMAM dendrimers from G2 to G6 using different force fields (DREIDING, COMPASS and CVFF) and coarse-grained models using the MARTINI [79]. To compare the performance of each FF the radius of gyration (Rg) was measured and compared to experimental values of SAXS (small angles X-ray scattering) [86]. All Rg values for the different all-atom FF were lower when compared to the Rg values determined by SAXS. Similar values were obtained for COMPASS and CVFF force fields with closer values to the experimental results.

DREIDING FF was the least reliable for smaller size dendrimers (G2–G4) and similar to the others for higher generations (G5 and G6). However, the scaling of size in the case of DREIDING FF was found to be similar to previous Brownian dynamic simulations ($Rg \sim N^{1/3}$) and the fractal dimensions (space occupied) were similar to those determined experimentally. For these reasons the authors concluded that DREIDING was the best for determining the Rg for PAMAM dendrimers.

**Table 1.** Examples of software used to build and simulate different types of dendrimers; * NA: the software was not disclosed; § Free use; ‡ Commercial use.

| Dendrimer Type | Software for Dendrimer Construct | Software Used for Simulations | Force Field | Aim of the Study |
|---|---|---|---|---|
| Conformational analysis | | | | |
| PAMAM G2 to G6 [87] | Insight II | Insight II ‡ CHARMM ‡ | CVFF CHARMM | Structural features at different pH and generations |
| PAMAM G5 [88] | NA* | MPsim | DREIDING | Effect of pH to study the water dynamics on dendrimers |
| PAMAM G50% and 90% acetylated [89] | Insight II | AMBER8 ‡ | GAFF | Effect of acetylation on structural features |
| Glycosylated PAMAM G3.5 [90] | XPLOR | Desmond § | OPLS_2005 | Effect of glycosylation on structural features |
| Triazine G3 and G5 with DOTA terminals [91] | AMBER 11 | AMBER 11 ‡ | GAFF and parm99 | Location of DOTA groups complexed with Gd ions |
| PEgylated PAMAM G3 to G5 [92] | NA * | GROMACS § | MARTINI | Effect of PEGylation on the structure and interparticle interaction |
| Pegylated triazine dendrimers linked with paclitaxel [72] | Material Studio 5 | AMBER 11 ‡ | parm99 | Effect of PEGylation on availability of linkers |
| Carboxylic modified PAMAM G5 with gold, fluorescein isothiocyanate (FI) and folic acid (FA) [93] | Insight II | Insight II ‡ | CVFF | Conformation and location of FI and FA |
| PAMAM G5 with amine, carboxyl and acetamide groups linked to fluorescein and folic acid [80] | Insight II | Insight II ‡ | CVFF | Location of folic acid and its availability |
| PAMAM G5 with methotrexate [29] | CHARMM | CHARMM ‡ | CHARMM | Location of MTX when directly linked or with a spacer |
| Poly(L-lysine) and Poly(amide) G4 dendrimers [94] | Starmaker (Silico) | NAMD § | OPLS-AA | Comparison of dendrimer architectures in solution |
| Dendrimer-small molecule interactions | | | | |
| PAMAM G5 with different terminal groups + methoxyestradiol [81] | Insight II | Insight II ‡ | CVFF | Influence of terminal groups on the complexation |
| PAMAM G4 + polyphenols [55] | ChemOffice Ultra 6.0 | HyperChem Pro 7.0 ‡ | MM+ | Free binding energies |
| PAMAM G3 + nicotinic acid, nicotinate and 3-pyridiniumcarboxylate [95] | HyperChem | NAMD § | CHARMM27 | Free energy of binding and the effect of pH variation on binding |
| Peptide dendrimers + hydroxypyrene trisulfonate butyrate ester [38] | CORINA | GROMACS § | GROMOS-96 43a1 | Conformation and docking site location |



**Table 1.** *Cont.*

| Dendrimer Type | Software for Dendrimer Construct | Software Used for Simulations | Force Field | Aim of the Study |
|---|---|---|---|---|
| PAMAM G5-Folic acid + Morphine and Tramadol [96] | ICM | NAMD § | CHARMM 27; ParamChem | Different pHs; Binding mechanism elucidadtion; Location of folic acid |
| PAMAM G5 + salicylic acid, L-alanine, phenylbutazone, primidone [97] | DBT/AMBER | AMBER9 ‡ | GAFF | Effect of pH on interaction and relation with drug release |
| Poly(L-lysine) G4 dendrimer + doxorubicin [83] | ChemBioOffice | Desmond § | OPLS-AA | Complex formation |
| Dendrimer-nucleic acid interaction | | | | |
| Triazine G2dendrimers + siRNA or DNA [98] | AMBER 10 | AMBER 10 ‡ | Parm99 | Binding mechanism and energy contributions |
| PAMAM ssDNA [49] | AMBER 7 | AMBER 7 ‡ | AMBER 95 (DNA) DREIDING (dendrimer) | Binding interaction and energy contributions |
| PAMAM G3 DNA [75] | NA * | NAMD § | CHARMM 27 | Complexation mechanism |
| PAMAM G0 and G1 + siRNA [43] | Material Studio 5 | AMBER9 ‡ | Ff99 FF for RNA GAFF for dendrimers | Effects of pH on the complexation |
| PAMAM G7 + siRNA [99] | Material Studio 5 | AMBER10 ‡ | GAFF (non-standard residues); parm99 | Complex interaction |
| Dendrimer-protein interaction | | | | |
| Glycosylated PAMAM G3.5 + MD-2 protein [52] | XPLOR | Desmond § | OPLS_2005 | Docking and interaction between active and non-active forms |
| PAMAM G4 Albumin [47] | NA * | NA * | DREIDING | Contact points between dendrimer-albumin at physiological pH |
| PAMAM G0 with guanidinium terminal groups α-chymotrypsinogen A [73] | NA * | NAMD § | CHARMM 27 | Site of interaction with the protein and effect of salt types |
| Dendrimer-lipid bilayer interaction | | | | |
| Acetylated and non-acetylated PAMAM G5 and G7 + DMPC [53] | Insight II | GROMACS § | MARTINI and adapted MARTINI | Effect of size, charge and concentration on dendrimer-membrane interaction |
| PAMAM G3 and G5 with different acetylation levels + DPPC [60] | Insight II | GROMACS § | MARTINI | Effect of size, charge and lipid phase on dendrimer-membrane interaction |
| PAMAM G3 with amine, acetyl and carboxyl terminals + DMPC [74] | CHARMM | CHARMM ‡ | CHARMM27 (lipid) and CHARMM 22 (dendrimer) | Effect of terminal groups and lipid phase |

The usefulness of DREIDING FF to predict the behavior of a PAMAM G4 dendrimer in solution was recently reported. This was the first report of a FF to be able to describe that the radius of gyration was independent from the pH and instead a reorganization of the internal structure occurs [85] (see Section 3 for more details). When compared to coarse-grain (CG) simulations, the Rg was found to be similar to those obtained by DREIDING FF. These studies confirmed the usefulness of the CG model when systems with larger length scales are simulated.

Finally, the surrounding environment should be defined as precisely as possible. This includes the presence of water molecules or other solvent, ions, lipid membranes or other molecules such as drugs. Although the dendrimer can be simulated in vacuum, this is not ideal due to the effects of solvent polarization on the structure. In the absence of explicit solvents and counter-ions, special care has to be taken since such approximations may lead to non-physiological conformations of the dendrimer. PAMAM G2 dendrimers were tested with different parameters to describe the implicit use of solvent and compare to the use of explicit solvent. It was observed that modifying the non-bonded cut-off distance and dielectric constant could led to radius of gyration different from those find with explicit solvent [87].

In simulation experiments, solvent molecules can be either modelled explicitly or implicitly. Explicit solvent calculations account for each individual water molecule, which is computationally demanding. Implicit simulations translate the behaviour of water into the forces experienced by the dendrimer. Although this introduces a simplification in the simulation, studies using both explicit and implicit solvents have shown good agreement [87,100].

Another way to simulate the solvent is through an intermediate approximation of a hybrid implicit/explicit solvation model. This approach uses explicit solvent only in the layer closer to the dendrimer ([35,101] for more information). This kind of approach was used to study the structural conformation of dendrimers in different solvents being able to reduce the computational costs and having an accurate solvation in the dendrimer interface [35]. After setting the parameters, the actual simulation is allowed to run. Several methods have been used but the majority of simulations performed on dendrimers have been (i) Brownian Dynamics (BD), (ii) Monte Carlo (MC) or (iii) molecular dynamics (MD).

BD uses simplifications that allow longer time-scale calculations. In these simulations individual dendrimers are treated as Brownian particles and evaluated for friction in the surrounding solvent (the flow) (reviewed [102]). This model was used to study the polyelectrolyte complexation between a charged G3 and G4 dendrimers and a linear polymer with the opposite charge. From these simulations it was observed that the polymer chain was adsorbed to the dendrimer in a higher amount than that required to neutralize the dendrimer [103].

MD and MC models are used to study the performance of dendrimers in biological systems including structural configuration and thermodynamic calculations. In general, dendrimers are defined with a starting configuration and then by assuming ergodic conditions, the system is minimized towards a low free energy. In this process, MC simulations use iterative random atomic displacements of the initial configuration to generate a new energy value which is then accepted or rejected by association of a probability function using Boltzmann statistics. This will depend on whether the study is performed in NVT (number of particles, volume and temperature constant) or NPT (number of particles, pressure and temperature constant) ensemble. The system is therefore evaluated to find a

minimum configuration potential energy. By setting up constrains, the number of degrees of freedom can be reduced to decrease the computational demand. For this reason, allowing only important rotatable bonds to change is usually a good approximation.

Significant improvements for dendrimer analysis have been performed by MC parameterization using Continuous Configuration Boltzmann Biased direct Monte Carlo (CCBB MC) [35]. With MC, the dendritic chains torsional angles are sampled in a step-by-step process [35], conversely with CCBB MC they are sampled using a weighting function ([104]). These types of simulation, however, do not provide dynamic information. Dendrimers can be highly flexible and therefore the number of sampling conformations can be very high. In order to acquire information about dendrimer dynamics, which is very relevant in a biological environment, molecular dynamics should be used.

Molecular dynamics decrease computed simulation time (compared to QM) by introducing simplifications that assume that molecules interact as particles via classical mechanics of motion. In MD simulations, atoms interact over time by addition of impositions (temperature, pressure, time), restrictions (neglect of quantum mechanics and relativistic effects) and the integration of equations of classical mechanics (Newton mechanics, which represents the motion of the system). This allows following the trajectory of atoms with a high spatial resolution.

Before performing the actual measurement, energy minimization is advised. This can be achieved with a short simulation with restrictions to the degrees of freedom. For example, in the case of a peptide bond, these can be restrained to maintain planarity. At this point it is necessary to be careful so that the initial structure does not end in a local minimum, which can be difficult to reverse. An interesting approach to circumvent this was proposed by changing the partial charge to +0.1e of all atoms followed by an increase in temperature to 500 K. This promotes the extension of the structure to be evaluated [105]. Another approach that can guarantee that the dendrimer branches are the farthest away from each other can be the addition of NOE constraints during the assembly of monomers using XPLOR [71].

After minimisation, the equations of motion are used in iterative time-steps to simulate the dendrimer and the surrounding system of desirable conditions. Depending on the simplification of the model (e.g., all-atom simulation, coarse grained) different information can be obtained from the simulations. All-atom simulations can be performed with dendrimers but might require high computational resources. This type of simulation gives relevant information including the 3D configuration and atomistic detailed interaction events.

Coarse-grained simulations can offer greater simplification allowing the system size and the simulation time-scale to be increased while still providing significant realistic details [42]. This can be accomplished by a reduction in the number of degrees of freedom. By defining an "atom" that represents an average of $n$ atoms (generally four non-hydrogen atoms) the simulation demand is decreased. This allows a broader range of simulations to be performed, but at a cost of losing an accurate reproduction of structural details (lower resolution). For example coarse-grained simulations do not provide information about hydrogen bonding [42]. Nonetheless, this method is still used as a valuable tool since it has shown to be valid for large systems including lipids and dendrimers (Section 3.3). As a result of reducing the number of particles and the number of degrees of freedom, the time-step can be greatly increased.

After performing a simulation, there are particular features that can be obtained and analysed. These include the radial distribution function (RDFs), solvent accessible surface area (SASA) and solvent excluded volume (SEV), radius of gyration (Rg), shape descriptors, counting number of hydrogen pairs, and the mechanistic interactions as well as the thermodynamic parameters associated with them. Together these features can provide a profile of a given dendrimer.

RDFs are especially interesting to evaluate dendrimers as drug delivery systems since they provide additional insight into the distribution of all the constituents of the system. A peak in this kind of representation indicates the distance from the centre of mass (for example) at which atoms remain in a locked conformation for a long time. In contrast a diffuse distribution can either mean a homogeneous distribution throughout the area of interest or a molecular movement. RDF can therefore be used to study the distribution of atoms such as water molecules, ions and drugs within the dendrimers' interior. For example, the distribution of Mefenamic acid in PAMAM G2 and G3 revealed that both dendrimers were able to encapsulate it through internal and external interactions giving an estimate of the number of molecules involved in these interactions [106]. It also measures the terminal group distribution which can be highly valuable to study the exposure of specific groups with targeting functions [72]. In this regard, the effect of surface groups was studied on the radial distance of folic acid from the center of mass. This study showed that depending on the dendrimers' surface group, the folic acid would be more or less exposed to the surface [80]. This can also be used to define the hydrodynamic radii of the solvated dendrimer by analyzing the solvent around [38].

SASA and SEV also give valuable information about dendrimer structure. These parameters allow the determination of geometrical shape, available non-solvent accessible internal space and the accessibility of groups of interest to the solvent (solvent accessible volume). As an example, if the release of a moiety is sensitive to the solvent, this information can be used to design dendrimers that can effectively burry or expose this molecule. Such case was studied by MD for the availability of labile linkers on different PEGylated dendrimers, to see if the linker was available, and could therefore act as a prodrug [72]. SASA and SEV examine the molecular surface with a spherical solvent probe to roll around the van der Waals spheres of the macromolecule. This modeling strategy can also provide information related to the internal cavities [107] and can be used to estimate how many molecules the dendrimer will be able to carry. This is particularly useful to characterize different types of dendrimers and compare which one has the highest potential. This strategy was applied to two families of denamide and denurea dendrimers where the measurement of the internal cavity size and volume was used to estimate the theoretical number of molecules that would fit into these cavities [107].

Finally, the Rg, which is correlated to the size, allows the comparison of simulation data with the experimental data and therefore the validation of the simulation model. When simulation values are similar to the experimental ones, it is expected that the simulation forces are well described. The analysis of Rg values can provide insight into the swelling or shrinkage of the dendrimer in the different conditions [85]. In particular several simulations have been performed on PAMAM dendrimers at different pH and salt concentrations to understand its behaviour in solution (see Section 3.1). The radius of gyration can also be calculated from the gyration tensor to provide insight into the shape of the dendrimer. In this case, several ratios between the various components of the gyration radius (in the x y z direction) can inform on whether the dendrimers is shaped like a sphere or more as an ellipsoid [105].

### *2.3. Molecular Docking of Dendrimers*

Before performing the actual docking of drugs into the structure, it is possible to estimate the potential of the dendrimer architecture to accommodate the drug inside. To illustrate this, two types of dendrimers (oxy-urea and oxy-amide groups) with varying branch lengths were evaluated for their cavity sizes that were available for host interaction with anti-parasitic drugs [107]. Equilibrated dendrimers were obtained from MD and the cavity dimensions in the interior were estimated from the difference between the van der Waals volumes and the solvent-excluded volumes. Since the size of the probe can over-estimate the molecular dimensions, an adequate probe size was first determined on the slight inflexion of the SASA curve *vs.* sphere radius. Measurements of cavity size were shown to be dependent on the increase of the generation but not significantly for branches derived from aliphatic chains. Also, oxy-urea dendrimers were less porous than oxy-amide, seemingly due to intramolecular interactions [107]. The oxy-amide dendrimer was found to be more adequate for the incorporation of molecules since it was more flexible and had more adequate size of cavities.

The measure of the cavity size can also be used to quickly estimate the maximum number of drug molecules that can be incorporated into the dendrimer [54]. However, these do not account for the favorable or unfavorable interaction energies that may occur between the dendrimer and candidate drugs. For this reason docking scores can be used to calculate free energies of individual binding sites. Modified PAMAM dendrimers were blindly docked with curcumin in Autodock using a grid box with 0.3750 Å spacing. Experimentally it was found that this dendrimer could accept up to 5 molecules and thus the most favorable energies calculated by the docking score (in the range of 4.04 and $-7.28$ kJ·mol$^{-1}$) were attributed to be the binding locations [108].

The alternative approach can also be used in which the docking conformations are first prepared to give the starting point structure for MD simulations. In this case the drugs can be placed in the interior of the dendrimer instead of randomly placed near the dendrimer with the hope that the drug will find the docking site along a trajectory in a short period of time. This is difficult to accomplish for large systems given the density of monomers on the interior. However this approach can prevent the possible clashing of atoms, which can occur when attempting to manually introduce the drug into voids of the dendrimer.

Using this random approach, four different drugs (salicylic acid, L-alanine, phenylbutazone and primidone) were docked to the interior of a PAMAM G5 where the grid box was limited to the center region in AutoDock Vina [97]. The best docking score conformations for each drug were then used as initial structure for further MD simulations with AMBER with explicit water as solvent. Another interesting way that has been reported to incorporate drugs into dendrimers is to artificially create cavities inside the dendrimer. This can be accomplished by applying a force to a select number of atoms and then inserting the drugs into those cavities with common docking software such as AutoDock [109].

Dendrimers can also be treated as the ligand instead and the receptor can be a protein. The protein model of A2A receptor homodimer linked to an agonist (CGS21680 molecule) was used as reference to study if multiple copies of this agonist linked to a PAMAM G3 would be able to simultaneously occupy both subunits of the receptor. To create this kind of docked molecule, a small part of the dendrimer was first docked into the protein and then the rest of the dendrimer was attached with the

favorable docked agonists already in place (see Figure 6). This created some clashes of overlapping branches with the protein which were then manually adjusted followed by minimization and subsequent MD simulation [48].

**Figure 6.** Docking strategies applied to dendrimer studies. Depending on the size either the dendrimer or the biomolecule can be described as the docking center. The docking site can be defined either in a small space of the dendrimer or in the whole structure (middle figures). The generated docking structures can then be submitted to MD simulations or the conformations from MD simulations can be used to dock the molecules (Bottom figures).

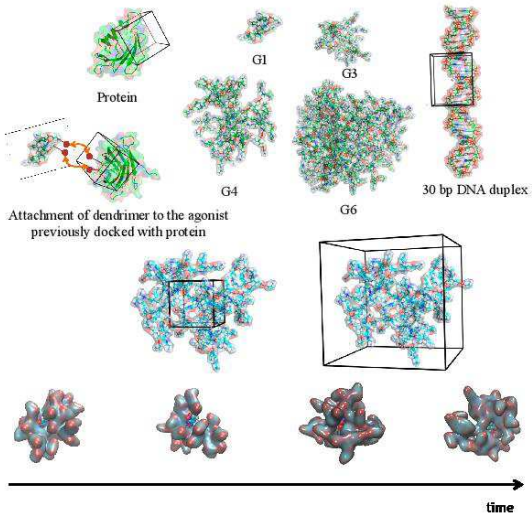


In contrast to this approach, the full size partially glycosylated and non-glycosylated (negative control) PAMAM dendrimers G3.5 were used as ligands in rigid docking against human MD-2 glycoprotein as a target. This was achieved using both Patchdock and Hex software for docking. Since both software packages were based on rigid docking, twenty different dendrimer conformations were obtained from MD. The partial glycosylation was found to promote better shape complementarity and showed a higher number of interactions compared to the non-glycosylated form. The docking interaction calculated with HEX showed that the partially glycosylated dendrimer co-operatively interacted with residues in the MD-2 entrance pocket revealing that not only shape but more importantly the electrostatic interactions were crucial for the biological activity of these dendrimers. The docked structures were then used as base for the MD simulations [52].

These examples illustrate the usefulness of docking methods to estimate free energy bindings, identify binding site locations and even to explore the potential of a dendrimer as a therapeutic agent. In fact, docking can be used as a preliminary filtering tool to optimize dendrimer structure. Specifically, it can be used to determine the potential use of a dendrimer to bind a guest molecule. Furthermore, if the *in vivo* behavior of the dendrimer is known and is interesting, docking methods can be used to evaluate a potential range of drugs that would fit the desired *in vivo* profile. Docking can be

used to check if drugs can be incorporated into the dendrimer in a similar process that is used in high throughput *in silico* screening performed for protein targets.

## 3. Modeling Dendrimers for Biomedical Applications

The design and development of dendrimers for biomedical applications is accelerated when there is an understanding of some of their properties in a physiological milieu. Molecular modeling techniques can provide the means to gain an increased understanding of important molecular structural features and dynamic behaviours that are fundamental to a biomedical application. Many methodologies have been developed and validated to model these molecules with good correlation with experimental results.

### *3.1. Impact of Solvent and Dendrimer Topology*

One of the primary applications of molecular modeling for the study of dendrimers has been to better understand conformational behaviour in solution. As expected dendrimer structure and topology appears to be dependent on the factors inherent to the dendrimer (generations, monomers length and their chemical properties) and factors related to the solvent (type of solvent, salt type and ionic strength) [107,110]. The combination of these factors affects the binding pockets to establish host-guest interactions as well as the possible moieties at the surface of dendrimers.

There has been a particular emphasis to understand the behaviour of PAMAM dendrimers in solution. This class of dendrimer is commercially available and there is vast array of experimental data that can be used for comparison. As a result, different levels of theory and force fields have been applied to PAMAM dendrimers from which Rg values have been measured and compared to experimental data (see Table 2). Although PAMAM dendrimers can have limited biomedical applications due to their inherent toxicity at higher generations (see [31]), these studies are important for methodology development and validation. Notably, PAMAM dendrimers exhibit different protonation levels at different pH value since they are composed of both primary and tertiary amines. Experimentally, it has been determined that for G4 [111] and G8 [112] the size of the dendrimers is independent of the pH with a variation of 4% and 2% respectively.

Since representing water and ions explicitly can be computationally demanding, the use of lower levels of theory is often considered and the solvent is treated implicitly. A way to overcome this problem is to perform an all-atom simulation with explicit solvent on a smaller generation and compare the radius of gyration and atom distribution with simulations performed with different implicit parameters [87]. From such studies it was found that the use of a distance-dependent dielectric constant without a cut-off distance had the best similarities to the explicit simulations for the neutral and low pH dendrimers and was reasonable for the high pH. However, when comparing the values of Rg obtained for a G4 dendrimer, this model was not able to predict the size invariability, previously was determined experimentally at different pH values [111]. One key aspect is that the implicit treatment of water may not fully represent the solvation to the necessary degree, including the diffusion of water molecules inside the dendrimer branches that contribute to swelling [110].

A good solvent system is essential for a reliable prediction of dendrimer size and conformation, and the evaluation of solvent penetration into dendrimer void spaces [113]. The water behaves differently depending on its position to a dendrimer. In the case of PAMAM dendrimers three classes of water

have been described: (i) buried water; (ii) surface water at the dendrimer-solvent interface and (iii) bulk water (*i.e.*, solvent) [113,114]. Water molecules are enthalpy favored near the dendrimer and buried water has lower entropy in relation to the bulk water. Therefore, the binding of a water molecule to a dendrimers molecule results in release of this difference of free energy [114].

Water molecules penetrate inside the dendrimer and compete for H-bonds between dendrimer residues [89,110]. However, other factors such as the force field employed may contribute to the correct prediction of experimental data (see Table 2). Recently, a study using all-atom simulations of PAMAM G4 with explicit solvent and counter-ions employing the DREIDING force field with optimized parameters (e.g., hydrogen bonding $Cl^{-}$-$^{+}HN(CH_3)_3$) [85] was able to predict the behaviour of these dendrimers at different pH. These simulations were not only able to predict the low variability of Rg (swelling of 4.9%) at different pH values, but they also elucidated the conformational mechanisms that the dendrimer underwent. It was observed by measuring the radial density distribution that the dendrimer underwent an intermolecular transition from a "dense core" at high pH to a "dense shell" at low pH. This mechanism of mass redistribution is important to interpret for example the encapsulation and the possible release mechanism of drugs from such dendrimers. This kind of behaviour of conformational change triggered by pH changes is highly desirable for intracellular delivery and is critical for the development of stimuli responsive polymers.

Different types of solvent can also promote structural modifications of the dendrimers that impact their properties. MD simulations were conducted in explicit solvent for dendrimers with a linear PEG chain in the core. Depending on the solvent (methanol *vs.* THF) the PEG was more extended or more compact in order to increase or decrease the interaction with the solvent. This resulted in burying of the dendrimer [35]. Although the solvent accessible surface area (SASA) was not measured for these dendrimers, the measurement of the radius of gyration revealed that in methanol the PEG core extends outwards and tends to wrap around the dendrimer as observed in the snapshots from the last frames of simulation. This study provided rationale for experimental results [115] where two structure forms were suggested (wrapping around *vs.* loops to the exterior). This is important as it gives a mechanistic view of the changes of the material in different solvents and can be used design dendrimers that respond differently in different solvent systems. Likewise, a PAMAM G5 dendrimer with amine terminal groups and 90% acetylation was simulated in explicit water and methanol using the General Amber Force Field (GAFF) in the presence of counter-ions. Measurements of the radius of gyration showed that the presence of acetylation promoted the dendrimer to shrink and become more compact compared to the non-acetylated dendrimer. The size of both dendrimers were similar to what was observed experimentally (2.50 nm (SEC) *vs.* 2.51 nm (MD) for G5 PAMAM and 2.35 nm (SEC) *vs.* 2.11 nm (MD) for PAMAM G5 acetylated and in methanol 2.41 (SAXS) *vs.* 2.57 nm (MD) for PAMAM dendrimer [89]).

**Table 2.** Non exhaustive list of PAMAM dendrimer simulations and their radius of gyration. For comparison the experimental values obtained by SAXS and SANS are displayed on top.

| FF | Solvent | G0 | G1 | G2 | G3 | G4 | G5 | G6 | G7 | G8 | G9 | G10 | Source |
|---|---|---|---|---|---|---|---|---|---|---|---|---|---|
| **SAXS** | Methanol | | | | 15.8 | 17.1 | 24.1 | 26.3 | 31.9 | 40.3 | 49.2 | 57.4 | [86] |
| **SAXS** | Methanol | 4.0 | 7.9 | 11.8 | 15.09 | 18.60 | 23.07 | 27.50 | 32.11 | 38.58 | - | - | [116] |
| **SANS** | D2O | - | - | - | - | 20.90–21.30 | - | - | - | - | - | - | [117] |
| **SANS** | D2O pH 4.97–10.25 | - | - | - | - | 20.64–21.58 | - | - | - | - | - | - | [111] |
| **SANS** | D2O pH 4.7–10.1 | - | - | - | - | - | - | - | - | 38.1–40.7 | - | - | [112] |
| **SANS** | Different solvents | - | - | - | - | - | 22.1 | - | - | 32.8–43.8 | - | - | [118] |
| **DREIDING** | Vacuum | 4.93 | 7.46 | 9.17 | 11.23 | 14.50 | 18.34 | 22.40 | 29.09 | 36.42 | 46.03 | 55.19 | [10] |
| **DREIDING optimized QM** | Water explicit | - | - | - | - | 21.07–22.11 | - | - | - | - | - | - | [85] |
| **DREIDING** | Water implicit | 4.97 | 7.03 | 9.77 | 13.01 | 16.36 | 21.67 | 27.62 | - | - | - | - | [35] |
| **DREIDING** | Water explicit High pH | - | 7.4 | 11.5 | 12.9 | 16.9 | 20.3 | 24.7 | 30.1 | - | - | - | [119] |
| **DREIDING** | Water explicit Low pH | - | 9.4 | 13.6 | 17.2 | 21.1 | 26.1 | 32.5 | 37.57 | - | - | - | [119] |
| **CHARMM 27** | Water explicit | - | - | - | 15.33 | 21.04 | 25.50 | 30.18 | - | - | - | - | [95] |
| **AMBER** | Water explicit pH 7.4 | - | - | - | 16.25 | 18.8–20 | 22.43–22.9 | 27.2 | - | - | - | - | [50] |
| **AMBER** | Water explicit pH 5 | - | - | - | - | 21.0 | 24.2 | 28.9 | - | - | - | - | [50] |
| **DREIDING** | Water explicit pH 4–12 | - | - | - | - | - | | - | - | 37.8–43.11 | - | - | [120] |
| **Coarse-Grained (MARTINI)** | Water explicit | - | - | - | - | 20.1 | 25.6 | - | - | - | - | - | [59] |
| **Coarse-Grained** | Water explicit | - | - | - | 13.1 | - | 23.20 | - | - | - | - | - | [60] |
| **DREIDING** | Water explicit pH 12 | - | - | - | - | 16.78 | 20.67 | 26.76 | - | - | - | - | [110] |
| **DREIDING** | Water explicit pH 7 | - | - | - | - | 17.01 | 22.19 | 27.28 | - | - | - | - | [110] |
| **DREIDING** | Water explicit pH 4 | - | - | - | - | 19.01 | 24.76 | 30.89 | - | - | - | - | [110] |
| **CVFF** | Water implicit Low pH | - | - | 16.6 | 22.8 | 29.9 | 38.0 | 46.8 | - | - | - | - | [87] |
| **CVFF** | Water implicit Neutral pH | - | - | 14.5 | 19.7 | 26.7 | 32.8 | 41.3 | - | - | - | - | [87] |
| **CVFF** | Water implicit High pH | - | - | 8.4 | 11.6 | 14.8 | 18.3 | 24.2 | - | - | - | - | [87] |
| **OPLS** | Vacuum | - | - | 11.0 | 13.7 | - | - | - | - | - | - | - | [121] |

Although water molecules led to more hydrogen bonding between the dendrimer and the solvent, the number of intra-molecular hydrogen bonds was found to be similar both in water and methanol. From the snapshots used to illustrate the H-bonds in the dendrimer, several cis-conformations of the amide bond can be observed. This could have resulted from not setting constraints to *trans* configuration while generating the dendrimer. Because of the large size of the dendrimer it would be hard to return to the most stable conformation. The results of this effect on the overall structure cannot therefore be assigned. Measurements of the relative shape anisotropy showed that both dendrimers correlated well the spherical model and that it was not affected by the solvent [89].

A combination of the effect of the solvent and the topological features of dendrimers was studied using coarse-grained MD with different dendrimers' generations (G4 to G7), different spacer lengths (1 to 6 molecules) and charges (neutral, partially and fully charged). From these structures it was observed that neutral dendrimers had a more spherical and compact structure compared to charged dendrimers, which had void spaces in their interior. It is expected that the resulting space left would be available to encapsulate drugs. It is also expected that with increasing size, higher volume will be obtained. Experimentally it was found that the increase in PAMAM generation from 4 to 6 increased the internal volume [122], which could also be observed by the measurement of solvent excluded surface of the simulated dendrimers [110]. Modifying the size of the spacer in the core was also observed to have an enormous effect on the size of the dendrimer as well as on its internal structure which changes from a compact almost sphere to a "blob-like" structure [123].

Another example where modeling can be crucial for designing dendrimers as potential drug carriers was studied in two families of an asymmetric (poly(L-lysine) and symmetric cationic G4 dendrimers at different pH. Both dendrimers were built in Starmaker and parameterized using the OPLS-AA FF. The simulations were performed with explicit solvent and counter-ions in NAMD for 10 ns. Both protonated dendrimers exhibited extended conformations (40% and 60% higher Rg for the SPAM and PLL respectively) whereas, in the neutral state a significant back-folding of terminal chains was observed [94]. The PLL dendrimer showed a higher deviation from the extended spherical form showing that the asymmetric nature of the dendrimer might facilitate other type of conformations.

Predicting this kind of "smart" or stimulus triggered behaviour has tremendous impact for applications as drug delivery systems since new dendrimers can be designed to encapsulate drugs in specified conditions (e.g., pH or other type of solvent), which then *in vivo* prevent the burst release from the entrapped drugs inside. It can also potentiate the design of a stimuli-responsive mechanism such as pH-triggered release, which can be useful for intracellular release.

### *3.2. Impact and Versatility of the End Groups*

Because of the hyperbranched topology of dendrimers, there are many end groups that can be tailored to participate in multiple specific or non-specific interactions simultaneously. A common practice for overcoming the potential toxicity of multiple charges at the surface has been the attachment of other groups such as acetyl, PEG or lipid moieties. The end groups can also be modified to carry targeting moieties, e.g., folic acid [80].

End group modifications can influence the overall dendrimer structure resulting in altered host-guest interactions or inefficient display of the targeting moieties. As an example, a common

observation for PAMAM dendrimers is the back-folding of the terminal end groups [110,120,124] as measured from the density distribution of the terminal groups from the centre of mass. If the intended goal is to protect a labile molecule from the external environment, this type of structure would be effective. However, in the case of a linked moiety (e.g., targeting molecule) this kind of structural arrangement would, most likely, be ineffective (see Figure 7). Both cases can be elucidated by molecular modeling, which help with structure design. Modeling approaches can sample the location of these groups and their available surface area to the solvent and provide some insight about the potential of modified end groups to be available to interact with a biological target.

**Figure 7.** Availability of the substituted terminal glucosamine groups on PAMAMs' surface. Reprinted from [90].

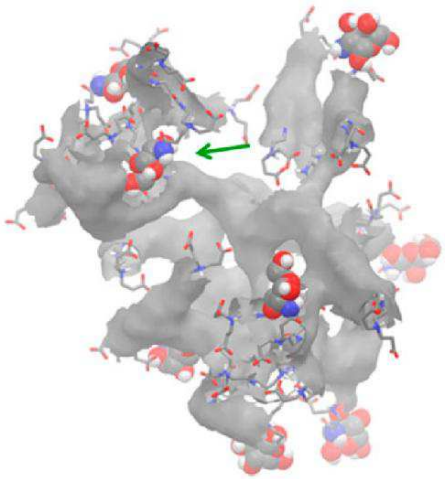

With the intent of examining the effect of terminal capping groups on the exposition of the folic acid to interact with the receptor, MD simulations were carried with CVFF in implicit solvent treated with a distance-dependent dielectric constant [80]. PAMAM G5 dendrimers with folic acid and terminal groups composed of amine, hydroxyl, carboxyl and acetamide, simulations showed that both dendrimers with charged groups internalized folic acid groups as measured by the mean distance of folic acid from the centre of mass and compared to the Rg. In contrast, in the case of the acetamide derivative the surface groups were extended away (mean distance of 26.7 Å *vs.* 19.8 of the Rg) suggesting potential capacity to interact with the receptor.It was suggested that the hydroxyl terminated dendrimer had higher exposition of the folic acid to the surface (mean distance of 27.2 Å *vs.* 21.8 of the Rg), although not as pronounced as in the case of acetamide derivative. Altogether these measurements correlated directly with the cell internalization assay of these dendrimers to KB cells [80].

Similarly, all-atom simulations with CHARMM 22 force field on PAMAM G3 terminated either with amine, hydroxyl groups or hydroxyl groups with four methotrexate (MTX) molecules were tested for the availability of MTX. The measurement of Rg for PAMAM-OH and PAMAM-MTX was smaller compared to PAMAM-NH2 (13.1, 14.0 and 18.8 Å respectively). Although more collapse

topologies (in comparison to PAMAM-NH2) were obtained, the snapshots of the equilibrated simulations indicated that the MTX remained at the surface. This result correlated positively with the binding affinity of these dendrimer found experimentally [125].

Considering a different approach, MD simulations were conducted to design dual labelled dendrimers in which the probes do not interfere with one another (by quenching or any other way) [126]. A PAMAM dendrimer was functionalized with both carboxy-fluorescein and tetramethyl-rhodamine. PEG spacers were introduced in order to study if it was able to maintain both fluorophores at a certain distance. The simulations were carried out in AMBER 11 with either no PEG or 44 monomers of PEG and an explicit water model was used with enough ions to neutralize the charges of the dendrimer together with 150 mM of NaCl to mimic experimental conditions. The analysis of the radial distribution function and fluorescein-to-rhodamine distance both suggested a suitable distance between dyes only in the presence of the PEG spacers. These results were in accordance with the quantum yield measured by optical spectroscopy [126]. Based on the validation by the modeling studies these dendrimers were used to probe the physiological/pathological microenvironments by measuring the fluorescence and making the assumption that both probes did not interfere with one another.

This type of approach has good potential to develop diagnostic tools. A practical and very beneficial application of this kind of molecular modeling design of dendrimers with several types of sensing probes would be for example in guided surgery by luminescence of tumour cells [127]. Dendrimers could be design to have sensing probes with targeting groups to selectively be internalized by cells. The probed would light up differently depending on whether or not they are tumour cells. This difference would help to identify areas surrounding the removed tumour and therefore a more efficient removal would be obtained instead of removing healthy tissue surrounding just for precaution. This approach would also be useful to identify metastasis that would not be identified by other methods [127].

Poly(ethylene glycol) (PEG) chains are also commonly used in biomedical applications to stabilize macromolecules (e.g., proteins) and increase their half-life. Coarse grained simulations with MARTINI FF in GROMACS were used to study PAMAM dendrimers of different generations linked to PEG chains of different size in order to study the conformation and aggregation of these dendrimers in solution [92]. Although CG simulations use a lower level of theory the measured Rg values was in close agreement to those measured experimentally (theoretical values: 5.98, 6.65 and 740 *vs.* 5.67, 7.06 and 7.67 nm measured experimentally) reassuring the usefulness of the predicted model. Altering the size of PEG chains in the PAMAM surface showed remarkable differences. When higher MW PEG chains were used, a completely coverage of the dendrimer was achieved and, although PEG tends to extend towards water, the spherical characteristics of dendrimers was maintained. Simulations up to 400 ns of binary systems of both lower and higher MW PEG chains revealed that no aggregation between two dendrimers was observed as measured by the distance of both centres of mass [92].

This interesting approach allows the study of the impact of surface modifications (e.g., linkage of targeting groups such as antibodies to the end of PEG chain) and the prediction of dendrimer behaviour to aggregate in solution that would make them ineffective. This kind of approach was also useful for the design of dendrimers with bio-labile linkages that were available to the solvent so that the degradation could occur [72]. Triazide dendrimers with paclitaxel were linked to different number of hexaPEG, nonaPEG or dodecaPEG and simulated in AMBER with parm99 all-atom force field. These simulations were performed to ensure that the bio-labile linker was available at the surface so

that it could be degraded and release the anti-cancer drug. Measuring the RDF it was found that increasing the PEGylation lead to a significant increase of PEG at the location of the linker [72]. Nevertheless, for all types of PEGylations, paclitaxel was found to be homogeneously distributed and close to the surface with only a small number of molecules back-folding.

Using a different approach, G5 dendrimers with different terminal groups, at different pH values, were build using Insight II software and simulated using CVFF to correlate the conformation of the dendrimer with the release and efficacy of an anticancer drug [81]. For this, seven 2-methoxyestradiol (2-ME) molecules were randomly incorporated in the simulation box. The position of 2-ME was measured from the centre of mass and was found to be farther for G5 with amine terminal groups and N-Glycine-OH. Except for G5-carboxyl all other structures exhibited open structures, which could be attributed to the release of the drug. These findings were consistent with the lower toxicity of G5-carboxyl observed in KB cells as the collapse structure would not allow the release. Although only a short simulation of 100 ps was performed the consistency with the structure obtained was achieved. However, the authors did not provide rationale for the superior encapsulation of 2-ME by ACE terminated dendrimers found experimentally, which might be caused by the aggregation of 2-ME inside the dendrimer that is neutral at this pH with the relative collapse of the structure in comparison to amine and carboxylic terminated dendrimers [81].

### *3.3. Dendrimers Interaction with Lipid Membranes*

Despite the tremendous developments of methods to study dendrimers, it is still a great challenge to develop novel dendrimers. Regardless of the applications for which dendrimers are used in nanomedicine, the fundamental knowledge of how these interact at the interface with cells is mandatory. Designing smart entities able to deliver their therapeutic payload to the site of action and circumvent physiological barriers is a promising strategy to achieve better therapeutic efficacy. Dendrimers interact with cells, and more specifically with the lipid bilayer. Cellular membranes are complex systems and a number of techniques have been used to address the interaction of dendrimers with these biomolecules including AFM, DLS, NMR, DSC and Raman Spectroscopy [128–132]. However, this is a difficult task, in part due to the extreme complexity of biological membranes. They contain a tremendous number of different lipids and proteins able to modulate the interaction between the dendrimer and the membranes.

Nevertheless, the results observed for model membranes have been well correlated with toxicity observed on cells. It is generally acknowledged that polymers with high density of cationic charge are more likely to cause disruptive effects on membranes [133]. In the case of PAMAM dendrimers these were found to have high deleterious effects both in model membranes [128,129] and cells [134,135]. In fact they were found to cause toxicity in a concentration, terminal charge density and generation dependent manner [136]. During this interaction, either the dendrimer creates holes (Figure 8), disrupts the membrane (particularly at higher generations) or is well accommodated in the lipid bilayer. Although this effect may mediate a higher cell transfection or even be useful as an anti-microbial activity [82,137] it is not suitable for drug delivery systems. Despite the experimental data that has been obtained, molecular dynamics simulations have been useful to elucidate the molecular mechanisms underlying these results [37,74,138]. In fact, molecular simulations allow testing

hypothesis that would be impossible to test experimentally. As an example, simulations of cationic G5 and G7 dendrimers of different concentrations on a DMPC membrane were tested with either short or long PME electrostatic interactions [53]. For the short PME electrostatic range no bending or insertion of the dendrimers was observed, suggesting that the long-range electrostatic interactions (*i.e.*, interactions with the inner layer of the membrane) are indeed necessary for prediction of dendrimer toxicity.

**Figure 8.** Proposed mechanism for high generation of PAMAM dendrimers; there is an initial attraction to the membrane governed by several forces (e.g., electrostatic); once the dendrimer is near the membrane the inner leaflet promotes interactions with the dendrimer. For high generation, the dendrimer is not able to flat and causes perturbation on the membrane leading to the formation of a vesicle encasing the dendrimers with subsequent formation of a pore.

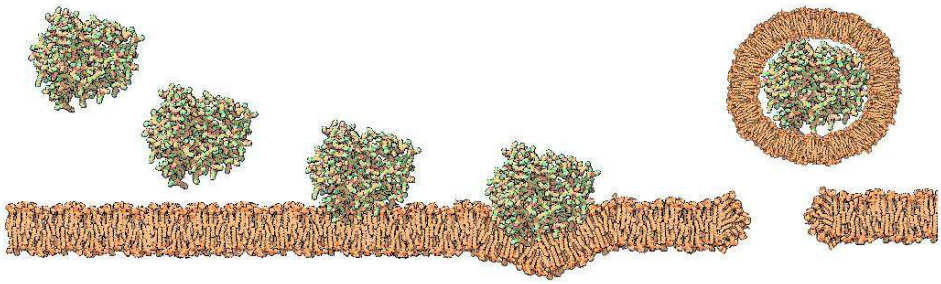

Until recently, molecular dynamics using all atoms and explicit solvent systems have been restricted by the size of the system. Although there has been great progress in computational sciences, this type of simulation is still limited in terms of timescale. Coarse-grained models loose some finer details such as hydrogen bonding but they provide an alternative to full atomistic simulations. Recent reports show they can successfully be used to generate predictive models of dendrimer-membrane interaction [53,77,139].

In general terms, from the various simulation studies, dendrimers first interact with lipid membranes through different forces and depending on their composition, size and concentration, as well as, the properties of the membrane, different phenomena can occur [60,74,77,138,140].

In order to settle the influence of size on the disruptive mechanism of PAMAM dendrimers in the lipid bilayers, coarse-grained simulations of G3, G5, G7 and G9 were performed with different tensionless membrane models (DMPC and two membranes with shorter and larger tails). The radius of gyration measurement showed that G3 and G5 dendrimers were able to flatten upon interaction of interaction with the DMPC membrane [77]. This effect has been widely observed in simulations including in all-atom simulations for differently terminated G3 dendrimers (amine, carboxyl and acetyl groups) [138] and has been attributed to the attempt of the dendrimer to maximize the interactions of all branches. However, at higher generations the flattening process upon interaction with the membrane is less evident due to the density of branches making it thermodynamically unfavorable [141]. As a result, the dendrimers keep their globular rigid conformation resulting in the pulling of the membrane instead. Upon interaction with the membrane, no pore formation was observed with for the PAMAM G5 in DMPC membrane [77]. This is clear agreement with experimental data where PAMAM G5 was

only able to expand existing defects but does not form new ones [133]. The measurements between the dendrimer and the membrane in the z-axis were evaluated as a measurement of dendrimer permeability. Dendrimers G3 and G5 showed small values consistent with the adsorption model in the membrane for all types of membranes. On the opposite side, G7 and G9 values were consistent with the embedded model in the membrane. The permeability also increased with the decrease in the tail size. From the snapshots, presented by the authors in the original publication, it is possible to observe significant distortions induced in the DMPC membrane while for shorter tail size membranes the G7 and G9 induced the formation of dendrimer-filled vesicles. On the contrary, for larger tail sizes the distortions induced by these dendrimers were smaller [77].

Dendrimer concentration has been other factor that showed to increase the toxicity of PAMAMs, experimentally. To explore this effect on membranes, a PAMAM G7 and G9 on a DMPC membrane were simulated using different simulation box sizes. These results showed that by increasing the area of the membrane, the cavities induced by the dendrimer became smaller [77]. However, this type of "dilution" may not capture the collective behavior of more than one dendrimer in the near space (higher concentration) as it only considers one dendrimer at the time. To overcome this, simulations of both positively charged and acetylated dendrimers were simulated in clusters in a DMPC bilayer [53]. An interesting observation from these simulations was that only 4 positive PAMAM G7 dendrimers were necessary to induce a strong bending on the membrane with insertion of some branches and pore formation while it required 16 positive G5 to induce some bending and insertion to the membrane. Furthermore, these effects were not observed for acetylated G5 dendrimers but these dendrimers aggregated instead [53]. Since the terminal groups can have such impact on dendrimers interaction, all atom simulations with implicit solvent were performed. A smaller system of a PAMAM G3 dendrimer with different terminal groups (amine, acetyl and carboxylic groups) on a DMPC bilayer were used to study the energy component involved in these interactions. The free energy binding was found to be 47, 36 and 26 kcal/mol for the PAMAM-carboxylic, PAMAM-amine and PAMAM-acetyl respectively and the attractive force was similar for both charged dendrimers [137]. These results are expected due to the zwitterionic character of DMPC lipid and therefore charged dendrimers interact more favorable than acetylated neutral ones.

Recently, a full all atom simulation was performed with a PAMAM G3 with amine terminal groups on a DPPC membrane and a discrepancy of 15 kcal/mol larger over the previous simulation was found. This result suggested that the explicit treatment of water significantly affects the adsorption thermodynamics as it contributed to the more entropic favorable interactions by releasing water molecules while pushing the dendrimer out of the water phase [142].

Lipid aggregation can also lead to the formation of fluid and gel phases. Experimentally AFM measurements of PAMAM G7 showed that the disrupting mechanism was abolished in gel phase of DMPC membrane [143]. Coarse-grained simulations of PAMAM G3 and G5 were simulated in DPPC bilayer at different temperature (277 K and 310 K) to simulate a more ordered phase compared to a more disordered phase. The results showed that during the simulation time no insertion of PAMAM G5 was observed at 277 K, contrary to the insertion observed at 310 K [60]. Similarly, all atom simulations of PAMAM dendrimers differently terminated (amine, carboxyl and acyl groups), with implicit solvent treatment, tested the fluidity of the membrane on dendrimers interaction. In this case, the gel phase was simulated by immobilization of the lipid tails from an equilibrated fluid phase

DMPC bilayer. In the case of the fluid membrane a depression was formed to accommodate the dendrimer while the dendrimer flatted to extend the number of interaction. On the contrary in the gel phase the dendrimers remained at the surface without inducing any kind of deformity.

Cell membranes, however, are much more complex than a simple unique lipid bilayer. For instance they are composed of different lipids and the combination of different lipids can lead to different properties. To address this issue, a recent study using coarse-grained description of three types of lipids (DPPC, DPPE and DPPS) were tested in different ratios (to mimic erythrocyte membrane) with G4 and G5 PAMAMs [59]. The asymmetry of the membrane showed to be correlated with the ability of the dendrimer to insert on it. In the case of symmetric membrane, PAMAM G4 remained at the surface of the outer leaflet. These differences were attributed to the electrostatic attraction between the inner leaflets of the membrane towards the dendrimer. Increasing the percentage of DPPS from 10% to 50% showed a decrease in the distance between centre of mass between dendrimer and the membrane, meaning that the insertion of the dendrimer was higher. Complementarily, the order parameter of the phospholipid tail (a measurement of the movements of lipid bilayers) revealed that the incorporation of the dendrimer decreased the lipid order. The PAMAM G5 created more perturbation in the lipid order that resulted in an observed the transient formation of a pore [59]. The type of lipids on the membrane can also have a specific role on the interaction with dendrimers. Using coarse-grained simulations of PAMAM G3, G4 dendrimer in bilayers composed of DPPC mixed with dipamitoylphosphatidyl-glycerol (DPPG) it was found that the dendrimers promoted the diffusion of the oppositely charged DPPG lipid from the inner to the outer leaflet [144,145]. This formation of microdomains of lipid rafts was also observed for PAMAM G7, G8 and G9 interacting with a bilayer mixture of 1,2-dimyristoyl-*sn*-*glycero*-3-phosphoglycerol (DMPG) with DMPC (3:7 ratio) lipids using coarse-grained simulations with the MARTINI force field. This simulation showed that the number of DMPG lipids near the dendrimer increased with the increase in dendrimer generation and a significant bending in the membrane was observed [146]. Overall these simulations are consistent with experimental data on dendrimers' toxicity. Dendrimers, particularly high in generation and cationic, can cause deleterious effects by disturbing the membrane. The particular interest of performing molecular dynamics is not only to explain how these effects occur but also to prevent them by designing structures that do not favour these types of interactions. In particular, it would be of high interest to develop dendrimers that could efficiently encompass a mechanism of lysosome escape without the disruptive mechanism. This would be useful for a vast range of therapeutic molecules including gene therapy.

### *3.4. Modeling Dendrimers for Drug Delivery Applications*

Combining the power of explanation of molecular mechanisms and construction of predictive models that can be applied to other kind of dendrimers gives a significant advantage to perform optimizations before even starting the synthesis of novel dendrimers. In terms of drug delivery applications, there are several factors where modeling and molecular dynamics can provide useful insights on how to optimize these carriers. Some of these factors include: (i) the stability of drug-dendrimer complexes; (ii) the strength of interactions that might compromise drug release; (iii) the availability of the targeting groups for interaction; (iv) the exposure of labile molecules to the solvent; (v) elucidate which forces govern the dendrimer-drug interaction and if those can be changed

and finally; (vi) if can the dendrimer withhold a significant number of molecules to make it attractive to drug delivery. The detailed analysis of these factors is also crucial to understand how these dendrimers will perform *in vivo*.

In the field of drug delivery, dendrimers could be designed to a vast range of drug molecules in order to solve problems such as solubility, drug release and targeting. Essentially, drugs can be incorporated into the dendrimer either covalently (e.g., prodrug) or non-covalently (surface or internal cavities). As observed in the classical structural behaviour of PAMAM dendrimers, the hydrophobicity of the interior (see Figure 9) can be modulated through pH and salt variations. These variations can be used to ascertain the conditions for encapsulation that will be different from the medium in which they are going to be released.

**Figure 9.** PAMAM dendrimers' hydrophilic surface (blue) and hydrophobic core (orange). Adapted from [45].

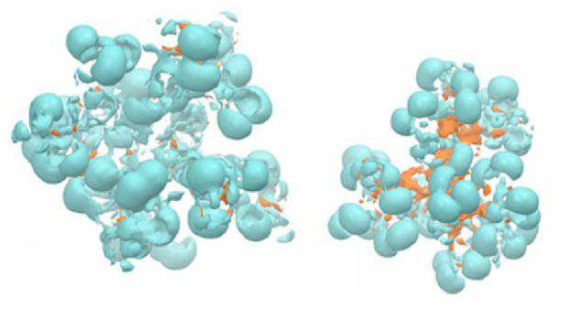

A classic example is the delivery of nonsteroidal anti-inflammatory drugs (NSAIDs). The particular interest in these drugs lies in their potential for encapsulation and controlled release. This would be technological beneficial as a prolonged analgesic effect could be achieved without increasing side effects such as ulceration. In particular, ibuprofen is a common model drug to test new drug delivery systems due to its small size and being a class II drug (high permeability but low solubility) and hence the availability is limited by their solvation rate. Experimentally, it was shown that PAMAM dendrimers were able to solubilize ibuprofen [147,148], it was shown that this effect was dependent on the pH and generation of the PAMAM dendrimers.

To probe how the interaction occurs, a PAMAM G3 was simulated at different pH with ibuprofen [54]. Using all-atom MD simulations, with the AMBER FF, the drug molecules were placed in the proximity of the dendrimer. The analysis of atom distributions showed that ibuprofen could penetrate more to the dendrimer core than water. Unlike at basic and neutral pH, at acidic pH the ibuprofen is located homogenously throughout the dendrimers' surface but cluster formation was observed. The measurement of the average distance between the ibuprofen and the PAMAM center of mass as a function of time also revealed a constant value at neutral and basic pH values, meaning the complexes formed are stable. At neutral pH conditions, hydrogen bonds are established between the dendrimer and the ibuprofen and this complex is mainly formed at the surface. On the contrary, at acidic pH, the ibuprofen diffuses away, this is seen by the increased values of mean distance [54]. This

was consistent with the experimental results where the solubility of PAMAM dendrimers decreases under acidic conditions [147].

In another study, the calculation of dendrimer-ibuprofen complexes with incorporation of different amounts of drugs was evaluated using MM2 calculations. From these calculations it was observed that incorporating more than 16 ibuprofen molecules inside the dendrimer was energetically unfavorable [107], which is a similar value to the one found experimentally (14 ibuprofen molecules) for a PAMAM G3 [148].

Similarly, PPI G5 were simulated with Bengal rose with the DREIDING force field and these simulations revealed that depending on the drug:dendrimer ratio, the number of molecules found in the interior would vary as measured by distance from the center of mass of each molecule, in clear agreement with experimental data [84].

This kind of study can also be applied to other drugs of the same class, to study, which one showed better binding affinity to the dendrimer. Thus a predictive model can be built of the drug more suitable for the carrier. In this case the design is based on the selection of the drug rather than the optimization of the carrier itself. In order to have a more accurate calculation of the binding energies of four different NSAIDs drugs, semi-empirical methods (PM6-DH+) were used [149]. However, this approach is limited by the size of the dendrimer to be included in the calculations. To overcome this limitation, several branches of the dendrimer were taken separately from structures originated from MD simulations in NAMD on PAMAM G4 with CHARMM FF. The conformational pairs between branches and drug were then generated by a Monte Carlo method and the energetics calculated using semi-empirical methods (PM6-DH+). The energy values obtained were directly correlated with the affinity degree found experimentally (naproxen > ketoprofen > ibuprofen > diflunisal) [149].

In a similar study, but applied to anti-cancer therapy, MD simulations were carried out to assess the molecular interactions between a series of 24 cytotoxic drugs and a G4 PAMAM dendrimer. The results indicate that the majority of drugs show high thermodynamic stability. The complete set of drugs showed to effectively interact with the dendrimer in an exothermic fashion, with bleomycin, orlistat and porfimer being the ones that most strongly interact with the PAMAM dendrimer [150].

These are encouraging results has one can predict from a pool of interesting drugs which ones will fit best into the features of a given dendrimer. This kind of approach has been tested on PAMAM G5 dendrimers with different drugs (salicylic acid, L-alanine, phenylbytazone and primidone) [98]. These drugs were docked to the dendrimer via AutoDock Vina and then the best scoring conformations were selected for MD simulations using AMBER with explicit water solvent. Umbrella samplings were performed between the center of mass of the dendrimer and the drugs. When plotting the potential mean force (PMF) among all drugs studied L-alanine showed lower free energy (better ability to be released) followed by salicylic acid, primidone and phenylbutazone. However, taking into account the experimental data, although L-alanine and salicylic acid had a lower free energy (semi-empirical calculations) they were difficult to encapsulate in the dendrimer due to absence of nonpolar groups. This is due to less van der Waals contributions and the hydrogen bonding that did not contribute significantly to the free energy barrier. The PMF was also found to be less when the drugs are bound to the non-protonated dendrimer. The authors suggest that drugs should be encapsulated at higher pH and once in physiological pH they will be more tightly bond making the release controlled [97].

Proposed alteration of pH to modulate the interaction, encapsulation and release of drugs was observed from MD/MM simulations of PAMAM G5 and folic acid-terminated PAMAM G5 with tramadol and morphine [96] as well as PPI dendrimers G5 with Famotidine and Indomethacin [44] where the affinity of these drugs decreased with the decrease in pH. Similarly, PAMAM G4 equilibrated using MM+ FF were docked with resveratrol, genistein and curcumin [55]. The MD simulations revealed that the free energy binding followed genistein > curcumin > resveratrol which was in different binding constants determined experimentally which followed the order of curcumin > genistein > resveratrol. The difference between the calculation of energy of binding and the binding constants found experimentally was attributed to the difficulty of the drug to access the interior of the dendrimer.

A way of accounting for this kind of behavior could be by using adaptive biasing force methods. This kind of approach was recently used to study the association of nicotinic acid with a PAMAM G3 at different pH (pH 3 and pH 6) [95]. Using a biasing force method the drugs were constrained in the z-axis to make sure that the drug moved along the selected sample direction but were allowed to move freely through the x and y axis. The energy profiles showed that the nicotinic acid interacted better with G3 at higher pH with an energy difference of −1 to −2.5 kcal in comparison to 3-pyridiniumcarboxylate and that this interaction was more favorable at the surface than in the interior [95]. Since nicotinic acid is also a poorly soluble drug and needs to be delivered to the interior of the cells, determining at which conditions it can be better encapsulated in the dendrimer and its location served as a guide future optimization of the carrier.

A different kind of approach was used to study the stability of complex formation between poly(L-lysine) G6 dendrimers with the anticancer drug doxorubicin to evaluate the potential as a drug delivery system. The drug-dendrimer complex was found to be favorable at 300 K but dissociated upon heating up to 1000 K. However, once the system was cooled again it reassembles again showing the favorable interaction between these two molecules and hence favorable for controlled release [83].

One of the most promising areas for the use of dendrimers as drug delivery systems is gene delivery. Dendrimers have long been recognized as potential carriers to nucleic acids due to their highly expressed positive charge, which allows them to form polyelectrolyte complexes (also known as dendriplexes). Both experimental and all-atom MD simulations have shown that nucleic acids have the ability to wrap around the dendrimer in a process that depends both on size and charge ratio. In this particular application MD simulations can probe with substantial detail whether a dendrimer will be a suitable carrier. The mechanistic details that can be probed, including how strongly the nucleic acid binds to the dendrimer, which will impact on the release. If the binding is too strong, the release could be jeopardized, however, if the interaction is not as strong, the nucleic acid will be available to be cleaved in solution.

MD simulations were carried out in AMBER7 with AMBER95 FF for ssDNA and the DREIDING FF for the dendrimer, with different levels of protonation. The various dendrimers were docked to the major groove of an ssDNA. Further simulations were carried out in explicit water and counter ions were added to neutralize the system. The simulations showed that for G2 and G3 the charge ratio was not enough to complete wrap the ssDNA onto the dendrimers, as evidenced by the radius of gyration of the complexes. On the other hand the G4 dendrimer was large enough to neutralize the charges of the ssDNA and promoted the collapse of the latter into the surface. This led to the formation of a compact complex with significant penetration inside as measured by the radial density distribution.

At neutral pH a higher degree of ssDNA penetration inside the dendrimer was observed. However, this may not constitute an advantageous phenomenon as it will prevent the release from the dendrimer and hence it is not useful as a gene delivery [49]. Similarly, protonated G3 and G4 PAMAM dendrimers with linked ssDNA were simulated using AMBER03 FF for ssDNA, GAFF for the linker and DREIDING FF for the dendrimer. Again, the ssDNA tended to loose helicity and wrap around the dendrimer with higher wrapping and DNA penetration in the case of G4 dendrimer [151].

Even when dsDNA (B-form) was simulated with G3 to G5 PAMAM dendrimers, a strong deformation of the DNA was observed [152]. Carrying MD simulations with AMBER03 FF in explicit water and added ions, the G5 expanded to try to cover the whole DNA while the DNA wrapped around the dendrimer as measured by the radius of gyration [152]. At the initial phase of the complex formation the dendrimer expands with increasing the contact between the dendrimer and DNA. Water molecules then suffer repulsion from the DNA backbone and DNA wraps on the dendrimer, forming a more stable complex. However, this phenomenon seems to be limited to the number of generation as it was shown by MD of PAMAM G7 dendrimers with siRNA, where the dendrimer behaved as a hard sphere with no variation in Rg after binding [99]. Higher charge ratio implies higher binding interaction [152]. Although the G3 is not enough to neutralize the DNA and a weak interaction occurs, this might be a better system as the release should be easier than in the case of a G4 or G5 [152].

In this regard, flexible triazine dendrimers of different generations and PEI polymer were simulated with DsiRNA in AMBER with parm99 FF to predict their efficacy [153]. Thermodynamically, dendrimers were found to be more stable than PEI with G2 being the most stable complex followed by G4 and G3. Furthermore, the charge neutralization of 1:1 complex predicted the stability of these complexes in solution as it was hypothesized that PEI only interacted partially with the DsiRNA. The authors suggested that the non-complexed part with both positive and negative charges promoted inter-particle interactions leading to aggregation. Finally *in vivo* studies showed that the G4 was more stable in comparison to the G2 (less excretion) but were significantly more uptake by the reticulo-endothelial system [153].

The sequence of the DNA also takes a role in the dendrimer-nucleic acid complex formation and thus the importance of using computational methods to predict this interaction. Using MD simulations with different strand composition it was found that the binding constant follows as polyG > polyC > polyA > polyT sequence as observed by the free energy calculations [49]. The flexibility or rigidity of dendrimers is another crucial point to form the polyelectrolyte complexes which was described to be due to the balance between the enthalpy and entropy of binding [98].

Dendrimers are also potential systems to be used as contrast agents since they can modulate the pharmacokinetic profiles and organ selection. Gadolinium-based triazine dendrimers with DOTA chelate groups was studied as contrast agent using MD simulations with AMBER FF. In this model, the G3 and G5 dendrimers had 24 and 96 chelates respectively [91]. The analysis of the radial distribution functions showed that the chelates were exposed to the solvent and available for chelation of Gd ions. In fact the high peaks in the RDF suggest that there is a reduced backfolding throughout the simulation time.

The multivalence of dendrimers is one of its upmost regarded advantages in which they can be design to perform multiple actions within the same structure. This is particularly useful in the application of imaging agents. In this regard, a PAMAM G5 linked to gold nanoparticles with randomly distributed

targeting ligand (folic acid) and imaging agent (fluorescein isothiocyanate) were simulated with CVFF [93]. The MD simulation was particularly useful in identifying that the fluorescent probe was at a significant distance from the gold metal and therefore a low quenching was expected but also that the folic acid was extended outwards making it available to interact. This system is interesting as it is an "all-in-one package". This dendrimer system could make selective targeting of the cancer, highlight where it is present and then laser hyperthermia could be induced on the gold nanoparticle.

### *3.5. Modeling Dendrimers as Therapeutic Agents*

Dendrimers due to their inherent similarity to biological macromolecules such as proteins can interact with other biomolecules and illicit biological responses [48,52]. Their high number of terminal groups promotes multivalent non-specific contacts that are beneficial for biological interactions. Furthermore, specific modifications can be introduced at the surface to promote binding. Using simulations on PAMAM G0 modified with guanidinium it was found that these modifications promoted simultaneously and cooperatively interactions with the protein surface of α-chymotrypsinogen A by hydrogen and cation-π interactions with the aminoacids [73]. This cooperative interaction was found to promote higher binding compared to a single unit.

Dendrimers can be designed and modelled to specifically interact with the desired target. PAMAM G3.5 dendrimers were modelled to predict the availability of glucosamine moieties at the surface and their influence on biological activity. Experimentally, PAMAM G3.5 (with carboxylic groups) with an average of 8 surface glucosamine molecules were found to inhibit the TLR5-MD-2-LPS complex formation [154]. Frontier molecular orbital theory (FMOT) was applied on smaller dendrimer dimensions to predict the reactivity (gap difference between HOMO and LUMO) of the dendrimer towards subsequent addition of glucosamine monomers [90]. These studies found that solely based on electronic properties of the dendrimer a maximum of 12 molecules cold be coupled to the structure. However, upon addition of more glucosamine steric effects of hindering the terminal groups started to occur as evidenced by MD simulations. Together these effects accounted to an average of 4–8 as the most favorable energetically [90].

These dendrimers were subsequently docked to MD-2 protein followed by a MD simulation. These results showed that the dendrimer could indeed act as an antagonist of the MD-2 receptor [52] (see Figure 10). Analysis of the trajectory showed that the PAMAM-glucosamine's groups could cooperatively bind to the hydrophilic residues at the entrance of the hydrophobic pocket [52]. This action was enough to block the entrance of LPS into it. This effect was very important as it was shown to prevent the formation of the TLR4-MD-MD-2-LPS from initiating the cytokine cascade. The predictive knowledge of this dendrimer-glucosamine derivative to the receptor was used as the basis for further design of the dendrimer architecture.

Active and non-active PETIM [155] dendrimers and Triazine-PAMAM hybrids [45] were modelled on the same basic principles. The modified PETIM dendrimers showed similar flexibility and the net surface charge was found to resemble that of the PAMAM derivative. This dendrimer was particularly interesting as it was a lower molecular weight compared to the original PAMAM dendrimer (easier synthesis and purification as well). The results from the non-active forms of this dendrimer revealed that the surface hydrophobicity did not contributed to the interaction with the MD-2 receptor. Similarly

in the case of the Triazine-PAMAM hybrids [45] it was found that the best architecture to promote antagonist effect was that of partially glycosylated G2 Triazine G1.5 PAMAM hybrid dendrimers. This dendrimer resembled the active PAMAM G3.5 glucosamine in key points such as polar surface area and globular shape (contrary to pure Triazine). These features facilitate the electrostatic interactions with the target and may justify its activity.

**Figure 10.** Docking between Dendrimer glucosamine and MD-2 protein and inhibition of TLR4-MD-2-LPS complex formation; adapted from [52].

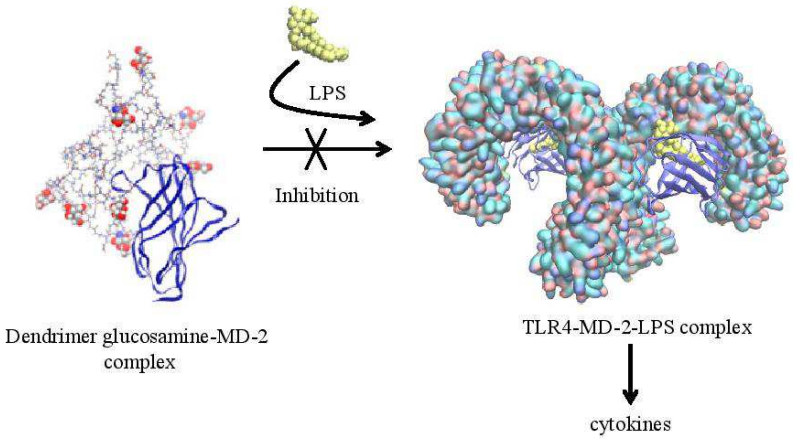


Another interesting application of dendrimers in the biomedical field is in the area of vaccination. Here the core base dendrimer can be used to attachment of multiple groups depending on the type of immunization required. Using a database of *Plasmodium falciparum* epitopes, several epitopes were selected and attached to the dendrimer [156]. These systems were simulated using CHARMM FF and explicit water, and the energetics of the different structures was calculated. Although not many details are given, this is an interesting application of MD simulations as one could estimate the availability of the epitopes to the solvent. It can also be used to see the effect of adding other groups such as recognition groups or even fluorophores to track the intracellular path of these dendrimers.

Even though dendrimers can be designed to specifically interact with certain proteins, while circulating in the plasma they will contact other proteins that can cause significant alteration of the pharmacokinetic profile. A common test is to study the binding affinity to albumin, the most abundant human plasma protein. In particular, dendrimers with their high number of terminal groups can promote unspecific binding and therefore bind to plasma proteins. Molecular modeling offers a potential test to evaluate and modulate these interactions. Using the previously described DREIDING FF that predicted the behavior of PAMAM at different pH, PAMAM dendrimers were simulated with human serum albumin to estimate the contacts between the two. It was suggested that the size and surface of terminal groups were crucial for this interactions. The interaction between dendrimer-HSA was due to electrostatic interactions between the charged groups as well as hydrogen and hydrophobic interactions. This interaction resulted in a backfolding conformation of PAMAM dendrimers with the

inner groups participating in this interaction [47]. SASA measurements were calculated to estimate relevant contact areas with different probe radii size. From both simulations and the NMR data it was suggested that PAMAM form weak complexes with HAS [47].

## 4. Challenges and Perspectives

Currently, there are over 100,000 entries in the protein databank (PDB) with experimentally determined structures of various biologically important molecules. In contrast there are only nine entries that have structures of dendrimer components reported. This is a clear indication that dendrimers have intrinsic properties that prevent experimental elucidation of their 3D structures and their interactions with components of biological systems. Computational modeling and molecular dynamics have been valuable tools for design and optimization of drug candidates and polymers in the past. Therefore, there is a growing interest in the opportunities to apply computational chemistry tools to study dendrimers. Molecular modeling when effectively applied on dendrimers will offer a means to study conformation and many features of the dynamic behavior of dendrimers on a molecular level that are difficult to probe experimentally. These approaches will also allow the elucidation of some of the key interactions of functionalized dendrimers with therapeutic molecules and biological systems such as proteins and lipid membranes.

There are currently two main challenges in the modeling of dendrimers. The first is to obtain the initial three dimensional coordinates of the dendrimer to be used in further computational studies. This task can be performed manually by sketching the dendrimer with common chemical drawing tools with relatively ease for small generation dendrimer. However with more interesting and larger generation dendrimer, this approach is prone to errors. Furthermore there are no guidelines on how the initial structure should be assembled although it can be easily imagined that a fully stretched starting structure should be obtained to prevent dendrimer being stuck in a local minimum of the initial structures [76,105].

To the best of our knowledge there are only two tools that attempt to generate the starting three dimensional coordinates of a dendrimer of interest. Dendrimer Builder Toolkit [70] is a graphical user interface written in PERL that interfaces with AMBERTOOLS to build dendrimers. The other tool, also written in Perl, is called Silico [69], which has a module named Starmaker that generates *mol2 file of dendrimers by building them layer by layer. Our group is developing a an alternative way of building dendrimers or other hyperbranched polymers using XPLOR [71] through the definition of a sequence of monomers and the way they are connected to each other through patch references. The structures generated using this approach can be converted to file formats with more general force fields from XPLOR topology and parameter files. We are currently working on a python GUI to automate the process of assembly.

Another major issue with computationally simulating dendrimer structures is that there is no dedicated force field for this kind of macromolecule. This is probably due to the wide range of chemical bonds used to make dendrimers and that there are only few crystal structures of dendrimers. As a result, studies often rely on force fields developed for other macromolecules such as proteins with optimization of specific parameters or the use of more general force fields and these have been shown to be generally appropriate to predict and clarify experimental data.

Developing more general atom types in force fields will allow the automated generation of dendrimer structures, which will help to determine structure-property correlations needed to gain insight into their conformational behavior. Furthermore these generated dendrimer structures could be used in docking experiments. These types of study allow a dendrimer to be used as targets for small molecules or as ligand for biopolymers (protein or DNA structures). The docking solutions can be used in MD simulations to explore detailed intermolecular interactions. Docking studies also allow for selection of optimal dendrimer architecture for synthesis and further optimization.

Despite the current challenges with the lack of dedicated force fields and tools to easily represent dendrimer structures, interest in dendrimers for biomedical applications remains high together with the increase use of computational methods to predict or validate experimental data. While most of the simulations have been conducted for PAMAM dendrimers, and to a lesser extent for poly(L-lysine) and triazine dendrimers, this is understandable by the availability of these dendrimers. It is hoped that sufficient MD data about other types of dendrimers will become available. Continued computation studies of dendrimer will yield new methods of analysis of their dynamic structural properties, which will be essential to their design and optimization. Finally, the expected increase in availability of computational power will allow the extension simulation times to probe more complex interactions, such as dendrimer-membrane interaction. Our hope is that the molecular modeling will become more widely used for dendrimers and its usefulness will compare to that which currently exists for proteins.

**Acknowledgments**

Nuno Martinho is thankful for the funding from FCT (Fundação para a Ciência e Tecnologia) with a doctoral fellowship (SFRH/BD/87838/2012). L.C. Silva acknowledges funding from Compromisso para a Ciência 2008 from FCT, Portugal Teresa Barata and Steve Brocchini are grateful for funding from the UK Engineering & Physical Sciences Research Council (EPSRC) for the EPSRC Centre for Innovative Manufacturing in Emergent Macromolecular Therapies. Financial support from the consortium of industrial and governmental users for the EPSRC Centre is also acknowledged. Steve Brocchini is grateful for funding from the National Institute of Health Research (NIHR) Biomedical Research Centre at Moorfields Hospital NHS Foundation Trust and UCL Institute of Ophthalmology, Moorfields Special Trustees, the Helen Hamlyn Trust (in memory of Paul Hamlyn), Medical Research Council, Fight for Sight and Freemasons Grand Charity.

**Author Contributions**

N.M. wrote the paper and conducted the main literature search; M.Z. and T.B. structured and supervised the manuscript. All authors conducted literature search and contributed to the sections on their specialty, H.F. cancer applications, L.S. membrane interactions, S.B. dendrimers chemistry, M.Z. and T.B. molecular modeling of dendrimers. All authors read and approved the final manuscript.

**Conflicts of Interest**

The authors declare no conflict of interests.

**References**


1. Tomalia, D.A. Birth of a new macromolecular architecture: Dendrimers as quantized building blocks for nanoscale synthetic polymer chemistry. *Prog. Polym. Sci.* **2005**, *30*, 294–324.
2. Ali, M.; Brocchini, S. Synthetic approaches to uniform polymers. *Adv. Drug Deliv. Rev.* **2006**, *58*, 1671–87.
3. Hodge, P. Polymer science branches out. *Nature* **1993**, *362*, 18–19.
4. Morefield, G.L.; Hawkins, L.D.; Ishizaka, S.T.; Kissner, T.L.; Ulrich, R.G. Synthetic Toll-like receptor 4 agonist enhances vaccine efficacy in an experimental model of toxic shock syndrome. *Clin. Vaccine Immunol.* **2007**, *14*, 1499–1504.
5. Klajnert, B.; Bryszewska, M. Dendrimers: Properties and applications. *Acta Biochim. Pol.* **2001**, *48*, 199–208.
6. Hawker, C.J.; Frechet, J.M.J. Preparation of Polymers with Controlled Molecular Architecture. A New Convergent Approach to Dendritic Macromolecules. *J. Am. Chem. Soc.* **1990**, *32*, 7638–7647.
7. Tomalia, D.A.; Naylor, A.M.; Goddard, W.A. Starburst Dendrimers: Molecular-Level Control of Size, Shape, Surface Chemistry, Topology, and Flexibility from Atoms to Macroscopic Matter. *Angew. Chem. Int. Ed. Eng.* **1990**, *29*, 138–175.
8. Mourey, T.H.; Turner, S.R.; Rubinstein, M.; Frechet, J.M.J.; Hawker, C.J.; Wooley, K.L. Unique behavior of dendritic macromolecules: Intrinsic viscosity of polyether dendrimers. *Macromolecules* **1992**, *25*, 2401–2406.
9. Jackson, C.L.; Chanzy, H.D.; Booy, F.P.; Drake, B.J.; Tomalia, D.A.; Bauer, B.J.; Amis, E.J. Visualization of Dendrimer Molecules by Transmission Electron Microscopy (TEM): Staining Methods and Cryo-TEM of Vitrified Solutions. *Macromolecules* **1998**, *31*, 6259–6265.
10. Maiti, P.K.; Çağın, T.; Wang, G.; Goddard, W.A. Structure of PAMAM Dendrimers: Generations 1 through 11. *Macromolecules* **2004**, *37*, 6236–6254.
11. Zeng, F.; Zimmerman, S.C. Dendrimers in Supramolecular Chemistry: From Molecular Recognition to Self-Assembly. *Chem. Rev.* **1997**, *97*, 1681–1712.
12. Tomalia, D.A.; Baker, H.; Dewald, J.; Hall, M.; Kallos, G.; Martin, S.; Roeck, J.; Ryder, J.; Smith, P. A new class of polymers starburst dendritic macromolecules. *Polym. J.* **1985**, *17*, 117–132.
13. Svenson, S. Dendrimers as versatile platform in drug delivery applications. *Eur. J. Pharm. Biopharm.* **2009**, *71*, 445–462.
14. Buhleier, E.; Wehner, W.; Vogtle, F. "Cascade"-and "Nonskid-Chain-like" Syntheses of Molecular Cavity Topologies. *Synthesis* **1978**, 155–158.
15. Fischer, M.; Appelhans, D.; Schwarz, S.; Klajnert, B.; Bryszewska, M.; Voit, B.; Rogers, M. Influence of surface functionality of poly(propylene imine) dendrimers on protease resistance and propagation of the scrapie prion protein. *Biomacromolecules* **2010**, *11*, 1314–1325.
16. Al-Jamal, K.T.; Al-Jamal, W.T.; Akerman, S.; Podesta, J.E.; Yilmazer, A.; Turton, J.A.; Bianco, A.; Vargesson, N.; Kanthou, C.; Florence, A.T.; *et al.* Systemic antiangiogenic activity of cationic poly-L-lysine dendrimer delays tumor growth. *Proc. Natl. Acad. Sci. USA* **2010**, *107*, 3966–3971.

17. Gillies, E.R.; Dy, E.; Fréchet, J.M.J.; Szoka, F.C. Biological evaluation of polyester dendrimer: Poly(ethylene oxide) "bow-tie" hybrids with tunable molecular weight and architecture. *Mol. Pharm.* **2004**, *2*, 129–138.
18. Lim, J.; Pavan, G.M.; Annunziata, O.; Simanek, E.E. Experimental and computational evidence for an inversion in guest capacity in high-generation triazine dendrimer hosts. *J. Am. Chem. Soc.* **2012**, *134*, 1942–1945.
19. Ciepluch, K.; Katir, N.; El Kadib, A.; Felczak, A.; Zawadzka, K.; Weber, M.; Klajnert, B.; Lisowska, K.; Caminade, A.-M.; Bousmina, M.; *et al.* Biological properties of new viologen-phosphorus dendrimers. *Mol. Pharm.* **2012**, *9*, 448–457.
20. Thomas, T.P.; Patri, A.K.; Andrzej, M.; Myaing, M.T.; Ye, J.Y.; Norris, T.B.; Baker, J.R., Jr. *In Vitro* Targeting of Synthesized Antibody-Conjugated Dendrimer Nanoparticles. *Biomacromolecules* **2004**, *5*, 2269–2274.
21. Jiang, L.-Y.; Lv, B.; Luo, Y. The effects of an RGD-PAMAM dendrimer conjugate in 3D spheroid culture on cell proliferation, expression and aggregation. *Biomaterials* **2013**, *34*, 2665–2673.
22. Hedden, R.C.; Bauer, B.J. Structure and Dimensions of PAMAM/PEG Dendrimer—Star Polymers. *Macromolecules* **2003**, *36*, 1829–1835.
23. Twyman, L.J.; King, A.S.H.; Martin, I.K. Catalysis inside dendrimers. *Chem. Soc. Rev.* **2002**, *31*, 69–82.
24. Degoricija, L.; Johnson, C.S.; Wathier, M.; Kim, T.; Grinstaff, M.W. Photo Cross-linkable Biodendrimers as Ophthalmic Adhesives for Central Lacerations and Penetrating Keratoplasties. *Investig. Ophthalmol. Vis. Sci.* **2007**, *48*, 2037–2042.
25. Šebestík, J.; Reiniš, M.; Ježek, J. Dendrimers as Biosensors and Imaging Tools. In *Biomedical Applications of Peptide-, Glyco- and Glycopeptide Dendrimers, and Analogous Dendrimeric Structures*; Springer Science & Business Media: Wien, Austria, 2012; pp. 191–195.
26. Grinstaff, M.W. Biodendrimers: New Polymeric Biomaterials for Tissue Engineering. *Chem. A Eur. J.* **2002**, 8, 2838–2846.
27. Shaunak, S.; Brocchini, S. Dendrimer-Based Drugs as Macromolecular Medicines. *Biotechnol. Genet. Eng. Rev.* **2006**, *23*, 309–315.
28. Shcharbin, D.G.; Klajnert, B.; Bryszewska, M. Dendrimers in gene transfection. *Biochemistry* **2009**, *74*, 1070–1079.
29. Tyssen, D.; Henderson, S.A.; Johnson, A.; Sterjovski, J.; Moore, K.; La, J.; Zanin, M.; Sonza, S.; Karellas, P.; Giannis, M.P.; *et al.* Structure Activity Relationship of Dendrimer Microbicides with Dual Action Antiviral Activity. *PLoS One* **2010**, *5*, e12309.
30. Darbre, T.; Reymond, J.-L. Peptide dendrimers as artificial enzymes, receptors, and drug-delivery agents. *Acc. Chem. Res.* **2006**, *39*, 925–934.
31. Jain, K.; Kesharwani, P.; Gupta, U.; Jain, N.K. Dendrimer toxicity: Let's meet the challenge. *Int. J. Pharm.* **2010**, *394*, 122–142.
32. Duncan, R.; Izzo, L. Dendrimer biocompatibility and toxicity. *Adv. Drug Deliv. Rev.* **2005**, *57*, 2215–2237.
33. McNerny, D.Q.; Leroueil, P.R.; Baker, J.R. Understanding specific and nonspecific toxicities: A requirement for the development of dendrimer-based pharmaceuticals. *Nanomed. Nanobiotechnol.* **2010**, *2*, 249–259.

34. Caminade, A.-M.; Laurent, R.; Majoral, J.-P. Characterization of dendrimers. *Adv. Drug Deliv. Rev.* **2005**, *57*, 2130–2146.
35. Cagin, T.; Wang, G.; Martin, R.; Zamanakos, G.; Vaidehi, N.; Mainz, T.; Iii, W.A.G. Multiscale modeling and simulation methods with applications to dendritic polymers. *Comput. Theor. Polym. Sci.* **2001**, *11*, 345–356.
36. Çagin, T.; Wang, G.; Martin, R.; Breen, N.; Goddard, W.A Molecular modeling of dendrimers for nanoscale applications. *Nanotechnology* **2000**, *11*, 77–84.
37. Lee, H.; Larson, R.G. Multiscale modeling of dendrimers and their interactions with bilayers and polyelectrolytes. *Molecules* **2009**, *14*, 423–438.
38. Javor, S.; Reymond, J.-L. Molecular dynamics and docking studies of single site esterase peptide dendrimers. *J. Org. Chem.* **2009**, *74*, 3665–3674.
39. Ranganathan, D.; Kurur, S. Synthesis of totally chiral, multiple armed, poly Glu and poly Asp scaffoldings on bifunctional adamantane core. *Tetrahedron Lett.* **1997**, *38*, 1265–1268.
40. Zloh, M.; Ramaswamy, C.; Sakthivel, T.; Wilderspin, A.; Florence, A.T. Investigation of the association and flexibility of cationic lipidic peptide dendrons by NMR spectroscopy. *Magn. Reson. Chem.* **2005**, *43*, 47–52.
41. Naylor, A.M.; Goddard, W.A.; Kiefer, G.E.; Tomalia, D.A. Starburst Dendrimers. 5. Molecular Shape Control. *J. Am. Chem. Soc* **1989**, *111*, 2339–2341.
42. Tian, W.; Ma, Y. Molecular dynamics simulations of a charged dendrimer in multivalent salt solution. *J. Phys. Chem. B* **2009**, *113*, 13161–13170.
43. Ouyang, D.; Zhang, H.; Parekh, H.S.; Smith, S.C. The effect of pH on PAMAM dendrimer-siRNA complexation: Endosomal considerations as determined by molecular dynamics simulation. *Biophys. Chem.* **2011**, *158*, 126–133.
44. Jain, V.; Maingi, V.; Maiti, P.K.; Bharatam, P.V. Molecular dynamics simulations of PPI dendrimer–drug complexes. *Soft Matter* **2013**, *9*, 6482–6496.
45. Barata, T.S.; Teo, I.; Lalwani, S.; Simanek, E.E.; Zloh, M.; Shaunak, S. Computational design principles for bioactive dendrimer based constricts as antagonists of the TLR4-MD-2-LPS complex. *Biomaterials* **2012**, *32*, 8702–8711.
46. Barnard, A.; Posocco, P.; Pricl, S.; Calderon, M.; Haag, R.; Hwang, M.E.; Shum, V.W.T.; Pack, D.W.; Smith, D.K. Degradable self-assembling dendrons for gene delivery: Experimental and theoretical insights into the barriers to cellular uptake. *J. Am. Chem. Soc.* **2011**, *133*, 20288–20300.
47. Giri, J.; Diallo, M.S.; Simpson, A.J.; Liu, Y.; Goddard, W.A.; Kumar, R.; Woods, G.C. Interactions of poly(amidoamine) dendrimers with human serum albumin: Binding constants and mechanisms. *ACS Nano* **2011**, *5*, 3456–3468.
48. Ivanov, A.A.; Jacobson, K.A. Molecular modeling of a PAMAM-CGS21680 dendrimer bound to an A2A adenosine receptor homodimer. *Bioorg. Med. Chem. Lett.* **2008**, *18*, 4312–4315.
49. Maiti, P.K.; Bagchi, B. Structure and dynamics of DNA-dendrimer complexation: Role of counterions, water, and base pair sequence. *Nano Lett.* **2006**, *6*, 2478–2485.
50. Pavan, G.M.; Albertazzi, L.; Danani, A. Ability to adapt: Different generations of PAMAM dendrimers show different behaviors in binding siRNA. *J. Phys. Chem. B* **2010**, *114*, 2667–2675.

51. Vasumathi, V.; Maiti, P.K. Complexation of siRNA with Dendrimer: A Molecular Modeling Approach. *Macromolecules* **2010**, *43*, 8264–8274.
52. Barata, T.S.; Teo, I.; Brocchini, S.; Zloh, M.; Shaunak, S. Partially Glycosylated Dendrimers Block MD-2 and Prevent TLR4-MD-2-LPS Complex Mediated Cytokine Responses. *PLoS Comput. Biol*. **2011**, *7*, e1002095.
53. Lee, H.; Larson, R.G. Coarse-grained molecular dynamics studies of the concentration and size dependence of fifth- and seventh-generation PAMAM dendrimers on pore formation in DMPC bilayer. *J. Phys. Chem. B* **2008**, *112*, 7778–7784.
54. Tanis, I.; Karatasos, K. Association of a weakly acidic anti-inflammatory drug (ibuprofen) with a poly(amidoamine) dendrimer as studied by molecular dynamics simulations. *J. Phys. Chem. B* **2009**, *113*, 10984–10993.
55. Abderrezak, A.; Bourassa, P.; Mandeville, J.-S.; Sedaghat-Herati, R.; Tajmir-Riahi, H.-A. Dendrimers bind antioxidant polyphenols and cisplatin drug. *PLoS One* **2012**, *7*, e33102.
56. Brocchini, S.; Godwin, A.; Balan, S.; Choi, J.; Zloh, M.; Shaunak, S. Disulfide bridge based PEGylation of proteins. *Adv. Drug Deliv. Rev.* **2008**, *60*, 3–12.
57. Uhlich, N.A; Darbre, T.; Reymond, J.-L. Peptide dendrimer enzyme models for ester hydrolysis and aldolization prepared by convergent thioether ligation. *Org. Biomol. Chem.* **2011**, *9*, 7071–7084.
58. Monticelli, L.; Kandasamy, S.K.; Periole, X.; Larson, R.G.; Tieleman, D.P.; Marrink, S.-J. The MARTINI Coarse-Grained Force Field: Extension to Proteins. *J. Chem. Theory Comput.* **2008**, *4*, 819–834.
59. He, X.; Qu, Z.; Xu, F.; Lin, M.; Wang, J.; Shi, X.; Lu, T. Molecular analysis of interactions between dendrimers and asymmetric membranes at different transport stages. *Soft Matter* **2014**, *10*, 139–148.
60. Lee, H.; Larson, R.G. Molecular dynamics simulations of PAMAM dendrimer-induced pore formation in DPPC bilayers with a coarse-grained model. *J. Phys. Chem. B* **2006**, *110*, 18204–18211.
61. Taylor, P.; Lee, H. Self-assembly of mixtures of a dendrimer and lipids : Effects of hydrophobicity and electrostatics. *Mol. Simul.* **2012**, *38*, 534–539.
62. Lozac'h, N.; Goodson, A.L.; Powell, W.H. Nobel Nomenclature—General Principles. *Angew. Chem. Int. Ed. Engl.* **1979**, *18*, 887–899.
63. Roberts, B.P.; Scanlon, M.J.; Krippner, G.Y.; Chalmers, D.K. The Dotted Cap Notation: A concise notation for describing variegated dendrimers. *New J. Chem.* **2008**, *32*, 1543–1554.
64. Florida, S.; Rouge, B. Systematic Nomenclature for Cascade Polymers. *J. Polym. Sci. Part A Polym. Chem.* **1993**, *31*, 641–651.
65. Friedhofen, J.H.; Vögtle, F. Detailed nomenclature for dendritic molecules. *New J. Chem.* **2006**, *30*, 32–43.
66. Hess, B.; Kutzner, C.; van der Spoel, D.; Lindahl, E. GROMACS 4 : Algorithms for Highly Efficient , Load-Balanced , and Scalable Molecular Simulation. *J. Chem. Theory Comput.* **2007**, *4*, 436–447.
67. Schwieters, C.D.; Kuszewski, J.J.; Tjandra, N.; Clore, G.M. The Xplor-NIH NMR molecular structure determination package. *J. Magn. Reson.* **2003**, *160*, 65–73.

68. Schwieters, C.; Kuszewski, J.; Mariusclore, G. Using Xplor–NIH for NMR molecular structure determination. *Prog. Nucl. Magn. Reson. Spectrosc.* **2006**, *48*, 47–62.
69. Charlmers, D.; Roberts, B. Silico—A Perl Molecular Modeling Toolkit. Available online: http://silico.sourceforge.net/Silico/Home.html (accessed on 1 August 2014).
70. Maingi, V.; Jain, V.; Bharatam, P.V.; Maiti, P.K. Dendrimer building toolkit: Model building and characterization of various dendrimer architectures. *J. Comput. Chem.* **2012**, *33*, 1997–2011.
71. Barata, T.S.; Brocchini, S.; Teo, I.; Shaunak, S.; Zloh, M. From sequence to 3D structure of hyperbranched molecules: Application to surface modified PAMAM dendrimers. *J. Mol. Model.* **2011**, *17*, 2741–2749.
72. Lim, J.; Lo, S.-T.; Hill, S.; Pavan, G.M.; Sun, X.; Simanek, E.E. Antitumor activity and molecular dynamics simulations of paclitaxel-laden triazine dendrimers. *Mol. Pharm.* **2012**, *9*, 404–412.
73. Schneider, C.P.; Shukla, D.; Trout, B.L. Effects of solute-solute interactions on protein stability studied using various counterions and dendrimers. *PLoS One* **2011**, *6*, e27665.
74. Kelly, C.V.; Leroueil, P.R.; Orr, B.G.; Banaszak Holl, M.M.; Andricioaei, I. Poly(amidoamine) dendrimers on lipid bilayers II: Effects of bilayer phase and dendrimer termination. *J. Phys. Chem. B* **2008**, *112*, 9346–9353.
75. Mills, M.; Orr, B.G.; Banaszak Holl, M.M.; Andricioaei, I. Attractive hydration forces in DNA-dendrimer interactions on the nanometer scale. *J. Phys. Chem. B* **2013**, *117*, 973–981.
76. Filipe, C.S.; Machuqueiro, M.; Darbre, T.; Baptista, M. Unraveling the Conformational Determinants of Peptide Dendrimers Using Molecular Dynamics Simulations. *Macromolecules* **2013**, *46*, 9427–9436.
77. Wang, Y.-L.; Lu, Z.-Y.; Laaksonen, A. Specific binding structures of dendrimers on lipid bilayer membranes. *Phys. Chem. Chem. Phys.* **2012**, *14*, 8348–8359.
78. Tian, W.; Ma, Y. Insights into the endosomal escape mechanism via investigation of dendrimer–membrane interactions. *Soft Matter* **2012**, *8*, 6378–6384.
79. Zhong, T.; Ai, P.; Zhou, J. Structures and properties of PAMAM dendrimer: A multi-scale simulation study. *Fluid Phase Equilib.* **2011**, *302*, 43–47.
80. Quintana, A.; Raczka, E.; Piehler, L.; Lee, I.; Myc, A.; Majoros, I.; Patri, A.K.; Thomas, T.; Mulé, J.; Baker, J.R. Design and function of a dendrimer-based therapeutic nanodevice targeted to tumor cells through the folate receptor. *Pharm. Res.* **2002**, *19*, 1310–1316.
81. Shi, X.; Lee, I.; Chen, X.; Shen, M.; Xiao, S.; Zhu, M.; Baker, J.R., Jr.; Wang, S.H. Influence of dendrimer surface charge on the bioactivity of 2-methoxyestradiol complexed with dendrimers. *Soft Matter* **2010**, *6*, 20–27.
82. Stach, M.; Maillard, N.; Kadam, R.U.; Kalbermatter, D.; Meury, M.; Page, M.G.P.; Fotiadis, D.; Darbre, T.; Reymond, J.-L. Membrane disrupting antimicrobial peptide dendrimers with multiple amino termini. *Med. Chem. Comm.* **2012**, *3*, 86–89.
83. Al-Jamal, K.T.; Al-Jamal, W.T.; Wang, J.T.-W.; Rubio, N.; Buddle, J.; Gathercole, D.; Zloh, M.; Kostarelos, K. Cationic poly-L-lysine dendrimer complexes doxorubicin and delays tumor growth in vitro and *in vivo*. *ACS Nano* **2013**, *7*, 1905–1917.
84. Miklis, P.; Tahir, C.; Iii, W.A.G. Dynamics of Bengal Rose Encapsulated in the Meijer Dendrimer Box. *J. Am. Chem. Soc.* **1997**, *7863*, 7458–7462.

85. Liu, Y.; Bryantsev, V.S.; Diallo, M.S.; Goddard, W.A PAMAM dendrimers undergo pH responsive conformational changes without swelling. *J. Am. Chem. Soc.* **2009**, *131*, 2798–2799.
86. Prosa, T.J.; Bauer, B.J.; Amis, E.J.; Tomalia, D.A.; Scherrenberg, R. A SAXS study of the internal structure of dendritic polymer systems. *J. Polym. Sci. Part B Polym. Phys.* **1997**, *35*, 2913–2924.
87. Lee, I.; Athey, B.D.; Wetzel, A.W.; Meixner, W.; Baker, J.R. Structural Molecular Dynamics Studies on Polyamidoamine Dendrimers for a Therapeutic Application: Effects of pH and Generation. *Macromolecules* **2002**, *35*, 4510–4520.
88. Lin, S.-T.; Maiti, P.K.; Goddard, W.A. Dynamics and thermodynamics of water in PAMAM dendrimers at subnanosecond time scales. *J. Phys. Chem. B* **2005**, *109*, 8663–8672.
89. Lee, H.; Baker, J.R.; Larson, R.G. Molecular dynamics studies of the size, shape, and internal structure of 0% and 90% acetylated fifth-generation polyamidoamine dendrimers in water and methanol. *J. Phys. Chem. B* **2006**, *110*, 4014–4019.
90. Barata, T.S.; Shaunak, S.; Teo, I.; Zloh, M.; Brocchini, S. Structural studies of biologically active glycosylated polyamidoamine (PAMAM) dendrimers. *J. Mol. Model.* **2011**, *17*, 2051–2060.
91. Lim, J.; Turkbey, B.; Bernardo, M.; Bryant, L.H.J.; Garzoni, M.; Pavan, G.M.; Nakajima, T.; Choyke, P.L.; Simanek, E.E.; Kobayashi, H. Gadolinium MRI contrast agents based on triazine dendrimers: Relaxivity and in vivo pharmacokinetics. *Bioconjug. Chem.* **2012**, *23*, 2291–2299.
92. Lee, H.; Larson, R.G. A molecular dynamics study of the structure and inter-particle interactions of polyethylene glycol-conjugated PAMAM dendrimers. *J. Phys. Chem. B* **2009**, *113*, 13202–13207.
93. Shi, X.; Wang, S.; Meshinchi, S.; van Antwerp, M.E.; Bi, X.; Lee, I.; Baker, J.R. Dendrimer-Entrapped Gold Nanoparticles as a Platform for Cancer-Cell Targeting and Imaging. *Small* **2007**, *3*, 1245–1252.
94. Roberts, B.P.; Krippner, G.Y.; Scanlon, M.J.; Chalmers, D.K. Molecular Dynamics of Variegated Polyamide Dendrimers. *Macromolecules* **2009**, *42*, 2784–2794.
95. Caballero, J.; Poblete, H.; Navarro, C.; Alzate-Morales, J.H. Association of nicotinic acid with a poly(amidoamine) dendrimer studied by molecular dynamics simulations. *J. Mol. Graph. Model.* **2013**, *39*, 71–78.
96. Carrasco-Sánchez, V.; Vergara-Jaque, A.; Zuñiga, M.; Comer, J.; John, A.; Nachtigall, F.M.; Valdes, O.; Duran-Lara, E.F.; Sandoval, C.; Santos, L.S. *In situ* and *in silico* evaluation of amine- and folate-terminated dendrimers as nanocarriers of anesthetics. *Eur. J. Med. Chem.* **2014**, *73*, 250–257.
97. Maingi, V.; Kumar, M.V.S.; Maiti, P.K. PAMAM dendrimer-drug interactions: Effect of pH on the binding and release pattern. *J. Phys. Chem. B* **2012**, *116*, 4370–4376.
98. Pavan, G.M.; Mintzer, M.A.; Simanek, E.E.; Merkel, O.M.; Kissel, T.; Danani, A. Computational insights into the interactions between DNA and siRNA with "rigid" and "flexible" triazine dendrimers. *Biomacromolecules* **2010**, *11*, 721–730.
99. Jensen, L.B.; Mortensen, K.; Pavan, G.M.; Kasimova, M.; Jensen, D.K.; Gadzhyeva, V.; Nielsen, H.M.; Foged, C. Molecular Characterization of the Interaction between siRNA and PAMAM G7 Dendrimers by SAXS, ITC, and Molecular Dynamics Simulations. *Biomacromolecules* **2010**, *11*, 3571–3577.

100. Huißmann, S.; Likos, C.N.; Blaak, R. Explicit *vs* Implicit Water Simulations of Charged Dendrimers. *Macromolecules* **2012**, *45*, 2562–2569.
101. Antosiewicz, J.M.; Shugar, D. Poisson-Boltzmann continuum-solvation models: Applications to pH-dependent properties of biomolecules. *Mol. Biosyst.* **2011**, *7*, 2923–2949.
102. Ballauff, M.; Likos, C.N. Dendrimers in solution: Insight from theory and simulation. *Angew. Chem. Int. Ed. Engl.* **2004**, *43*, 2998–3020.
103. Lyulin, S.V.; Darinskii, A.A.; Lyulin, A.V. Computer Simulation of Complexes of Dendrimers with Linear Polyelectrolytes. *Macromolecules* **2005**, *38*, 3990–3998.
104. Sadanobu, J.; Goddard, W.A. The continuous configurational Boltzmann biased direct Monte Carlo method for free energy properties of polymer chains. *J. Chem. Phys.* **1997**, *106*, 6722–6729.
105. Filipe, L.C.S.; Machuqueiro, M.; Baptista, A.M. Unfolding the conformational behavior of peptide dendrimers: Insights from molecular dynamics simulations. *J. Am. Chem. Soc.* **2011**, *133*, 5042–5052.
106. Barra, P.A.; Barraza, L.; Jiménez, V.A.; Gavín, J.A.; Alderete, J.B. Complexation of Mefenamic Acid by Low- Generation PAMAM Dendrimers: Insight from NMR Spectroscopy Studies and Molecular Dynamics Simulations. *Macromol. Chem. Phys.* **2014**, *215*, 372–383.
107. Evangelista-Lara, A.; Guadarrama, P. Theoretical evaluation of the nanocarrier properties of two families of functionalized dendrimers. *Int. J. Quantum Chem.* **2005**, *103*, 460–470.
108. Cao, J.; Zhang, H.; Wang, Y.; Yang, J.; Jiang, F. Investigation on the interaction behavior between curcumin and PAMAM dendrimer by spectral and docking studies. *Spectrochim. Acta A Mol. Biomol. Spectrosc.* **2013**, *108*, 251–255.
109. Vergara-Jaque, A.; Comer, J.; Monsalve, L.; González-Nilo, F.D.; Sandoval, C. Computationally efficient methodology for atomic-level characterization of dendrimer-drug complexes: A comparison of amine- and acetyl-terminated PAMAM. *J. Phys. Chem. B* **2013**, *117*, 6801–6813.
110. Maiti, P.K.; Çağın, T.; Lin, S.-T.; Goddard, W.A. Effect of Solvent and pH on the Structure of PAMAM Dendrimers. *Macromolecules* **2005**, *38*, 979–991.
111. Chen, W.; Porcar, L.; Liu, Y.; Butler, P.D.; Magid, L.J. Small Angle Neutron Scattering Studies of the Counterion Effects on the Molecular Conformation and Structure of Charged G4 PAMAM Dendrimers in Aqueous Solutions. *Macromolecules* **2007**, *40*, 5887–5898.
112. Nisato, G.; Ivkov, R.; Amis, E.J. Size Invariance of Polyelectrolyte Dendrimers. *Macromolecules* **2000**, *33*, 4172–4176.
113. Gorman, C.B.; Smith, J.C. Effect of repeat unit flexibility on dendrimer conformation as studied by atomistic molecular dynamics simulations. *Polymer* **2000**, *41*, 675–683.
114. Blaak, R.; Lehmann, S.; Likos, C.N. Charge-induced conformational changes of dendrimers. *Macromolecules* **2008**, *41*, 4452–4458.
115. Gitsov, I.; Fre, J.M.J. Stimuli-Responsive Hybrid Macromolecules: Novel Amphiphilic Star Copolymers With Dendritic Groups at the Periphery. *J. Am. Chem. Soc.* **1996**, *118*, 3785–3786.
116. Rathgeber, S.; Monkenbusch, M.; Kreitschmann, M.; Urban, V.; Brulet, A. Dynamics of star-burst dendrimers in solution in relation to their structural properties. *J. Chem. Phys.* **2002**, *117*, 4047–4062.
117. Porcar, L.; Hong, K.; Butler, P.D.; Herwig, K.W.; Smith, G.S.; Liu, Y.; Chen, W.-R. Intramolecular structural change of PAMAM dendrimers in aqueous solutions revealed by small-angle neutron scattering. *J. Phys. Chem. B* **2010**, *114*, 1751–1756.

118. Topp, A.; Bauer, B.J.; Tomalia, D.A.; Amis, E.J. Effect of Solvent Quality on the Molecular Dimensions of PAMAM Dendrimers. *Macromolecules* **1999**, *32*, 7232–7237.
119. Maiti, P.K.; Messina, R. Counterion Distribution and ζ-Potential in PAMAM Dendrimer. *Macromolecules* **2008**, *41*, 5002–5006.
120. Maiti, P.K.; Goddard, W.A. Solvent quality changes the structure of G8 PAMAM dendrimer, a disagreement with some experimental interpretations. *J. Phys. Chem. B* **2006**, *110*, 25628–25632.
121. Carbone, P.; Müller-Plathe, F. Molecular dynamics simulations of polyaminoamide (PAMAM) dendrimer aggregates: Molecular shape, hydrogen bonds and local dynamics. *Soft Matter* **2009**, 2638–2647.
122. Li, T.; Hong, K.; Porcar, L.; Verduzco, R.; Butler, P.D.; Smith, G.S.; Liu, Y.; Chen, W.-R. Assess the Intramolecular Cavity of a PAMAM Dendrimer in Aqueous Solution by Small-Angle Neutron Scattering. *Macromolecules* **2008**, *41*, 8916–8920.
123. Huißmann, S.; Likos, C.N.; Blaak, R. Conformations of high-generation dendritic polyelectrolytes. *J. Mater. Chem.* **2010**, *20*, 10486–10494.
124. Tian, W.; Ma, Y. Theoretical and computational studies of dendrimers as delivery vectors. *Chem. Soc. Rev.* **2013**, *42*, 705–727.
125. Zhang, Y.; Thomas, T.P.; Lee, K.-H.; Li, M.; Zong, H.; Desai, A.M.; Kotlyar, A.; Huang, B.; Holl, M.M.B.; Baker, J.R. Polyvalent saccharide-functionalized generation 3 poly(amidoamine) dendrimer-methotrexate conjugate as a potential anticancer agent. *Bioorg. Med. Chem.* **2011**, *19*, 2557–2564.
126. Albertazzi, L.; Brondi, M.; Pavan, G.M.; Sato, S.S.; Signore, G.; Storti, B.; Ratto, G.M.; Beltram, F. Dendrimer-based fluorescent indicators: *In vitro* and *in vivo* applications. *PLoS One* **2011**, *6*, e28450.
127. Alcala, M.A; Kwan, S.Y.; Shade, C.M.; Lang, M.; Uh, H.; Wang, M.; Weber, S.G.; Bartlett, D.L.; Petoud, S.; Lee, Y.J. Luminescence targeting and imaging using a nanoscale generation 3 dendrimer in an *in vivo* colorectal metastatic rat model. *Nanomedicine* **2011**, *7*, 249–258.
128. Mecke, A.; Uppuluri, S.; Sassanella, T.M.; Lee, D.-K.; Ramamoorthy, A; Baker, J.R.; Orr, B.G.; Banaszak Holl, M.M. Direct observation of lipid bilayer disruption by poly(amidoamine) dendrimers. *Chem. Phys. Lipids* **2004**, *132*, 3–14.
129. Mecke, A.; Majoros, I.J.; Patri, A.K.; Baker, J.R.; Holl, M.M.B.; Orr, B.G. Lipid bilayer disruption by polycationic polymers: The roles of size and chemical functional group. *Langmuir* **2005**, *21*, 10348–10354.
130. Gardikis, K.; Hatziantoniou, S.; Viras, K.; Wagner, M.; Demetzos, C. A DSC and Raman spectroscopy study on the effect of PAMAM dendrimer on DPPC model lipid membranes. *Int. J. Pharm.* **2006**, *318*, 118–123.
131. Ionov, M.; Gardikis, K.; Wróbel, D.; Hatziantoniou, S.; Mourelatou, H.; Majoral, J.-P.; Klajnert, B.; Bryszewska, M.; Demetzos, C. Interaction of cationic phosphorus dendrimers (CPD) with charged and neutral lipid membranes. *Colloids Surf. B. Biointerfaces* **2011**, *82*, 8–12.
132. El-Sayed, M.E.H.; Ghandehari, H.; Ginski, M.; Rhodes, C.A. Influence of Surface Chemistry of Poly (Amidoamine) Dendrimers on Caco-2 Cell Monolayers. *J. Bioact. Compat. Polym.* **2003**, *18*, 7–22.

133. Hong, S.; Leroueil, P.R.; Janus, E.K.; Peters, J.L.; Kober, M.-M.; Islam, M.T.; Orr, B.G.; Baker, J.R.; Banaszak Holl, M.M. Interaction of polycationic polymers with supported lipid bilayers and cells: Nanoscale hole formation and enhanced membrane permeability. *Bioconjug. Chem.* **2006**, *17*, 728–734.
134. Domański, D.M.; Klajnert, B.; Bryszewska, M. Influence of PAMAM dendrimers on human red blood cells. *Bioelectrochemistry* **2004**, *63*, 189–191.
135. Kitchens, K.M.; Foraker, A.B.; Kolhatkar, R.B.; Swaan, P.W.; Ghandehari, H. Endocytosis and interaction of poly (amidoamine) dendrimers with Caco-2 cells. *Pharm. Res.* **2007**, *24*, 2138–2145.
136. Kitchens, K.M.; El-Sayed, M.E.H.; Ghandehari, H. Transepithelial and endothelial transport of poly (amidoamine) dendrimers. *Adv. Drug Deliv. Rev.* **2005**, *57*, 2163–2176.
137. Calabretta, M.K.; Kumar, A.; McDermott, A.M.; Cai, C. Antibacterial activities of poly(amidoamine) dendrimers terminated with amino and poly(ethylene glycol) groups. *Biomacromolecules* **2007**, *8*, 1807–1811.
138. Kelly, C.V.; Leroueil, P.R.; Nett, E.K.; Wereszczynski, J.M.; Baker, J.R.; Orr, B.G.; Banaszak Holl, M.M.; Andricioaei, I. Poly(amidoamine) dendrimers on lipid bilayers I: Free energy and conformation of binding. *J. Phys. Chem. B* **2008**, *112*, 9337–9345.
139. Ainalem, M.-L.; Campbell, R.A.; Khalid, S.; Gillams, R.J.; Rennie, A.R.; Nylander, T. On the Ability of PAMAM Dendrimers and Dendrimer/DNA Aggregates To Penetrate POPC Model Biomembranes. *J. Phys. Chem. B* **2010**, *114*, 7229–7244.
140. Ting, C.L.; Wang, Z.-G. Interactions of a charged nanoparticle with a lipid membrane: Implications for gene delivery. *Biophys. J.* **2011**, *100*, 1288–1297.
141. Lipid, D.; Kelly, C.V.; Liroff, M.G.; Triplett, Ḱ.L.D.; Leroueil, P.R.; Mullen, Ḱ.D.G.; Wallace, J.M.; Meshinchi, Ḱ. S.; Baker, J.R.; Orr, B.G.; *et al.* Stoichiometry and Structure of Poly(amidoamine) Dendrimer-Lipid Complexes. *ACS Nano* **2009**, *3*, 1886–1896.
142. Kim, Y.; Kwak, Y.; Chang, R. Free energy of PAMAM dendrimer adsorption onto model biological membranes. *J. Phys. Chem. B* **2014**, *118*, 6792–6802.
143. Mecke, A.; Lee, D.-K.; Ramamoorthy, A.; Orr, B.G.; Holl, M.M.B. Synthetic and natural polycationic polymer nanoparticles interact selectively with fluid-phase domains of DMPC lipid bilayers. *Langmuir* **2005**, *21*, 8588–8590.
144. Tian, W.; Ma, Y. pH-responsive dendrimers interacting with lipid membranes. *Soft Matter* **2012**, *8*, 2627–2632.
145. Tu, C.; Chen, K.; Tian, W.; Ma, Y. Computational Investigations of a Peptide- Modified Dendrimer Interacting with Lipid Membranes. *Macromol. Rapid Commun.* **2013**, *34*, 1237–1242.
146. Xie, L.; Tian, W.; Ma, Y. Computer simulations of the interactions of high-generation polyamidoamine dendrimers with electronegative membranes. *Soft Matter* **2013**, *9*, 9319–9325.
147. Milhem, O.M.; Myles, C.; McKeown, N.B.; Attwood, D.; D'Emanuele, A. Polyamidoamine Starburst dendrimers as solubility enhancers. *Int. J. Pharm.* **2000**, *197*, 239–241.
148. Kolhe, P. Drug complexation, *in vitro* release and cellular entry of dendrimers and hyperbranched polymers. *Int. J. Pharm.* **2003**, *259*, 143–160.

149. Avila-Salas, F.; Sandoval, C.; Caballero, J.; Guiñez-Molinos, S.; Santos, L.S.; Cachau, R.E.; González-Nilo, F.D. Study of Interaction Energies between the PAMAM Dendrimer and Nonsteroidal Anti-Inflammatory Drug Using a Distributed Computational Strategy and Experimental Analysis by ESI-MS/MS. *J. Phys. Chem. B* **2012**, *116*, 2031–2039.
150. Radhika, R.; Rohith, V.; Anil Kumar, N.C.; Varun Gopal, K.; Krishnan Namboori, P.K.; Deepak, O.M. Insilico Analysis of Nano Polyamidoamine ( PAMAM ) Dendrimers for Cancer Drug Delivery. *Int. J. Recent Trends Eng. Technol.* **2010**, *4*, 142–144.
151. Satish Kumar, M.V.; Maiti, P.K. Structure of DNA-functionalized dendrimer nanoparticles. *Soft Matter* **2012**, *8*, 1893–1900.
152. Nandy, B.; Maiti, P.K. DNA compaction by a dendrimer. *J. Phys. Chem. B* **2011**, *115*, 217–230.
153. Merkel, O.M.; Zheng, M.; Mintzer, M.A.; Pavan, G.M.; Librizzi, D.; Maly, M.; Höffken, H.; Danani, A.; Simanek, E.E.; Kissel, T. Molecular modeling and in vivo imaging can identify successful flexible triazine dendrimer-based siRNA delivery systems. *J. Control. Release* **2011**, *153*, 23–33.
154. Shaunak, S.; Thomas, S.; Gianasi, E.; Godwin, A.; Jones, E.; Teo, I.; Mireskandari, K.; Luthert, P.; Duncan, R.; Patterson, S.; *et al.* Polyvalent dendrimer glucosamine conjugates prevent scar tissue formation. *Nature* **2004**, *22*, 977–984.
155. Teo, I.; Toms, S.M.; Marteyn, B.; Barata, T.S.; Simpson, P.; Johnston, K.A.; Schnupf, P.; Puhar, A.; Bell, T.; Tang, C.; *et al.* Preventing acute gut wall damage in infectious diarrhoeas with glycosylated dendrimers. *EMBO Mol. Med.* **2012**, *4*, 866–881.
156. Isea, R.; Hoebeke, J.; Mayo-García, R. Designing a Peptide-dendrimer for Use as a Synthetic Vaccine Against Plasmodium falciparum. *Am. J. Bioinforma. Comput. Biol.* **2013**, *1*, 1–8.

The results of this chapter are presented as a published original papers that originated from this work.

# PAPER 2 (Results) – Practical computational toolkits for dendrimers and dendrons structure design

J Comput Aided Mol Des
DOI 10.1007/s10822-017-0041-6

## Practical computational toolkits for dendrimers and dendrons structure design

**Nuno Martinho[1,2,4] · Liana C. Silva[1,3] · Helena F. Florindo[1] · Steve Brocchini[2] · Teresa Barata[2] · Mire Zloh[4]**

Received: 7 December 2016 / Accepted: 6 July 2017


**Abstract** Dendrimers and dendrons offer an excellent platform for developing novel drug delivery systems and medicines. The rational design and further development of these repetitively branched systems are restricted by difficulties in scalable synthesis and structural determination, which can be overcome by judicious use of molecular modelling and molecular simulations. A major difficulty to utilise in silico studies to design dendrimers lies in the laborious generation of their structures. Current modelling tools utilise automated assembly of simpler dendrimers or the inefficient manual assembly of monomer precursors to generate more complicated dendrimer structures. Herein we describe two novel graphical user interface toolkits written in Python that provide an improved degree of automation for rapid assembly of dendrimers and generation of their 2D and 3D structures. Our first toolkit uses the RDkit library, SMILES nomenclature of monomers and SMARTS reaction nomenclature to generate SMILES and mol files of dendrimers without 3D coordinates. These files are used for simple graphical representations and storing their structures in databases. The second toolkit assembles complex topology dendrimers from monomers to construct 3D dendrimer structures to be used as starting points for simulation using existing and widely available software and force fields. Both tools were validated for ease-of-use to prototype dendrimer structure and the second toolkit was especially relevant for dendrimers of high complexity and size.

**Keywords** Dendrimer · Dendrons · Linear polymers · Molecular modelling · 3D structure generation

**Electronic supplementary material** The online version of this article (doi:10.1007/s10822-017-0041-6) contains supplementary material, which is available to authorized users.

✉ Teresa Barata
t.barata@ucl.ac.uk

✉ Mire Zloh
m.zloh@herts.ac.uk

[1] Research Institute for Medicines (iMed.ULisboa), Faculty of Pharmacy, Universidade de Lisboa, Av. Professor Gama Pinto, 1649-003 Lisbon, Portugal

[2] Department of Pharmaceutics, UCL School of Pharmacy, University College London, 29/39 Brunswick Square, London WC1N 1AX, UK

[3] Centro de Química-Física Molecular and Institute of Nanoscience and Nanotechnology, Instituto Superior Técnico, Universidade de Lisboa, Av. Rovisco Pais, 1049-001 Lisboa, Portugal

[4] School of Life and Medical Sciences, University of Hertfordshire, College Lane, Hatfield AL10 9AB, UK

## Introduction

Dendrimers and dendrons are a type of hyper-branched macromolecules characterised by a well-defined three-dimensional branching architecture with a high degree of monodisperse molecular weight characteristics emanating from a multifunctional core [1]. They are often defined by the composition and chemistry of their core, branching (internal monomers) and by their multivalent terminal groups (surface groups). This results in a wide diversity of different topologies described in the literature since different core precursor and branching monomers can be used in their preparation. In particular, the use of different types of monomers can have dramatic changes in the size, volume, shape, flexibility, physicochemical properties and available space (interior density) of dendrimers [2, 3]. These features provide an excellent platform for potential applications of dendrimers for various purposes, for example: enhancing solubility and

Published online: 15 September 2017

delivery of drugs [4–8], optimization of therapeutic agents toxicity [9, 10], developing sensors [11], diagnostic agents [4] and transfection reagents [12]. The multivalent surface of dendrimers can also be utilized for passive or active targeting by modification of terminal groups using small molecules or macromolecules to employ relevant molecular recognition mechanisms [12–17].

Dendrimers are prepared following a wide range of synthetic routes. Divergent routes essentially proceed from the core outwards, and convergent routes tend to proceed from branched end groups to the core. Due to the hyperbranched character of dendrimers, the size of the structure, complexity and branching increases with each additional generation. The increase of each generation often results in the doubling the number of end groups with the possibility that intricate branched structures can be formed. Eventually dendrimers reach a generation number where end-group crowding results in restricted chemical accessibility self-interruption of synthesis [18]. The conformation of dendrimers at lower generation numbers can be different from higher number generation dendrimers and their conformation in solution is highly dependent on chemical structure and requires analysis on a case-by-case basis. For example, generations 1 and 3 of equilibrated triazine dendrimers in water assume a globular-like configuration with a dense core and flexible surface, generation 5 becomes less spherical but having still dense core, while generations 7 and 9 are porous and open to the penetration to the solvent [19]. As with most polymers, the behaviour of end groups depends on the nature of the terminal groups, in some cases the end groups may be flexible [19] or folded into the interior of the dendrimer [18].

The size and flexibility of structures of many dendrimers prevent the unequivocal determination of their conformation using common experimental techniques. Currently, there are only 15 reported structures of dendrimers determined by X-ray crystallography in the protein data bank (PDB) [20]. There is a significant progress in analysis of dendrimers using NMR from distinguishing the signals of different generations and signal assignments [21, 22] to understanding the dynamics and mobility of dendrimers [23]. However, the full three dimensional structure determination of dendrimers using NMR is still hindered due to the repetitive nature of monomers in each generation of the dendrimer that leads to ambiguous assignments of nOe signals. The use of biophysical and physicochemical techniques can provide information on complexes that dendrimers form with other molecules of interest [24], however the detailed structural information that can be obtained experimentally remains limited.

Due to the large variation in chemical structures of monomers that can be used to prepare dendrimers, it is increasingly difficult to envision their important properties, such as shape, flexibility and interior flexibility. Molecular modelling and simulations has become a powerful tool to probe and model molecular structural information. Molecular modelling has been increasingly used to rationally design dendrimers for biomedical applications with special focus on studying their structure and dynamic response to environment stimulus (e.g. pH change) as well as interactions of dendrimers with other molecules [23, 25–28]. Modelling studies of dendrimers have been conducted using different force fields developed for proteins and small molecules, including CHARMM [29], AMBER [30], CVFF [31], Dreiding [32], GROMOS [33], COMPAS [34] and OPLS [35]. Although these types of molecular modelling studies provide information that corroborate experimental data, it still remains difficult to generate the three dimensional models of relevant dendrimers in silico. This is particularly true for larger generations or for non-regular dendrimers or dendrons with complex structures. Several molecular modelling tools are suited to build regular dendrimers and hyper-branched polymers, namely Starmaker (part of Silico toolkit) [36, 37], Dendrimer Building Toolkit [30], Dendrimer Builder in Materials Studio [38] and HBP builder [39]. However, there are still opportunities to automate process of generation of the structures of more complex dendrimers or dendrons. We have previously developed a method to describe dendrimer structures as a sequence of monomers accompanied by a "connectivity table" [40] for use in generating structure using XPLOR-NIH software [41]. This method still required the manual description of the sequence and the "connectivity table" and thus lacked the automation required for general use. Therefore, there is still a demand for a GUI that allows building frameworks of dendrimers and dendrons with different chemistries and being able to use different force fields in a reliable manner.

This manuscript concerns the description of an algorithm presented in a GUI to generate the sequence of monomers and connectivity tables to be exported to XPLOR to generate topology files of dendrimers and complete 3D structure to be used in MD simulation packages. Additionally, we also provide an automated method to generate 2D structure and smiles of dendrimers for fast prototyping and database management of these macromolecules. Both tools were shown to provide a faster and easier way to assemble dendrimers in preparation for further computational studies.

## Results and discussion

Our approach aims to provide a framework of tools to build dendrimers and dendrons in a reliable and consistent way using two approaches according to the level of parameterization and complexity of the dendrimer required. As with other dendrimer building strategies, the principle is to construct the dendrimer framework from the set of monomers needed to increase the dendrimer generation number.

We focused on tools written in Python language that allow the design of different chemistry templates with varying complexity. In cases where parameterization for further MD simulation of dendrimers is not required and only the assembly is important we provide a GUI to generate 2D mol files of dendrimers (Toolkit 1). When parameterization is required to further model the dendrimers, we created a GUI to automate our previously reported method [40]. This new GUI generates the input file containing the sequence of monomers and their connectivity to be used in XPLOR to generate the pdb and psf files that can then be submitted to MD simulations (Toolkit 2). This tool is not restricted to build large dendrimers but was also focused on being able to build complex dendrimer and dendrons frameworks. For example, a more complex dendrimer may comprise a small number of generations derived from one type of monomer (e.g. flexible, hydrophobic), which is then followed by another type of monomer (e.g. rigid, hydrophilic) with variations of multiplicity and length of linear sequences.

**Toolkit 1: quick generation of 2D mol files**

While generating the 3D structure of dendrimers is a key goal when assembling dendrimers, there are several computational applications that do not require 3D coordinates. Having a quick and reliable way to generate 2D structure of dendrimers in silico is useful for various applications including database management for dendrimers, creation of images, rapid prototyping and in cheminformatics, such as QSAR, data mining and machine learning models. It is therefore useful to have an automated tool for building dendrimers without the need for more complex modelling tools and parameterization. Thus, we developed a GUI using PyQt4 (Fig. 1) using the RDKit library in Python to have a flexible tool to rapidly generate 2D mol files of dendrimers, which include the smiles, a 2D image and a mol file with no coordinates.

RDKit is an open-source cheminformatics software with a large collection of algorithms to perform in silico manipulation of molecules. In particular this library has functions to describe and apply chemical transformations using the SMARTS-based language similar to Daylight's Reaction SMILES [42]. This module is commonly used for virtual chemical library generation to quickly generate big libraries of compounds for virtual high throughput screening [43]. In order to "synthesize" a new compound, the algorithm requires the smiles of both reactants and the reaction between both described in SMARTS language. The functional groups required for the reactions are then mapped onto both precursors and linked accordingly to the description. For example, a generic peptide bond formation can be expressed as an amine ($–CNH_2$) reacting with a carboxyl (–COO) and would be described in SMARTS as [**C**X4][**N**H2].[**C**X3](=0)[**O**X1]>>[**C**X4][**N**X3][**C**X3](=O), where each reactant is separated by a "." and the final product of this reactions is given by the ">>" indicator (in this case –CNCO–). One of the difficulties observed in using this library to assemble dendrimers is that all mapped

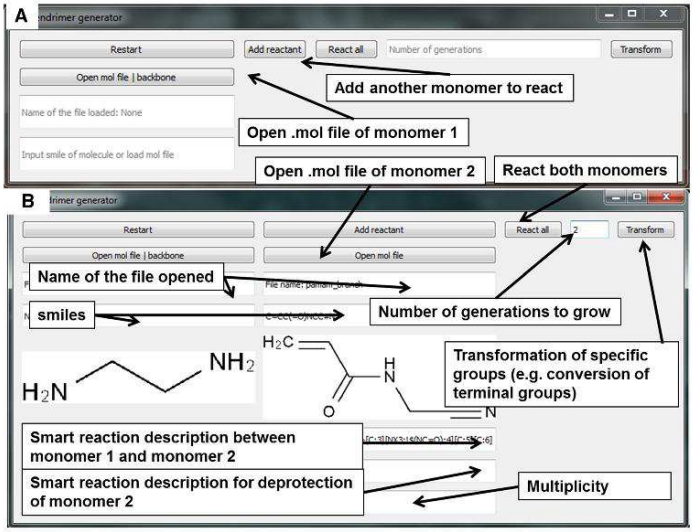


**Fig. 1** Graphical user interface for assembling 2D structures of dendrimers showing a way how to assemble PAMAM dendrimers. The application utilizes mol files of the precursor's monomers and information on how these are reacted using SMARTS reaction description. **a** Snapshot of the GUI of the first step in building a dendrimer and requires an entry to load the core; **b** snapshot of the GUI after adding a reactant and adding relevant information into entry boxes

substructures (all functional groups) would react to give rise to all possible intermediate products which themselves could undergo further reaction. This results in a massive number of products, expensive computational time and it is difficult to retrieve the intended product from the pool of compounds that are generated.

To prevent this issue, we followed the same approach in the synthesis of dendrimers where branch monomers not allowed to react were conjugated with protecting groups (e.g. ester group of a carboxylic) or with groups that would not be mapped by the SMARTS identifier (e.g. a triple bond instead of a double). These protected groups do not undergo reaction to generate side products. Consequently, this allows application of transformation functions available in the RDKit library (.ReactionFromSmarts; .RunReactants; .ReplaceSubstructure) to link all mapped monomers that are allowed to react and obtain the product. This is followed by deprotection of the protecting groups in the newly formed layer, and repetition of the previous reaction until the desired generation is obtained. Since some functional groups can react more than once (e.g. amines), multiplicity has to be set to instruct how many times each group reacts. A specific examples is shown in Fig. 2. A standard procedure goes as follows:

1. Click on open file to open a mol file of the monomer of the core. Once the file is loaded the name of the file is displayed on a text box as well as the smiles of the mol file and an image of the 2d structure of the input mol file. Alternatively, SMILES can be input directly in the text box.
2. Click add reagent and open the mol file of the monomer that will be attached to the core structure. The name of the file, the smiles and the d structure of the input mol file will be displayed.
3. Add the SMARTS reaction between the core and the branching monomers in the corresponding text box.
4. Add the SMARTS reaction for the deprotection reaction of the branching monomers.
5. Add the multiplicity of the reaction and the number of generations intended.
6. Press React all to create the smiles, 2D image of the dendrimer as well as a mol file without 3D coordinates.

Alternatively, a mol file of the dendrimer can be loaded to perform single modification, such as change of the terminal group chemistry by pressing the transform button and executing the SMARTS reaction for this modification. A key limitation of this tool is to achieve the balance between the use of protecting groups and types of reaction between the core and the branching monomers. A way to overcome these problems is by creating different layers of the dendrimer one by one and using it as the backbone input each

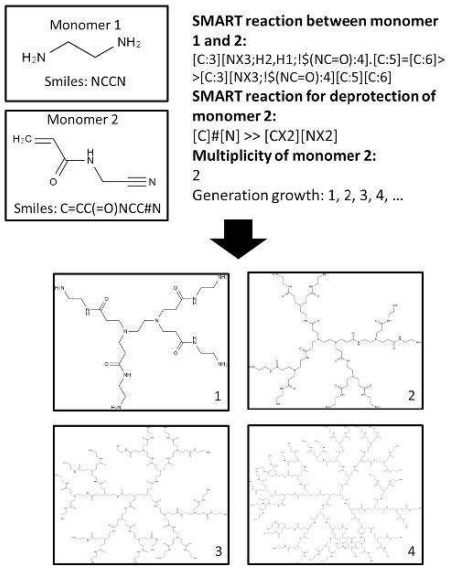


**Fig. 2** Example of 2D structure of a dendrimer generated using the RDKit library. Smiles, SMARTS of the reactions, multiplicity and generation desired were used as the input to generate different generations of a dendrimer. The application generated the smiles, a mol file without coordinates and an image

time. Furthermore, the generation of more complex dendrimers and dendrons can be challenging, since the mol file generated does not have 3D coordinates, random generation of coordinates of higher generations dendrimers leads to entangled branches or monomers and thus not be suited for 3D visualization. Nevertheless, this tool proved to be highly flexible and allowed the rapid prototyping of differently types and families of dendrimers (Fig. 3).

### Toolkit 2: generation of 3D structures for MD simulations

We previously reported a method where dendrimers were described as a linear sequence of monomers and were then assembled through the description of a connectivity table (similar to the creation of a disulfide bond in linear peptides, Figs. 4, 5) [40]. As shown in Fig. 4, a generation 1 polylysine (PLL) dendrimer can be easily described by the core monomer and the two generations monomers translating into a sequence of "core; generation 0: monomer 1 and 2; generation 1: monomer 1,2,3 and 4" for a total of 7 monomers, lysine amino acids. However, contrary to a linear sequence,

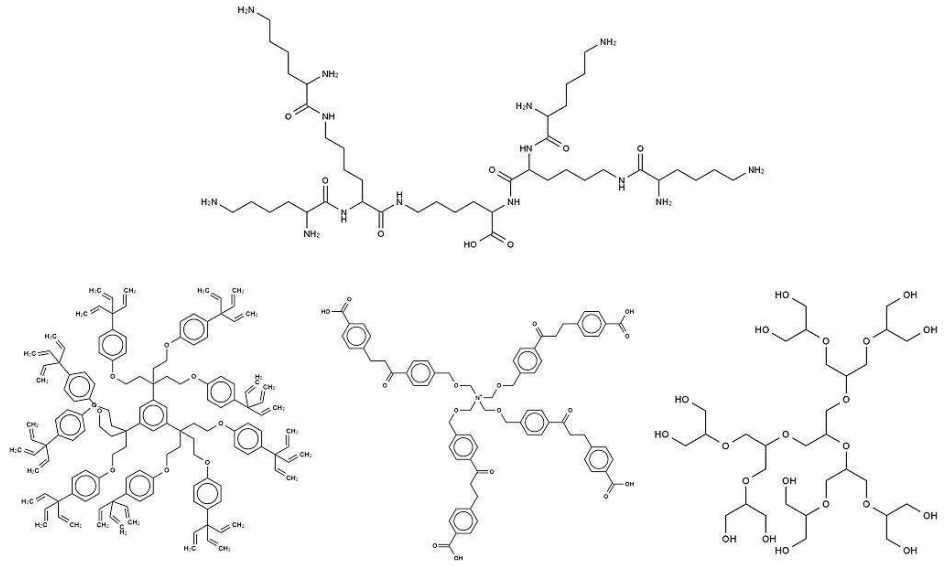

**Fig. 3** Examples of different types of dendrimers generated as 2D mol files using the RDKit module

in order for XPLOR to understand how to assemble the dendrimer sequence, a "connectivity table" has to be provided. In this case of the PLL dendrimers, the monomer 1 (the core) was attached to the monomer 2 (branch 1) through the patch reference 1 (peptide bond through the amine group of the alpha carbon) and the monomer 3 (branch 2) through the patch reference 2 (peptide bond through the amine from the side chain). Then each of the branch monomers was further connected two times with another lysine monomer given the same patch reference. This can be repeated until the intended generation is obtained. Although this can be feasible to describe manually for small generations it becomes increasingly more difficult and prone to errors for higher generations. Consequently, in order to automate this process, we developed a python GUI application using PyQt4 library (Fig. 5) that generates a text file containing the sequence and connectivity table to be used in XPLOR.

Our python toolkit allowed a fast generation of the sequence and the "connectivity table" by using essential information only in an interactive way and resulting in a pdb file with preserved monomer names. Using a classical example, we firstly demonstrate the use of this toolkit on the assemble of PAMAM dendrimers (see Fig. 5). Since XPLOR requires the topology and parameters of the monomers, these had to be generated in the first instance. PDB files of monomers were first generated in Avogadro and used as input on XPLO2D [44] to automatically generate a generic topology and parameters file. Simultaneously, monomers were used as input in ParamChem [45] to assign atom types, charges and bonded parameters of the CHARMM General Force Field (CGenFF). The topology and parameter files were then modified with the ParamChem data. Furthermore, patch references were manually assigned for individual connectivity (all functional groups) between monomers with the parameters given by ParamChem.

The sequence of monomers and the connectivity table were then created using our toolkit (Fig. 5). The toolkit requires the name of the monomers and patch references, as described in the topology file, as well as the multiplicity of the monomers. A standard protocol goes as follows:

1. The first input command requires the name of the first monomer (described as the core) as given in the topology file and its multiplicity (for example 4 in the case of PAMAM core) to which individual patch reference names should be provided. Then press New Layer.
2. Depending on the multiplicity provided in step 1, new entry boxes will open to match the multiplicity, each patch reference between the core and the branching monomers should have individual names since patches between monomers are described individually in the

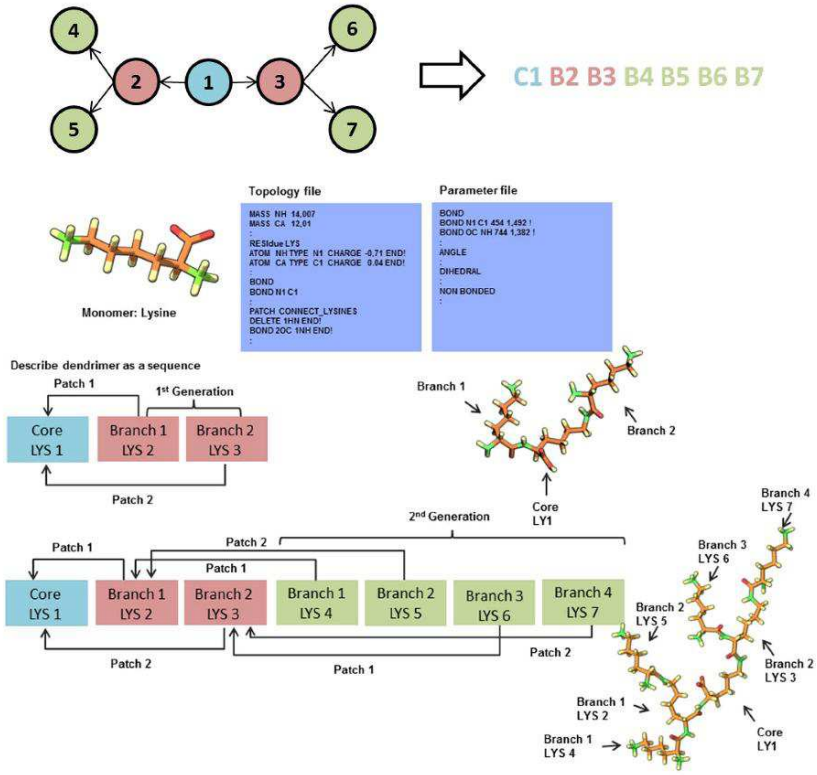


**Fig. 4** Method description for a dendrimer assembly using a linear sequence of monomers and describing how they connect to each other through a "connectivity table"

topology file because atoms are deleted and bonded individually.

3. After, the name of the branching monomer is provided, which in the case of the PAMAM dendrimers is the same for all branching points of the core (in this example named BMA, Fig. 5). Since the toolkit recognizes all the branches monomers as the same name, it will only open a new entry for all of them, asking for the number of generations they are intended to grow. If different names are provided (e.g. different monomers used such as in the case of dendrons) it will open entries for each individual monomer and thus allowing for the versatility of building branched polymers or dendrons. It is important to note that the original names of the monomers are preserved in the final output files.
4. If more than one generation is to be grown then a multiplicity input entry pops up. In this case, multiplicity of 2 was given for the branching monomers and thus two new entry boxes appear to provide the patch reference to connecting the next layer.
5. Again, individual patching references should be given for individual functional group of the monomers.
6. The toolkit then produces an input text file for XPLOR containing the normal instructions for XPLOR to assemble a macromolecule and the sequence of monomers and how they are connected automatically (see Fig. 5).

This protocol showed versatility in types of dendrimers and dendrons that could be built and the types of force fields to be used as parameterization. In particular, since amino

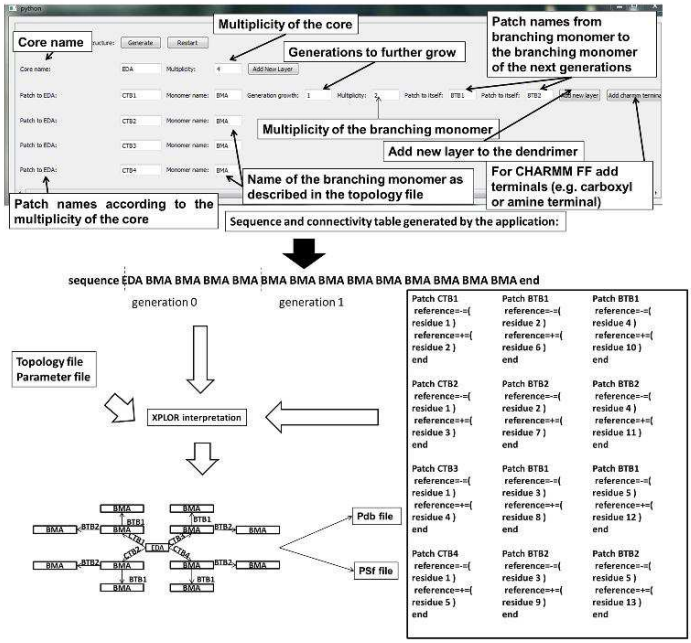


**Fig. 5** Example for PAMAM G1 dendrimer generation using the GUI application to generate the sequence and connectivity table and how XPLOR interprets this information to generate the final 3D structure

acids were already described in XPLOR format using the CHARMM 22 FF and peptide dendrimers are relevant for biomedical applications, we implemented a feature where the caps for the amino acids (e.g. carboxyl or amine) can be added automatically for the terminal groups. To this, once the terminal layer is described we provided a "add charmm terminal" button that opens a new window for an input entry to specify the terminal cap, as described in the topology file.

Overall, this application extended on our previous approach to build dendrimers from sequence [40] allowing a flexible, fast, easy and reliable way to produce not only dendrimers, but also other linear or branched polymers such as dendrons. Depending on the practical use and type of modelling required, there are several ways where the use of this application is beneficial. Comparing to the original method, we improved the automation by making use of XPLO2D [41] to generate generic (indiscrimination of atom types) topology and parameters files with the Engh & Huber ball-park force field [46] (but lacking atom charges) and generation of the sequence and connectivity table automatically. This has considerably decreased the time necessary to assemble the dendrimer. Since XPLOR does not require a dedicated dendrimer force field just to assemble the dendrimer or dendrons, this means that the assembly can be performed just by updating the charges in the topology file provided by XPLO2D (generic atom charges) and by manually describing the patch references. A major advantage of using XPLOR is that during the handle of the simulated annealing protocols it allows atoms to cross over each other, and thus prevents the formation of entangled branches and, if specified, it can provide a fully extended dendrimer. Then once the dendrimer is assembled, the pdb generated can be imported to other software where force field development can be performed (e.g. MAESTRO, AMBER). On the other hand, the topology and parameter files of the monomers can be modified with the desired force field (e.g. CHARMM, OPLS, AMBER) at this early step generate the dendrimer and then use the same files in NAMD to run MD simulations (Fig. 6).

Using this protocol (Fig. 6) we were able to apply our scripts and generate the 3D structure of different classes of polymers (Fig. 7). As depicted in Fig. 7, more complex structures could be generated including *n*-acetyl cysteine terminated PAMAM dendrimers [47] or peptide dendrimers [48] showing the versatility of this tool.

These structures in a pdb can be readily used for further modelling studies and MD simulations using different software packages, such Desmond [49], NAMD [50] and

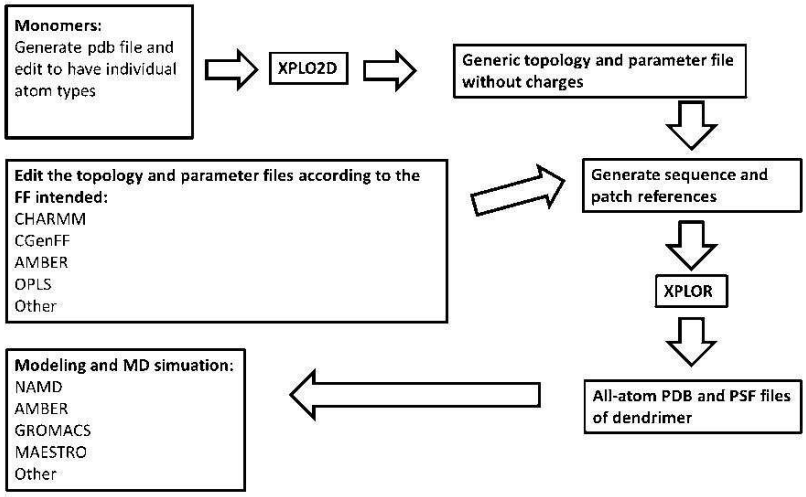


**Fig. 6** Schematic protocol making use of the XPLO2D, XPLOR and our application to quickly and reliably generate dendrimers for MD simulation

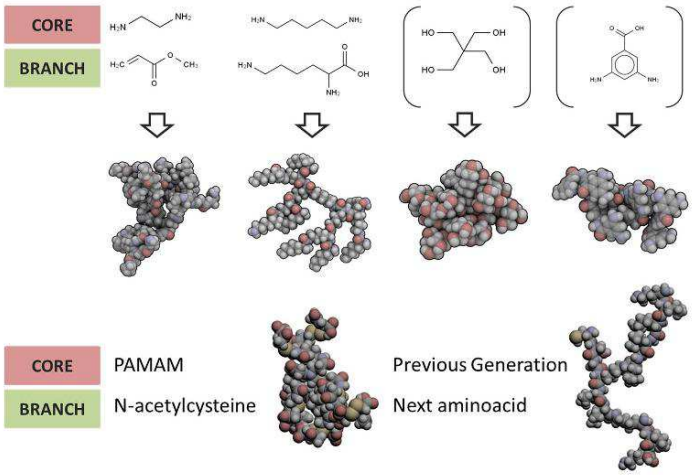


**Fig. 7** Different G0 and G1 dendrimers generated using our protocol. Even without specific force field development, different classes of dendrimers can be easily assembled to generate a pdb file that can then be subsequently used in modelling studies. More complex structures can be generated including differently terminated structures (*N*-acetylcysteine terminated PAMAM dendrimers, *bottom left*) and peptide dendrimers (*bottom right*) should be generated using toolkit 2

XPLOR-NIH [41] with minimal modifications of generated structures and preparation of input files. The same files can be used in preparation of systems for simulation using AMBER [51] and Gromacs [52], albeit after generating adequate topologies and parametrization of the monomers and patches. Some of the examples of simulated systems and results of the simulations using Desmond and NAMD software are shown in the supplementary information (Figs. S1–S6).

Although we focused on dendrimers, this application can be applied to other types of polymers including linear polymers and dendrons, as long as, a specific defined topology is required. In many respects our tools have similarity with already available tools for building dendrimers such as builder in Material Studio [38], Starmaker [36] and DBT [30] tools. These are also able to generate regular dendrimers but are limited when a molecule is not defined solely by a same monomer in higher generations of branches, in a case of dendrimers, or if one or more branches are completely different in cases of dendrons. Dendrimer Builder Tookit (DBT) is a Perl written graphical user interface that uses the antechamber module of AMBER to assemble the dendrimer with a main limitation as it can use only a maximum of three types of monomers to define a core, branches and terminal groups. This prevents building dendrimers with different building blocks in different generations. Starmaker can be used to overcome such limitations, however the attachment point has to be defined for each monomer that can be a complex task without a GUI.

Our toolkit is not suited for the generation of random copolymers, hyperbranched polymers with random branching and dendrigrafts. These features can be found in molecules builders available in Material Studio or HBP [39] and therefore those resources should be used instead.

Our toolkit is particularly useful in cases when only resources that are freely available to academia and industry can be used to generate 3D structures of dendrimers with different monomers in different generations; or to generate dendrons as it is possible to build a molecule comprising individual branches that have different structures.

## Conclusion

Two different GUI applications using a Python were written to rapidly and reliably produce structures of dendrimers and dendrons. The first toolkit is intended for an easy use and intuitive way for rapid prototyping of 2D structures for in silico methods in chemoinformatics. The second toolkit is aimed to further improve and automate our previously published method making it easier to produce 3D structures of higher dendrimer generations and different types of branched macromolecules without having to manually write the connectivity table. The major advantage of both applications is their flexibility for the assembly of monomers to obtain structures of dendrimers, dendrons or linear polymers with defined topologies for further molecular modelling studies.

## Methods

### Generation of 2D mol files and smiles for fast prototyping and database management

A python GUI was built using the PyQt4 library to generate 2D mol files of dendrimers. The core assembly of this application follows the same principles of dendrimers synthesis-wise where protected monomers (e.g. ester forms of carboxyl groups) are used and subsequently deprotected for the next layer to be added. This interface takes mol files or smiles to describe the monomers and interprets them using the RDKit library package [43]. These were then subsequently reacted by providing the SMARTS reaction description [42] on how to connect both monomers and how to deprotect the monomers for subsequent layer. Once the SMARTS reaction description was mapped onto the monomers, it connected all identified groups and in cases where each group reacted multiple times (e.g. amines), a multiplicity value was provided. In cases where the modification of terminal groups was required (e.g. change of amines to carboxyl) the assembled dendrimer could then be imported again as a mol file, and the mapped groups changed to any other desired group. This application produced 2D mol files that could then be imported to different modelling software packages (e.g. Avogadro, Maestro/Desmond, Gabedit) where parameterization and molecular simulations could be performed. Furthermore, smiles as well as rendered png 2D images of the assembled dendrimers were produced, which can be used for database management of dendrimers.

### Generation of 3D pdb and psf files of dendrimers using an automated tool for generation of a linear sequence and connectivity table

The assembly of 3D dendrimers followed a similar protocol previously published by our group [40]. Monomers' topology and parameter files in the XPLOR format were automatically generated using XPLO2D [53], and subsequently manually modified according to the CGenFF by ParamChem [45] or simply by adding charges calculated using the HF/6-31G* ESP method. For peptide dendrimers, the topology and parameters were already described in XPLOR format using the CHARMM22 force field and therefore were used without modification. The connection between monomers was described as patch references by describing the charges, atom types and the angles formed as previously reported [40].

A GUI application was written in Python using the PyQt4 library to produce the XPLOR input file containing the sequence and "connectivity table" of the desired dendrimers. The application takes the name of the core, the core's multiplicity, the name of the patches to connect to

the core, the name of the branch, multiplicity of the branch monomers as well as the number of generations to grow. The text file created containing the instructions to XPLOR with the sequence of monomers and the "connectivity table" was used as input in XPLOR-NIH similarly to the previously published method [40]. The 3D structure of dendrimers was obtained as a pdb and psf file, which could be further simulated using Gromacs [52], NAMD [50] or MAESTRO using DESMOND [49].

**Acknowledgements** Nuno Martinho is thankful for the funding from FCT (Fundação para a Ciência e Tecnologia) with a doctoral fellowship (SFRH/BD/87838/2012) and iMed.ULisboa grant (UID/DTP/04138/2013). L.C. Silva acknowledges funding from Investigador FCT 2014 (IF/00437/2014), Portugal. Teresa Barata and Steve Brocchini are grateful for funding from the UK Engineering & Physical Sciences Research Council (EPSRC) for the EPSRC Centre for Innovative Manufacturing in Emergent Macromolecular Therapies. Financial support from the consortium of industrial and governmental users for the EPSRC Centre is also acknowledged. Steve Brocchini is grateful for funding from the National Institute of Health Research (NIHR) Biomedical Research Centre at Moorfields Hospital NHS Foundation Trust and UCL Institute of Ophthalmology, Moorfields Special Trustees, the Helen Hamlyn Trust (in memory of Paul Hamlyn), Medical Research Council, Fight for Sight and Freemasons Grand Charity. Mire Zloh acknowledges support by University of Hertfordshire.

## References

1. Svenson S, Tomalia DA (2005) Dendrimers in biomedical applications: reflections on the field. Adv Drug Deliv Rev 57:2106–2129. doi:10.1016/j.addr.2005.09.018
2. Astruc D, Boisselier E (2010) Dendrimers designed for functions: from physical, photophysical, and supramolecular properties to applications in sensing, catalysis, molecular electronics, photonics, and nanomedicine. Chem Rev 110:1857–1959
3. Dong S, Zheng B, Wang F, Huang F (2014) Supramolecular polymers constructed from macrocycle-based host–guest molecular recognition motifs. Acc Chem Res 47:1982–1994. doi:10.1021/ar5000456
4. Kalomiraki M, Thermos K, Chaniotakis NA (2016) Dendrimers as tunable vectors of drug delivery systems and biomedical and ocular applications. Int J Nanomed 11:1–12. doi:10.2147/IJN.S93069
5. Ghosh S, Chakraborty P, Chakrabarti A et al (2016) Biological activity of dendrimer-methylglyoxal complexes for improved therapeutic efficacy against malignant cells. RSC Adv 6:6631–6642. doi:10.1039/C5RA23477H
6. Tanis I, Karatasos K (2009) Association of a weakly acidic anti-inflammatory drug (ibuprofen) with a poly(amidoamine) dendrimer as studied by molecular dynamics simulations. J Phys Chem B 113:10984–10993. doi:10.1021/jp9039176
7. Al-Jamal KT, Al-Jamal WT, Wang JTW et al (2013) Cationic poly-L-Lysine dendrimer complexes doxorubicin and delays tumor growth in vitro and in vivo. ACS Nano 7:1905–1917. doi:10.1021/nn305860k
8. Hsu H-J, Bugno J, Lee S, Hong S (2017) Dendrimer-based nanocarriers: a versatile platform for drug delivery. Wiley Interdiscip Rev 9:e1409. doi:10.1002/wnan.1409
9. Luong D, Kesharwani P, Deshmukh R et al (2016) PEGylated PAMAM dendrimers: enhancing efficacy and mitigating toxicity for effective anticancer drug and gene delivery. Acta Biomater 43:14–29. doi:10.1016/j.actbio.2016.07.015
10. Nguyen TTC, Nguyen CK, Nguyen TH, Tran NQ (2017) Highly lipophilic pluronics-conjugated polyamidoamine dendrimer nanocarriers as potential delivery system for hydrophobic drugs. Mater Sci Eng C 70:992–999. doi:10.1016/j.msec.2016.03.073
11. Brown CW, Buckhout-White S, Díaz SA et al (2017) Evaluating dye-labeled dna dendrimers for potential applications in molecular biosensing. ACS Sensors 2:401–410. doi:10.1021/acssensors.6b00778
12. Cai X, Zhu H, Zhang Y, Gu Z (2017) Highly efficient and safe delivery of VEGF siRNA by bioreducible fluorinated peptide dendrimers for cancer therapy. ACS Appl Mater Interfaces 9:9402–9415. doi:10.1021/acsami.6b16689
13. Barata TS, Teo I, Brocchini S et al (2011) Partially glycosylated dendrimers block MD-2 and prevent TLR4-MD-2-LPS complex mediated cytokine responses. PLoS Comput Biol. doi:10.1371/journal.pcbi.1002095
14. Öztürk K, Esendağlı G, Gürbüz MU et al (2017) Effective targeting of gemcitabine to pancreatic cancer through PEG-cored Flt-1 antibody-conjugated dendrimers. Int J Pharm 517:157–167. doi:10.1016/j.ijpharm.2016.12.009
15. Jatczak-Pawlik I, Gorzkiewicz M, Studzian M et al (2017) Sugar-modified poly(propylene imine) dendrimers stimulate the NF-κB pathway in a myeloid cell line. Pharm Res 34:136–147. doi:10.1007/s11095-016-2049-3
16. Arima H, Motoyama K, Higashi T (2017) Potential therapeutic application of dendrimer/cyclodextrin conjugates with targeting ligands as advanced carriers for gene and oligonucleotide drugs. Ther Deliv 8:215–232. doi:10.4155/tde-2016-0064
17. Li N, Li N, Yi Q et al (2014) Amphiphilic peptide dendritic copolymer-doxorubicin nanoscale conjugate self-assembled to enzyme-responsive anti-cancer agent. Biomaterials 35:9529–9545. doi:10.1016/j.biomaterials.2014.07.059
18. Jishkariani D, MacDermaid CM, Timsina YN et al (2017) Self-interrupted synthesis of sterically hindered aliphatic polyamide dendrimers. Proc Natl Acad Sci USA 114:E2275–E2284. doi:10.1073/pnas.1700922114
19. Raut S, Enciso AE, Pavan GM et al (2017) Intrinsic fluorescence of triazine dendrimers provides a new approach to study dendrimer structure and conformational dynamics. J Phys Chem C 121:6946–6954. doi:10.1021/acs.jpcc.6b11110
20. Berman HM, Westbrook J, Feng Z et al (2000) The protein data bank. Nucleic Acids Res 28:235–242
21. Zloh M, Ramaswamy C, Sakthivel T et al (2005) Investigation of the association and flexibility of cationic lipidic peptide dendrons by NMR spectroscopy. Magn Reson Chem 43:47–52. doi:10.1002/mrc.1508
22. Pinto LF, Riguera R, Fernandez-Megia E (2013) Stepwise filtering of the internal layers of dendrimers by transverse-relaxation-edited NMR. J Am Chem Soc 135:11513–11516. doi:10.1021/ja4059348
23. Pinto LF, Correa J, Martin-Pastor M et al (2013) The dynamics of dendrimers by NMR relaxation: interpretation pitfalls. J Am Chem Soc 135:1972–1977. doi:10.1021/ja311908n
24. Alberto R, Joao R, de los Angeles M-F et al (2017) Principal physicochemical methods used to characterize dendrimer molecule complexes used as genetic therapy agents, nanovaccines or drug carriers. Curr Pharm Des 23:1–1. doi:10.2174/1381612823666170220164535
25. Martinho N, Florindo H, Silva L et al (2014) Molecular modeling to study dendrimers for biomedical applications. Molecules 19:20424–20467. doi:10.3390/molecules191220424
26. Kim SH, Lamm MH (2012) Multiscale modeling for host-gues chemistry of dendrimers in solution. Polymers 4:463–485

27. Bello M, Fragoso-Vázquez J, Correa-Basurto J (2017) Theoretical studies for dendrimer-based drug delivery. Curr Pharm Des 23:1–1. doi:10.2174/1381612823666170228142429
28. Ahmed S, Vepuri SB, Kalhapure RS, et al (2016) Interactions of dendrimers with biological drug targets: reality or mystery: a gap in drug delivery and development research. Biomater Sci 4:1032–1050. doi:10.1039/C6BM00090H
29. Barata TS, Shaunak S, Teo I et al (2011) Structural studies of biologically active glycosylated polyamidoamine (PAMAM) dendrimers. J Mol Model 17:2051–2060. doi:10.1007/s00894-010-0907-1
30. Maingi V, Jain V, Bharatam PV, Maiti PK (2012) Dendrimer building toolkit: model building and characterization of various dendrimer architectures. J Comput Chem 33:1997–2011. doi:10.1002/jcc.23031
31. Quintana A, Raczka E, Piehler L et al (2002) Design and function of a dendrimer-based therapeutic nanodevice targeted to tumor cells through the folate receptor. Pharm Res 19:1310–1316
32. Liu Y, Bryantsev VS, Diallo MS, Goddard WA (2009) PAMAM dendrimers undergo pH responsive conformational changes without swelling. J Am Chem Soc 131:2798–2799. doi:10.1021/ja8100227
33. Javor S, Reymond J-L (2009) Molecular dynamics and docking studies of single site esterase peptide dendrimers. J Org Chem 74:3665–3674. doi:10.1021/jo802743c
34. Razmimanesh F, Amjad-Iranagh S, Modarress H (2015) Molecular dynamics simulation study of chitosan and gemcitabine as a drug delivery system. J Mol Model 21:165. doi:10.1007/s00894-015-2705-2
35. Roberts BP, Krippner GY, Scanlon MJ, Chalmers DK (2009) Molecular dynamics of variegated polyamide dendrimers. Macromolecules 42:2784–2794. doi:10.1021/ma8021579
36. Chalmers DK, Roberts BPS, A perl molecular toolkit. http://silico.sourceforge.net
37. Naylor AM, Goddard WA, Kiefer GE, Tomalia DA (1989) Starburst dendrimers: 5. Molecular shape control. J Am Chem Soc 111:2339–2341
38. Vacas-Córdoba E, Maly M, De Mata FJ, Gómez R et al (2016) Antiviral mechanism of polyanionic carbosilane dendrimers against HIV-1. Int J Nanomed 11:1281–1294
39. Yu C, Ma L, Li S et al (2016) HBP Builder: a tool to generate hyperbranched polymers and hyperbranched multi-arm copolymers for coarse-grained and fully atomistic molecular simulations. Sci Rep 6:1–15. doi:10.1038/srep26264
40. Barata TS, Brocchini S, Teo I et al (2011) From sequence to 3D structure of hyperbranched molecules: application to surface modified PAMAM dendrimers. J Mol Model 17:2741–2749. doi:10.1007/s00894-011-0966-y
41. Schwieters CD, Kuszewski JJ, Tjandra N, Marius Clore G (2003) The Xplor-NIH NMR molecular structure determination package. J Magn Reson 160:65–73. doi:10.1016/S1090-7807(02)00014-9
42. Daylight SMARTS: A language for describing molecular patterns
43. Landrum G RDKit: Open-source chemoinformatics
44. Kleywegt G, Jones T (1997) Model-building and refinement practice. Methods Enzymol 277:208–230
45. ParamChem
46. Kleywegt G (2005) XPLO2D manual
47. Mishra MK, Beaty CA, Lesniak WG et al (2014) Dendrimer brain uptake and targeted therapy for brain injury in a large animal model of hypothermic circulatory arrest. ACS Nano 8:2134–2147
48. Kwok A, Eggimann GA, Reymond J-L et al (2013) Peptide dendrimer/lipid hybrid systems are efficient dna transfection generations reagents: relationships highlight the role of charge distribution across dendrimer. ACS Nano 7:4668–4682
49. Bowers KJ, Sacerdoti FD, Salmon JK, et al (2006) Molecular dynamics: scalable algorithms for molecular dynamics simulations on commodity clusters. In: Proceedings of the 2006 ACM/IEEE conference on supercomputing (SC'06). doi:10.1145/1188455.1188544
50. Phillips JC, Braun R, Wang W et al (2005) Scalable molecular dynamics with NAMD. J Comput Chem 26:1781–1802. doi:10.1002/jcc.20289
51. Case DA, Cheatham TE, Darden T et al (2005) The Amber biomolecular simulation programs. J Comput Chem 26:1668–1688. doi:10.1002/jcc.20290
52. Berendsen HJC, van der Spoel D, van Drunen R (1995) GROMACS: a message-passing parallel molecular dynamics implementation. Comput Phys Commun 91:43–56. doi:10.1016/0010-4655(95)00042-E
53. Kleywegt G, Jones T (1998) Databases in protein crystallograhy. Acta Cryst D 54:1119–1131

**PAPER 3 (Results) – Rational design of novel, fluorescent, tagged glutamic acid dendrimers with different terminal groups and in silico analysis of their properties**

International Journal of Nanomedicine

Dovepress
open access to scientific and medical research

Open Access Full Text Article

ORIGINAL RESEARCH

# Rational design of novel, fluorescent, tagged glutamic acid dendrimers with different terminal groups and in silico analysis of their properties

Nuno Martinho[1–3]
Liana C Silva[1,4]
Helena F Florindo[1]
Steve Brocchini[2]
Mire Zloh[3]
Teresa S Barata[2]

[1]Research Institute for Medicines (iMed.ULisboa), Faculty of Pharmacy, Universidade de Lisboa, Lisbon, Portugal; [2]Department of Pharmaceutics, UCL School of Pharmacy, London, [3]School of Life and Medical Sciences, University of Hertfordshire, Hatfield, UK; [4]Centro de Química-Física Molecular and IN – Institute of Nanoscience and Nanotechnology, Instituto Superior Técnico, Universidade de Lisboa, Lisboa, Portugal

**Abstract:** Dendrimers are hyperbranched polymers with a multifunctional architecture that can be tailored for the use in various biomedical applications. Peptide dendrimers are particularly relevant for drug delivery applications due to their versatility and safety profile. The overall lack of knowledge of their three-dimensional structure, conformational behavior and structure–activity relationship has slowed down their development. Fluorophores are often conjugated to dendrimers to study their interaction with biomolecules and provide information about their mechanism of action at the molecular level. However, these probes can change dendrimer surface properties and have a direct impact on their interactions with biomolecules and with lipid membranes. In this study, we have used computer-aided molecular design and molecular dynamics simulations to identify optimal topology of a poly(L-glutamic acid) (PG) backbone dendrimer that allows incorporation of fluorophores in the core with minimal availability for undesired interactions. Extensive all-atom molecular dynamic simulations with the CHARMM force field were carried out for different generations of PG dendrimers with the core modified with a fluorophore (nitrobenzoxadiazole and Oregon Green 488) and various surface groups (glutamic acid, lysine and tryptophan). Analysis of structural and topological features of all designed dendrimers provided information about their size, shape, internal distribution and dynamic behavior. We have found that four generations of a PG dendrimer are needed to ensure minimal exposure of a core-conjugated fluorophore to external environment and absence of undesired interactions regardless of the surface terminal groups. Our findings suggest that NBD-PG-G4 can provide a suitable scaffold to be used for biophysical studies of surface-modified dendrimers to provide a deeper understanding of their intermolecular interactions, mechanisms of action and trafficking in a biological system.

**Keywords:** dendrimers, peptide dendrimers, molecular dynamics, fluorescence, CHARMM, structure-activity, surface properties

## Introduction

Dendrimers belong to a class of hyperbranched polymers with well-defined radial architecture that has been extensively studied for biomedical applications.[1] The topology of dendrimers can be described by their core, internal branches (or spacers) and terminal groups. By using various monomers to build different topological architectures, it is possible to design their size, their shape, the surface groups available for interaction and overall physicochemical properties.[2–4] Similar to other drug delivery systems, one of the key requirements is to have an adequate safety profile.[5] In this regard, peptide dendrimers consisting of natural amino acids are attractive candidates for use in biological systems due to their potential biodegradability and biocompatibility.[6] Peptide dendrimers can be synthesized either by linear combinations of amino acids

Correspondence: Mire Zloh
School of Life and Medical Sciences, University of Hertfordshire, College Lane, Hatfield AL10 9AB, UK
Email m.zloh@herts.ac.uk

Teresa S Barata
Department of Pharmaceutics, UCL School of Pharmacy, 29/39 Brunswick Square, London WC1N 1AX, UK
Email t.barata@ucl.ac.uk

submit your manuscript | www.dovepress.com
Dovepress
http://dx.doi.org/10.2147/IJN.S135475

assembled at a branching point[7,8] or by using amino acids as focal branching points themselves (eg, glutamic acid [GLU],[9] lysine [LYS][10,11] and aspartic acid[12]). Owing to side chain size and the combination of amino acids, these peptide dendrimers might have an asymmetric arrangement that will create different local microenvironments within the dendrimer and be suitable to different surface modifications.[13–15]

Although extensively studied, the mechanism of action of bioactive dendrimers is still difficult to probe experimentally.[16] One way to track dendrimers during their interaction with biomolecules and cells is to conjugate a fluorescent probe at the surface of these carriers. However, there are two main drawbacks of using this approach. First, fluorescent probes may randomly be distributed at the surface. This would result in a heterogeneous population of dendrimers, ranging from non-labelled dendrimers to dendrimers with multiple fluorophores, where the proximity between the probes might lead to possible quenching effects.[17] Second, the fluorophore probes can themselves interact with cells and interfere or mask the real interaction of dendrimers with these biological systems.[18,19] Furthermore, the targeted drug delivery achieved by conjugation of different monomers to surface groups[13,14] may be affected by the introduction of a fluorophore on the surface.

In order to avoid this kind of interferences, phosphorus dendriplexes with a fluorophore attached to the core have been synthesized to study their interaction with cells.[20] Thus, designing dendrimers that have a defined number of probes that are hindered from the external environment is of uppermost importance. However, there is still an overall lack of knowledge of the behavior of these molecules at the atomistic level,[8] and consequently, computational methods can provide a suitable tool to explore the behavior of these macromolecules.

Prediction and rationalization of the 3D structure of dendrimers can be a difficult task due to their structural complexity and due to the lack of a dedicated force field (FF). The latter is particularly difficult to develop due to the diversity and high degree of chemical space that dendrimers encompass. Several degrees of complexity from coarse grained to full-atom simulations[21,22] have been utilized to understand how dendrimers interact with drugs and other biomolecules at the molecular interface. In this regard, molecular dynamics (MD) simulations have been shown to be a suitable method to predict the behavior of dendrimers and structure[15,22] and therefore are useful for the rational design of dendrimers.

The aim of this work was to study the potential of a poly(L-glutamic acid) (PG) dendrimer backbone for its ability to incorporate a fluorophore (of different size) into its core. The goal of this approach was to determine the generation at which the fluorophore can be protected from the external environment, thus ensuring that the probe does not interfere with the interaction of PG dendrimers with other biomolecules. Furthermore, different surface modifications were studied to determine their overall effect on the structural properties of the modified core dendrimers. We have used all-atom MD simulations using the CHARMM FF as an FF suitable to study structural properties of dendrimers.[23] These simulations were used to describe the structure and conformational behavior of PG dendrimers, as well as the effects of modifying the dendrimer core by attaching different size fluorophores, namely, nitrobenzoxadiazole (NBD) or Oregon Green 488 (ORG). NBD was chosen due to its small size and optical properties that are suitable to monitor polarity changes in the surrounding environment, whereas the ORG was selected due to its bigger size and suitable spectroscopic properties to be used in monitoring cell events. We further evaluated the effects of diverse terminal groups with different charges on the structure of the dendrimers by using GLU, LYS or tryptophan (TRP; Figure 1). This study demonstrates the use of MD simulation to provide an insight into the versatility of the PG dendrimers that can be further explored for different biomedical applications.

## Methods

### Monomer parameterization

Sets of parameters for GLU, LYS and TRP residues were prepared to be compatible with CHARMM 36a FF. These parameters, already available in the XPLOR format as CHARMM 22 FF, were updated to match the syntax of the CHARMM 36a. Moreover, additional parameters were added for a peptide bond between the side chain of the GLU and a new residue using a procedure similar to one previously reported in the literature.[24] The topology blocks and parameters for NBD and ORG were obtained using ParamChem,[25,26] assuming the transferability of the CGenFF FF and its compatibility with CHARMM 36a FF.[25,26] The patches for new bonds between both fluorophores and GLU residues were assigned using ParamChem, ensuring that the overall charge was maintained.

### Dendrimer assembly and equilibration

Initial dendrimer structures were generated by their in silico assembly, resembling their divergent synthesis (from core to terminal groups). The dendrimers were written as a sequence of monomers, and the patches for their assembly

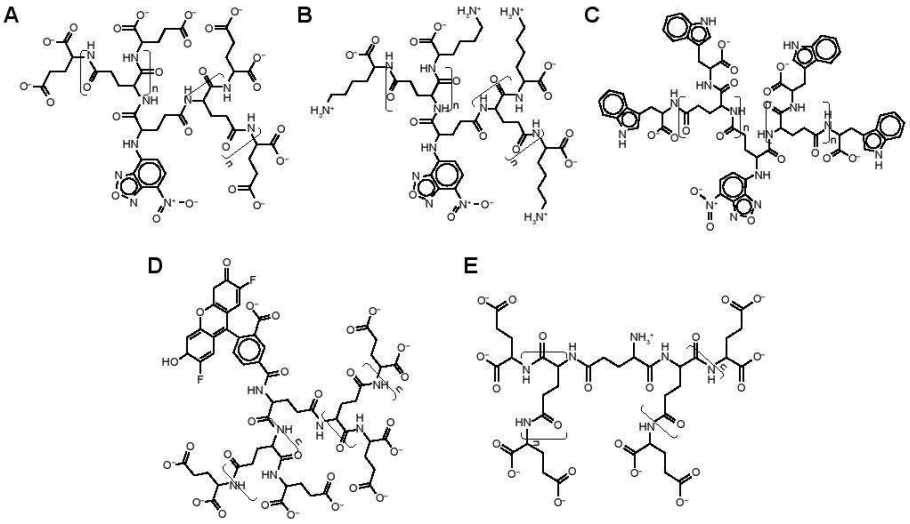


**Figure 1** Chemical structures of PG dendrimers with different cores and terminal groups.
**Notes:** The following nomenclature were used to name the dendrimers: core – internal monomers – terminal monomers. NBD-PG-GLU (**A**), NBD-PG-LYS (**B**), NBD-PG-TRP (**C**), ORG-PG-GLU (**D**)and $NH_2$-PG-GLU (**E**).
**Abbreviations:** PG, poly(L-glutamic acid); NBD, nitrobenzoxadiazole; GLU, glutamic acid; LYS, lysine; TRP, tryptophan.

were prepared using a previously published procedure[27] implemented in scripts for automation.[28] The first monomer of GLU served as a trifunctional selective core, in which two focal points (carboxyl groups) were used for branching, while the third one (amine group) was used to connect a selected fluorophore. Files to generate the 3D structures of dendrimers containing the sequences of monomers (eg, NBD GLU GLU GLU …) and the connectivities established between the monomer residues through the description of patches were prepared as input files for XPLOR. These were then used in the XPLOR v3.4[29] to generate the 3D structure of the dendrimer through a series of simulated annealing protocols in a vacuum. The peptide bonds were kept in a *trans* conformation by introducing restraints since this is the most likely conformation to occur in hyperbranched dendrimers due to their peptidic nature.

Dendrimers were then immersed in a TIP3P water box model, with a distance between 15 and 20 Å in all directions, using the solvate module in VMD v.1.9.1, followed by the addition of ions, enough to neutralize the charge of the system and obtain a NaCl concentration of 150 mM, using autoionize module. The solvated system was then submitted to minimization and simulated annealing protocol in NAMD v.2.9[30] using periodic boundary conditions. The system was heated up to 500 K to remove a possible misfolding of the dendrimer by increasing the temperature 5 K each time and simulating for 1,000 fs at 1 fs/step for each temperature increase. The system was then cooled down in a similar way to 310 K. This also allowed rectifying steric clashes due to inappropriate contacts of water with the dendrimer.[2]

## MD settings

Production runs were carried out in NAMD v.2.9.[30] Dendrimers were first minimized for 2,500 steps through a steepest-descendent minimization. Each dendrimer was then submitted to MD simulation run for 45 ns at a constant pressure of 1 bar. Each run was performed with periodic boundary conditions and the integration step of 2 fs/step. The temperature was kept constant at 310 K using Langevin thermostat with a coupling constant of 5 $ps^{-1}$, and the integration time step was 2 fs. The SHAKE algorithm was used to keep all covalent bonds at their equilibrium value. Electrostatics were evaluated using smooth particle mesh Ewald (PME) method with the van der Waals (vdW) cutoff defined as 12 Å, with a pair list of 10 Å and a real space cutoff of 14 Å.

## Analysis

The obtained trajectories were analyzed using VMD, XPLOR, PyMOL, Bio3D,[31,32] ProDy, MDTraj and in-house tools. The end of equilibration of the simulations for each system was assessed using a radius of gyration and root-mean-square deviation (RMSD). The trajectories of production runs were analyzed by calculating a range of molecular properties, including solvent surface accessible area, monomer density distribution, hydrogen interactions and shape properties.

### RMSD and root-mean-square fluctuation (RMSF)

The RMSD was calculated using all dendrimer atoms to quantify the dissimilarity of the two structures once superimposed. The similarity between conformers was calculated after translational and rotational superimposition of structures.[33] The RMSD values of superimposed structures were calculated using the following equation:

$$\mathrm{RMSD}(A, B) = \sqrt{\frac{1}{N}\sum_{i=1}^{N}(r_i(A) - r_i(B))^2} \quad (1)$$

where $r_i(A)$ and $r_i(B)$ are the Cartesian coordinates of the $i$th atom in the conformations $A$ and $B$ and $N$ is the total number of atoms. Contrary to symmetric peptide dendrimers,[33] no special overlap rules have to be introduced during RMSD measurement. In fact, PG dendrimers are asymmetric as they contain the fluorophore, and thus, the superimposition always occurs between the correct monomers.

### Principal component analysis (PCA)

PCA was performed to reduce the dimensionality of the data and identify the conformational space that a molecule occupies during the simulation. The translational and rotational motions of all alpha carbon atoms (since they are common in all the amino acids used) were eliminated by superimposing the structures, and the $3N \times 3N$ covariance matrix was created with the Cartesian coordinates (Equation 2). The sets of eigenvectors and eigenvalues that represent the motion were generated by the diagonalization of the covariance matrix.[34,35] PCA was performed on the last 10 ns of each production simulation. The covariance matrix was defined as:

$$C = <(x(t) - <x>)(x(t) - <x>)^T> \quad (2)$$

where $<>$ denotes the average ensemble and $x(t)$ is the structure at time $t$.

### Radius of gyration ($R_g$)

The radius of gyration was calculated from the gyration tensor, a size descriptor based on the distribution of atoms from the center of mass (cm; Figure 2):

The diagonalization of the matrix renders the principal axis, $\lambda_1$, $\lambda_2$, $\lambda_3$ (Equation 4), where

$$Tr\, S = \lambda_1 + \lambda_2 + \lambda_3 = R_g^2 \quad (3)$$

These eigenvalues correspond to the variances of the coordinates along the principal axes and were used to calculate other related shape properties.

Alternatively, the size of the dendrimer (when it reaches a spherical entity) can be measured by the embedding sphere radius ($R$) or span (Equation 4). This was measured by calculating the farthest atoms from the center of mass, ie, the radius that encompasses completely all atoms of the molecule:[36]

$$R = \max_i r_i \quad (4)$$

where $r_i$ is the distance of the $i$th atom from the center of mass.

### Hydration radius ($R_H$)

Hydration radius ($R_H$) is a representation of an effective radius for molecules, and it can be correlated to experimental data, such as viscosity or pulsed field gradient spin-echo NMR.[11] The values of $R_H$ for both symmetric and asymmetric branching dendrimers were calculated from $R_H = \sqrt{\frac{5}{3}}R_g$, using $R_g$.[11,37] Additionally, $R_H$ was evaluated by measuring

$$S = \frac{1}{N}\begin{pmatrix} \sum_i (x_i - x_{cm})^2 & \sum_i (x_i - x_{cm})(y_i - y_{cm}) & \sum_i (x_i - x_{cm})(z_i - z_{cm}) \\ \sum_i (x_i - x_{cm})(y_i - y_{cm}) & \sum_i (y_i - y_{cm})^2 & \sum_i (y_i - y_{cm})(z_i - z_{cm}) \\ \sum_i (x_i - x_{cm})(z_i - z_{cm}) & \sum_i (y_i - y_{cm})(z_i - z_{cm}) & \sum_i (z_i - z_{cm})^2 \end{pmatrix} \quad (5)$$

**Figure 2** Matrix for the determination of the distance of atoms from the center of mass averaged for all atoms.
**Note:** The diagonalization of this matrix allows the calculation of the principal axes, which are related to the radius of gyration.

the distribution of water molecules inside the dendrimer and the distance from the center of mass, where the water density reaches 95% of the bulk value.[11] These values were calculated from the radial pair distribution function, determined from the center of mass of the dendrimer, and relate to the different layers of hydration in these dendrimers.

### Solvent accessible surface area (SASA)

SASA was obtained by following the rolling sphere method using a radius of either 1.4 Å for the whole dendrimer or 3 Å for the fluorophore using the SASA module available in VMD.

### Hydrogen bonding

The total number of hydrogen bonds was determined by monitoring the hydrogen bond formation for each frame. Hydrogen bonds were defined using a geometrical criterion with a maximum donor–acceptor distance of 3.5 Å and a hydrogen–donor–acceptor angle inferior to 30°.

### Radial distribution of atoms

The distribution of mass was measured through the radial pair distribution function from either the fluorophore or the center of mass of the whole dendrimer. From these two points, several mass distribution functions were calculated:[38]

1. Distribution of all atoms belonging to the dendrimers
2. Distribution of the terminal groups
3. Distribution of water
4. Distribution of ions

The probability distribution of finding an atom in a spherical volume of radius $r$ from a center of mass, a selected atom or a selected group is given in Equation 6. This probability was measured by

$$\rho(r) = \frac{1}{4\pi r^2} \sum_{i}^{N_a} m_i \delta(r - r_{\text{Com}}) \quad (6)$$

where $N_a$ is the number of atoms, $m_i$ is the $i$th atom mass and $r_{com}$ is the distance from the dendrimer center of mass or alternatively from the fluorophore.

### Shape of dendrimers

The relative shape anisotropy ($\kappa^2$ in Equation 7),[39] or asphericity, was calculated from the eigenvalues of the gyration tensor.

$$\kappa^2 = 1 - \frac{3(\lambda_1\lambda_2 + \lambda_2\lambda_3 + \lambda_1\lambda_3)}{(\lambda_1 + \lambda_2 + \lambda_3)^2} \quad (7)$$

This parameter is limited to the values between 0 and 1. For highly symmetric spherical structures, the value is close to 0, and it reaches 1 for ideal chains (when all points lie on a line). Alternatively, asphericity parameter $b$ can also be calculated (Equation 8),[39] which measures the deviation from a spherical symmetry:

$$b = \lambda_1 - \frac{1}{2}(\lambda_2 + \lambda_3) \quad (8)$$

Analogously, the sphericity index can also describe the deviation from spherical symmetry (Equation 9):

$$\Omega_S = \frac{3 \times \lambda_3}{\lambda_1 + \lambda_2 + \lambda_3} \quad 0 \le \Omega_S \le 1 \quad (9)$$

The values are limited between 0 for flat molecules and 1 to describe perfect spheres.

## Results and discussion

### Generation of PG dendrimers

We have developed a scaffold composed of a PG skeleton by linking fluorophores of different sizes to the core via free amine and adding variable terminal groups to allow functionalization of dendrimers for different applications (Figure 1).

The initial structures of dendrimers were relaxed using a simulated annealing protocol in a vacuum, which resulted in a significant increase in RMSD for all dendrimers within the first few nanoseconds during equilibration. The RMSD change increased in higher generations of dendrimers (Figure S1). This may be attributed to the removal of initial steric clashes between monomers and unfavorable interactions of PG dendrimers with solvent molecules. Depending on the dendrimer generation, simulations took between 5 and 25 ns to equilibrate, which is similar to other dendrimer simulations.[8] Therefore, the last 20 ns of each simulation was used to ensure that the equilibrated systems were used during the evaluation of the properties of PG dendrimers. Despite the possibility of dendrimers being highly flexible and that the RMSD might not by itself indicate that equilibration was truly reached, this sampling should be sufficient to account for the dynamic behavior of PG dendrimers.

### Effect of the presence of a small fluorophore in the dendrimer core

MD simulations were carried out on all PG dendrimers with a free $-NH_3$ group on the core GLU and with a small fluorophore (NBD) attached to the core GLU to reveal the lowest



**Note**: Equation 6 should read as:

$$\rho(r) = \frac{1}{4\pi r^2} \sum_{i}^{N_a} m_i \delta(r_i - r_{com})$$

generation of the dendrimer in which the fluorophore was fully hidden from the solvent.

The radius of gyration and hydration radius, the ratio between the gyration tensors, the relative shape anisotropy and asphericity were calculated to evaluate the differences in the overall size and shape of the dendrimers following the incorporation of the NBD to the PG core. The size of the dendrimers can be represented by its radius of gyration ($R_g$). These values showed to be constant for each dendrimer throughout the trajectories, suggesting that there is no significant variation of the size of dendrimers due to the change in their conformations. Moreover, no significant differences in size between the $NH_3$- and NBD-PG series were observed as exemplified by their maximum radius ($R_{max}$; Table 1). The distribution of $R_g$ follows a normal distribution with a narrow variation in size indicating no major shift in the conformation throughout the simulation time (Table 1 and Figure 3, top).

The $R_g$ for both series increased exponentially with the number of generations and molecular weight (MW). This is a common observation in dendrimers and results from the increase in MW being much faster than the molecular volume. This also indicated that no restrictions in an incremental increase of generations due to a higher number of terminal groups were observed.

These similarities are also reflected in the snapshots of the vdW representation of these PG dendrimers (Figure 3, bottom). Similar to the previously described peptide poly-L-lysine (PLL) dendrimers,[11] PG dendrimers become spherical at higher generations and have a porous structure. This type of architecture is useful as there is potential to incorporate drug molecules within the dendrimer[40] and can adopt different conformations. Even at G4, NBD-PG dendrimers showed different conformations, ranging from a more tubular form with the extension of a single branch, exposing the interior of the dendrimer to a more spherical and compact structure (Figures S2 and S3). Since most of the charged groups are located on the surface, the different conformations can lead to distinctive local charge distributions that may affect their interactions with biomacromolecules.

In previous studies, the correlation between the MW and $R_g$ of dendrimers was found to be described by a power law of $R_g \sim MW^X$, where $X$ was found to be equal to 0.34 for spherical particles with an average density of monomers (ie, the similar distribution of monomers throughout the dendrimer).[11,37] The correlation between MW and $R_g$ for both $NH_3$- and NBD-PG dendrimer series was found to have a correlation factor of 0.35 and 0.39, respectively. As a result, the $NH_3$-PG series followed a similar trend to previously studied peptide dendrimers,[37] whereas the NBD-PG series had a slightly higher value of 0.39. This minor difference in the correlation is attributed to the higher density in the core from the NBD without significant changes in the $R_g$.

The $R_H$ values, additional indicators of effective radii, measured by the water distribution showed 5%–20% higher than those calculated directly from the $R_g$ (Table 2). These higher values can be attributed to the porous and extended structure of PG backbone allowing water to penetrate deeply into dendrimer interior and interact strongly with the terminal groups as well. On the other hand, the $R_H$ values calculated from $R_g$ did not consider the properties of terminal groups and their interactions with the water, thus correlating only to the size of the molecules. Overall, both calculations were higher than $R_g$, which is attributed to the presence of higher number of interactions of these dendrimers with water, where the hydration layer at G4 was ~0.7 nm for both dendrimers, with and without NBD. Notably, no significant differences in the radii of gyration, maximum radii and hydration radii were observed at G4.

To further explore the possible differences caused by the introduction of NBD, the shape descriptors of the dendrimers

**Table 1** Radius of gyration ($R_g$), maximum radius ($R_{max}$), hydration radius calculated from the radius of gyration ($R_H$) and hydration radius calculated from water distribution ($R_H$ [95% W])

| Generation | Core | $R_g$ (nm), mean ± SD | $R_{max}$ (nm), mean ± SD | $R_H$ (nm) | $R_H$ (95% W, nm) |
|---|---|---|---|---|---|
| 0 | $NH_3$ | 0.489±0.025 | 0.415±0.033 | 0.631 | 0.715 |
| | NBD | 0.497±0.021 | 0.468±0.061 | 0.641 | 0.755 |
| 1 | $NH_3$ | 0.671±0.041 | 0.891±0.090 | 0.866 | 0.905 |
| | NBD | 0.632±0.029 | 0.999±0.104 | 0.816 | 0.945 |
| 2 | $NH_3$ | 0.890±0.045 | 1.238±0.122 | 1.148 | 1.335 |
| | NBD | 0.928±0.030 | 1.239±0.094 | 1.198 | 1.425 |
| 3 | $NH_3$ | 1.131±0.047 | 1.725±0.145 | 1.460 | 1.801 |
| | NBD | 1.148±0.040 | 1.830±0.111 | 1.482 | 1.655 |
| 4 | $NH_3$ | 1.400±0.029 | 2.181±0.121 | 1.807 | 2.051 |
| | NBD | 1.384±0.030 | 2.078±0.318 | 1.786 | 2.045 |

**Abbreviation:** NBD, nitrobenzoxadiazole.

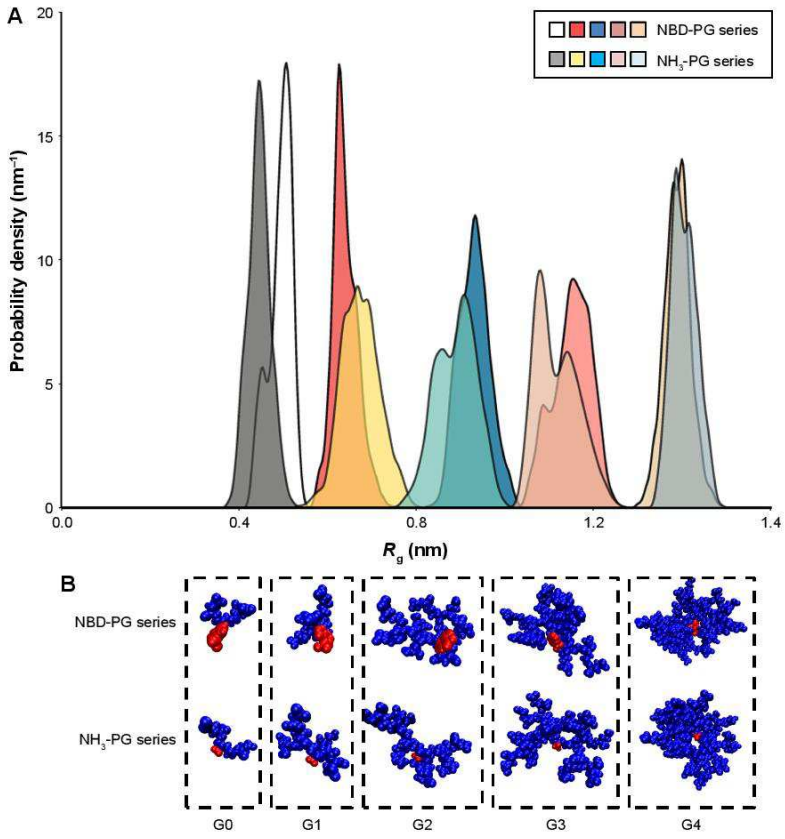


**Figure 3** Effects of the incorporation of the NBD fluorophore into the core of the PG dendrimers.
**Notes:** $R_g$ normal density distribution of $NH_3$-PG and NBD-PG series (**A**). Snapshot conformations taken from trajectories generated during simulations of NBD-PG and $NH_3$-PG dendrimers for generations G0–G4 (**B**). Dendrimers are displayed in vdW representation. Blue color represents the GLU monomers, and red color highlights the NBD and $NH_3$ groups in the core. $R_g$, radius of gyration.
**Abbreviations:** NBD, nitrobenzoxadiazole; PG, poly(L-glutamic acid); vdW, van der Waals.

**Table 2** Comparison of the ratios of the gyration ($R_g$) tensor and the sphericity values ($\Omega$) for generations G0–G4 of two types of PG dendrimers

| Generation | Core | Ratio $R_{gx}:R_{gy}:R_{gz}$ | Ω |
|---|---|---|---|
| 0 | NBD | 1:0.7:0.4 | 0.250 |
| | $NH_3$ | 1:0.9:0.3 | 0.348 |
| 1 | NBD | 1:0.6:0.5 | 0.461 |
| | $NH_3$ | 1:0.8:0.4 | 0.533 |
| 2 | NBD | 1:0.7:0.5 | 0.442 |
| | $NH_3$ | 1:0.8:0.5 | 0.585 |
| 3 | NBD | 1:0.7:0.5 | 0.511 |
| | $NH_3$ | 1:0.8:0.5 | 0.680 |
| 4 | NBD | 1:0.8:0.6 | 0.588 |
| | $NH_3$ | 1:0.9:0.7 | 0.780 |

**Abbreviation:** NBD, nitrobenzoxadiazole.

were calculated. Since the shape of the dendrimers can ultimately contribute to their interaction with the biological target, the decomposition of the radius of gyration tensors is a good approach to explore the distribution of residues in the three dimensions and thus their shape. The ratios of $R_{gy}/R_{gx}$ and $R_{gz}/R_{gx}$ can be used to evaluate the shapes of molecules with values closer to 1, indicating spherical shape for dendrimers at higher generations (Table 2). These ratios ($R_{gy}/R_{gx}$ and $R_{gz}/R_{gx}$) were similar for $NH_3$- and NBD-PG dendrimers at generations G3 and G4, while differences were observed for lower generations (Table 2). This is a result of the significant influence of NBD on the center of

mass and the gyration tensors at lower generations. The increase in generations also resulted in the increase in the spherical shape of the dendrimers, albeit these molecules are not forming a perfect sphere as observed by the differences in the $R_{g2}/R_{g1}$ (Table 2).

The increase in spherical nature of both series of dendrimers was also pinpointed by measuring the asphericity ($\kappa^2$) of these dendrimers, where at higher generations, a value close to zero was observed (Figure 4). Except for generation 0, no significant differences were observed between the NBD- and $NH_3$-PG series, reiterating that NBD does not significantly affect the shape at higher generations. Similar values of $\kappa^2$ were reported for PLL dendrimers,[11] and it was found to be a feature present in both symmetric (eg, poly(amidoamine) [PAMAM]) and asymmetric dendrimers.[11] Overall, these results further support the previous observations that the incorporation of NBD did not influence the shape of the dendrimers at higher generations and that the PG dendrimers are not perfect spheres.

Other than just the overall size and shape, the internal structure and motion of the dendrimers also take an important role in their behavior while interacting with biological systems. Dendrimers exhibit both local and collective motions (essential movements) that happen at the same time, and their visualization throughout the MD simulation is difficult. They appear as random movements; however, the motions follow defined patterns. PCA was used to identify the overall dominant conformational patterns and overall patterns of motion in the trajectories of dendrimers (Figure S4). Except for $NH_3$-PG-G0, the first principal component (PC) accounted for 30%–50% of the overall motion. Furthermore, three to five PCs were sufficient to explain 70%–80% of the total variance in motion. In the case of $NH_3$-PG-G0, the first two PCs described the overall behavior of the dendrimer due to the lower complexity of the structure. For both series at lower generations, the overall space occupied was similar, whereas at higher generations, the space explored had differences for PC2 and PC3 of dendrimers with different cores. This could be due to the fact that at higher generations, one type of motion might be occurring on different branches for various dendrimers possibly due to their asymmetry. Nevertheless, in visual inspection of all PG dendrimer motions, one to five PCs showed to be related to twisting, stretching and bending of the terminal branches (example of three major PCs is shown for a small G1 NBD-PG dendrimer in Figure 5).

For higher generations, the projection of the two major PCs reveals a U-shape form. This type of shape has been attributed to random diffusion of motion in proteins, allowing only to inform on more accessible degrees of freedom.[41] However, for dendrimers, due to their specific connections between monomers, this may be the only degrees of freedom allowed since they cannot be denatured. As a result, both types of dendrimers, with and without NBD, revealed similar motions and dynamics. Furthermore, the data showed that the terminal groups contributed more to the dynamic behavior of the dendrimers and that the introduction of the NBD did not significantly impair the natural motion of PG dendrimers.

Dendrimer mass distribution was measured through the radial mass density from the center of mass (Figures 6 and S5). For both $NH_3$ and NBD series, the density was higher in the core and thus in agreement with the core-dense

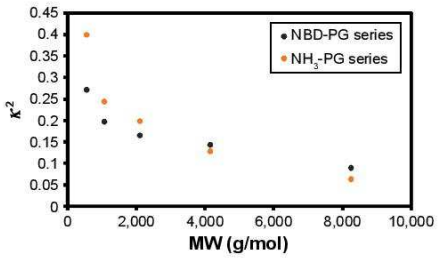


**Figure 4** Influence of MW on asphericity ($\kappa^2$) in NBD-PG-GLU dendrimers from G0 to G4.
**Notes:** The exponential decay shows that the higher the MW of the dendrimers results in their more spherical shape. No substantial differences in asphericity were found for both series of dendrimers except for the G0 where the introduction of the fluorophore has a substantial influence on the geometry of the dendrimer.
**Abbreviations:** MW, molecular weight; NBD, nitrobenzoxadiazole; PG, poly(L-glutamic acid); GLU, glutamic acid.

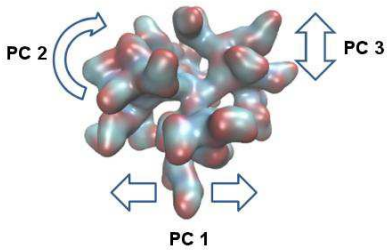


**Figure 5** An example of the general movements on NBD-PG dendrimers characterized by the first three PCs.
**Note:** The major dynamics observed for PG dendrimers were related to twisting (PC 1), bending (PC 2) and stretching (PC 3) for the exemplified dendrimer (NBD-PG-G1).
**Abbreviations:** NBD, nitrobenzoxadiazole; PG, poly(L-glutamic acid); PC, principal component.

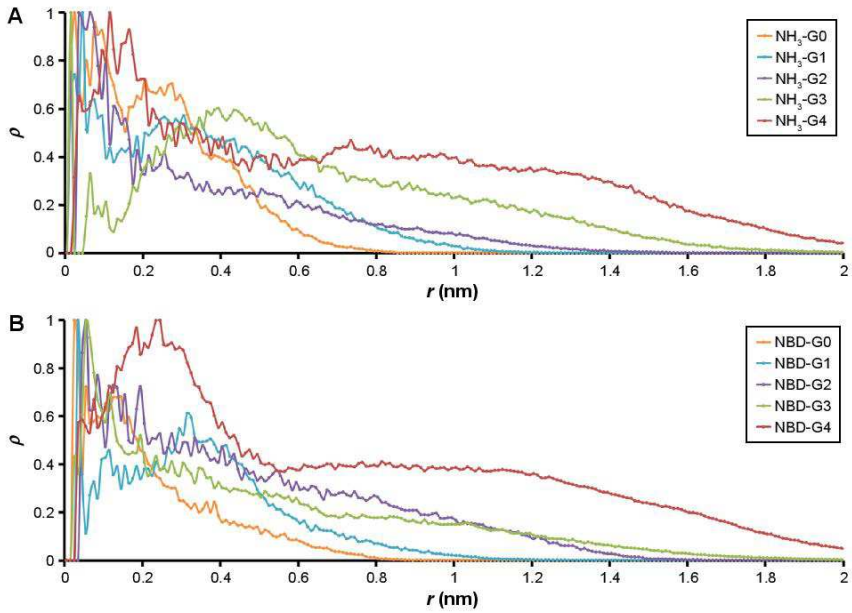


**Figure 6** Density distribution of atoms from the center of mass of $NH_3$-PG dendrimers series (**A**) and NBD-PG dendrimer series (**B**).
**Notes:** Color coding: orange, G0; blue, G1; purple, G2; green, G3; red, G4.
**Abbreviations:** PG, poly(L-glutamic acid); NBD, nitrobenzoxadiazole.

model of dendrimers found for PAMAM or PLL dendrimers. Both series of PG dendrimers ($NH_3$-PG and NBD-PG) showed similar distributions with only minor differences at lower generations again due to the deviation of the center of mass upon NBD incorporation. Therefore, at G3 and G4, the NBD no longer had a major influence on the mass distribution, and therefore, no significant differences were observed for both series.

Regarding the distribution of ions around dendrimers, it was observed that negatively charged ions ($Cl^-$) had a lower distribution around the dendrimer than positively charged ions ($Na^+$), as it would be accepted for a dendrimer with a negatively charged terminal group. These ions accumulated near the dendrimer surface with higher generation dendrimers for both series, showing the maximum peak distribution at the same distance as the terminal groups (Figure S5). This suggests that ions are complexed with charged terminal groups in the same manner. Consequently, it is expected that cationic charged molecules will be attracted to the dendrimer, whereas anionic molecules will be repelled. This will result in different sets of molecules that could be conjugated to promote specific interactions with biomacromolecules.

Overall, the introduction of the NBD fluorophore did not influence the most relevant properties of size, shape, internal structure and motion of dendrimers from two series. Therefore, generations G0–G4 of the NBD dendrimers were evaluated to determine at which generation the fluorophore could be incorporated inside the scaffold with minimal interaction with the external environment. SASA measurements were carried out for the fluorophore (NBD) residue. The classic rolling probe of 1.4 Å showed not to be adequate for this measurement, as the probe would enter inside the dendrimer into the void space and would not give adequate representation of their exposure to the external environment. As a result, a 3 Å probe was found to be an adequate size to perform these measurements.

SASA values for the NBD showed that there was a significant decrease in NBD SASA values at G4 (Figure 7). This is also observed by visual inspection throughout the trajectory,

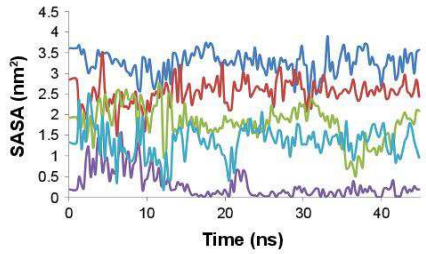


**Figure 7** SASA measurements of the NBD fluorophore along the trajectory for the NBD series: G0 (blue), G1 (red), G2 (green), G3 (cyan) and G4 (purple).
**Notes:** The increase in generation is directly correlated to its ability to prevent the exposure of the NBD to the aqueous medium. Only G4 was effective in fully preventing NBD's exposure after 20 ns when the dendrimer structure was fully equilibrated.
**Abbreviations:** SASA, solvent accessible surface area; NBD, nitrobenzoxadiazole.

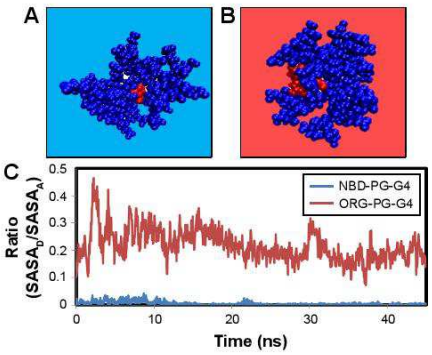


**Figure 8** Analysis of molecular dynamics simulations of dendrimers with two different cores.
**Notes:** Snapshot conformations taken from trajectories generated during simulations of NBD-PG-G4 (**A**) and ORG-PG-G4 (**B**). The ratio of SASA of ORG (gray color) and NBD fluorophore (yellow) in comparison with SASA value of respective free fluorophore (**C**). Dendrimers are displayed in their vdW representation. Blue spheres represent atoms of PG backbone and the red spheres represent atoms of NBD and ORG. The ratio is calculated from the SASA of the fluorophore in the dendrimer over the SASA of the unconjugated fluorophore.
**Abbreviations:** NBD, nitrobenzoxadiazole; PG, poly(L-glutamic acid); ORG, Oregon Green 488; SASA, solvent accessible surface area; vdW, van der Waals.

in which it is apparent that the NBD is well embedded inside the dendrimer at this generation. All analyses from the obtained trajectories indicate that generation 4 is required to fully cover the fluorophore and that at this generation, the incorporation of this small fluorophore has minimal to none interference with the overall surface properties. Thus, G4 was selected to study further modifications on the dendrimer to understand how the overall structure can be tuned for different applications.

## Effect of using a bigger fluorophore

Since different probes with distinct spectra might be required to study multiple phenomena experimentally, ORG was linked to the core at G4 to evaluate the effect of the introduction of a bigger fluorophore (Figure 8).

As observed in Figure 8, no major structural differences could be observed between NBD-PG-G4 and ORG-PG-G4. However, the gyration tensor and sphericity showed that ORG-PG-G4 dendrimer is more spherical than NBD-PG-G4 as the ratios of the gyration tensor and the sphericity were found to be 1:0.9:0.7 and 0.795, respectively. This can be attributed to the incorporation of a bulkier monomer that introduces the bias on the gyration tensor calculations. However, the bulkier nature of ORG prevented a complete coverage of the fluorophore by the dendrimer, even at the G4 (Figure 8). This is because ORG is big enough to extend to the terminal groups resulting in ~20% of the fluorophore still exposed to the solvent, as shown by SASA measurements. In order to fully encompass ORG, a higher generation of PG dendrimers might be necessary. However, producing dendrimers with generations higher than G4 increases the difficulty of their synthesis and potentially could lead to increased toxicity. Nevertheless, ORG-PG-G4 could still potentially be useful as a probe since the introduction of the larger fluorophore did not cause any major structural modifications, and 80% of ORG's volume was embedded within the interior of the dendrimer.

## Surface modification by changing the terminal groups

The interaction of dendrimers with biomolecules is often driven by their terminal groups. For this reason, we further modified the NBD-PG dendrimers to display different surface groups and thus potentially modulate their biological interaction. Two modifications were pursued by having a G4 dendrimer with LYS or TRP at the surface. These modifications allow the NBD-PG dendrimer to display a zwitterionic behavior (LYS terminal groups) or have a hydrophobic surface while being water-soluble type of dendrimer (TRP terminal groups). These modifications may also allow the conjugation of different types of therapeutics, thus ensuring their delivery using these dendrimers.

The LYS modification had no effect on the overall $R_g$ of PG dendrimers (Table 3). However, the modification with TRP significantly increased the $R_g$ (1.424 nm, Student's *t*-test, $p<0.05$) compared to any other G4 so far described. This can be attributed to the bulkier side chain of TRP and the fact that the ring decreases the flexibility of the side chain and forms pi–pi stacking interactions, thus locking the dendrimer

**Table 3** Radius of gyration ($R_g$), maximum radius ($R_{max}$), radius of hydration ($R_H$) calculated using two different approaches and sphericity (Ω) of NBD-PG-LYS-G4 and NBD-PG-TRP-G4

| Name | $R_g$ (nm) | $R_{max}$ (nm) | $R_H$ (nm) | $R_H$ (95% W) | Ratio $R_{gx}$:$R_{gy}$:$R_{gz}$ | Ω |
|---|---|---|---|---|---|---|
| NBD-PG-LYS-G4 | 1.367±0.022 | 1.576±0.342 | 1.764 | 2.125 | 1:0.8:0.7 | 0.702 |
| NBD-PG-TRP-G4 | 1.424±0.020 | 1.596±0.336 | 1.838 | 2.245 | 1:0.8:0.6 | 0.573 |

**Abbreviations:** NBD, nitrobenzoxadiazole; PG, poly(L-glutamic acid); LYS, lysine; TRP, tryptophan.

terminal groups to prevent their folding into the interior. This can also be observed by the number of particles at the surface and thus to the extended gyration tensor.

Both dendrimers were found to be in more compact conformations throughout the simulated time. The $R_{max}$ for dendrimers with LYS and TRP surface modifications branches (1.576 and 1.596 nm, respectively) was smaller in comparison with the GLU terminal residues (2.078 nm; Table 3). This is due to the electrostatic interactions established between the carboxyl and amine groups for the LYS substitution and the pi–pi stacking in the case of TRP. In fact, some snapshots showed pi–pi interactions between the rings of the NBD and the TRP, and evidenced the backfolding of some of the terminal groups toward the interior of the dendrimer (Figure 9). This also results in a more oblate shape (gyration tensor ratio of 1:0.8:0.6), even though only minor differences in asphericity were found for LYS and TRP surface modifications, 0.0488 and 0.0813 respectively.

This observation was further supported by hydrogen bonding calculations. Dendrimers, and in particular peptide dendrimers, display a complex hydrogen bonding network as the internal groups are near each other. This can translate into increasing compactness of structure and higher stabilization of conformers. NBD-PG-G4, $NH_3$-PG-G4 and ORG-PG-G4 showed a similar average number of hydrogen bonds per residue, ie, 1.86, 2.15 and 1.7, respectively. On the other hand, substituting the terminal groups with TRP and LYS increased hydrogen bonding, 3.1 and 9.69 hydrogen bonds per residue, respectively. The higher number of hydrogen bonds is expected since hydrogen donors were introduced for both residues and, in the case of LYS, a charged protonated amine was also introduced. This may be important as the number of hydrogen bond acceptors and donors, as well as the number of intramolecular hydrogen bonds that can be formed, may influence the number and type of intermolecular interactions established between dendrimers and biomolecules.

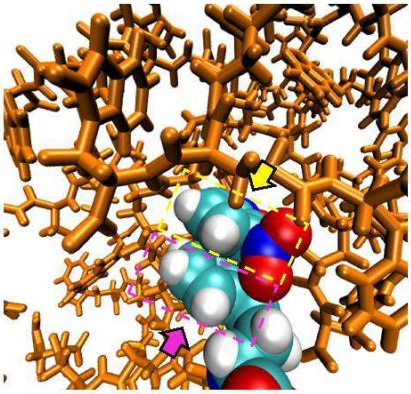

**Figure 9** Pi–pi interactions between NBD and a terminal TRP group.
**Note:** Both aromatic groups are shown in the vdW representation (yellow arrow indicates the NBD, and purple arrow indicates TRP), while the PG interior is shown as a orange stick representation.
**Abbreviations:** NBD, nitrobenzoxadiazole; TRP, tryptophan; vdW, van der Waals.

The surface charge was also considerably different for dendrimers with distinct surface modifications (Figure 10), which enable substantially distinct intermolecular interactions with biomolecules to occur. Therefore, these dendrimers are potentially suitable for modification to achieve multiple applications. For example, NBD-PG-LYS-G4 could be used to complex with nucleic acid molecules, whereas the TRP substitution can complex with molecules that present both positive and negative charges, as well as hydrophobic surfaces.

Overall, we showed that it is possible to change the terminal groups of the NBD-PG dendrimer to display different charges and hence lipophilicity of their surface while keeping the fluorophore from interacting with the external environment. Other modifications can, therefore, be pursued in order to obtain the desired properties according to intended application. Finally, G4 seems to be the potential candidate generation for drug delivery, presenting a plausible size range for synthesis purposes and affording a range of surface modifications tailored to multiple applications.

## Conclusion

Predicting structure of dendrimers to design effective carriers can be a difficult endeavor. Herein, MD simulations were performed to predict the 3D structure of PG dendrimers with different surface modifications to study their capacity

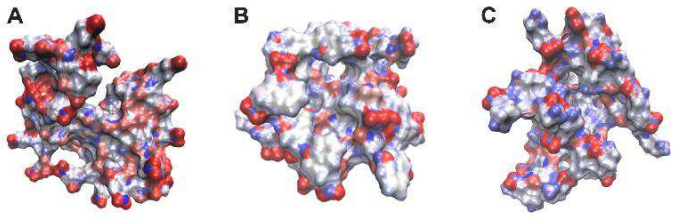


**Figure 10** Electrostatic potential surface of NBD-PG-G4 (**A**), NBD-PG-TRP-G4 (**B**) and NBD-PG-LYS-G4 (**C**).
**Notes:** Surfaces are colored according to charge: negatively, red; neutral, gray and positively, blue charged surfaces.
**Abbreviations:** NBD, nitrobenzoxadiazole; PG, poly(L-glutamic acid); TRP, tryptophan; LYS, lysine.

to incorporate a fluorophore as an imaging agent. We showed that a G4 PG dendrimer could fully encompass a small fluorophore, without affecting the intermolecular interactions that the dendrimer can form with biomacromolecules. The addition of NBD in the core of G4 PG dendrimers did not introduce significant changes in their size and shape. The incorporation of a bigger fluorophore (ORG) was also inspected. A G4 PG dendrimer did not completely incorporate the fluorophore with 80% of its surface in the dendrimer interior, rendering the use of this fluorophore as an imaging agent possible, albeit not ideal. Finally, dendrimer surface modifications by different amino acids, LYS and TRP, were further explored. These differed not only in size but also in the charges of the surface compared to GLU-terminated dendrimer. The study showed that these different amino acids induce different topological features compared to GLU-terminated PG dendrimers while maintaining the ability to encompass NBD fully. These changes in charge distribution and shape can, therefore, be used to tailor the surface of NBD-PG-G4 for different biological applications via introducing desired interactions with targets. NBD-PG-G4 dendrimers with different surface modifications provide a suitable scaffold to be used to monitor the distribution of dendrimers in a biological system without NBD interfering with interactions with targets or other biomolecular systems.

## Acknowledgments

Funding from the UK Engineering & Physical Sciences Research Council (EPSRC) for the EPSRC Centre for Innovative Manufacturing in Emergent Macromolecular Therapies is gratefully acknowledged. Financial support from the consortium of industrial and governmental users is also acknowledged. NM, LCS and HFF acknowledge Fundação para a Ciência e a Tecnologia – Ministério da Ciência; Tecnologia e Ensino Superior (FCT-MCTES), Portugal (PhD Grant SFRH/BD/87838/2012 (NM); Investigador FCT IF/00437/2014 to LCS and iMed.ULisboa grant UID/DTP/04138/2013). The University of Hertfordshire is acknowledged for providing support to this project.

## Author contributions

All authors contributed toward data analysis, drafting and revising the paper and agree to be accountable for all aspects of the work.

## Disclosure

The authors report no conflicts of interest in this work.

## References

1. Svenson S, Tomalia DA. Dendrimers in biomedical applications – reflections on the field. *Adv Drug Deliv Rev*. 2005;57:2106–2129.
2. Maingi V, Kumar MVS, Maiti PK. PAMAM dendrimer-drug interactions: effect of pH on the binding and release pattern. *J Phys Chem B*. 2012;116(14):4370–4376.
3. Milhem OM, Myles C, McKeown NB, Attwood D, D'Emanuele A. Polyamidoamine Starburst(R) dendrimers as solubility enhancers. *Int J Pharm*. 2000;197:239–241.
4. Shi X, Lee I, Chen X, et al. Influence of dendrimer surface charge on the bioactivity of 2-methoxyestradiol complexed with dendrimers. *Soft Matter*. 2010;6(11):20–27.
5. De Jong WH, Borm PJ. Drug delivery and nanoparticles: applications and hazards. *Int J Nanomedicine*. 2008;3(2):133–149.
6. Sadler K, Tam JP. Peptide dendrimers: applications and synthesis. *Rev Mol Biotechnol*. 2002;90(3–4):195–229.
7. Javor S, Delort E, Darbre T, Reymond JL. A peptide dendrimer enzyme model with a single catalytic site at the core. *J Am Chem Soc*. 2007;129(43):13238–13246.
8. Filipe LCS, Machuqueiro M, Darbre T, Baptista AM. Unraveling the conformational determinants of peptide dendrimers using molecular dynamics simulations. *Macromolecules*. 2013;46(23):9427–9436.
9. Twyman L, Beezer A, Mitchell J. The synthesis of chiral dendritic molecules based on the repeat unit L-glutamic acid. *Tetrahedron Lett*. 1994;35(25):4423–4424.
10. Vlasov GP, Korol'kov VI, Pankova GA, et al. Lysine dendrimers and their starburst polymer derivatives: possible application for DNA compaction and in vitro delivery of genetic constructs. *Russ J Bioorganic Chem*. 2004;30(1):12–20.

11. Falkovich S, Markelov D, Neelov I, Darinskii A. Are structural properties of dendrimers sensitive to the symmetry of branching? Computer simulation of lysine dendrimers. *J Chem Phys*. 2013;139(64903):1–8.
12. Ranganathan D, Kurur S. Synthesis of totally chiral, multiple armed, poly Glu and poly Asp scaffoldings on bifunctional adamantane core. *Tetrahedron Lett*. 1997;38(7):1265–1268.
13. Li N, Cai H, Jiang L, et al. Enzyme-sensitive and amphiphilic PEGylated dendrimer-paclitaxel prodrug-based nanoparticles for enhanced stability and anticancer efficacy. *ACS Appl Mater Interfaces*. 2017;9(8):6865–6877.
14. Li N, Li N, Yi Q, et al. Amphiphilic peptide dendritic copolymer-doxorubicin nanoscale conjugate self-assembled to enzyme-responsive anti-cancer agent. *Biomaterials*. 2014;35(35):9529–9545.
15. Bouvier B. Optimizing the multivalent binding of the bacterial lectin LecA by glycopeptide dendrimers for therapeutic purposes. *J Chem Inf Model*. 2016;56(6):1193–1204.
16. Caminade AM, Laurent R, Majoral JP. Characterization of dendrimers. *Adv Drug Deliv Rev*. 2005;57(15):2130–2146.
17. Franc G, Mazères S, Turrin CO, et al. Synthesis and properties of dendrimers possessing the same fluorophore(s) located either peripherally or off-center. *J Org Chem*. 2007;72(23):8707–8715.
18. Yoo H, Juliano RL. Enhanced delivery of antisense oligonucleotides with fluorophore-conjugated PAMAM dendrimers. *Nucleic Acids Res*. 2000;28(21):4225–4231.
19. Kitchens KM, Kolhatkar RB, Swaan PW, Eddington ND, Ghandehari H. Transport of poly(amidoamine) dendrimers across Caco-2 cell monolayers: influence of size, charge and fluorescent labeling. *Pharm Res*. 2006;23(12):2818–2826.
20. Kazmierczak-Baranska J, Pietkiewicz A, Janicka M, et al. Synthesis of a fluorescent cationic phosphorus dendrimer and preliminary biological studies of its interaction with DNA. *Nucleosides Nucleotides Nucleic Acids*. 2010;29(3):155–167.
21. Bello M, Fragoso-Vázquez J, Correa-Basurto J. Theoretical studies for dendrimer-based drug delivery. *Curr Pharm Des*. Epub 2017 Feb 28.
22. Martinho N, Florindo H, Silva L, Brocchini S, Zloh M, Barata T. Molecular modeling to study dendrimers for biomedical applications. *Molecules*. 2014;19(12):20424–20467.
23. Kanchi S, Suresh G, Priyakumar UD, Ayappa KG, Maiti PK. Molecular dynamics study of the structure, flexibility, and hydrophilicity of PETIM dendrimers: a comparison with PAMAM dendrimers. *J Phys Chem B*. 2015;119(41):12990–13001.
24. Gumbart JC, Beeby M, Jensen GJ, Roux B. *Escherichia coli* peptidoglycan structure and mechanics as predicted by atomic-scale simulations. *PLoS Comput Biol*. 2014;10(2):e1003475.
25. Vanommeslaeghe K, MacKerell AD Jr. Automation of the CHARMM General Force Field (CGenFF) I: bond perception and atom typing. *J Chem Inf Model*. 2012;52(12):3144–3154.
26. Vanommeslaeghe K, MacKerell AD Jr. Automation of the CHARMM general force field (CGenFF) II: assignment of bonded parameters and partial atomic charges. *J Chem Inf Model*. 2012;52(12):3155–3168.
27. Barata TS, Brocchini S, Teo I, Shaunak S, Zloh M. From sequence to 3D structure of hyperbranched molecules: application to surface modified PAMAM dendrimers. *J Mol Model*. 2011;17(11):2741–2749.
28. Martinho N, Silva LC, Florindo HF, Brocchini S, Barata T, Zloh M. Practical computational toolkits for dendrimer and linear polymer structure design. *J Comput Aided Mol Des*. Epub 2017.
29. Schwieters CD, Kuszewski JJ, Tjandra N, Marius Clore G. The Xplor-NIH NMR molecular structure determination package. *J Magn Reson*. 2003;160(1):65–73.
30. Phillips JC, Braun R, Wang W, et al. Scalable molecular dynamics with NAMD. *J Comput Chem*. 2005;26(16):1781–1802.
31. Grant BJ, Rodrigues APC, ElSawy KM, McCammon JA, Caves LSD. Bio3d: an R package for the comparative analysis of protein structures. *Bioinformatics*. 2006;22(21):2695–2696.
32. Skjærven L, Yao X, Scarabelli G, Grant BJ. Integrating protein structural dynamics and evolutionary analysis with Bio3D. *BMC Bioinformatics*. 2014;15:1–11.
33. Filipe LCS, MacHuqueiro M, Baptista AM. Unfolding the conformational behavior of peptide dendrimers: insights from molecular dynamics simulations. *J Am Chem Soc*. 2011;133(13):5042–5052.
34. Hayward S, de Groot BL. Normal modes and essential dynamics. *Methods Mol Biol*. 2008;443:89–106.
35. Berendsen HJC, Hayward S. Collective protein dynamics in relation to function. *Curr Opin Struct Biol*. 2000;10:165–169.
36. Todeschini R, Consonni V. Descriptors from molecular geometry. *Handbook of Chemoinformatics*. Wiley-VCH: Weinheim, Germany; 2000:1004–1033.
37. Neelov I, Falkovich S, Markelov D, Paci E, Darinskii A, Tenhu H. Molecular dynamics of lysine dendrimers. Computer simulation and NMR. *Dendrimers in Biomedical Applications*. Royal Society Of Chemistry: Cambridge, UK; 2013:204.
38. Tian W, Ma Y. Effects of valences of salt ions at various concentrations on charged dendrimers. *Soft Matter*. 2010;6:1308–1316.
39. Arkin H, Janke W. Gyration tensor based analysis of the shapes of polymer chains in an attractive spherical cage. *J Chem Phys*. 2013;138(5):1–9.
40. Al-Jamal KT, Al-Jamal WT, Wang JTW, et al. Cationic poly-L-Lysine dendrimer complexes doxorubicin and delays tumor growth in vitro and in vivo. *ACS Nano*. 2013;7(3):1905–1917.
41. Wolf A, Kirschner KN. Principal component and clustering analysis on molecular dynamics data of the ribosomal L11·23S subdomain. *J Mol Model*. 2013;19(2):539–549.

## Supplementary materials

The following files are available free of charge: document containing information regarding the RMSD and RMSF analysis of the different dendrimer series and further detail on conformational analysis, density profiles and PCA of the different dendrimers under study (PDF).

### RMSD analysis of the different series of PG dendrimers

RMSD was used to determine when dendrimers' structure reached equilibrium. It was observed that the higher the generation, the longer it took to reach equilibrium. For this reason, only the last 20 ns of each simulation was taken and analyzed (Figure S1).

### 2D and 3D representation of GLU dendrimers bearing NBD

2D representation of dendrimers is not enough for topological characterization of the dendrimers. Visualization of the 3D structure highlighting the fluorophore showed that G4 is required to fully prevent NBD exposure (Figure S2).

### NBD-PG-G4 dendrimer conformations

Once dendrimers' simulation reached equilibrium, several conformational changes were observed. Most of these corresponded to rotation movements of the terminal monomers where no major changes in the overall structure were observed (Figure S3).

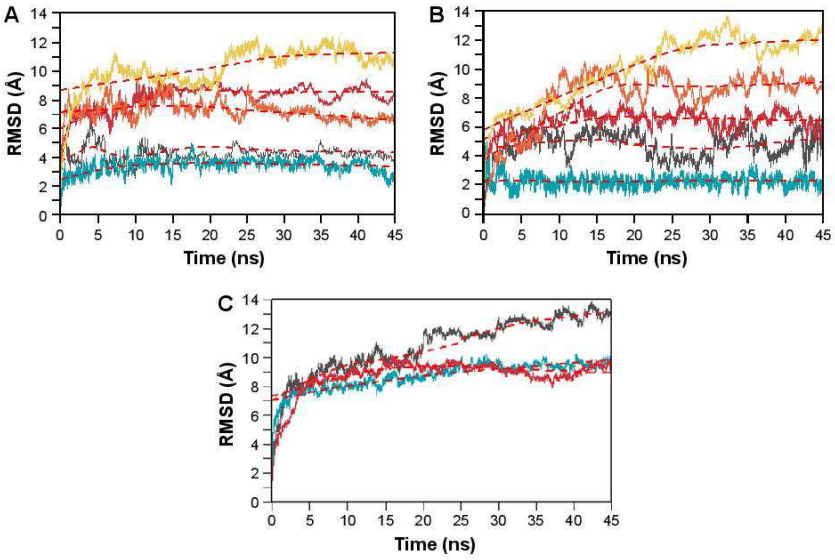


**Figure S1** RMSD for the different series of PG dendrimers (heavy atoms).
**Note:** NBD-PG dendrimers (**A**), $NH_2$-PG dendrimers (blue, G0; gray, G1; red, G2; orange, G3; yellow, G4; **B**) and (gray, NBD-PG-LYS-G4; red, NBD-PG-TRP-G4; blue, ORG-PG-G4; **C**).
**Abbreviations:** RMSD, root-mean-square deviation; PG, poly(L-glutamic acid); NBD, nitrobenzoxadiazole; LYS, lysine; TRP, tryptophan; ORG, Oregon Green 488.

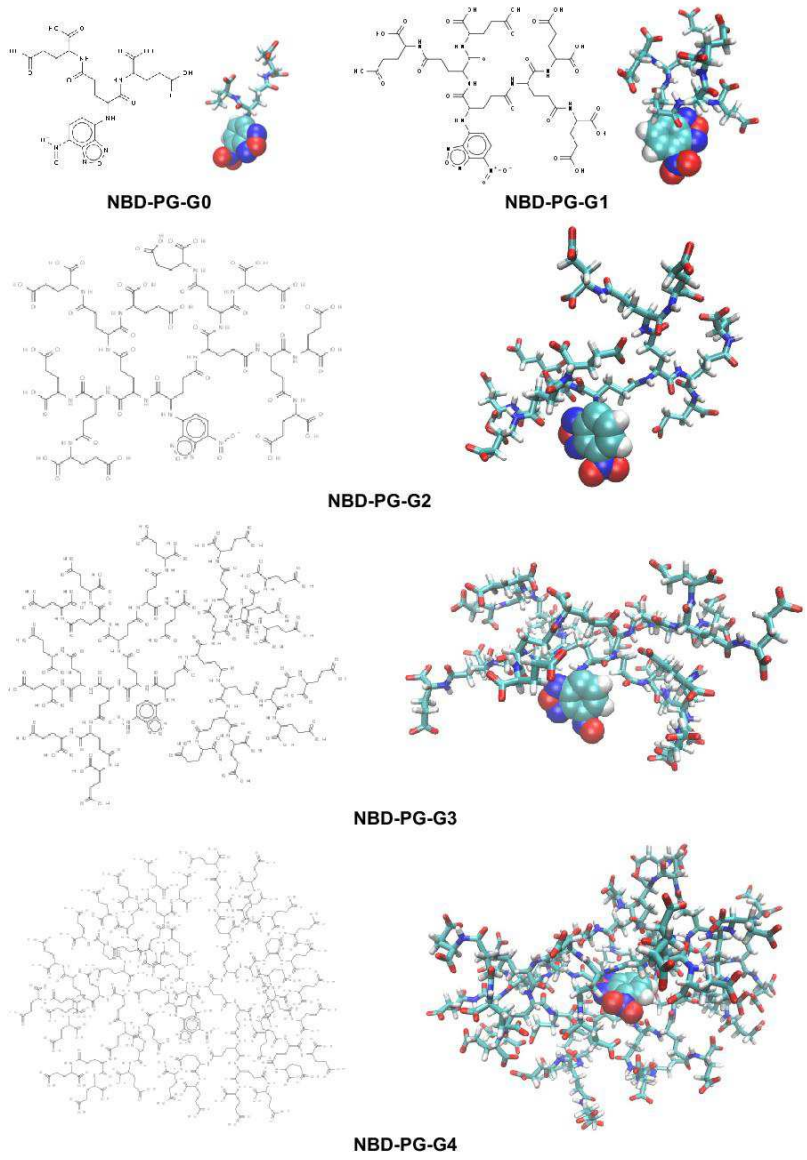


**Figure S2** (*Continued*)

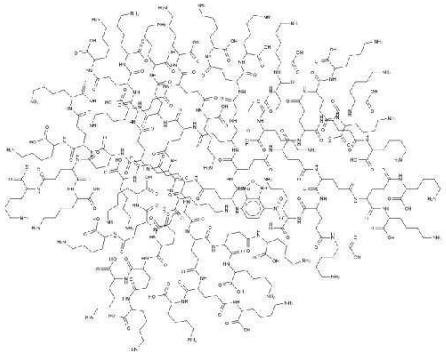

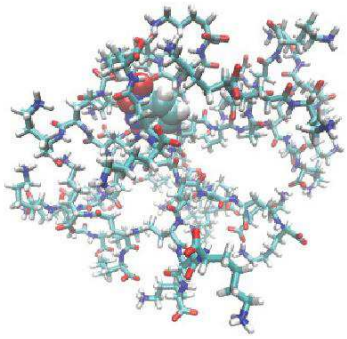

NBD-PG-LYS-G4

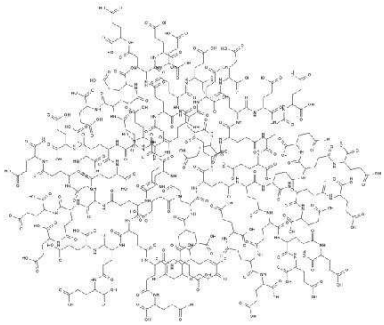

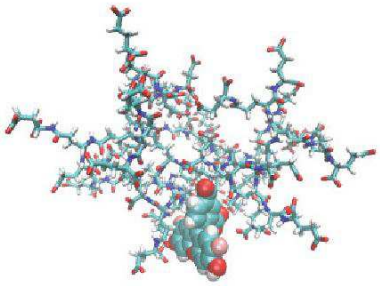

ORG-PG-G4

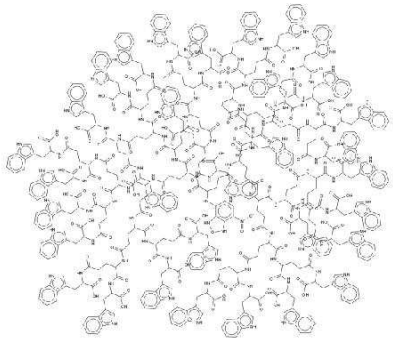

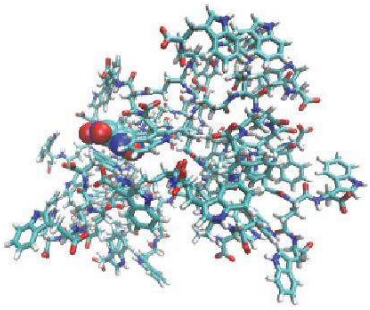

NBD-PG-TRP-G4

**Figure S2** 2D and 3D representations of GLU dendrimers bearing NBD; NBD is highlighted with vdW representation to allow the visualization of the burying capacity by the dendrimer.
**Abbreviations:** GLU, glutamic acid; NBD, nitrobenzoxadiazole; vdW, van der Waals; PG, poly(L-glutamic acid); LYS, lysine; ORG, Oregon Green 488; TRP, tryptophan.

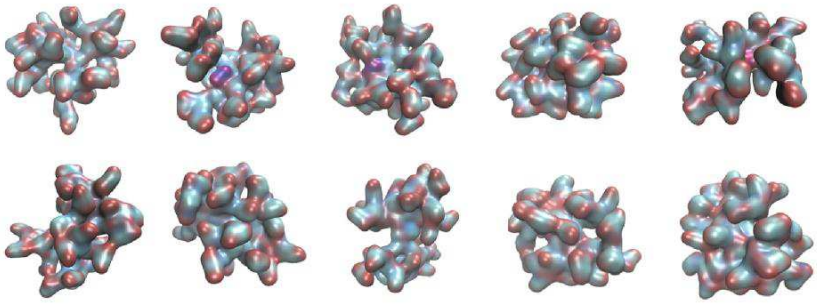

**Figure S3** Snapshots of the different conformations observed throughout the trajectory of NBD-PG-G4 dendrimer.
**Abbreviations:** NBD, nitrobenzoxadiazole; PG, poly(L-glutamic acid).

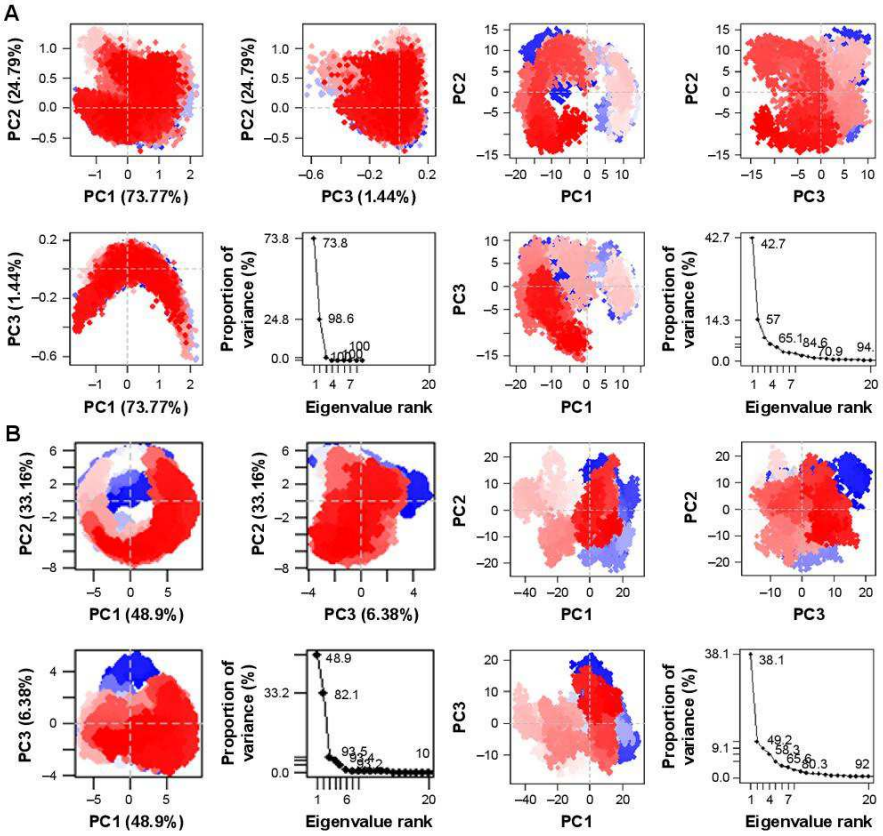


**Figure S4** *(Continued)*

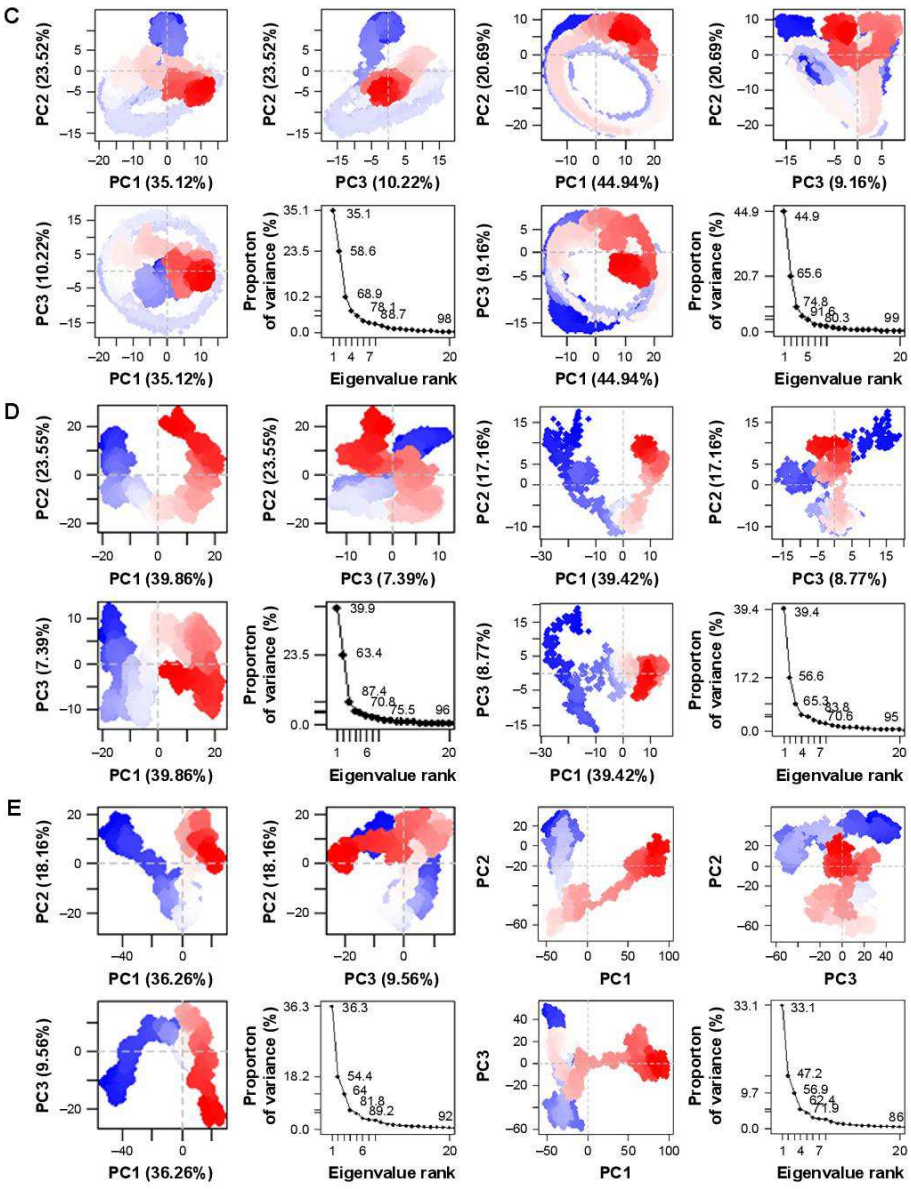


Figure S4 (*Continued*)

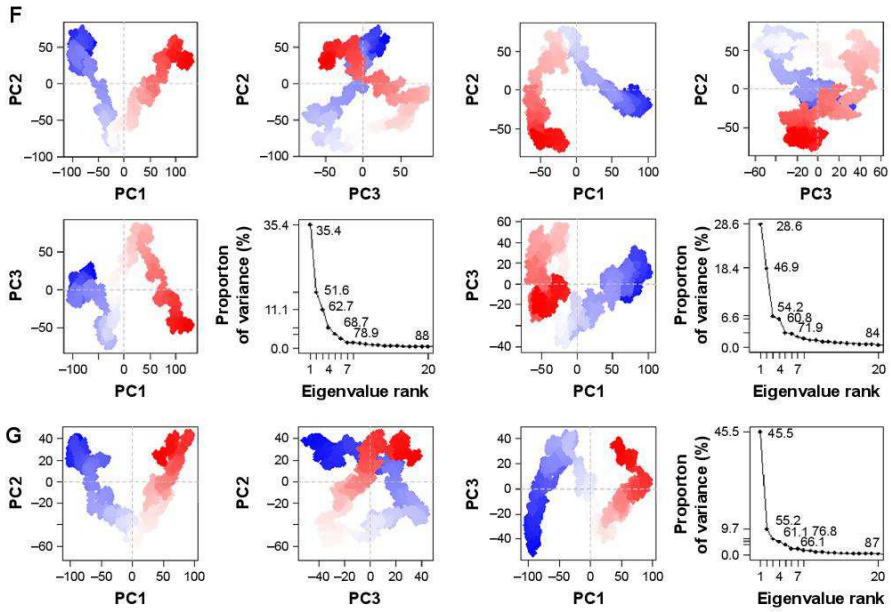


**Figure S4** PCA of PG dendrimers: (**A**) G0 series (left: $NH_3^+$, right: NBD-), (**B**) G1 series (left: $NH_3^+$, right: NBD-), (**C**) G2 series (left: $NH_3^+$, right: NBD-), (**D**) G3 series (left: $NH_3^+$, right: NBD-), (**E**) G4 series (left: $NH_3^+$, right: NBD-), (**F**) LYS-PG-G4 and TRP-PG-G4 and (**G**) ORG-PG-G4.
**Abbreviations:** PCA, principal component analysis; NBD, nitrobenzoxadiazole; LYS, lysine; PG, poly(L-glutamic acid); TRP, tryptophan; ORG, Oregon Green 488.

## Principal component analysis

PCA was performed to determine the conformational space that a molecule occupies and the general motion of these dendrimers. For most of the simulations, three to five PCs were sufficient to explain most of the motions of dendrimers. Most of these motions can be attributed to movements of the terminal monomers (Figure S4).

## Density distribution of PG dendrimers

The density of atoms distributed from the center of the molecule was calculated for all series of dendrimers. Modification of the terminal groups with different charge resulted in a different ion distribution. This indicated the formation of ion complexation with the dendrimer. Water molecules were found to be well embedded in the dendrimer and formed a layer around the dendrimer as well (Figure S5).

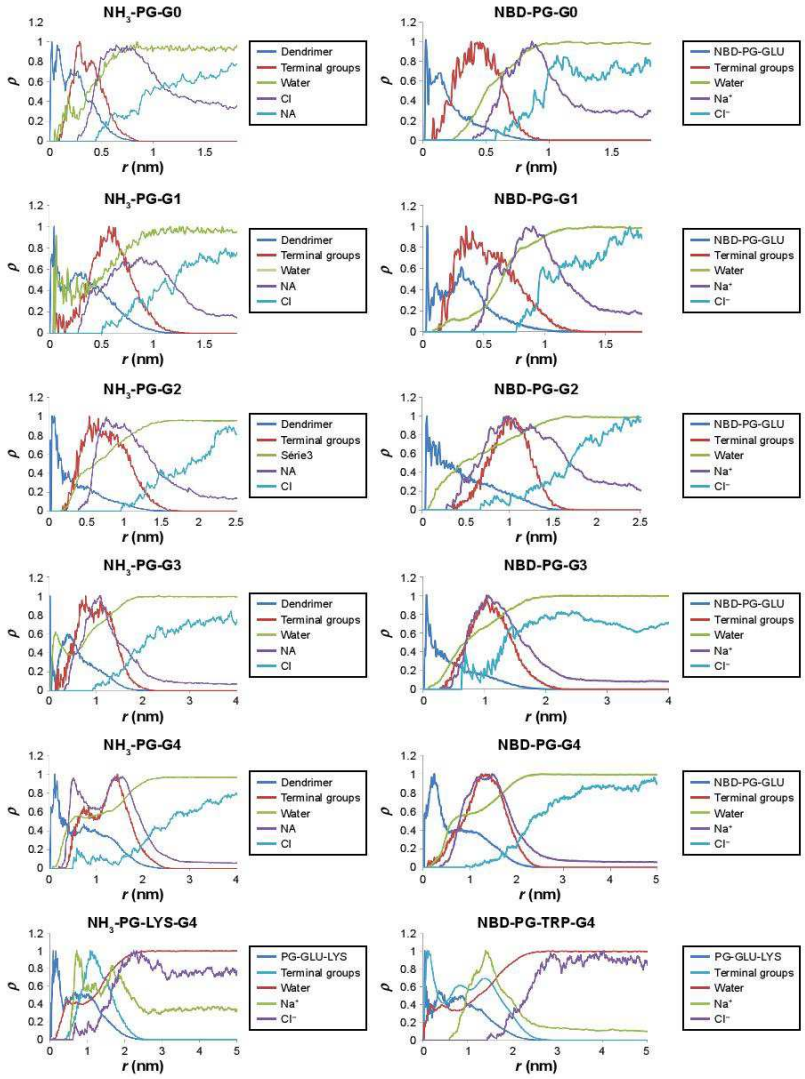


**Figure S5** PG dendrimers density distribution for $NH_3$ series (left) and NBD series (right).
**Note:** The density distribution of all atoms of the dendrimer, the atoms from the terminal monomers, water molecules (measured for the oxygen atom) and sodium and chloride atoms was determined individually from the center of mass of the dendrimer.
**Abbreviations:** PG, poly(L-glutamic acid); NBD, nitrobenzoxadiazole; NA, not applicable.

# CHAPTER III
# SYNTHESIS OF PG DENDRIMERS

# CHAPTER III: Synthesis of poly-glutamic acid (PG) dendrimers

## 3.1. Introduction

### 3.1.1. General considerations on dendrimers synthesis

Despite the tremendous amount of investment in developing new method for synthesis of dendrimers, producing novel dendrimers is still a great challenge. Contrary to traditional synthesis of polymers where statistical variations of their molecular weight are common, dendrimers are synthesized precisely. Therefore, a high degree of synthetic control has to be achieved by high-yield and high-selectivity reactions so that monodisperse populations can be obtained.

Because dendrimers can virtually be made of any building blocks (monomers) the synthetic route chosen will be dependent on the type of functional groups available in the monomer. Regardless of the route of synthesis, dendrimers can be produced though a convergent or divergent approach (or a mix method of both) in a step-wise manner[1–3]. In the divergent synthesis approach, the reaction is carried out outward from the core in an exponential-like growth. In this approach the core reacts with monomers that are generally capped by protecting groups and these are then de-protected to generate the intermediary backbone that is used to grow the next generation. The main problem associated with this synthetic approach is the possible inconsistencies caused by side-reactions and/or incomplete reactions that can lead to defective dendrimers. This is particularly relevant at higher generations where a higher number of groups have to be conjugated. In order to cope with this challenge, it is common to use excess amounts of reagents and longer reactions times which can be highly inefficient. Moreover, at higher generations there is a need to perform an increasingly number of reactions and the purification becomes increasingly more difficult due to number of defective dendrimers with similar biophysical properties. Furthermore, highly selective reactions are necessary since every small percentage of unreacted groups have dire consequences when growing the dendrimer (i.e. fully incomplete arms that scale up).

On the contrary, the convergent route requires an initial step of building the dendrons (individual branches) or the building blocks (e.g. linear sequence of monomers) that will constitute the layer separately before attaching them to the multifunctional core in the final step. The major advantage of using this route is the easier purification step since the products are very distinct from side-products. Moreover, the lower number of

reactions that need to occur at each step minimizes the defects in the final structure. However, there are restrictions when using this approach that arise from a potential steric hindrance effects at higher generations, and for very bulky and/or rigid monomers[4]. Additionally, the pre-formed branches may have groups that are incompatible with the intended reaction to conjugate them to the core and thus may hinder the possibility of using this route.

Finally, using mixed methods, where both convergent and divergent routes are combined, can minimize the problems associated with each individual approach. In this approach the number of reactions can be reduced to achieve the desired generation. However, not all dendrimer types benefit from this approach or have the functional groups necessary for this approach. Ultimately, the route should be selected using a case-by-case evaluation.

Upon continuous increase in dendrimers size, the exterior surface starts to become crowded due to the number of monomers that can be found close to each other. This results in restriction of the availability of the functional groups to further react. In fact, dendrimers grow faster than their volume and become densely packed which results in smaller space necessary to accommodate all additional groups necessary for the next layer (sometimes referred as "Malthusian packing paradox")[5,6]. The dense packing concept of the surface was further explored by de Gennes and Hervet[7], which introduced a theoretical approach to show the limitation of growth (a finite generation) due to steric hindrance effects. For this reason, this effect is often referred to as the "de Gennes packing"[8]. Even though this can be a limiting factor for most dendrimers, it was recently reported the synthesis of a dendrimer up to the size of a small virus (~30 nm)[9].

### 3.1.2. General considerations on synthesis of peptide dendrimers

In regards to peptide dendrimers, both carboxylic acid and amino groups are present in the monomers. Because of their nature they are expected to have protein-like behavior and thus its reactivity is similar to proteins. As there are many natural and un-natural amino acids there are other different synthetic approaches that can then be undertaken depending on the side chain groups. Amino acids can be present in the backbone or as terminal groups and this dictates the synthetic approach to be taken. Commonly, peptide dendrimer syntheses involve the formation of a peptide bond (amide bond formation) between the carboxyl and the amine. This approach has been used for therapeutic peptide synthesis and a plethora of other small drug molecules[10] and thus its translation to dendrimers synthesis should be straightforward. Indeed, this type of

reaction is commonly employed in the synthesis of PLL dendrimers using N-Boc protected lysine derivatives (Figure 3.1). The protecting groups are then removed using TFA to release the free amine and continually grow the dendrimer.

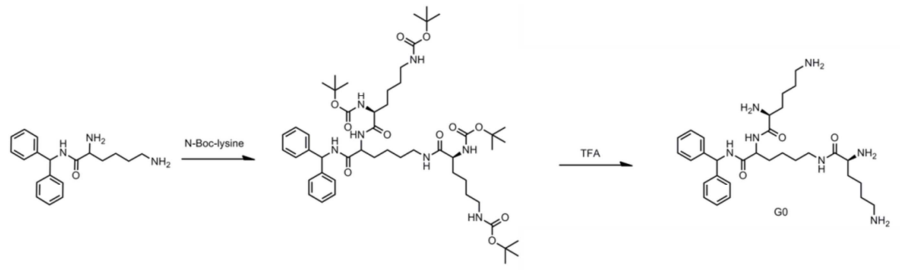


**Figure 3.1 – Synthesis of PLL dendrimers G0.** The core lysine amino acid with the carboxyl group capped with a protecting group is reacted with amine-capped branching lysines using the Boc protecting group to prevent further reaction of the amines.

Similarly to lysine, glutamic acid also has 3 functional groups (1 amine and 2 carboxylic acid groups) and therefore has inherent branching directionality. Depending on which groups are protected, it originates a complex variety of chemistry scaffolds that can be further modified. This has resulted in different types of PG dendrimers described in the literature, in which linear sequences of glutamic acid or dendrons have been attached to different core monomers (naphthoic, adamantine, oxalyl, silsesquioxane, CBZ- and porphyrin-glutamic acid), using both convergent and divergent approaches (Figure 3.2)[11–15]. However, the reactions necessary for the synthesis of PG dendrimers in this work concerns only the reactions between carboxylic acid and amine groups.

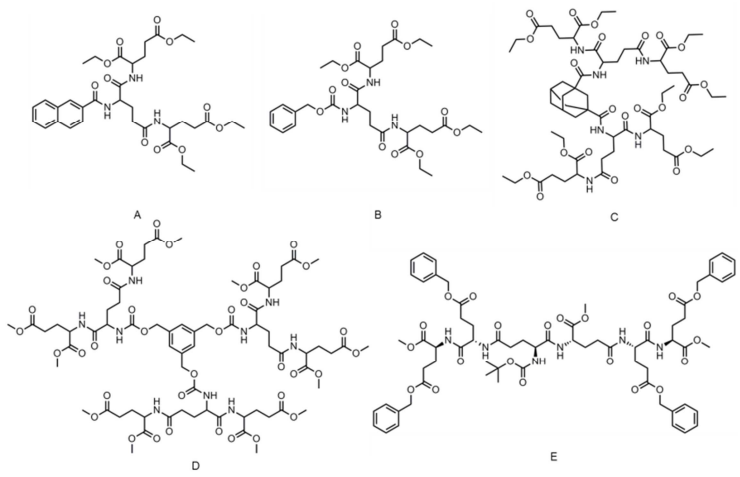


**Figure 3.2 – Examples of PG dendrimers G0 described in the literature using different cores and different capping groups[11–15].** Despite Glu being used to grow the different dendrimers, the use of different cores resulted in very different scaffolds. In fact the type of core can have (A-B) mono-, (C) bi- and (D) tri-functionality meaning that for the same generation the architecture and size of the dendrimer vary. (E): Similarly using a core composed of a di-glutamic acid results in a different final scaffold.

### 3.1.3. Coupling reagents used for peptide synthesis

As the production of dendrimers requires the reactions to be simple with fewer synthetic steps, the reagents should be compatible with the precursors (in terms of stability, reactivity and steric constraints) while maintaining minimal racemization and having high coupling efficiency. This stems from the nature of dendrimers synthesis where, at each step, multiple similar reactions have to occur simultaneously. Additionally, small defects at low generations will have deleterious effects when growing larger dendrimers. Peptide dendrimers synthesis can be carried using solid phase peptide synthesis (SPPS)[16,17] or in liquid phase. SPPS is particularly useful in the divergent method since the dendrimer is attached to a solid surface at all times. This allows washing off the unreacted reagents as well as side products formed during the reaction without compromising the main product. On the other hand, both convergent and divergent synthesis can be carried out in liquid phase, but this requires the purification of the dendrimer at each step. Nevertheless, in both approaches, the amide bond formation is usually carried out by *in situ* pre-activation of the carboxylic acid prior to the addition of the amine. This approach aims to enhance the electrophilic nature of the carboxylate groups to make it a better leaving group, and thus moving the reaction forward at higher rates, while preventing unwanted side reactions and racemization. In this regard, the most common reagents used include acyl halides, acyl azides, carbodiimides, uranium salt and acylimizadoles.

The activation of carboxyl by acyl halides is commonly carried out by using thionyl chloride, $SOCl_2$ or oxalyl cholaride[10]. In this reaction, the carboxylic acid is treated to form the corresponding acyl halide, which is a very reactive derivative since the halide is a good leaving group. Therefore, in the presence of amines a nucleophilic reaction occurs forming the corresponding amide (Figure 3.3). The problems occurring from acyl chlorides are the formation of acidic by-products that can be incompatible with the use of acid-sensitive groups, such as Boc-protected groups, and the formation of the amine salt rendering it non-nucleophilic. This can be minimized by the use of acyl fluoride and/or base[10]. However, this type of reaction is also commonly prone to hydrolysis and racemization and commonly suffers from poor yields.

Similarly, acyl azides (e.g. sodium azide, diphenylphosphoryl azide, dimethylphosphinothioylazide) are also commonly used for coupling. This reagent uses two-step activation process in which the methyl esters are converted into hydrazine and that is subsequently nitrosated to form the acyl azide. Even though the racemization is kept low it can lead to the isocyanate form[10] which can be difficult to

handle. Furthermore the obtained yield may be lower than in the case of other amide coupling reagents[10,18].

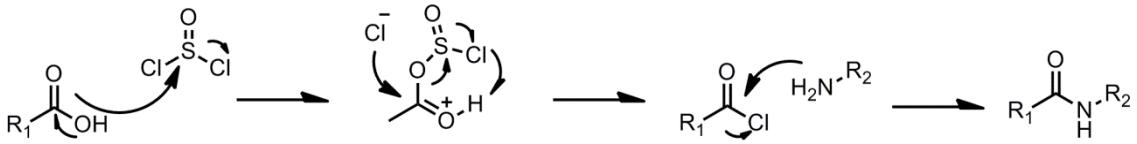


**Figure 3.3 – Mechanism reaction of acyl halides for amide formation.** During the reaction there is formation of gases that are extracted and further drive the reaction forward.

On the other hand, carbodiimides have been one of the most popular activators used for peptide synthesis and have also been commonly used for dendrimers synthesis. Examples of common carbodiimides include the DCC (N,N'-dicyclohexylcarbodiimide) [19–21], DIPC (N,N′-Diisopropylcarbodiimide) and the more aqueous soluble version EDC (1-Ethyl-3-(3-dimethylaminopropyl)carbodiimide)[14,22]. Among them, DCC is by far the most commonly used and it is highly soluble in several organic solvents but insoluble in water. During the reaction, DCC also forms an insoluble urea (dicyclohexylurea) in most organic solvents that precipitates and therefore drives the reaction forward. However, small amounts of dicyclohexylurea remain in the solution and can be difficult to remove. To prevent this, DIPC has been commonly used as an alternative to DCC since the formed urea is soluble in organic solvents which can sometimes facilitate the purification process. Finally, EDC is a carbodiimide whose urea is soluble in water facilitates the purification step on organic solvents (e.g. acidic wash). However, EDC is generally associated with lower yields in comparison to DCC[18]. The mechanism of carboxylic activation by carbodiimides involves the formation of an O-acylisourea, which can then be substituted by the amine or form the unreacted N-acylurea (undesirable) by acyl transfer[10] (Figure 3.4). Methods to reduce this unwanted by-product include carrying out the activation of the carboxyl at low temperature, or addition of an intermediary nucleophile such as HOBt (hydroxybenzotriazole), NHS (N-hydroxysuccinimide) or DMAP (4-dimethylaminopyridine) that compete for the acyl transfer. In fact, DCC/NHS is a very common combination of reagents and has been shown to have minimal racemization[23].

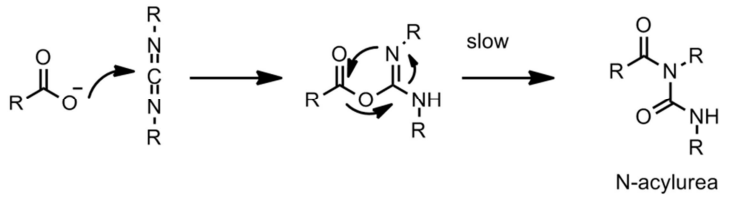


**Figure 3.4 – Side product of carbodiimides reacting with carboxyl group resulting in the formation of the N-acylurea.**

Uronium salts (HBTU, TBTU, HOBt)[14,24] are reagents that have been starting to replace the carbodiimides. Similarly to carbodiimides, uronium reagents are also prone to side products generation by guanidinylation formation. Therefore, HOBt and HOAt (1-hydroxy-7-azabenzotriazole) triazoles are commonly used to keep the racemization levels low since they form a less reactive intermediate, and therefore lower the propensity for racemization. Furthermore, the orientation of the reagents can also have a pronounced effect on coupling by promoting chelation/neighbouring effects (e.g HOAt chelation with both precursors Figure 3.5).

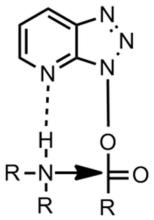

**Figure 3.5 - Neighboring effect of HAOt with the precursors favoring the homing effect.** This orientates both precursor reagents and facilitates their reaction.

Finally, acylimidazoles and in particular CDI (carbonyl diimidazole) are another class of coupling reagents that can be used in an one-pot syntheses that are commonly used in large-scale[25]. The acylimidazole is formed *in situ* by pre-activating the carboxyl with CDI (not requiring an additional base) followed by addition of the amine (Figure 3.6). The major advantage of this reagent is the compatibility with acid salts of amines and the by-product is carbon dioxide, making it easier to purify. The presence of a weakly acidic moiety has the advantage that the partial protonation of the imidazolide leads to an enhanced reaction rate[25].

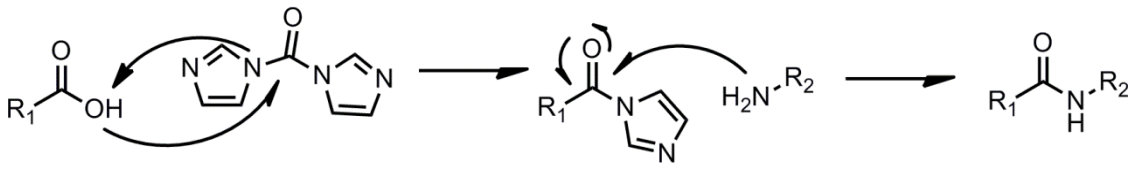

**Figure 3.6 – Mechanism of reaction of CDI with carboxyl to form an amide bond.**

### 3.1.4. Related work on PG dendrimer synthesis

Regardless of the coupling agents used in syntheses, the purification of dendrimers remains a difficult task. This is particularly relevant for biomedical applications where larger dendrimers have to be synthesized via a higher number of reactions with potentially unsatisfactory yield. When comparing the outcome of PG G0 dendrimers syntheses carried out from CBZ-glutamic acid with di-ethyl ester using DCC/NHS/DMAP to those using HBTU/HOBt as coupling reagents, a higher yield of 92% was obtained for the latter in comparison to 58% yield for the former[24]. Moreover, it has been observed that these reagents have significantly higher success for lower generations and limited success for higher generations. Using divergent approaches, glutamic acid diethyl ester was grown from a napthyl-; oxalyl or benzyloxycarbonyl-protected glutamic acid[15,26,27] using DCC as coupling agent and de-protecting the ester using NaOH. The benzyloxycarbonyl-PG-ethyl ester G0, G1 and G2 were obtained as 89%, 84% and 51% yield, respectively[15], demonstrating a large loss in yield at higher generations. Similar trends in yields were observed in divergent synthesis from a porphyrin core (4 branching groups) using different glutamic acid derivatives (carboxyl, allyl, ethyl and benzyl), using DCC/pyridine in THF as coupling method. The yields for G0 varied from 65-85%, whereas G1 was obtained in 21-42%, and the G2 had an even lower yield of 12-16%[28]. The decrease in yields is particularly noticeable in the convergent synthesis. CBZ-PG-ethyl esters were synthesized in a convergent manner with HBTU/HOBt to yield G0, G1 and G2 as 92%, 50% and 43% respectively[24]. As it can be observed for the second generation the yield decreases to half, and the same was observed for PG-methyl esters, where the convergent approach had a loss in yield from 81% to 37% from the increase of one generation[27]. This effect may be due to steric and crowding effects related to the side chain and protecting groups of the glutamic acid. When using both glutamic acid and aspartic acid to produce G1 and G2 dendrimers from an 1,3-adamantane dicarbonyl core, significantly lower yields were obtained with aspartic acid, which was attributed to steric effects[29]. Similar results were obtained using a convergent approach with a 1,3,5-benzene tricarbonyl chloride or 1,3-benzene tricarbonyl chloride as core and DCC/NHS as coupling reagents to generate a G2 dendrimer[30]. In this study, using a tri-functional core instead of a di-functional core decreased the yield of the reaction from 52% to 40% showing that steric effects of bulky branches hinder further addition. Finally, the effect of spacing between functional groups in the side chain on the yield of higher generation can also be observed on a different construct of PG dendrimers. When growing the dendrimer using a di-peptide composed of glutamic acids where one of the side chains is capped with methyl ester,

it was possible to synthesize a G2/G4 of high molecular weight (5689 g.mol$^{-1}$) with high yields of 91%[31]. This can be attributed to the larger spacing between branching points, which reduces the steric effects. Nevertheless, further reaction to form the next generation was not possible due to the steric hindrance that shielded the reaction sites.

A positive characteristic of PG dendrimers is their versatility to further modification. PG G2 were synthesized using a divergent approach from a octa(3-aminopropyl)silsesquioxane core using glutamic acid di-*tert*-butyl ester as a branching amino acid. Reactions were carried out using HBTU/HOBt/DIPEA in DMF and de-protection of the capping groups with TFA[13,14]. These dendrimers were then modified at the surface with carbazic acid *tert*-butyl ester via EDC/HOBt/DIPEA to subsequently attach biotin and doxorubicin[14]. Using a similar approach, linear PG was attached to PAMAM G4 where the side chain of the glutamic acid was de-protected and used to couple with PEI polymer[11]. Linear PG has also been attached to PAMAM[32–34] by ring-opening polymerization, using HBr to study their structure and in particular their binding capacity to other molecules. Because of their charged nature that can be controlled by the solvent or pH, PG dendrimers can form different macromolecular structures. In fact, PG-benzyl ester G0 dendrimers attached to an aliphatic octadecanoyl core were able to adapt different architectures in response to changes the environment (e.g. ions)[35–37].

### 3.1.5. Designing fluorescence-based tracking strategies

As peptide dendrimers are not expected to have intrinsic fluorescent properties that can be observed at physiological pH, it would be beneficial to attach a tag molecule with this type of properties. This would allow the direct tracking of dendrimers within the biological milieu and enable the study of their biological interactions with other biomolecules. The NBD-Cl (7-chloride-4-nitrobenz-2-oxa-1,3-diazole, NBD) was first introduced in 1969 as a non-fluorescent and chromogenic pale-yellow compound that becomes highly fluorescent once it reacts in the 7-position with amino groups (or thiols). This fluorescence is also intensified in environments of low polarity (red shift from non-polar to polar environment)[38–42]. Due to this strong fluorescence properties, NBD has been commonly used in bioanalytical chemistry including labelling of amino acids, peptides and proteins[38,42], lipids[43], sugars(glycoproteins, glycolipids and lectins)[40,44] and other bioactive molecules[45], with some derivatives having even demonstrated biological activity[40,46,47]. Synthetically, NBD is particularly useful since it is a cheap compound and is considerably stable in aqueous solutions and other solvents[44]. The coupling mechanism in the synthesis of NBD-derivatives is based on nucleophilic substitution (e.g. chloride) via a $S_NAr$ reaction (Figure 3.7) by the amine

(either primary or secondary)[44,45]. This reaction generally produces high yields (i.e. 50-100%) but some amines produce very low yields attributed to steric hindrance effects, or due to the presence of competing molecules, such as, hydroxyl groups coming from solvent[44]. As a result NBD is a suitable probe to be conjugated to non-fluorescent dendrimers and in particular to PG dendrimers since these have available amines to react at the core.

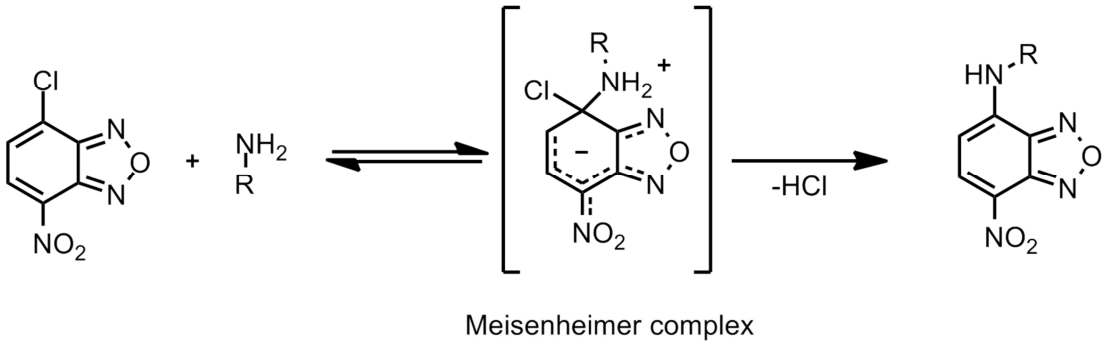


**Figure 3.7 – Reaction scheme of coupling the NBD to the amine[47].** The nucleophilic nature of amines displaces the chloride of NBD.

In this chapter, the synthesis of PG G4, designed by molecular modelling, was attempted. Different coupling reagents (carbodiimides, uronium salts and CDI) were tested in different conditions and different purification methods were used. Moreover, the step at which NBD coupling should be carried out on the dendrimer backbone was evaluated. Finally, different terminal groups were synthesized for attachment to the PG dendrimer backbone as well as different cores. Due to the amount of similar compounds described in this chapter, their naming is followed by a description number referencing the ordering by which they appear in the methods section 3.3, where the 2D structure and structural analysis of these compounds are also provided.

## 3.2 Results and Discussion

### 3.2.1. Synthesis of PG dendrimers using DCC as coupling agent

As described above, syntheses of dendrimers requires a series of repetitive step-by-step reactions. The decision of using a divergent approach over the convergent approach is highly dependent on the dendrimers generation required and the chemical constraints of the monomers. Moreover, a mix of both a convergent and divergent synthesis could reduce the number of reactions necessary to achieve the G4. In this regard, purely on a theoretical reasoning, synthesizing the N-protected-PG G0 with free carboxyl groups and the $NH_2$-PG-Ester G1 and combining them together would afford

the N-protected-PG-Ester G3 directly. This would be a good compromise between synthesizing lower generations (which are expected to produce higher yields and easier to purify), while having lower steric hindrance constraints in larger dendrimers as well as the number of reactions required (i.e. sets of de-protection and formation of new layers). Moreover, having the last step to generate the G4 in this approach would be the most optimized approach since the different terminal groups could be added at this step. However, as reported in the literature for PG dendrimers, it is expected steric hindrance of the G1 when combining with the short side chain of the glutamic acid[24,29,30]. Consequently, combining both $NH_2$-PG-Ester G0 and N-protected PG-OH G0 to obtain the N-protected PG-Ester G2 would be a better strategy to pursue as a first approach to minimize the number of reactions required (Figure 3.8).

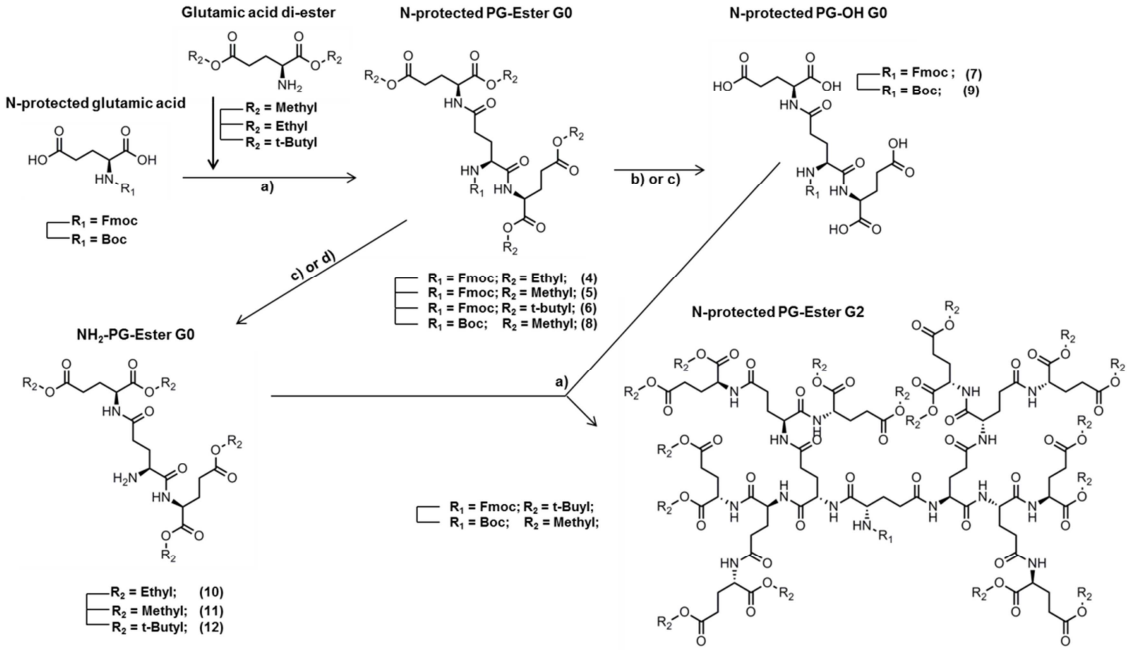


**Figure 3.8 – Initial intended synthetic approach to generate N-protected PG-Ester G2;** a) coupling reagents (typically DCC/NHS; HBTU/HOBt; CDI); b) basic hydrolysis with NaOH or LiOH; c) acid hydrolysis with TFA or concentrated HCl/sulfuric acid; d) Fmoc-removal with piperidine

In order to use glutamic acid both as the core and as branching monomers, different analogues of glutamic acid have to be used. This is necessary to prevent the nucleophilic amine of glutamic acid from reacting with itself. Free amines are usually protected with CBZ, Fmoc or N-Boc groups in peptide coupling. The protection results in loss of nucleophilicity since the nitrogen lone pairs are shared to the carboxy group. The use of CBZ-Glutamic acid was reported in the previously published of the PG dendrimers synthesis, but showed some problematic lack of compatibility with other protecting groups when the de-protection was carried out[30]. On the other hand, Fmoc

and N-Boc are versatile protecting groups that are compatible with ester protection and are well-established and extensively studied in peptide synthesis. Furthermore, N-Boc has been commonly used for the production of PG dendrimers[31,35–37], where its removal can be easily achieved with acidic hydrolysis in high yields. On the other hand, Fmoc protecting group provides many advantages such as suitable solubility in organic solvents. It is also stable in acidic conditions while being easily removed in the mild basic conditions.

To explore the reactivity of reagents to form the first generation dendrimer, Fmoc-PG-OEt G0 (4) and two additional intermediates were synthesized (Figure 3.9). Firstly, Fmoc-L-glutamic acid 5-*tert*-butyl ester was pre-activated with DCC/NHS, and upon addition of 1 equivalent of glutamic diethyl ester the desired dipeptide Fmoc-Glu(OtBu)-Glu-OEt (3) was obtained (for more information see method section 3.3). Alternatively, Fmoc-L-glutamic acid was reacted with 2 equivalents of DCC/NHS and subsequently either purified to obtain the Fmoc-Glu-NHS (1) intermediate, or immediately reacted with L-glutamic acid diethyl ester to obtain the first generation Fmoc-PG-OEt G0 (4).

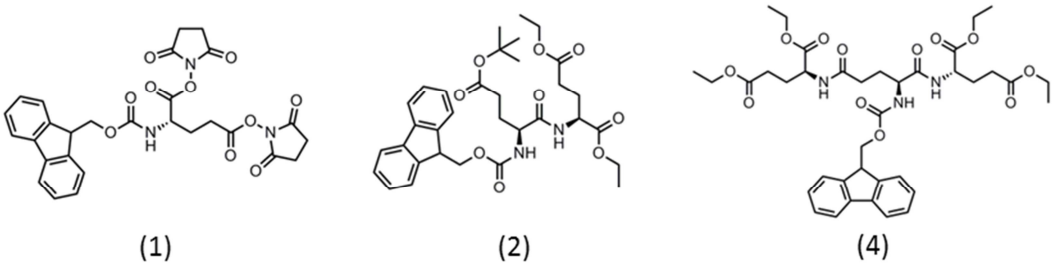


**Figure 3.9 – Chemical structure of two synthesized intermediates (Fmoc-GLU-NHS (1) and Fmoc-GLU(OtBu)-GLU-OEt (2)) and first generation Fmoc-PG-OEt G0 (4) dendrimer**

All reactions were carried out until completion as monitored by thin layer chromatography (TLC). Even though all three products were obtained in high yields, there were distinctive differences in the outcomes of the different synthetic approaches. Fmoc-Glu-NHS (1) was obtained with 65% yield and was subsequently used as the precursor to react with 2 equivalents of glutamic acid diethyl ester to form the first generation Fmoc-PG-OEt G0 (3) with 97% yield (with urea still present). Alternatively, the di-peptide Fmoc-Glu(OtBu)-Glu-OEt (2) was obtained with 98% yield, and was subsequently hydrolyzed to remove the *tert*-butyl-ester in quantitative yield to obtain the Fmoc-Glu(OH)-Glu-OEt (3) with the free carboxyl. The latter was then reacted with 1 equivalent of glutamic acid di-ethyl ester using the DCC/NHS coupling again to obtain the dendrimer Fmoc-PG-OEt G0 (4) (yield: 97%). On the other hand, the direct one-pot synthesis of Fmoc-PG-OEt G0 (4) by reacting Fmoc-L-glutamic acid with 2 equivalents

of glutamic acid di-ethyl ester via DCC/NHS coupling resulted in 78-89% yield after purification. Overall, the direct reaction of Fmoc-PG-OEt G0 (4) was shown to be the best approach in terms of overall yield and lower number of synthetic steps. Even though the Fmoc-Glu-NHS (1) was an interesting precursor to obtain since it could be subsequently used to generate the higher generations (and therefore be synthesized in one big batch), it afforded a lower yield in comparison and was prone to hydrolysis during handling (new bromocresol active spots on TLC were observed– data not shown). On the other hand, the synthesis of the di-peptide had no benefit in the synthesis of the dendrimer but could be an interesting moiety to subsequently be used as a terminal group instead.

Since reactions were carried out with DCC, the N-acylurea (DCU) byproduct was formed in all reactions. This urea is almost insoluble in most organic solvents and even though it precipitates, it still remains in detectable amounts in most of solvents. Moreover, in order to eliminate the unreacted DCC, acetic acid was added to the mixture and allowed to react for 1 hour to convert the DCC to DCU. The newly formed urea was then filtrated out with but small amounts remained in the solvent. Nevertheless, in all cases single spots in the TLC showed that only one product was formed (data not shown) and thus no side reaction products derived from the isomerization of the DCC (O-acylurea) on the carboxyl groups were expected. This result was expected since NHS was used concomitantly. NHS controls the racemization by rapid addition to the DCC activation. Moreover, the reactions were carried out in solvents of low dielectric constant (DCM) which accelerates the reaction together with the catalytic amounts of DMAP. Additionally, when the reaction was carried out without NHS, the yield of the reaction was significantly lower and the TLC showed multiple spots below the dendrimer spot.

The Fmoc-PG-OEt G0 (4) was then purified by several methods including column chromatography. For this, different eluents were tested: (a) DCM/THF (3:1 v/v); (b) THF/n-hexane (1:2 v/v); (c) ethyl acetate/n-hexane (3:1 v/v); and (d) methyl acetate/methanol (95:5 v/v). All eluents were able to separate the urea to a certain extent while the ethyl acetate/n-hexane (3:1 v/v) and methyl acetate/methanol (95:5 v/v) showed better separation from impurities to yield the product as a white solid. The $^{1}$H NMR confirmed the product to be pure (Figure 3.10). Moreover, both trituration from methanol with water and crystallization with acetonitrile were also able to purify the dendrimer but had significantly lower yields. Low generation PG dendrimers were previously shown to be able to crystalize which was attributed to formation of supramolecular assemblies with strong hydrogen bonding[29,48]

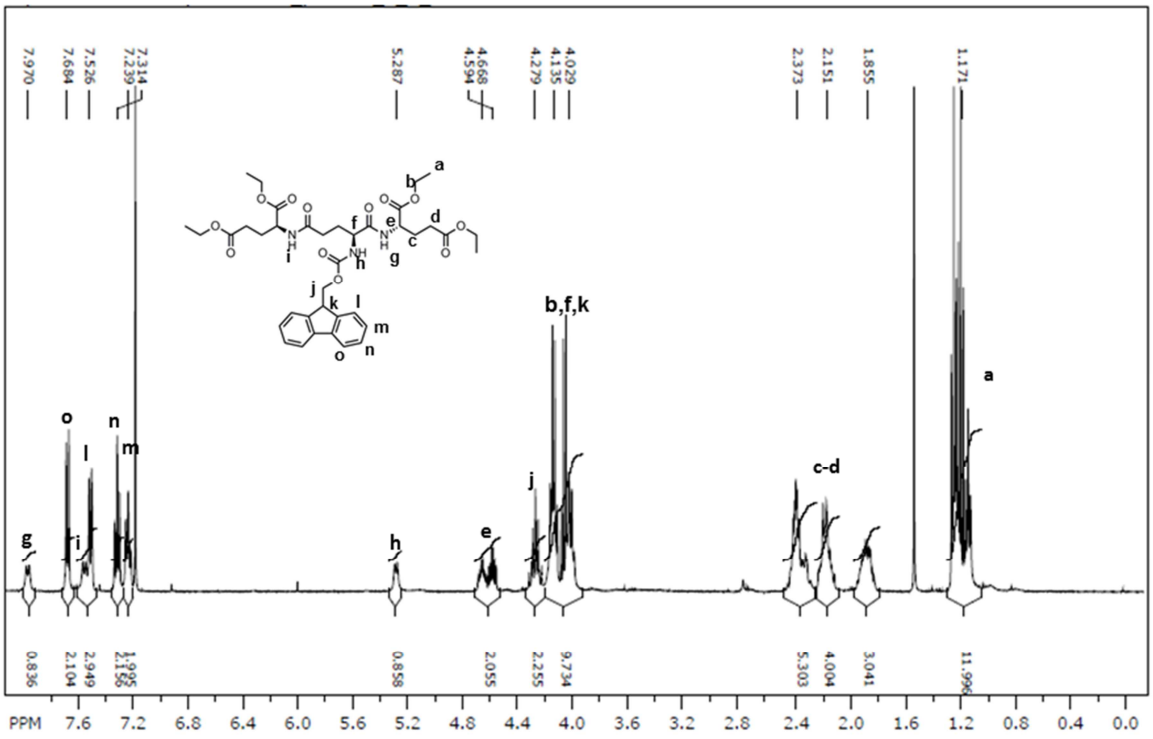


**Figure 3.10 – $^{1}$H NMR of Fmoc-PG-OEt G0 (4) in deuterated chloroform as single pure product;** the esters were used as reference and are in a proportional ratio to the Fmoc groups. Under these conditions the amides (7.97, 7.56 and 5.28 ppm) (h, i, g) were visible further evidencing the coupling to both sides of glutamic acid and the different microenvironment these amines are exposed to.

As shown in figure 3.10 all peaks in the $^{1}$H NMR of the product obtained could be easily assigned to the hydrogen atoms of the dendrimer. Moreover, all α-carbons of glutamic acid (4.27, 4.59 and 4.66 ppm) and amides (7.97, 7.68 and 5.28 ppm) showed distinctive signal. Furthermore, the ratio of esters correlated to the β and γ carbon hydrogens, and the COSY NMR also showed the correct correlation between the $CH_3$ and $CH_2$ groups of the esters as well as correct correlation of the Fmoc hydrogens (data not shown). These results strongly suggested that there was no formation of side products and that both carboxyl groups of the core reacted. The distinct nature of the peaks has also been observed in other PG dendrimers where it has been attributed to the involvement of the amide bonds in intramolecular hydrogen bonding[29].

The Fmoc-PG-OEt (4) was then reacted with piperidine in DMF or DCM to remove the Fmoc group and generate the intermediate $NH_2$-PG-OEt (10) to serve as scaffold to further grow the dendrimer (Figure 3.8.). The Fmoc removal occurs due to the slightly more acidic nature of the hydrogen in the fluorenyl group due to charge stabilization by the aromatic rings. This results in the removal of this hydrogen in presence of excess of base which subsequently decomposes the carbamate to form the dibenzofulvene

intermediate together with carbon dioxide. This reaction then releases the amine (Figure 3.11)[49]. Furthermore, the dibenzofulvene is highly reactive and thus can react with the excess of piperidine to form a stable product.

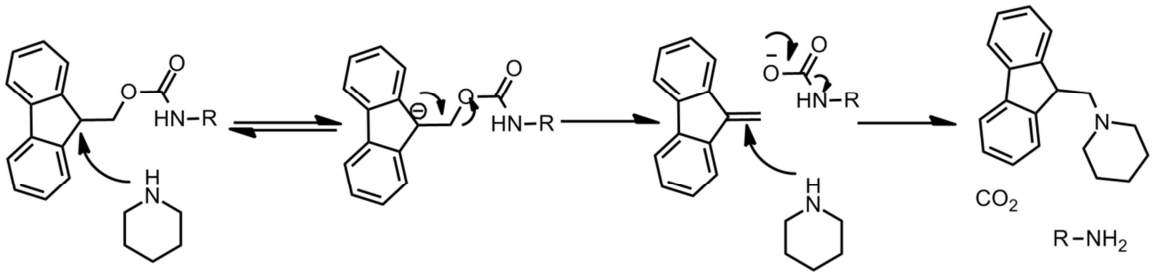


**Figure 3.11 – Chemical scheme of Fmoc removal mechanism.** This reaction releases the free amine and the fulvene intermediate that subsequently reacts with piperidine to form a stable product

The Fmoc removal was monitored spectrophotometrically as well as by TLC (ethyl acetate/methanol 95:5 v/v) (data not shown). The 209.5 nm pre-reaction peak shifted to 218 nm and reached a plateau after 2 hours. On the other hand, the 265 nm peak shifted to 255 nm after 2 hours and returned to 262 nm after 4 hours. This could probably be attributed to de-protection of the fulvene and reaction with the piperidine. This is in accordance with the TLC results where after 2 hours two top UV spots were observed and after 4 hours only one spot was observed.

The obtained reaction mixture containing the dendrimer then was purified by silica column chromatography using ethyl acetate/methanol (95:5 v/v) as eluent to effectively separate the Fmoc-piperidine and the $NH_2$-PG-OEt (10). However a low recovery yield was obtained (yield: 50-60%), which could be only slightly increased by doping the eluent with TEA to an improved yield of 66%. The first eluted product (rf 0.7 and UV positive) was identified to be solely the Fmoc-piperidine by $^1$H NMR (Figure 3.12), and by mass spectrometry with a m/z of 264 Da. This confirmed that all the fulvene molecules released during the reaction were converted to a single product that could be removed. Also, the $^1$H NMR spectrum allowed the characterization of the reaction completion since the Fmoc peaks showed significant shifts and produced distinctive peaks.

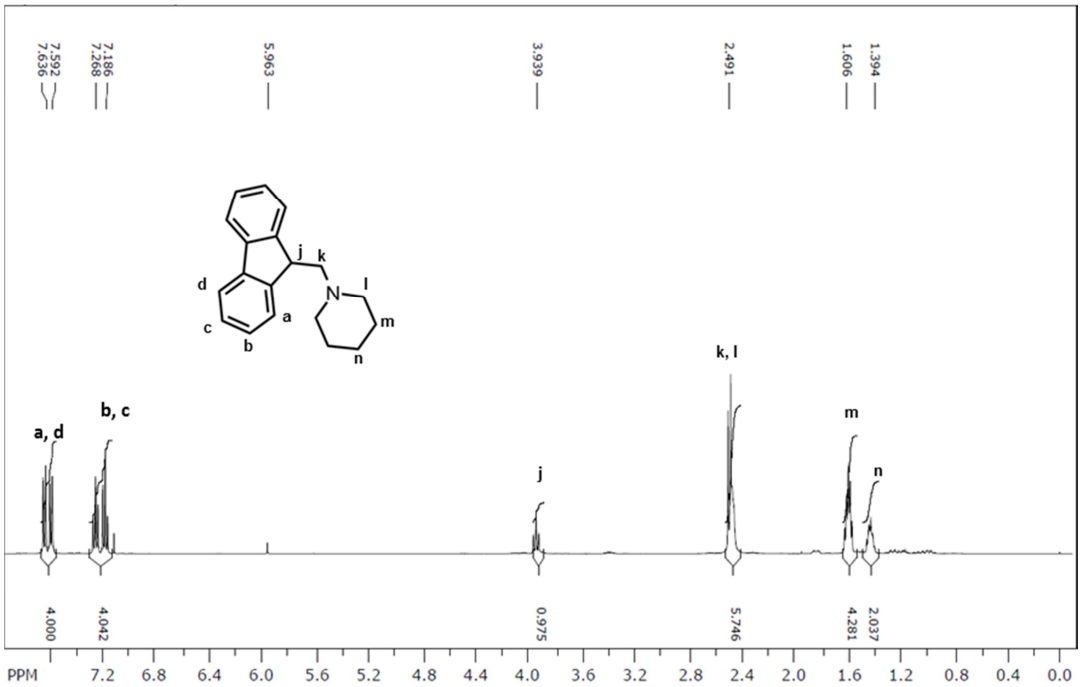


**Figure 3.12 – $^{1}$H NMR of Fmoc-piperidine that is formed as a side product when reacting with the fulvene released.** Particularly, the Fmoc peaks (7.18-7.63 ppm) (a-d) are at slightly different position to those when coupled to the dendrimer.

The second eluted product (rf 0.5 and reactive to ninhydrin) was obtained as a yellow oil which was characterized by $^{1}$H NMR (Figure 3.13) and $^{13}$C NMR (methods section 3.3). The $^{1}$H NMR showed similar peaks to its precursor but the Fmoc-related peaks completely disappeared (around 7 ppm), showing that the product was pure. Moreover, the NMR peaks are in agreement to those previously published for this molecule[24]. The product was also characterized by MS where an m/z of 540.23 Da was found [Na + $NH_2$-PG-OEt G0 (10)].

In the attempt to improve the yield two additional methods were tested. The first method relied on the poor solubility of the Fmoc-piperidine in cold methanol, and thus multiple cycles of cold methanol and removal of the precipitate were carried out. However, to fully remove the impurity, the yield of recovery of the intended product was low (yield: 40%) due to the number of cycles required. The second method followed a published protocol based on partition of the Fmoc-piperidine between polar solvents (e.g. DMF) and an immiscible hydrocarbon solvent[50]. This method showed efficient transfer of the Fmoc-piperidine to the n-hexane layer phase and improved the yield of PG dendrimer recovery to 78%.

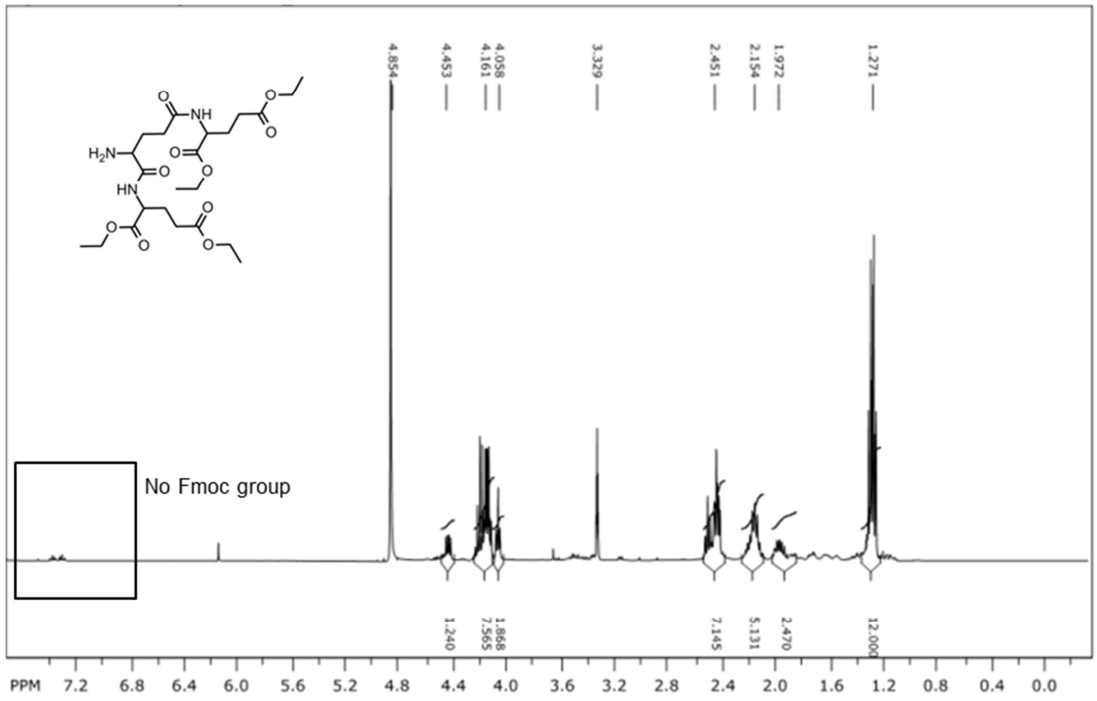


**Figure 3.13 – $^{1}$H NMR of $NH_2$-PG-OEt G0 (10) in deuterated methanol;** all peaks attributed to the Fmoc were completely absent (around 7 ppm and 4 ppm). The free amine hydrogens were also detected at around 2.1-2.4 ppm. All other peaks are similar to those found to Fmoc-PG-OEt G0 (4)

In order to synthesize the G2 directly from two G0, the Fmoc-PG-OEt G0 (4) had to also to be hydrolyzed. Ester hydrolysis to form a free carboxyl can be carried out in aqueous methanol or THF using both basic or acidic conditions[20,51,52]. However, basic hydrolysis could not be carried out due to the nature of the Fmoc that would be de-protected concomitantly. Even carrying out the reaction with LiOH in the presence of $CaCl_2$, which has been reported to increase the stability of the Fmoc[53], showed limited success with the majority of Fmoc undergoing de-protection (data not shown). Thus, acidic hydrolysis with concentrated acid under reflux was tested to remove the esters. However, due to the harsh conditions of the heating cycle, the dendrimer was found to be degraded forming a tar-like precipitate. Analysis of the solution also showed that the esters were not completely removed.

In order to carry out the hydrolysis in milder conditions, the methyl ester derivative of the branching glutamic acid was used instead. The reaction to generate the dendrimer was similar to the Fmoc-PG-OEt G0 (4) using DCC/NHS, affording the Fmoc-PG-OMe G0 (5) in similar yield (88-95%) in pure form (Figure 3.14). Again the NMR peaks were easily attributed to each functional group. As observed, the Fmoc (7.24-7.66 ppm and 4.00-4.27 ppm) and the α (4.14-4.69 ppm), β and δ (1.89-2.38 ppm) carbon hydrogen peaks remained similar, whereas the ester is identifiable as group of single peaks at

3.57-5.70 ppm. Nevertheless, attempts on hydrolysis under acidic conditions resulted in multiple species due to incomplete ester hydrolysis similarly to the Fmoc-PG-OEt G0 (4) as determined by the NMR (data not shown). As a result, this synthetic route was deemed unsuitable since it would be detrimentally for higher generation dendrimers where a high number of hydrolyses have to occur.

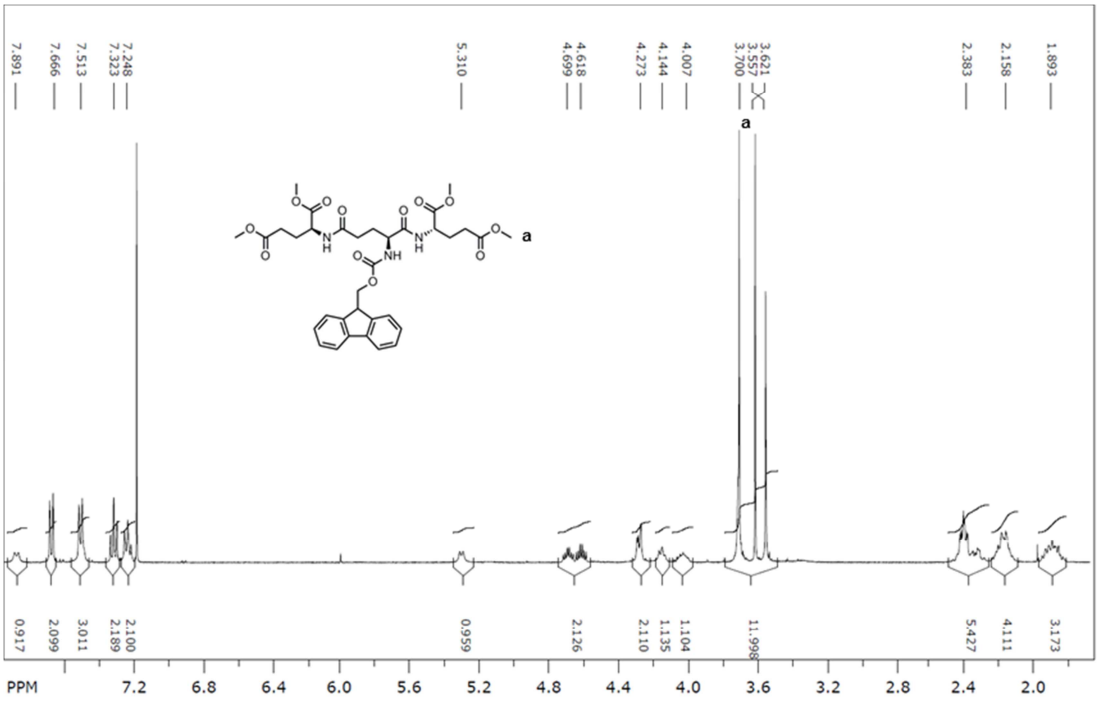


**Figure 3.14 – $^{1}$H NMR of Fmoc-PG-OMe G0 (5) in deuterated chloroform;** the protecting ester groups were differentiated between 3.5-.3.7 ppm (a) and the amides were clearly observed at 7.89, 7.51 and 5.31 ppm further evidencing coupling to both sides of the core. All other peaks were similar to Fmoc-PG-OEt G0 (4)

In order to prevent the issue of ester hydrolysis being incompatible with the Fmoc group, two alternatives were devised: (1) change of the Fmoc to an N-Boc and carry out hydrolysis of the esters under basic conditions; and (2) change of the ester (ethyl or methyl) to an acid-sensitive ester such as *tert*-butyl ester. Even though both ethyl and methyl esters can be sensitive to acid hydrolysis this process is slow under conditions employed for N-Boc removal[52]. Moreover, the N-Boc is stable to nucleophile reagents and thus suitable for ester hydrolysis under basic conditions. It has also been previously reported the selective de-protection of the N-Boc in the presence of *tert*-butyl esters by concentrated sulfuric acid in t-BuOAc or with $MeSO_3H$ in t-BuOAc[54]. The mechanism of this reaction does not rely on selective de-protection of N-Boc but rather on the re-esterification of the carboxylic acid that is formed during the reaction[52]. Even though this was a convenient approach, adding more steps in the same reaction

when producing a dendrimer may not be the best approach since it can lead to more defects at higher generations. However, theoretically the N-Boc-PG-OtBu G0 could be synthesized to produce the $NH_2$-PG-OH G0 using a single de-protection reaction with acidic conditions (Figure 3.15).

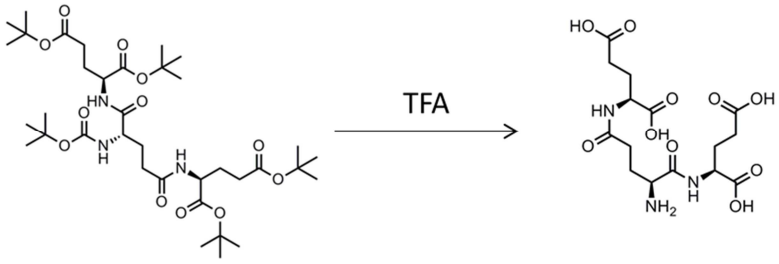


**Figure 3.15 – Theoretical synthesis of $NH_2$-PG-OH G0 using a single de-protection reaction to remove all t-Boc groups with an acid**

As a result, both PG derivatives above described were synthesized in a similar manner to the Fmoc-PG-OEt (4) and Fmoc-PG-OMe (5) using the DCC/NHS coupling method (Figure 3.8). Both resulted in similar yield of 97% for N-Boc-PG-OMe G0 (8) and 95% for Fmoc-PG-OtBu (6). The N-Boc-PG-OMe G0 (8) was then hydrolyzed under basic conditions with either NaOH or LiOH, whereas Fmoc-PG-OtBu G0 (6) was hydrolyzed under acidic conditions using TFA (Figure 3.16).

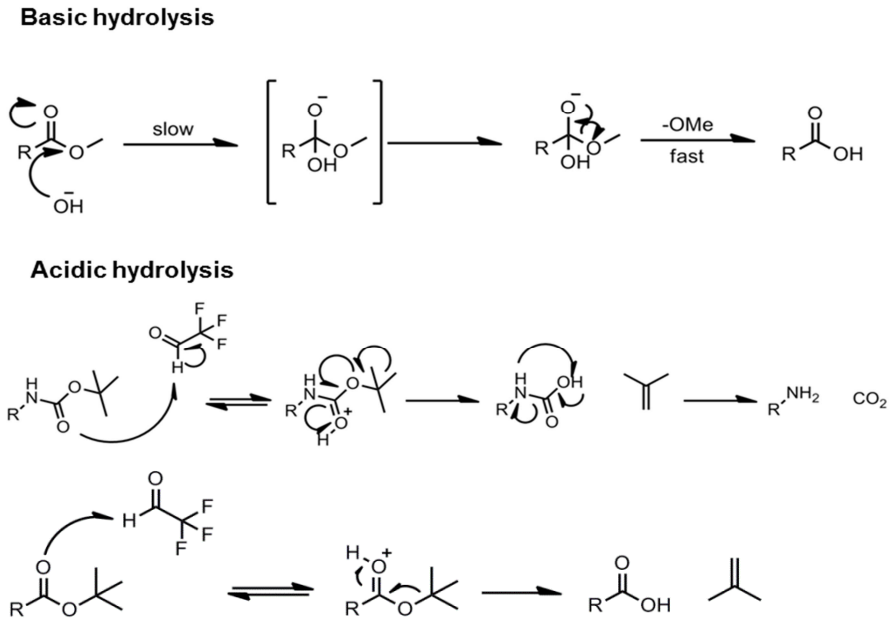


**Figure 3.16 – Reaction mechanism of basic hydrolysis of methyl esters using LiOH and acidic hydrolysis N-Boc and *tert*-butyl esters using TFA**

When using basic hydrolysis, the hydroxide ions attack the carbon of the ester and form a tetrahedral intermediate that collapses to reform the carbonyl resulting in the release of the alcohol and generating the free carboxylic acid group (Figure 3.16). On the other hand, in acidic conditions, the acid donates the proton to the carbonyl with subsequent release of the 2-methylprop-1-ene and the free carboxyl (Figure 3.16). Both routes showed complete hydrolysis of the esters in high yields (similar to other reported PG dendrimers[55]) producing the desired free carboxylic acid products in the form of N-Boc-PG-OH G0 (9) ($^1$H NMR showed in Figure 3.17) and Fmoc-PG-OH G0 (7) ($^1$H NMR showed Figure 3.18) to be further used as the core for the PG dendrimers G2.

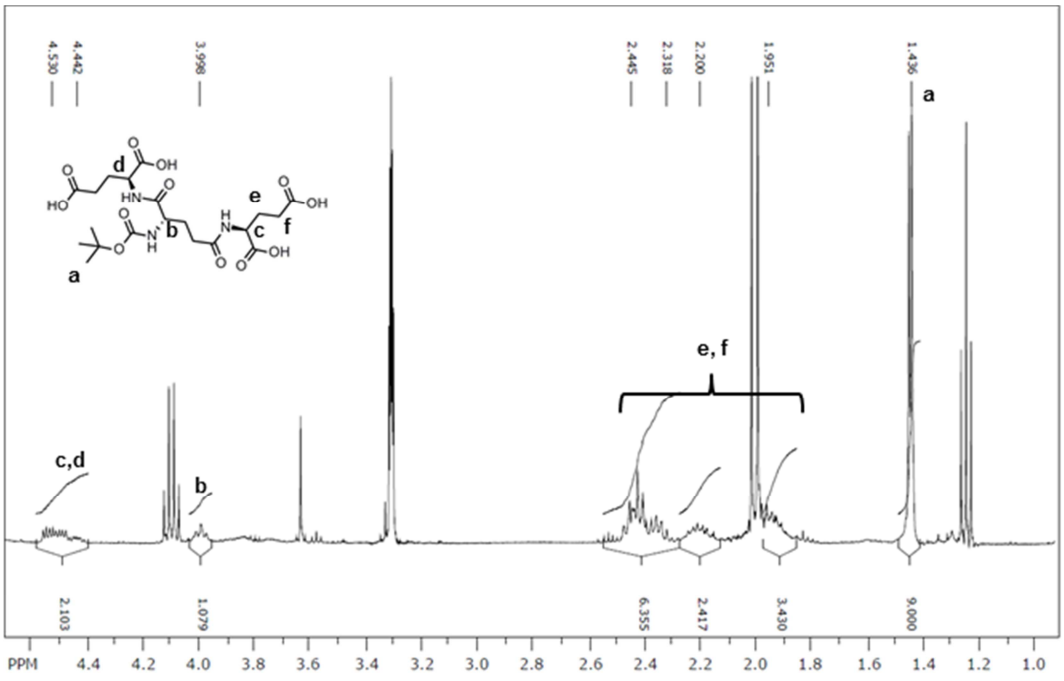


**Figure 3.17 – $^1$H NMR of N-Boc-PG-OH G0 (9) in deuterated methanol;** the N-Boc peak at 1.43 ppm was used as reference; solvent peaks are still present.

Since the N-Boc group is resistant to basic conditions the G2 could be formed by the conjugation of the N-Boc-PG-OH G0 (9) with the previously synthesized $NH_2$-PG-OEt G0 (10) (Figure 3.8). However, because the methyl esters are more suitable since they can be hydrolyzed in less harsh conditions, a new intermediate derivative was synthesized. To this, the Fmoc-PG-OMe (5) was reacted with piperidine to generate the $NH_2$-PG-OMe (11) as an oil (yield: 40-68%). Alternatively, the Fmoc-PG-OtBu G0 (6) was reacted with piperidine to yield $NH_2$-PG-OtBu G0 (12) (yield: 65-79%), to be combined with the Fmoc-PG-OH G0 (7) (Figure 3.8).

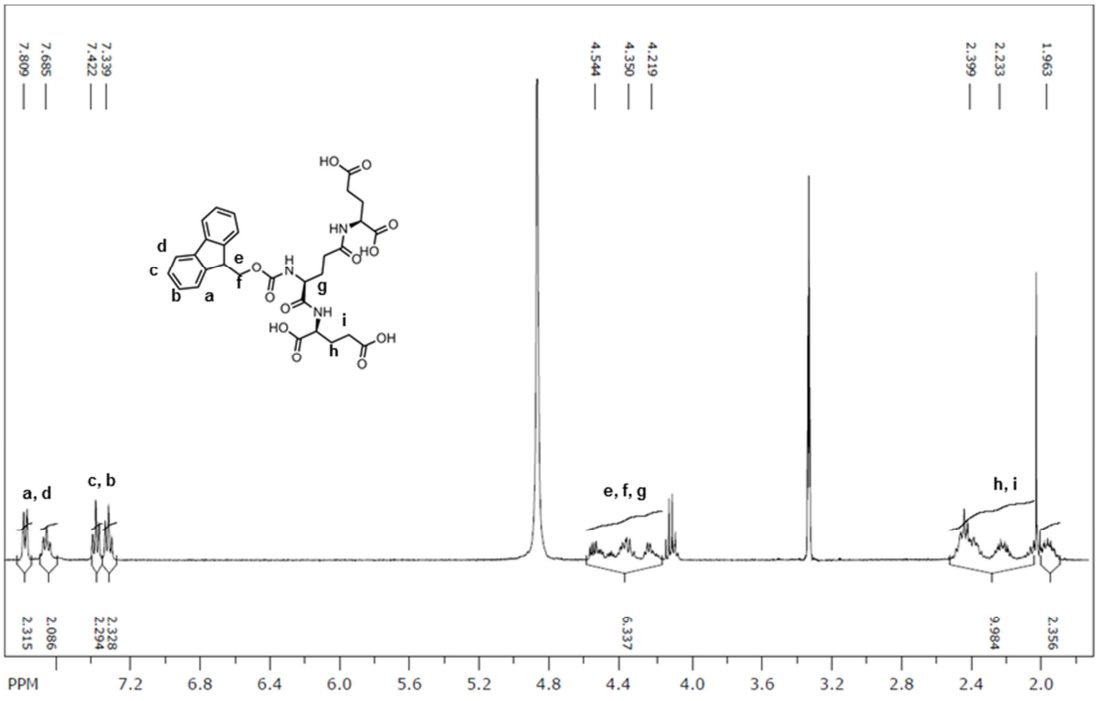


**Figure 3.18 – $^{1}$H NMR of Fmoc-PG-OH G0 (7) in deuterated methanol;** Fmoc group was used as reference and no evidence of hydrolysis of this group was evident in the spectra.

The synthesis of N-protected-PG-Ester G2 was then attempted using the different combinations of the previous synthesized precursors. The first was carried out by combining the Fmoc-PG-OH G0 (7) with $NH_2$-PG-OMe G0 (11) by DCC/NHS coupling. The second was carried out by combining N-Boc-PG-OH G0 (9) with $NH_2$-PG-OMe (11) by DCC/NHS coupling. The TLC for both couplings showed a complex mixture of products (data not shown). Multiple close peaks were observed which suggested the formation of both mono- and di-substitutions. The reaction was extended to 120 hours without change and the analysis by $^{1}$H NMR showed a complex mixture of peaks that could not be assigned to the G2. The incomplete substitution was probably due to the steric hindrance effects. Therefore once one carboxyl is substituted, the G0 may be too bulky for the substitution of another G0.

Consequently, two new synthetic routes to synthesize a G1 were tested and compared. Using a convergent approach, $NH_2$-PG-OEt G0 (12) was coupled to Fmoc-L-glutamic acid to form the G1. Similarly to the attempted synthesis of the G2, this approach yield multiple TLC spots which upon purification of the product yielded the Fmoc-PG-OEt G1 (13) in 44% yield. On the other hand, using a divergent approach combining the Fmoc-PG-OH (7) with glutamic acid di-ethyl ester afforded the product with a much higher yield (73-88%). These results further corroborated the effects of steric hindrance to limit the growth of PG dendrimers. Furthermore, as observed in $^{1}$H NMR (Figure 3.19), the

isolated product still showed the presence of small amounts of DCU urea. Several eluents mixtures in various ratios (ethyl acetate, methanol, diethyl ether, ether) were tested for the separation of the DCU but all showed similar rf to the dendrimer by TLC, and thus the separation by silica column chromatography was not complete. Moreover, running the product through a gradient of water/acetonitrile in a C18 column was not able to separate the product and most of it partitioned to the first fraction of 5% water in acetonitrile. This suggested that the dendrimer established strong interactions with the DCU urea.

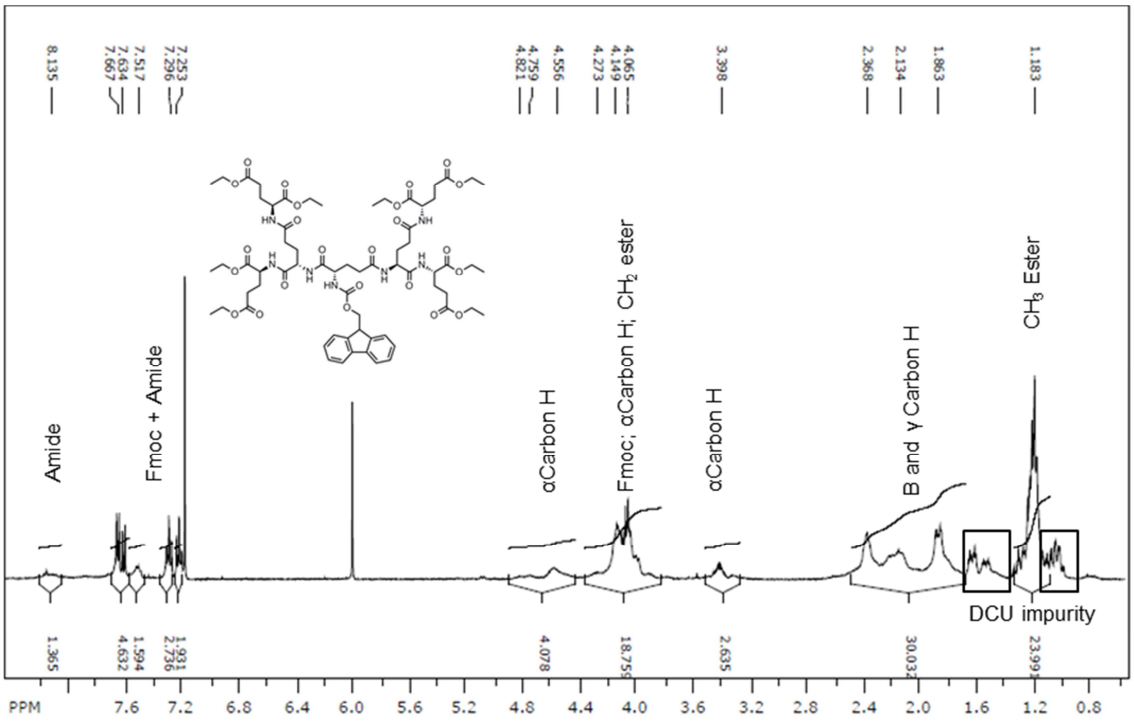


**Figure 3.19 – $^{1}$H NMR of Fmoc-PG-OEt G1 (13) in chloroform;** urea was still present in significant amounts as it can be observed by the peaks at 1.0-1.7 ppm; comparing to the $^{1}$H NMR of the G0, the signals were broader due to the exponential growth of signaling by each monomer. However, the Fmoc groups were still distinct and in proportional ratio to the ester groups which suggested complete reaction of all branches.

The Fmoc group was subsequently removed using piperidine to afford the $NH_2$-PG-OEt G1 (22) as a thick yellow oil. The TLC showed incomplete reaction where the initial product was still present even after extension of the the reaction time for 48 hours. The product was then purified by flash chromatography from a dry loading to afford the product with a low yield of 34%. To further test the availability of the Fmoc group for de-protection, the N-Boc-PG-OMe G1 (20) analogue was synthesized from reaction of the N-Boc-PG-OH (9) with glutamic acid di-methyl ester via DCC/NHS coupling. This compound was then reacted with 10 equivalents of TFA in an ice bath to remove the N-Boc[13]. A common problem that can arise during the N-Boc de-protection with TFA is

the cyclization of the glutamic acid[56]. To optimize the reaction, the small N-Boc glutamic acid was reacted with TFA and cyclization was indeed observed as the product did not react with ninhydrin and the integration of the $^1$H NMR did not match both esters (data not shown). However, when carrying out the reaction with N-Boc-PG-OMe G0 (8) and N-Boc-PG-OMe G1 (20) no cyclization were observed (ninhydrin reaction positive). Furthermore, the $^1$H NMR confirmed the peak corresponding to N-Boc group completely disappeared (Figure 3.20). In both cases, the products were obtained in quantitative yield (91-97%), therefore suggesting that the bulkiness of the group in the core is essential for the success of the de-protection reaction.

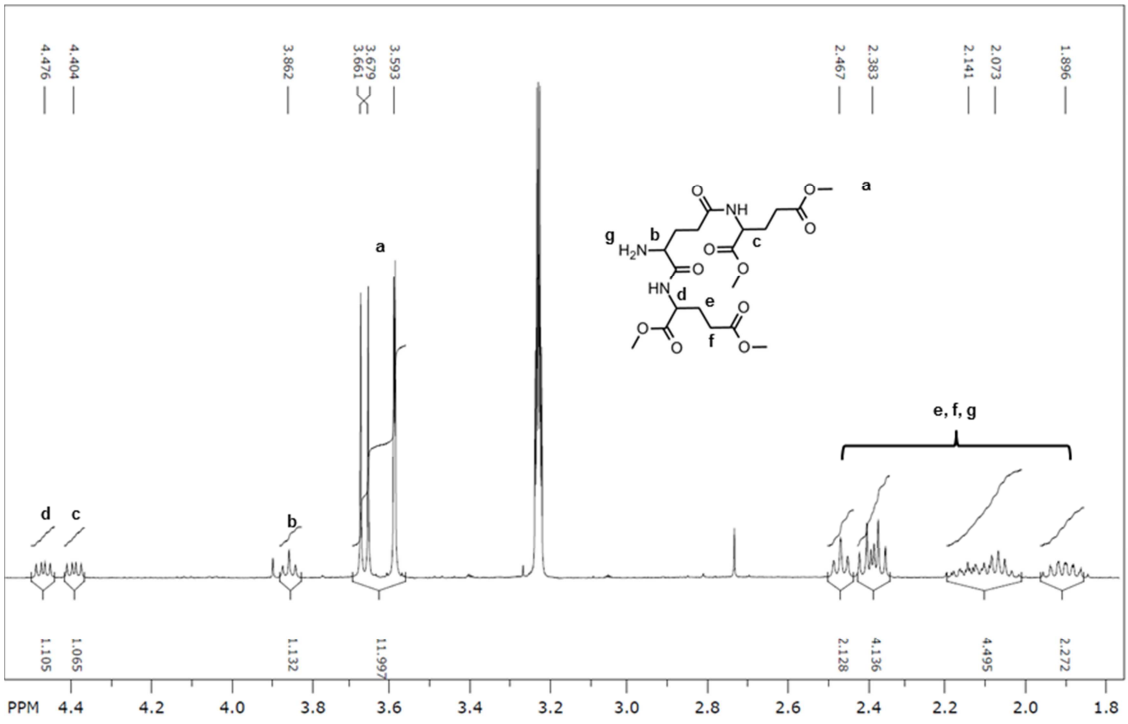


**Figure 3.20 – 1H NMR of $NH_2$-PG-OMe G0 (11) in deuterated methanol;** the N-Boc was not visible suggesting complete hydrolysis

The newly synthesized $NH_2$-PG-OEt G1 (22) was then coupled to Fmoc-L-glutamic acid in a convergent manner to form the G2 intermediary. However, as expected multiple peaks appeared in the TLC and upon isolation of these products the $^1$H NMR showed multiple complex peaks that indicated a complex mixture of multiple Fmoc and esters peaks close to each other together with urea and unknown peaks. Altogether, these results suggested that the divergent synthesis may be a more suitable route for the synthesis of this type of dendrimers since the bulkiness of the dendrons prevents complete substitution of both carboxyl groups of the GLU monomer.

Consequently, the divergent approach was further explored. To this, the N-Boc-PG-OMe G1 (20) was hydrolyzed with LiOH/MeOH/THF/water to obtain the N-Boc-PG-OH G1 (21) (Figure 3.21) as an yellow oil with an yield of 38%. Alternatively, the Fmoc-PG-OtBu G0 (6) was synthesized via DCC/NHS (yield: 96%) and then hydrolyzed to form Fmoc-PG-OH G0 (7) in quantitative yield. This was subsequently used to form the G1 via DCC/NHS to afford the Fmoc-PG-OtBu G1 (15) (yield: 85%). Finally, the later was then hydrolyzed with TFA to afford the Fmoc-PG-OH G1 (16) (Figure 3.21) with a yield of 55%. These results showed that the de-protection of *tert*-butyl esters had an improved yield in comparison to the methyl esters. However, as observed previously, the ability to de-protect the Fmoc is harder than the N-boc. Nevertheless, to further explore the best approach, both compounds were used to synthesize PG G2 dendrimers.

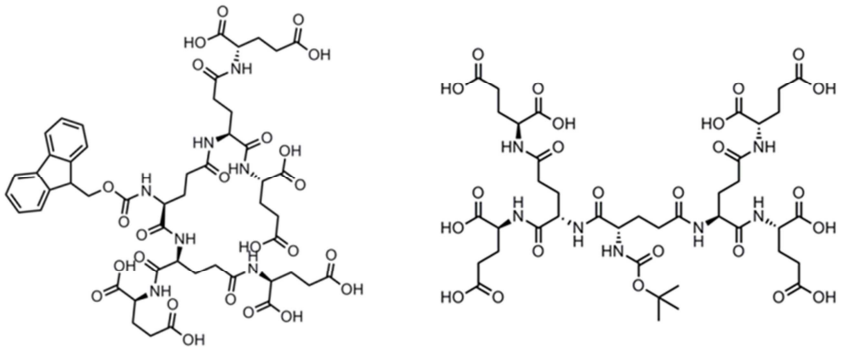

**Figure 3.21 – 2D structure of the Fmoc-PG-OH G1 (16) (left) and N-Boc-PG-OH G1 (21) (right)**

As a result, Fmoc-PG-OH G1 (16) was reacted with L-glutamic acid di-*tert*-butyl-ester whereas the N-Boc-PG-OH G1 (21) was reacted with L-glutamic acid di-methyl ester via DCC/NHS coupling to afford the corresponding G2. However, both products were obtained in low yield (5-21%). Moreover, the purification of the G2 showed to be particularly difficult since no suitable eluent was found to effectively separate the high amounts of urea even at high salt concentrations as well as in acidic conditions on both silica column chromatography and C18 column (with varied ratios of water/acetonitrile). Moreover, the $^{1}$H NMR showed to be extremely complex and high amounts of urea peaks were present (e.g. $^{1}$H NMR of Fmoc-PG-OtBu G2 (24) in Figure 3.22). In fact, due to the high number of repetitive monomers the integration of the signal and attribution of the peaks is considerably harder and cannot be done properly to determine whether the urea is associated or coupled to the main dendrimer backbone. The COSY NMR also displayed a complex signal that did not allow the determination of whether the urea was bonded to the dendrimer (data not shown).

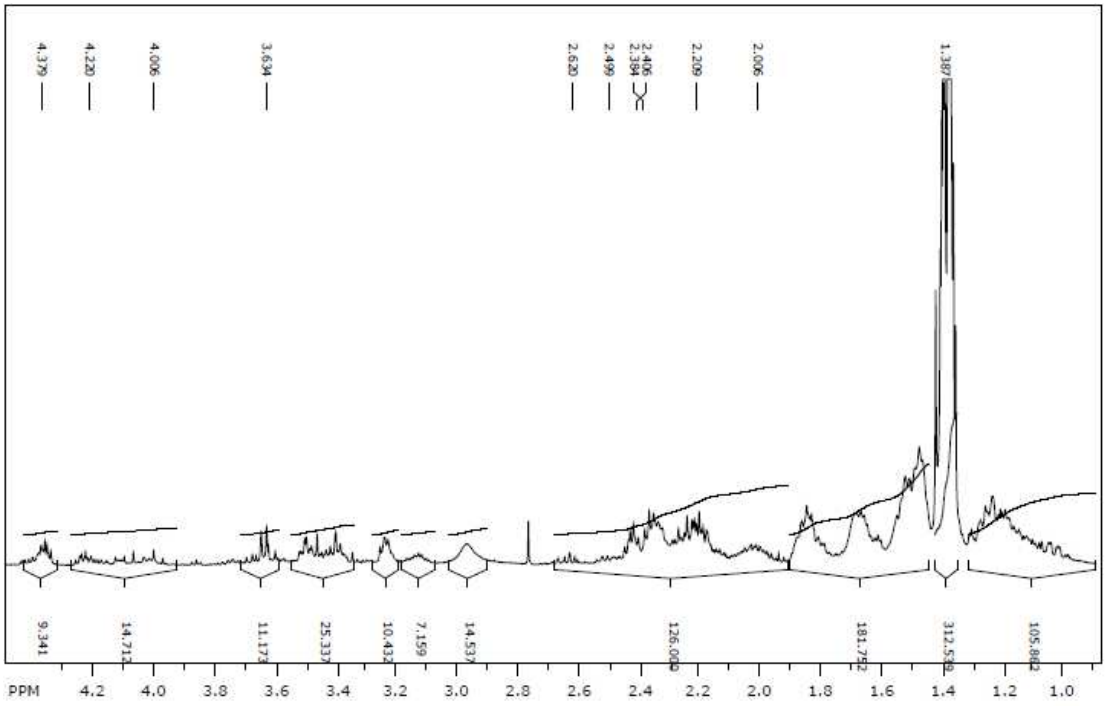


**Figure 3.22 – $^{1}$H NMR of the Fmoc-PG-OtBu G2 (24) in deuterated chloroform.** The NMR spectra started to become very complex. However, high amounts of urea can be observed demonstrating the difficulty in purification for the bigger dendrimers.

Furthermore, even after hydrolysis of the N-Boc-PG-OMe G2 (24) with LiOH, the DCC remained in the water phase after washings with organic solvents. Therefore, it was not possible to ascertain whether or not the DCC was linked or complexed to the dendrimer. Nonetheless, it is plausible that these form a stable complex (Figure 3.23) between the carboxylic acid and the urea group and when in the ester form, the PG may work as a host molecule for the DCC/DCU. On the other hand, because there are a higher number of terminal groups the reaction may be slower for the substitution of the NHS and thus leading to the side product. This is also evidenced by the fact that even at high salt concentrations there was no evident reduction of the DCU. Nevertheless, the yield of recovery was extremely low (~11%) and thus not suitable as a method for further growth of the dendrimer.

Previous studies of PG dendrimers have described high yield for the G0 (around 65-92%)[15,28] and G1 (58-92%)[15],[24] which drop drastically for the G2 (33-51%)[15,24,29]. One reason for lower yields at higher generations may be due to the crowding effect resulting in steric hindrance. This could be observed when comparing glutamic acid and aspartic acid as building blocks for dendrimers using a convergent method where aspartic acid based dendrimers had a yield of 10% for G2, whereas this was slightly higher (33%) for PG dendrimers[29]. This can also occur in the core as observed for

benzene tricarbonyl or dicarbonyl cores, where 40 and 50% yield was obtained respectively. In the convergent approach, the N-protected group has to be removed. In the case of N-benzyloxycarbonyl groups this could be removed with high yields with iodotrimethylsilane for G0 (94%) but not for G1 where the slow cleavage allowed the ester degradation and thus Pd-C/$H_2$ had to be used, which afforded a good yield (73%)[15]. Therefore, taking into account the results obtained in this work together with the ones reported in the literature, the synthesis of higher generations PG dendrimers should be carried out by divergent synthesis. As a result, given that DCC is a bulky reagent and it is difficult to remove, different coupling reagents were tested to ascertain the ability to improve the yield and purification of PG dendrimers.

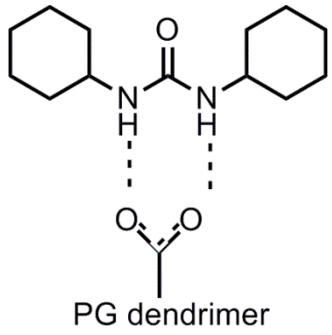


**Figure 3.23 – Possible complex between urea the carboxylic groups of the PG dendrimer**

### 3.2.2. Synthesis of PG dendrimers using alternative coupling agents

The Fmoc-PG-OtBu G0 (6) was chosen as a reference to study the ability of different coupling reagents to afford the PG dendrimers with high yield and ease of purification. These reagents included: (a) DCC; (b) DIPC; (c) EDC; and (d) CDI. Results for the synthesis of this dendrimer are displayed in table 3.1. It can be observed that different coupling reagents resulted in varied yield of recovery. Even though some reactions had lower yield they are comparatively similar to the others previously described since these reagents (EDC and CDI) can be easily removed by aqueous washings.

Similarly to the results obtained with DCC coupling, the DIPC coupling produced higher yields in the presence of NHS. However, contrary to the DCC, the urea of DIPC did not precipitate. In order to remove it, column chromatography had to be carried out for purification. On the other hand, using the water soluble carbodiimide EDC showed a significantly drop in the yield. However, the purification was much easier since all side products and precursors can be extracted to the aqueous layer under acidic conditions. Nevertheless, the major consensus on using this reagent is that it can result in lower yields in comparison to other reagents[35]. This comparatively lower yield was also

observed in the synthesis of both Fmoc-PG-OEt G0 (4) and N-Boc-PG-OMe (8), where a yield in the range of 44-60% was achieved. This is in contrast with the work carried out with EDC for other PG dendrimers where high yields were attained[57]. Again, the limited spacing between both carboxyl groups in the same GLU may contribute to this issue, since in these dendrimers di-glutamic acid (instead of a single GLU) were used as monomers for branching. Thus, when single GLU are used, it is possible that after one of the carboxylic acid groups reacted with EDC, the side chain of the latter may interfere by forming a salt bridge with the other carboxylic acid in the other side chain of the GLU, thus slowing the reaction.

**Table 3.1 – Yield obtained for Fmoc-PG-OtBu G0 (6) reaction using different coupling reagents**

| Coupling reagents | Yield (% expected mass) |
|---|---|
| DCC/NHS | 96%* |
| DIPC | 44%** |
| DIPC/NHS | 80%** |
| EDC/HOBt | 55% |
| CDI | 78-88% |

Notes: * urea present; ** after column purification; DCC: *N,N'*-Dicyclohexylcarbodiimide; NHS: N-hydroxysuccinimide; DIPC: N,N′-Diisopropylcarbodiimide; HOBt: Hydroxybenzotriazole; CDI: 1,1'-Carbonyldiimidazole

Finally, CDI was also tested as coupling reagent. CDI, similarly to EDC, offers a valuable benefit for amide formation since the work up is easily carried out by washing of the organic phase with acidic solutions and phase separation. Moreover, with the use of glutamic acid ester hydrochloride monomers, the acid protonates the remaining CDI, promoting its precipitation in solution. As observed in table 3.1., CDI afforded the small dendrimers in high yield. Moreover, the dendrimer was obtained with minimal loss in the purification process and no side products were obtained after purification. Consequently, this reagent was chosen to carry out further synthesis of PG dendrimers.

To this, the Fmoc-PG-OtBu G0 (6) was then hydrolysed using TFA to afford a viscous yellow oil in quantitative yield. The obtained Fmoc-PG-OH G0 (7) was then pre-activated with CDI and coupled with L-glutamic acid di-*tert*-butyl ester to afford the Fmoc-PG-OtBu G1 (15) with a yield of 62-80%. The $^{1}$H NMR (Figure 3.24) showed that the dendrimer was obtained pure, and the integration of peaks correlated with the substitution of all carboxyl groups.

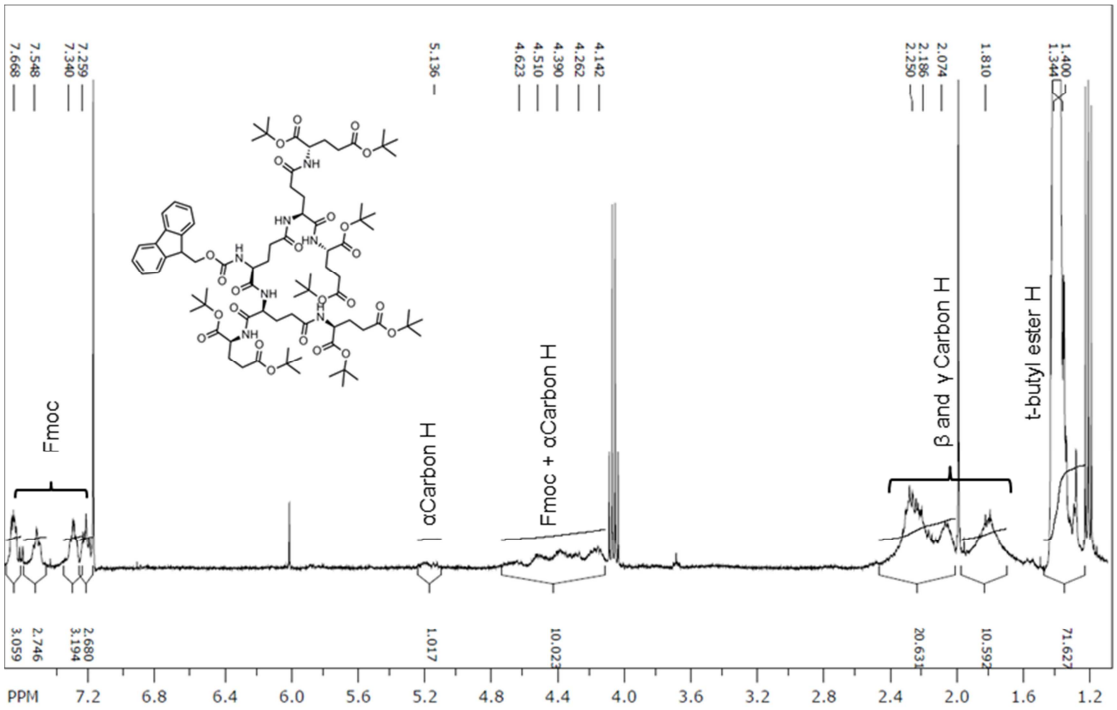


**Figure 3.24 – $^{1}$H NMR of Fmoc-PG-OtBu G1 (15).** The NMR showed the Fmoc group signal between 7.29-7.66 ppm and around 4.26-4.51 ppm similarly to the previous PG dendrimers. Solvent peaks were still present.

Because *tert*-butyl esters are bulky, a different type of coupling reagent was also tested. HATU (Hexafluorophosphate Azabenzotriazole Tetramethyl Uronium) and HBTU (Hexafluorophosphate Benzotriazole Tetramethyl Uronium) are generally potent coupling reagents that have high success for bulky amino acids. In fact, the combination of HATU/DIPEA has previously been used in the synthesis of tryptophan-terminated dendrimers with tert-butyl esters[55]. Therefore, these reagents were first tested on their ability to synthesize Fmoc-PG-OEt G0 (4) and Fmoc-PG-OMe G0 (5) since they are cheaper derivatives of glutamic acid. These reagents showed the ability to produce these dendrimers in highly pure forms with minimal purification steps (yield 70-92%). However, when using these reagents in the synthesis of Fmoc-PG-OMe G1 (14), the NMR showed a mixture of multiple Fmoc peaks including the ones previously determined to correspond to fulvene peaks. However, whether the coupling reagents were responsible for acting as a base for de-protection of the Fmoc or the product was degraded during handling was not determined.

Therefore, the previously obtained Fmoc-PG-OtBu G1 (15) was then hydrolysed using TFA and extracted to an organic solvent to obtain the Fmoc-PG-OH G1 (16) as a

dense orange oil (yield 56-72%). The $^{1}$H NMR (Figure 3.25) showed complete removal of *tert*-butyl esters as observed by the disappearance of the 1.40 ppm peak.

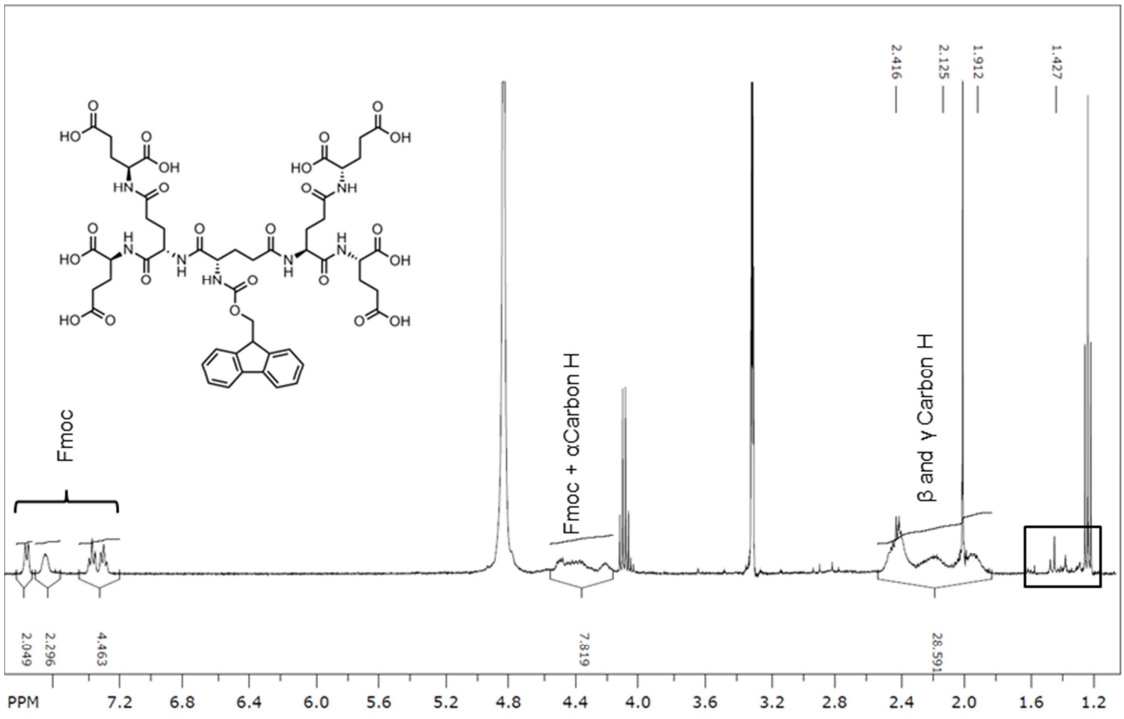


**Figure 3.25 – $^{1}$H NMR of Fmoc-PG-OH G1 (16) in deuterated methanol;** solvent peaks were still present; the *tert*-butyl ester groups were not present at 1.40 ppm indicating that the hydrolysis was complete.

Continuing the synthesis cycle, the Fmoc-PG-OH G1 (16) was then activated with CDI for 24 hours. Following the reaction by TLC, it was possible to observe a multitude of peaks arising from the origin point (data not shown). After 24 hours, no change in the peaks was observed even after adding more CDI and thus the L-glutamic di-*tert*-butyl ester was added and the reaction was allowed to continue for 7 days. After purification, the Fmoc-PG-OtBu G2 (17) was obtained as a sticky white plastic-like product with a very low yield of 5%. This low yield is expected as the *tert*-butyl esters are very bulky and thus may restrict the coupling on both sides of the glutamic acid. Nevertheless, the obtained dendrimer was then subjected to hydrolysis with TFA to yield the Fmoc-PG-OH G2 (18) as a very dense turquoise oil (yield 11%) that showed low solubility in methanol. The analysis of the $^{1}$H NMR (Figure 3.26) showed some impurities around 1.05-1.35 pm which can be expected due to the multitude in carboxyl groups that may establish complexes with impurities present in solvents. It is also noticeable that the color of the oil obtained for G0, G1 and G2 varied from yellow, orange and turquoise respectively. Furthermore, at this point, very small yields were obtained probably due to the amount of acid that has to be used in the hydrolysis reaction, which probably

degraded the dendrimer. Nevertheless, the small amounts of Fmoc-PG-OH G2 (18) obtained were activated with CDI and coupled to the tert-butyl derivative but very small amounts of a product were obtained (even the precipitate of CDI was analyzed to determine if the dendrimer had been precipitated). Because the amounts were low and the signals were weak and very broad it was not possible to assign the peaks to the NMR.

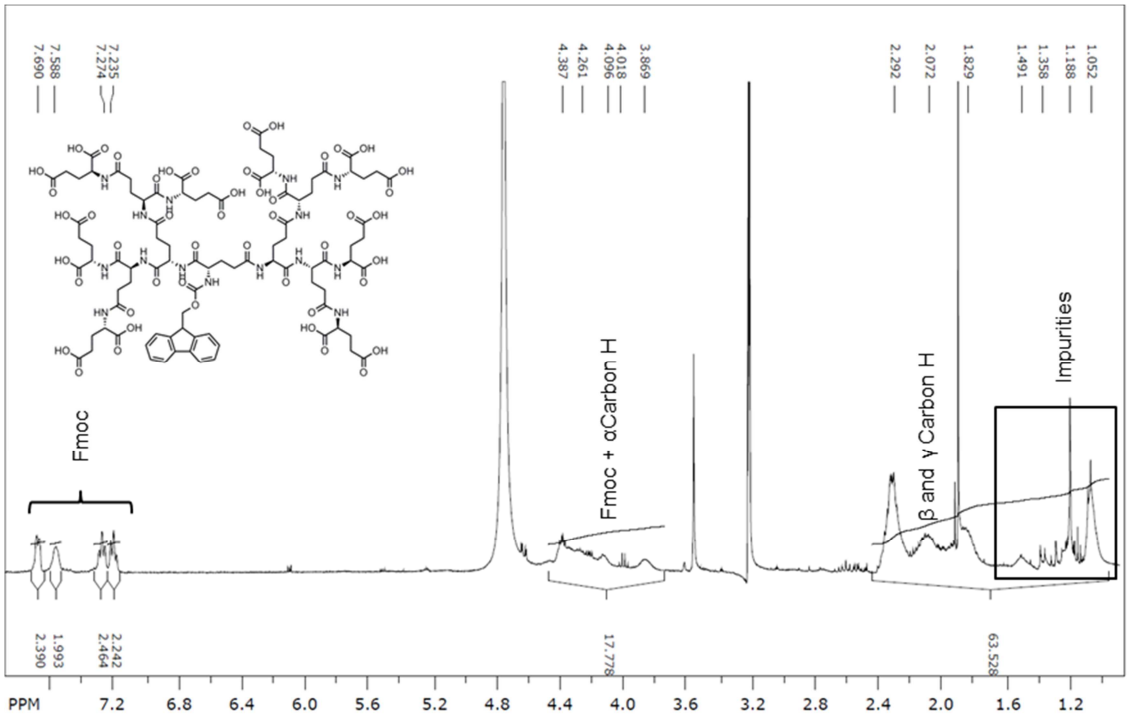


**Figure 3.26 – $^{1}$H NMR of Fmoc-PG-OH G2 (18) in deuterated mthanol.** The tert-butyl ester groups were not present at 1.40 ppm showing that the hydrolysis was complete.

Due to the bulkiness of the *tert*-butyl esters and the previously described difficulties of removing the Fmoc at higher generations, a different alternative was explored that would facilitate the integration of the NBD at this point. Despite the limited success at ester removal via basic hydrolysis for methyl esters, the fact that these are compatible with N-Boc and are less bulky, suggested that higher generations could be easier to synthesize. As a result, the N-Boc-PG-OMe G0 (8) was synthesized using CDI, HBTU/HOBt/DIPEA[58] or HATU/HBTU/DIPEA as coupling agents and all reactions were obtained in high yields (86-99%). Again, the product was obtained by washing the organic solvent with aqueous solutions and afforded the dendrimer as a pure product (Figure 3.27). The amides displayed distinct peaks (7.17, 7.51 and 5.00 ppm) in deuterated methanol and all three $\alpha$-carbon hydrogens had distinct signals (4.69, 4.60 and 3.91 ppm).

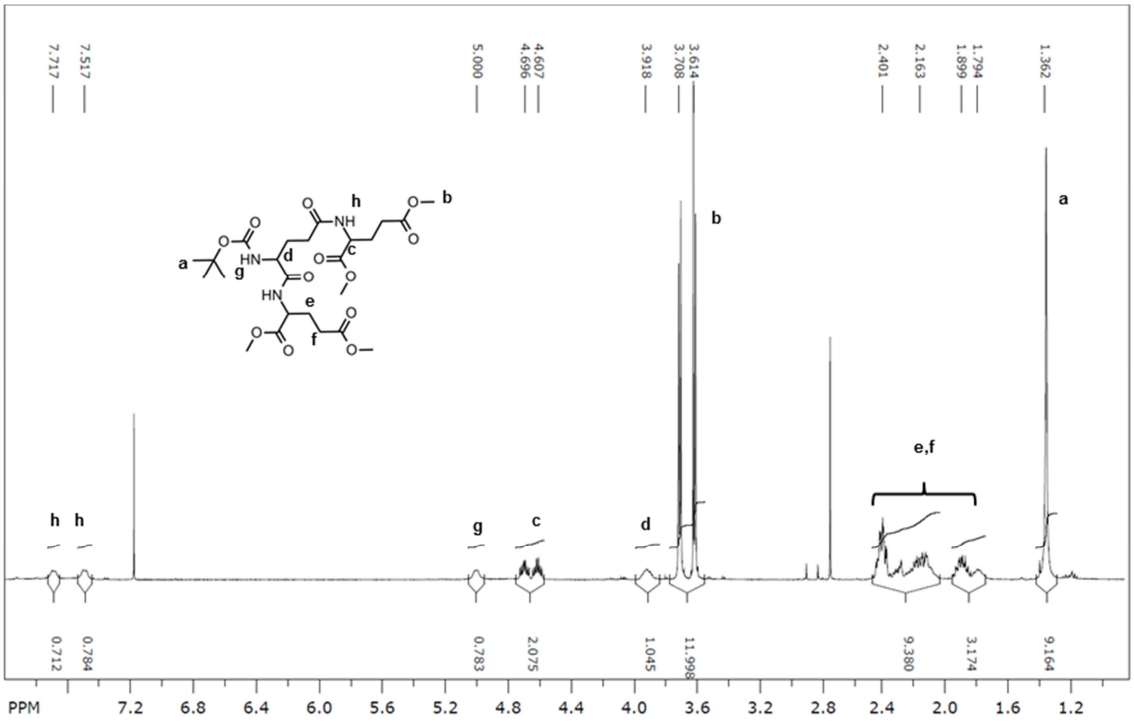


**Figure 3.27 – $^{1}$H NMR N-Boc-PG-OMe G0 (8) in deuterated methanol.** The 3 amides and 3 α-carbon hydrogens can be observed as distinct signals.

The N-Boc-PG-OMe G0 (8) was then hydrolyzed with LiOH/THF/MeOH/water to afford the N-Boc-PG-OH (9) as a sticky yellow oil (yield: 65-86%) and subsequently reacted with L-glutamic acid di-methyl ester via CDI coupling to generate the N-Boc-PG-OMe G1 (20) as a yellow oil (Yield: 50%). This product was then hydrolyzed again to yield a dense yellow oil with poor yield (yield: 38%). The next generation was then obtained via HBTU/HOBt/DIPEA coupling to obtain the N-Boc-PG-OMe G2 (24) with an improved yield of 45%, which was similar to the one reported in the literature for similar PG dendrimers and reagents[24]. However, when analyzing the $^{1}$H NMR (Figure 3.28) the assignment of peaks was not in agreement to the ones reported for similar dendrimers using an adamantane core[29], as well as the peaks observed for the N-Boc-PG-OMe G0 (8). The disparity in the obtained $^{1}$H NMR concerns the number of α-carbon hydrogens present, where only a broad peak at 4.44 ppm can be observed (Figure 3.28). Also, a shift of the N-Boc to 0.770 ppm was observed but this could have been due to N-Boc being buried inside the dendrimer. Using the methyl groups at 3.61-3.70 ppm as a reference (accounting for 48 hydrogens) and assuming that the α-carbon hydrogens shifted, the integration of all peaks between 1.22 and 2.70 account for the possible missing α-carbons hydrogens as well as the internal β and γ carbon hydrogens. Given this is a reasonable assumption, the product was obtained pure. Therefore, further analysis including $^{13}$C NMR and MS should be conducted to

determine the purity of the compound or whether it is a degraded product. Because the overall yield to obtain the G2 was low taking into consideration both coupling and de-protection reactions, new synthetic alternatives should be considered. This could be carried by using solid phase synthesis to facilitate the purification process of by altering the scaffold of PG dendrimers.

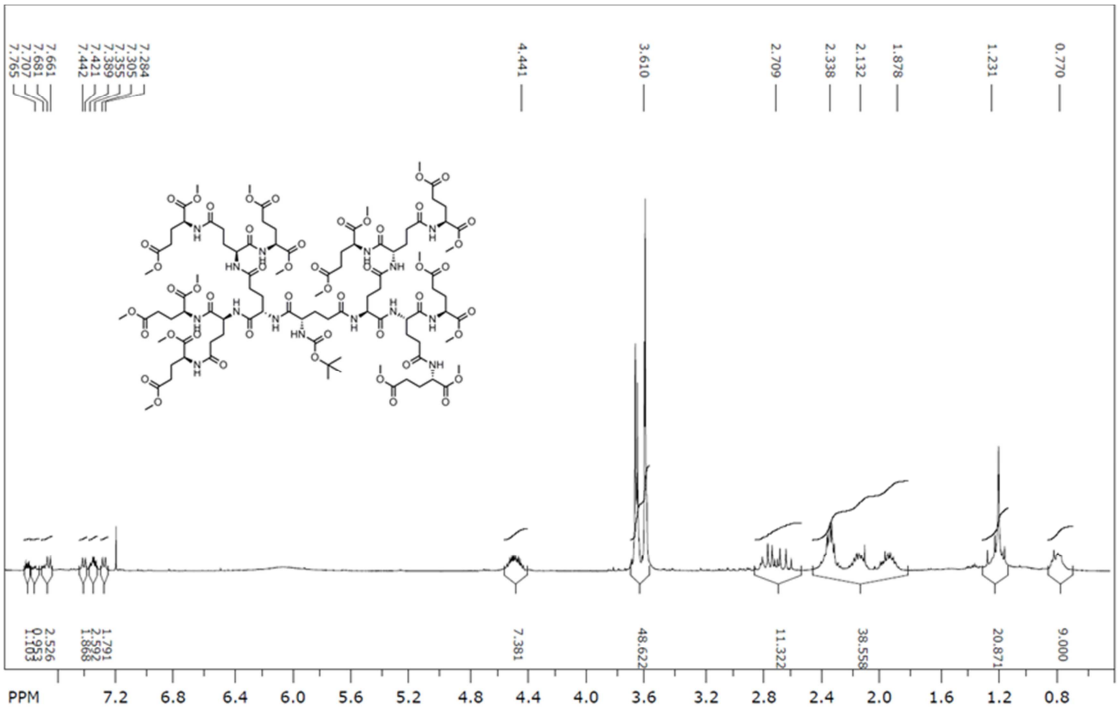


**Figure 3.28 – $^{1}$H NMR N-Boc-PG-OMe G2 (24) in deuterated chloroform; the N-Boc at 0.770 ppm as well as the methyl groups at 3.610 ppm were used as reference.**

### 3.2.3. Attachment of NBD to the core of PG dendrimers

Coupling of GLU and PG dendrimers to NBD was concomitantly studied in order to ascertain at which step it would benefit its coupling. Based on the experimental results of Fmoc removal, and on literature data regarding the convergent synthesis of PG dendrimers[24], even for the synthesis of G1, the yield of the reaction was expected to be lower. This suggests that the amine of the core may be unavailable to react. The coupling of various fluorophores such as dansyl, rhodamine, nitrobenzoxadiazole and phthalamine are generally carried out by coupling to an amine[59]. In particular, several different amino acids have been coupled to NBD using different conditions including different solvent (methanol, ethanol and ethanol/sodium acetate, DCM, DMF acetonitrile, methanol:water), different bases (potassium acetate, sodium hydrogen carbonate, triethylamine, $Na_2B_4O_7$, $K_2CO_3$) and different temperatures (from room temperature to 80$^{o}$C) and for different extensions of time (5 min to 48h)[38–41,43,44,60].

Common side products observed when coupling amino acids to NBD is the substitution by hydroxyls present in the solvent resulting in impurities such as NBD-OH[43] and NBD-O-$CH_3$[41].

Therefore the applicability of NBD to PG dendrimers was studied using different derivatives of GLU (L-glutamic acid, L-glutamic di-ethyl ester, L-glutamic di-methyl ester and L-glutamic di-*tert*-butyl ester; Figure 3.29) in different conditions (varying both bases and solvents) to optimize the coupling reaction.

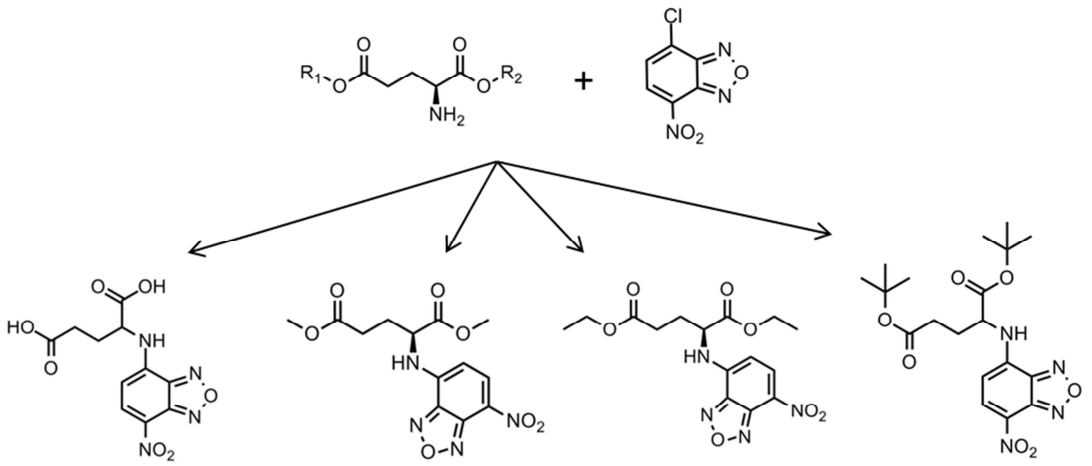

**Figure 3.29 – Reaction scheme of the different obtained products tested to optimize GLU coupling to NBD**

Table 3.2 outlines all conditions tested for the coupling reaction. A common feature observed across all reactions was that the reaction started with a light orange color that evolves to a darker color of blue, brown, red and black tones. The difference in tones was dependent not only on the GLU derivative but also on the impurities formed. All reactions were followed by TLC (ethyl acetate/hexane (1:1 v/v)) and were terminated once the GLU spot did not test positive to ninhydrin. The results showed clear trends that both DMF and acetonitrile were the favorable solvents and that DIPEA and $Cs_2CO_3$ were the better bases. In fact, when using carbonate bases a clear trend of increasing yield was observed. For example the glutamic acid di-ethyl ester reaction with NBD had a yield of 50%, 73% and 88% when using $Na_2CO_3$, $K_2CO_3$ and $Cs_2CO_3$ respectively. This is in line with previous reports of high yield reactions for conjugation of NBD to putrescine, tri-Boc-spermine or N-Boc-piperazine using $Cs_2CO_3$ as base in acetonitrile. Furthermore, the yield was increased with *tert*-butyl and methyl esters suggesting that the type of ester may contribute to the reaction. On the other hand, using strong bases, such as KOH, or methanol as solvent was detrimental for the

reaction. This was due to the formation of the side products as a consequence of direct reaction with NBD (Figure 3.30)[43,61].

**Table 3.2 – Different conditions tested for coupling of NBD to different glutamic acid derivatives; $R_1$ and $R_2$ denote the carboxyl portion of glutamic acid;**

| $R_1$; $R_2$ group | Solvent | Base | Yield / % |
|---|---|---|---|
| Carboxyl | DMF | $K_2CO_3$ | 0% |
| | DCM | DIPEA | 40% |
| | Acetonitrile | DIPEA | 51% |
| Ethyl ester | MeOH | $Na_2CO_3$ | 16% |
| | MeOH | TEA | 15% |
| | Acetonitrile | TEA | 98% |
| | DMF | $Na_2CO_3$ | 50% |
| | DMF | TEA | 53% |
| | DMF | KOH | 27% |
| | DMF | $K_2CO_3$ | 71% |
| | DMF 80$^oC$ | $K_2CO_3$ | 73% |
| | DMF | $Cs_2CO_3$ | 88% |
| | Acetonitrile | $K_2CO_3$ | 73% |
| | DCM | $K_2CO_3$ | 71% |
| Methyl ester | DMF | DIPEA | 96% |
| | DMF | $K_2CO_3$ | 88% |
| | DMF | $Cs_2CO_3$ | 92% |
| t-butyl | Acetonitrile | $Cs_2CO_3$ | 82% |
| | Acetonitrile | DIPEA | 92% |
| | DCM | $Cs_2CO_3$ | 97% |
| | DCM | $K_2CO_3$ | 88% |
| | DMF 80$^oC$ | $Cs_2CO_3$ | 90% |
| | DMF | $Cs_2CO_3$ | 97% |
| | DMF | DIPEA | 98% |

The pure NBD-GLU-OMe (26) and NBD-GLU-OtBu (27) (Figure 3.31) were then used to study the effects of acid and basic hydrolysis on these compounds. For this purpose, basic hydrolysis of methyl esters was carried out with LiOH/THF/Water, and acidic hydrolysis of *tert*-butyl esters was carried out with TFA. The basic hydrolysis showed multiple NBD peaks on the TLC and the hydrolysis was incomplete. Among the obtained products the common NBD-OH peaks were found on the $^1H$ NMR. Similarly,

the TFA reaction produced several NBD peaks on the TLC, and the $^{1}$H NMR showed significant shift on the α-carbon hydrogen, which could be caused by the probable cyclization of the glutamic acid (data not shown).

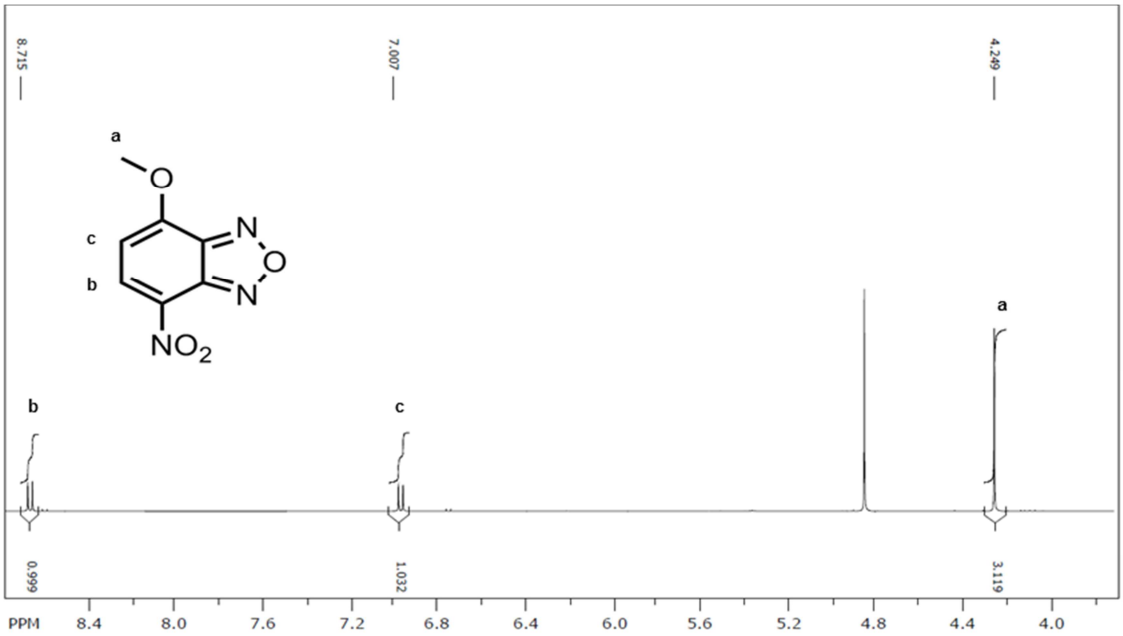


**Figure 3.30 – $^{1}$H NMR of a side product from the reaction of glutamic acid with NBD where the methanol directly substitute the chloride.**

Extending the NBD coupling to PG dendrimers, the fluorophore was reacted with $NH_2$-PG-OEt G0 (10), $NH_2$-PG-OMe G0 (11) and NH2-PG-OtBu G0 (12) in DMF with $Cs_2CO_3$ or DIPEA, and the conjugates were obtained with a yield of 65%, 68% and 44%, respectively. Similarly to the results obtained in the convergent synthesis approach, the bulkier derivative resulted in lower yield. Again, these results suggest that steric hindrance prevents the orthogonal attack of the amine to the NBD.

The NBD-PG-OMe G0 (30) was then hydrolyzed with LiOH in THF/MeOH/water to afford the NBD-PG-OH G0 (31) as dark colored oil with a yield of 53%. However, the TLC showed that both precursors and the NBD-OH impurity were still present. On the other hand, the NBD-PG-OtBu G0 (32) was hydrolyzed with TFA and recovered with a yield of 35%. The $^{1}$H NMR showed multiple peaks for the dendrimer and NBD, which could be related to polymerization. It is therefore possible that the conversion of the secondary amine to a quaternary one may result in the release of NBD. However, no further experiments were carried to elucidate these low yields. The NBD-PG-OH G0 (31) obtained from both hydrolysis was then activated with HBTU/HOBt/DIPEA and coupled to L-glutamic acid di-*tert*-butyl ester to afford the NBD-PG-OtBu G1 (33) (yield

of 55%). The TLC however showed multiple colored spots which suggested that NBD is not stable under the experimental conditions.

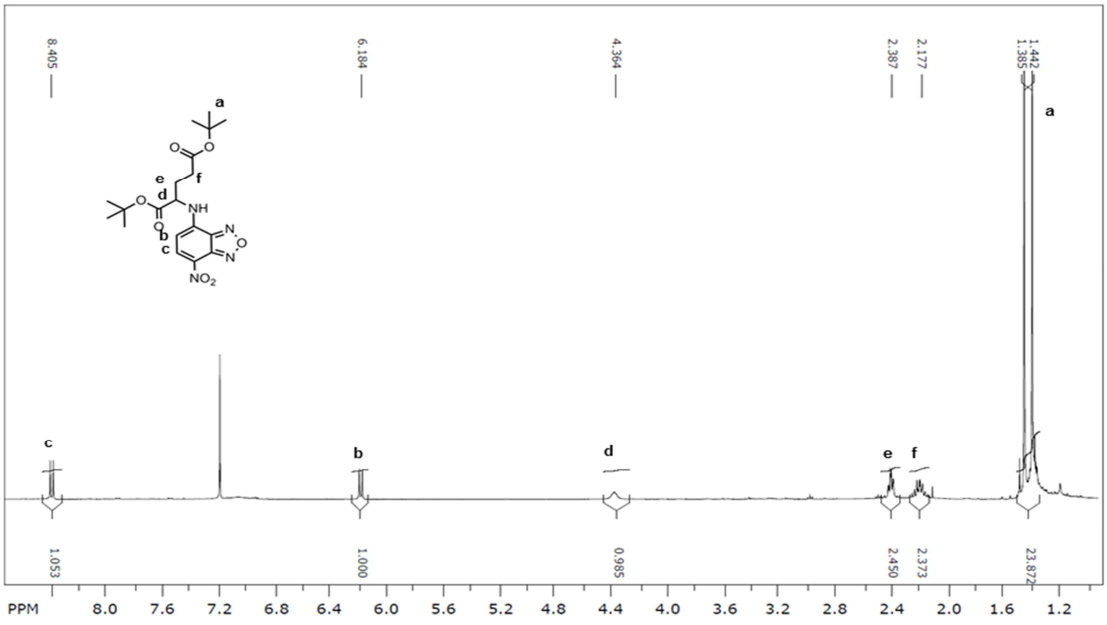


**Figure 3.31 – $^{1}$H NMR of NBD-GLU-OtBu (27) in deuterated chloroform**

### 3.2.4. Derivatization reactions of the core amine

Because secondary amines can still be reactive (e.g. react with CDI[62]), the transformation of the amine of GLU was further studied. In order to test the viability of using a secondary amine to couple NBD, L-proline methyl ester was first used to optimize the reaction. The latter was coupled to the NBD using DIPEA or $Cs_2CO_3$ as base and afforded the NBD-proline-OMe (44) with a yield of 59% and 37% respectively. This suggested that secondary amines are still able to couple to NBD and therefore the modification of GLU amine should be a viable strategy. Alkylation of amines is widely used and this approach has been previously reported for the synthesis NBD-tri-Boc-spermine[60]. However, alkylation reactions can sometimes also methylate carboxylic acids[63] or even the $\alpha$-carbons[64] depending on the type of strong base (LDA, methyl iodide (MeI)) used. Nevertheless, this is not problematic for the PG dendrimers since the core is restricted from the external environment, and these alterations are not expected to impact the overall structure (i.e. branching). As a result, mono-methylation of GLU was carried using different bases ($Cs_2CO_3$, LDA or NaH) in DMF as previously reported in the literature[65,66]. The direct alkylation with alkyl halides is a common practice for the formation of secondary amines but it is limited due to the possible over-alkylation that creates a mixture of primary, secondary and tertiary

amines as well as quaternary salts[67]. Both the starting amine and the product amine are nucleophiles and consequently it will be alkylated a second time when competing with the starting material. To this, the addition of an inorganic base in a polar aprotic solvent (DMF, DMSO, MeCN) is commonly used to prevent the overalkylation. In fact, $Cs_2CO_3$ has shown to not only promote mono-N-alkylations but also to suppress overalkylations, favoring secondary amine formation over tertiary amines[67]. However, performing the reaction in these conditions afforded the N-alkyl-GLU-OMe (36) and N-alkyl-GLU-OH (37) in very low yields of around 10-34%. Subsequently, using the N-alkyl-GLU-OMe (36) to further react with NBD-Cl in the presence of $Cs_2CO_3$ resulted in a TLC with multiple NBD peaks suggesting that the conversion of the amine promoted the formation of NBD side products (possibly due to slower reaction rate). Therefore, as an alternative, the NBD-GLU-OtBu (27) previously synthesized was reacted with MeI in the presence of $Cs_2CO_3$ to afford the N-alkyl-NBD-GLU-OtBu (40) (Figure 3.32). Again the TLC showed multiple spots of NBD and the desired product was obtained by preparative TLC in low yields. However, contrary to the previously observed cyclization of glutamic acid after TFA hydrolysis, the N-alkyl-NBD-GLU-OH (41) was obtained pure as a salt (Figure 3.33). On the other hand, when alkaline hydrolysis[68] was used for the N-alkyl-NBD-GLU-OMe (39) it resulted in removal of the NBD, which limits this synthetic route.

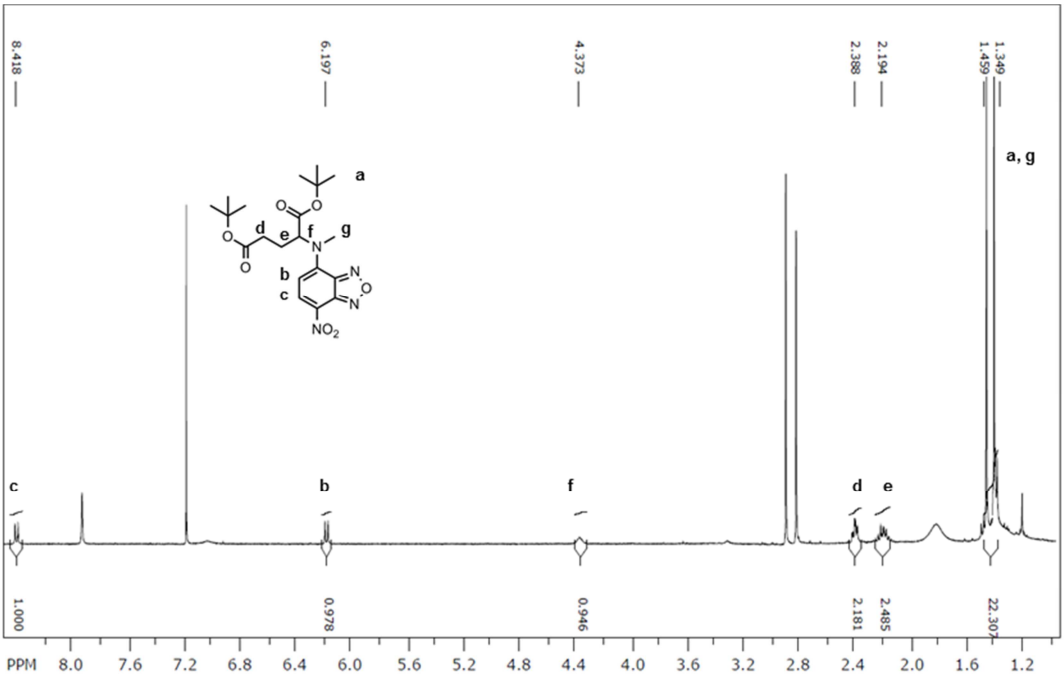


**Figure 3.32 – $^1$H NMR of N-alkyl-NBD-GLU-OtBu (40) in deuterated chloroform.** The NBD peaks have a ratio of 1:1 to the α-carbon hydrogens and 1:2 ratio to the β and γ carbon hydrogens. Solvent peaks are still present

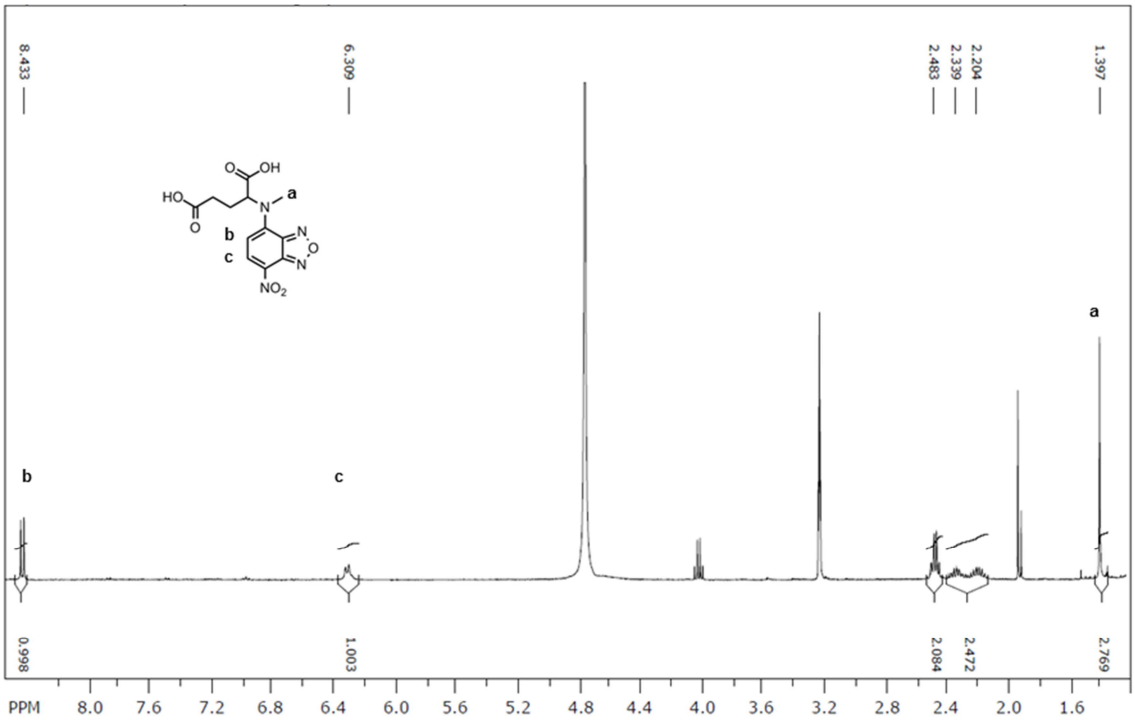


**Figure 3.33 –$^{1}$H NMR of N-alkyl-NBD-GLU-OH (41) in deuterated methanol.** The 1.39 ppm single peak corresponds to the alkyl group in a ratio of 1:3 of NBD to Alkyl. Solvent peaks are still present

To further explore other amine modifications to use GLU-NBD as the core, the N-Boc-glutamic acid was alternatively used since the amine is not primary but rather in resonance with the carbonyl. In this strategy, the alkylation of the amine[69–71] would be followed by subsequently hydrolysis of the N-Boc and the secondary amine would then react with the NBD to afford the tertiary amine. It was previously reported that selective N-methylation of Boc-protected valine using MeI in the presence of NaH occurred because the carboxylate was protected by chelation with $Na^{+}$ ions[72]. Moreover, based on previous reports, the use $K_2CO_3$ should not methylate the N-Boc amine[73]. Therefore, to test this approach, methylation of the amine was tested with $Cs_2CO_3$. As a base, $Cs_2CO_3$ has shown advantages over bases in terms of yield and reaction time. In particular this base is advantageous when reactions are too sensitive towards strong bases or reactions that required a balanced base, stronger than other carbonates but weaker than hydroxides or alkoxides[74]. However, carrying the reactions with $Cs_2CO_3$ it was observed that the reaction did not progress. This may be due to the fact that the base is not strong enough to deprotonate the NH group as previously reported[72]. Therefore, NaH was used alternatively as base since in combination with MeI in DMF it has been reported to be able to methylate N-boc protected amines[70].However, when tested with GLU, NaH only afforded the N-Boc-alkyl-GLU (38) in low yield of 10-15%. Furthermore, using NaH to directly conjugate the N-Boc-glutamic acid to NBD resulted

in multiple products (but not the desired product) and cyclization of the product was observed (data not shown) which is in accordance with previous reports[75].

Finally, formation of a sulfonamide[76] of glutamic acid di-methyl ester was alternatively synthesized using NaH to afford the N-sulfonamide-GLU-OMe (43) (Figure 3.34). Sulfonamides can be obtained by the classical $SN_2$ or acyl substitution displacements and are commonly used in drugs[77,78]. The product was obtained as a yellow oil with an improved yield of 32%. However, further attempts of reaction of this intermediate with NBD failed and therefore novel methods have to be attempted.

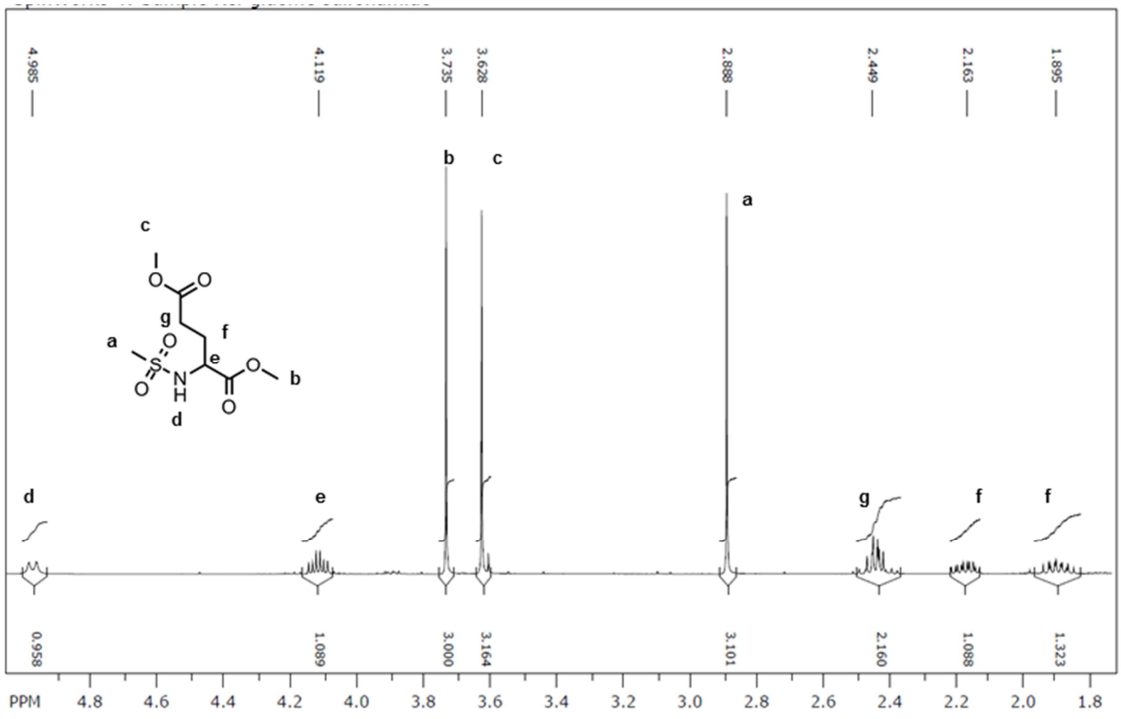


**Figure 3.34 – $^1$H NMR of N-Sulfonamide-GLU-OMe (43) in chloroform.** The singlet peak at 2.88 ppm corresponds to the $CH_3$ of the sulfonamide group and the amide group can be observed at 4.98 ppm.

Overall, different core glutamic acid derivatives have the potential to be synthesized but the conditions need to be optimized since very low yields were obtained. In particular the N-alkyl-NBD-GLU-OH (41) could be a starting point to further grow the dendrimer. On the other hand, the N-sulfonamide-GLU-OMe (43) could also potentially be used but a base suitable for the NBD coupling should be investigated.

### 2.2.5. Synthesis of different PG terminal groups

As with other macromolecules and drug delivery systems only a portion of them reaches the intended tissues and most of it just accumulates in non-targeted areas. Being able to among other things, modulate the ability to cross cellular barriers, toxicity and elimination is also important alongside bioactivity. In this regard, dendrimers are valuable scaffolds due to the ease of functionalization of the terminal groups. Different terminal groups can determine cell viability even if made of amino acids, which can be attributed to conformation and charge distribution at the surface[79]. From the molecular modelling studies carried out earlier in this work for the PG dendrimers (Chapter 2), tryptophan and lysine were chosen to be present at the surface. However, these two reagents were not available at the time these experiments were performed and thus two other alternative reagents with similar chemistry were used. Therefore, instead of tryptophan, phenylalanine was chosen to optimize the reactions since it was the most similar in structure. As a result, small branches were synthesized to study if the reactions used for PG dendrimer could be applied to synthesize the terminal groups (Figure 3.35 and 3.36). However, it should be noted that even though the reactions between these branches on the PG G2 dendrimer would directly afford the desired G4, due to the previous results in the synthesis of PG dendrimers this was highly unlike to occur due to steric hindrance and therefore suitable strategies should be developed in order to accomplish this route.

The L-phenylalanine methyl ester hydrochloride was reacted with Fmoc-glutamic acid using CDI as the coupling reagent to afford the Fmoc-glu-(phenylalanine)$_2$ (47) as a white plastic-like product and with a similar yield (89%) to that obtained for the other G0 dendrimers. Contrary to similar reactions with PG dendrimers, this reaction took more time to full completion and even after 12 hours the mono-substitution was still evidenced by TLC and therefore the reaction as extended for 24 hours. The product was then purified and the Fmoc was removed with piperidine affording the $NH_2$-GLU-(Fmoc)$_2$ (45) as a white solid (Yield: 69%). Therefore, these results suggest that the conditions developed to PG dendrimers can also be applied for the synthesis of this terminal group.

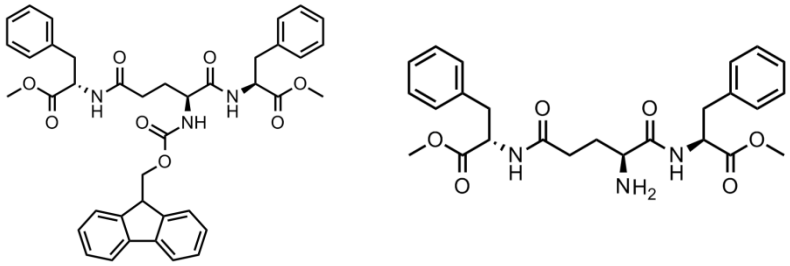

**Figure 3.35 – Structure of the hydrophobic terminal group synthesized as a small branch that would be coupled to the PG dendrimer.**

To further explore different types of terminal groups, Fmoc-ethylamine was coupled to N-Boc glutamic acid using the CDI coupling. The product of this reaction, N-Boc-GLU-$(Fmoc)_2$ (44), was obtained in considerably high yield (98%) since it precipitated in the solvent, and therefore could easily be recovered. Similarly to the Fmoc-GLU-$(phenylalanine)_2$ (47) the reaction took longer than the reactions for PG dendrimer. The product was however found to be insoluble in methanol, acetone, acetonitrile and hexane and soluble in DMSO and DMF. Therefore, the N-Boc was subsequently removed with TFA in DMF to afford the NH2-GLU-$(Fmoc)_2$ (48) as a salt in quantitative yield. Theoretically, this branch would then be attached at the surface, and then de-protected with piperidine to release the two amines. However, this compound would not be suitable since it is most likely to produce an insoluble polymer (due to the amount of terminal groups in the PG G3 dendrimer). Therefore, if this dendrimer were to be synthesized a different derivate and method (e.g. SPPS) would have to be explored.

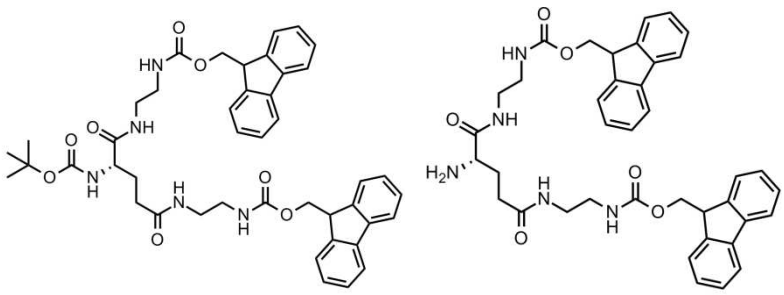

**Figure 3.36 – 2D structure of the positive derivative to attach to the PG backbone**

Finally, a smaller terminal group that would present zwitterionic properties once de-protected was tested. To this, Fmoc-glutamic acid 5-tert-butyl ester was reacted with ethylamine using the CDI coupling to afford the N-Boc-GLU(OtBu)-ethylamine (48) (Figure 3.37). This reaction was carried out by statistical selectivity. In this type of

reaction, the N-Boc-Glu(OtBu)(OH) was first activated with 1 equivalent of CDI. Once the reaction was finished, as monitored by TLC, this compound was slowly added to a solution with 20 equivalents of ethane-1,3-diamine. Because only small amounts are added at each time there is a higher amount of diamine precursors and therefore the monosubstitution is more likely to take place. However, under the conditions tested, the di-substitution still occurred in high amounts and therefore the desired product was only obtained with low yield (20%).

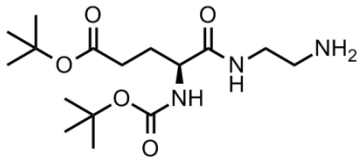

**Figure 3.37 – 2D structure of the zwitterionic intermediate to attach to the PG backbone.**

## 3.3 Materials and Methods

All reactions were conducted under an inert atmosphere at room temperature unless otherwise specified. All solvents were purchased from common chemical suppliers and utilized as received without further purification.

### 3.3.1 Materials

L-glutamic acid diethyl ester hydrochloride (GLU-OEt), *N,N,N′,N′*-Tetramethyl-*O*-(1*H*-benzotriazol-1-yl)uronium hexafluorophosphate (HBTU), **1**-Hydroxybenzotriazole hydrate (HOBt), 1-Hydroxy-7-azabenzotriazole (HOAt)**,** *N*-[(Dimethylamino)-1*H*-1,2,3-triazolo-[4,5-*b*]pyridin-1-ylmethylene]-*N*-methylmethanaminium hexafluorophosphate *N*-oxide (HATU), Triethylamine (TEA), N,N-diisopropylethylamine (DIPEA), (dimethylamino)pyridine (DMAP), dicyclohexylcarbodiimide (DCC), diisopropylcarbodiimide (DIPC), *N*-(3-Dimethylaminopropyl)-*N′*-ethylcarbodiimide (EDC), Bromocresol, 4-chloro-7-nitrobenzofurazan (NBD-Cl), dichloromethane (DCM), tetrahydrofuran (THF), methanol (MeOH), ethanol (EtOH), dimethylformamide (DMF), hexane, cyclohexane, diethyl ether, ethyl acetate, acetone, acetonitrile (ACN), dimethyl sulfoxide (DMSO), n-butanol, isopropanol, ninhydrin, silica gel 60 (50-70 mesh). From Bachem it was acquired Fmoc-L-glutamic acid (Fmoc-Glu(OH)). From Nova Biochem was acquired glutamic acid di-tert-butyl ester hydrochloride (Glu-(OBoc)) were all acquired from Sigma-Aldrich. N-Hydroxysuccinimide was acquired from AlfaAesar.

$^{1}$H and $^{13}$C NMR spectrum were recorded in deuterated solvent (chloroform, methanol, water, dimethylsulfoxide) using a Bruker Avance system 400 MHz with ultrashield Bruker magnet and Broadband probe or in a 500 MHz Oxford magnet and QNP cryoprobe. Tetramethylsilane (TMS) was used as internal standard in organic deuterated chloroform. All NMR data was analysed using SpinWorks 4 and chemical shifts are expressed in parts per million (ppm). Peaks are described as follows: singlet (s), doublet (d), triplet (t), quartet (q), multiplet (m) and for undistinguished peaks classified as broad (br)

Liquid chromatography-mass spectrometry (LC/MS) was used to determine the mass spectra and compound purity using a Shimadzu LC/MS 2020 (pump: Shimadzu LC-20AD; autosampler: Shimadzu-SIL20AC HT); detector: Shimadzu-SPD-20A between 220-254 nm). The nebulizing gas flow was set to 1.5 L/min and the system was fitted in a Xterra MS C18 column from Waters with a flow rate set to 1 mL/min with a mobile phase of water and acetonitrile both spiked with 0.1% formic acid.

Thin Layer Chromatography (TLC) was carried out in TLC silica gel 60 F254 Analytical Chromatography. Staining solutions included: PMA, crystal iodine, bromocresol, ninhydrin.

### 3.3.2 Synthesis

**Fmoc-GLU-NHS (1);**

**IUPAC: (S)-bis(2,5-dioxopyrrolidin-1-yl) 2-((((9H-flupren-9-yl) methoxy)carbonyl) amino)pentanedioate**

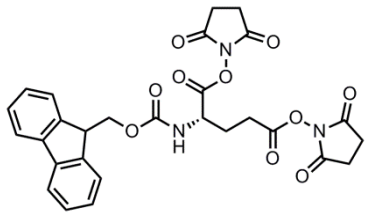

Fmoc-glutamic acid (0.2M) was suspended in DCM and mixed with 2.1 equivalents of NHS and 2.1 equivalents of DCC for 1 hour at 0$^{o}$C. The reaction mixture was then allowed to warm to room temperature for another 2 hours. The white crystalline precipitate composed of the DCC urea (DCU) was then removed by filtration and the reaction mixture was then washed with water and brine and dried with anhydrous $MgSO_4$. The organic layer was evaporated under vacuum on a rotary evaporator to give a white solid (Yield: 65%).

Rf 0.5 on TLC (methanol:ethyl acetate 95:5 v/v).

$^{1}$H NMR ($CDCl_3$, 400MHz, 300K) δ(ppm): 7.69 (d, 2H, Fmoc CH), 7.53 (d, 2H, Fmoc CH), 7.32 (t, 2H, Fmoc CH), 7.26 (t, 2H, Fmoc CH), 4.37 (br, 2H, Fmoc $CH_2$), 4.16 (br, 2H, Fmoc CH + αC CH), 3.14 (br, 1H, $CH_2$), 2.75 (br, 8H, NHS $CH_2$), 2.57 (br, 1H, $CH_2$), 2.38 (br, 1H, $CH_2$), 2.28 (br, 1H, $CH_2$).

**Fmoc-GLU(OtBu)-GLU-OEt (2);**

**IUPAC: (S)-diethyl 2-((S)-2-((((9H-fluoren-9-yl)methoxy) carbonyl)amino)-5-(tert-butoxy)-5-oxopentanamido)pentanedioate**

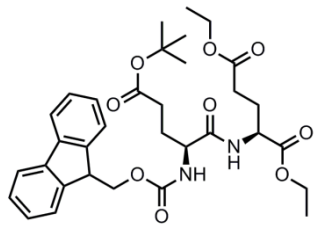

Fmoc-GLU(OtBu)(OH) (0.2M) was dissolved in DCM and 2.1 equivalents of NHS and 2.1 equivalents of DCC were added to react for 30 min at 0$^{o}$C. A mixture of glutamic acid diethyl ester (2.2 eq.) and TEA (2.2 eq.) pre-activated *in situ* in ice-cold DCM was then slowly added. The reaction was carried out at 0$^{o}$C for 45 minutes after which was allowed to warm to room temperature and stirred for 24 hours. The mixture was filtered to remove the DCU, and the filtrated DCM was washed with citric acid, water and brine. The organic

layer was then dried over anhydrous $MgSO_4$ and evaporated to afford a white solid (Yield: 98% in presence of DCU).

Rf 0.7 on TLC (methanol:ethyl acetate 95:5 v/v).

$^1$H NMR ($CDCl_3$, 400MHz, 300K) δ(ppm): 8.00 (d, 1H, NH), 7.67 (d, 2H, Fmoc CH), 7.51 (d, 2H, Fmoc CH), 7.32 (t, 2H, Fmoc CH), 7.23 (t, 2H, Fmoc CH), 6.31 (d, 1H, NH), 5.30 (br, 1H, αC), 4.50 (br, 1H, αC), 4.46 (br, 1H, Fmoc CH), 4.2 (m, 2H, Fmoc $CH_2$), 4.10 (m, 4, Ester $CH_2$), 2.63 (m, 4H, $CH_2$), 2.10-2.00 (m, 4H, $CH_2$), 1.40-1.28 (m, 15H, $CH_3$)

**Fmoc-GLU(OH)-GLU-OEt (3);**

**IUPAC: (S)-4-((((9H-fluoren-9-yl)methoxy)carbonyl)amino)-5-(((S)-1,5-diethoxy 1,5-dioxopentan-2-yl)amino)-5-oxopentanoic acid**

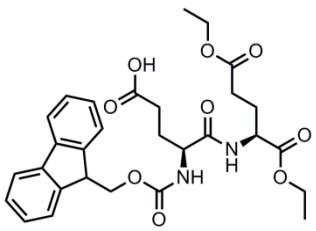

Ten equivalents of TFA were added dropwise to a solution of Fmoc-GLU(OtBu)-GLU-OEt (**2**) in DCM in ice for a period of 1 hour. The reaction mixture was then stirred for another 2 hours and monitored using TLC. After two hours TLC showed complete disappearance of the initial spot and the appearance of a UV spot that was reactive towards bromocresol (yellow color). The solvent was then removed under vacuum and co-evaporated several cycles with a mixture of THF and ethyl acetate to give a crystalline white solid (in quantitate yield) that was used without further purification or analysis.

**Fmoc-PG-OEt G0 (4);**

**IUPAC: (2S, 2'S)-tetraethyl 2,2'(((S)-2-((((9H-fluoren-9-yl)methoxy)carbonyl)amino) pentanedioyl)bis(azanediyl)dipentanedioate**

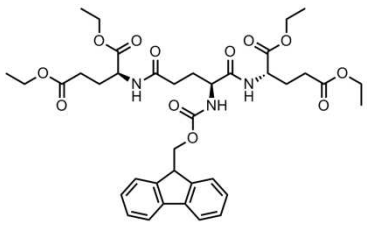

**(A) DCC coupling:** Fmoc-glutamic acid (0.2-0.3M) was suspended in ice-cold DCM in a round-bottom flask flushed with nitrogen and pre-activated for 30 minutes with DCC (2.05-2.5 eq) in the presence of NHS or HOBt (2.05-2.5 eq) and catalytic amounts of DMAP. Significant amounts of crystalline urea precipitate formed composed of DCU. Glutamic acid diethyl ester hydrochloride was neutralized *in situ* to generate the free amine with TEA or DIPEA in ice-cold DCM and was then added dropwise to the previous mixture and allowed to react for 45 minutes before warming to room temperature and left stirring overnight. The precipitate composed of DCU was filtered

out and glacial acetic acid was added to the reaction mixture to decompose the unreacted DCC for 1 hour. The remaining newly precipitated DCU was then filtered and the solvent was replaced with ethyl acetate and washed with cold 0.1M HCl (or 0.1M sulfuric acid or 10% critic acid), ice cold water, ice cold 5% bicarbonate and brine, dried over $MgSO_4$ or $NaSO_4$ and concentrated under vacuum in a rotary evaporator to give a transparent solid (Yield: 88-98%). Further purification included short silica gel column chromatography with chloroform:methanol (92:8 or 95:5 v/v), ethyl acetate:methanol (95:5) or THF:n-hexane (1:2 v/v), trituration from cold ethanol or methanol upon addition of water or crystallization using cold acetonitrile. Cold ethyl ether was added to remove small amounts of impurities which were then removed by centrifugation at 2000 rpm. Alternatively, using the same protocol, Fmoc-GLU(OH)-GLU-OEt (**3**) was used as the core molecule to react with 1.1 eq. of DCC and 1.1 eq. of NHS and 1.1 eq. of glutamic acid diethyl ester to yield the Fmoc-PG-OEt G0 (Yield: 92%).

**(B) DIPC coupling:** Similar to DCC coupling, the reaction was carried out with 2.5 eq. of DIPC instead of DCC. After 12 hours stirring at room temperature, glacial acetic was added to the reaction mixture and stirred for 1 hour. The reaction mixture was then washed with 0.1 HCl, water, 5% $NaHCO_3$ and brine and dried over $MgSO_4$. The solvent was then evaporated and the product was purified through a silica gel column chromatography using ethyl acetate:methanol (95:5) as eluent (Yield: 80%).

**(C) EDC coupling:** This reaction was carried out according to previous protocols[69]. The Fmoc-glutamic acid (0.15-0.2 M) was mixed with HOBt (2.1- 2.5 eq.) or NHS (2.1-2.5 eq.) in DMF or DCM at $0^oC$, and cold EDC (2.1-2.5 eq) was then added to the mixture. After stirring for 30 min, glutamic acid diethyl ester (2.1-2.5 eq) generated *in situ* with DIPEA or HOBt was added to the reaction mixture and the reaction was carried out for 24h-48h at room temperature. The solvent was then removed under vacuum on a rotary evaporator and the product was dissolved in ethyl acetate and washed with aqueous HCl (0.1M), water and brine. The organic phase was then removed in vacuum to give a white solid (Yield: 44-60%) and no further purification was performed.

**(C) HATU coupling:** Fmoc-glutamic acid (0.2M) in a round-bottom flask flushed with argon was reacted with 2.05 of HATU in anhydrous DMF for 1 hour at $0^oC$. Excess of glutamic acid diethyl ester hydrochloride (2.2-3 eq) was then slowly added dropwise and the solution became yellow. The reaction mixture was stirred for 10 minutes after which DIPEA (2.2-10 eq) was added dropwise under argon. The reaction mixture was

then allowed to react at 0$^{o}$C for 45 minutes, warm up to room temperature and stirred for 8 hours. The DMF was then removed and the product was re-dissolved in chloroform or ethyl acetate and washed with 10% citric acid, saturated $NaHCO_3$, water and brine. The organic phase was then dried over $MgSO_4$ and the solvent was removed under vacuum to afford a white solid (Yield: 70-75%).

Rf 0.7 in THF/n-hexane (1:4 v/v); 0.8 in ethyl acetate:methanol 95:5 or 90:10 v/v)

$^{1}$H NMR ($CDCl_3$, 400MHz, 300K) δ(ppm):1.07-1.26 (12H, m, $CH_2CH_3$), 1.75-2.44 (12H,m, $CHCH_2CH_2$), 3.94-4.19 (10H, m, $CH_2CH_3$ and $CHCH_2CH_2$ and CH-$CH_2$-O), 4.59 (2H, q, CH-$CH_2$-O), 4.66 (2H, $CHCH_2CH_2$), 5.28 (1H, d, NH), 7.241 (2H, t, Ar), 7.32 (2H, t, Ar), 7.51 (2H, d, Ar), 7.59 (1H, d, NH), 7.68 (2H, d, Ar), 7.97 (1H, d, NH).

$^{13}$C NMR ($CDCl_3$): δH (400 MHz); 14.01(CH2CH3), 14.13(CH2CH3), 14.20(CH2CH3), 26.67(CH2), 26.82(CH2), 29.35 (CH2), 30.42 (CH2), 30.59(CH2), 32.15(CH2), 47.11(Ar-CH), 51.58(CH), 51.62(CH), 53.53(CH), 60.56(CH2CH3), 60.70(CH2CH3), 62.28(CH2CH3), 62.27(CH2CH3), 67.04(R-CH2), 76.85(CH$Cl_3$, solvent), 120.21(ArC), 125.00(ArC), 127.0(ArC), 127.70(ArC), 141.22(ArC), 143.89(R-CH2-O-CO), 143.9 (R-CH2-O-CO), 172.43(CO), 172.46(CO), 172.62(CO), 173.88(CO), 174.03 (CO).

$C_{38}H_{49}N_3O_{12}$ requires 739.80 g.mol$^{-1}$; MS found $MH^+$ 740.35 MW; M-$Na^+$ 762.78 MW

**Fmoc-PG-OMe G0 (5);**

**IUPAC: (2S, 2'S)-tetramethyl 2,2'(((S)-2-((((9H-fluoren-9-yl)methoxy)carbonyl) amino)pentanedioyl)bis(azanediyl)dipentanedioate**

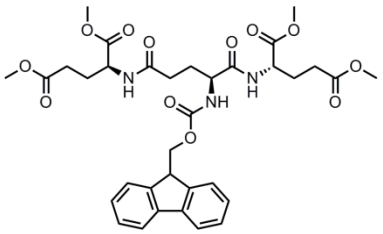

**(A) DCC coupling:** Similar procedure was followed as that used for Fmoc-PG-OEt G0 (**4**) by using the DCC/NHS/DMAP coupling method and by using the glutamic di-methyl ester hydrochloride for adding the branching layer. Yield: 88-95%.

**(B) HATU or HBTU coupling:** Similar procedure to a ppreviously published protocol was used[13,80]. Briefly, Fmoc-glutamic acid (0.2-2M) was activated with HBTU (2.1 eq) or HATU (2.1 eq) and HOBt (2.2 eq) and DIPEA (4 eq) in anhydrous DCM, DMF or DMA for 30 min to 1 h at 0$^{o}$C or room temperature followed by addition of the glutamic acid dimethyl ester hydrochloride (2.2 eq). After 10 minutes the reaction was allowed to warm to RT and reacted for 8 hours. The solvent was then evaporated and the product was re-dissolved in ethyl ester and washed with 10% citric acid, water, $NaHCO_3$ and brine. The organic phase was dried over MgSO4 and the solvent removed under

reduced-pressure evaporation. Further purification was carried out by recrystallization in acetonitrile (Yield: 88-92%).

**(C) CDI coupling:** Fmoc-glutamic acid (0.2-0.3M) was mixed with 2.05-2.5 eq. of CDI in dry THF or dry DCM under argon for 3 hours before adding 2.15 eq. of glutamic acid di-methyl ester over a period of 30 min. The reaction was then stirred for 24 hours at room temperature. Additional CDI or glutamic acid di-methyl ester was added as required by monitoring the reaction by TLC. The solvent was then evaporated and the product re-dissolved in ethyl ester and washed with 10% critic acid, water, NaHCO3 and brine. The organic phase was then dried over $MgSO_4$ and the solvent evaporated under vacuum to afford a white crystaline plastic-like solid (Yield 97%).

Rf 0.7 in THF/n-hexane (1:4 v/v); 0.8 in ethyl acetate:methanol 95:5 or 90:10 v/v).

The product may be further purified by flash chromatography (eluent: ethyl acetate: hexane 3:1 v/v or chloroform:methanol 95:5) if required.

$^1$H NMR ($CDCl_3$, 400MHz, 300K) δ(ppm): 7.89 (d, 1H, NH), 7.67 (d, 2H, Fmoc CH), 7.50 (d, 3H, Fmoc CH + NH), 7.33 (t, 2H, Fmoc CH), 7.24 (t, 2H, Fmoc, CH), 5.31 (d, 1H, NH), 4.69-4.59 (m, 2H, αC), 4.2 (m, 2H, Fmoc $CH_2$), 4.13 (m, 2H, Fmoc CH), 4.01 (m, 1H, αC), 3.70-3.50 (s, 12H, Ester $CH_3$), 2.39-1.87 (m, 12H, $CH_2$)

**Fmoc-PG-OtBu G0 (6);**

**IUPAC: (2S, 2'S)-tetra-*tert*-butyl 2,2'(((S)-2-((((9H-fluoren-9-yl)methoxy)carbonyl) amino)pentanedioyl)bis(azanediyl)dipentanedioate**

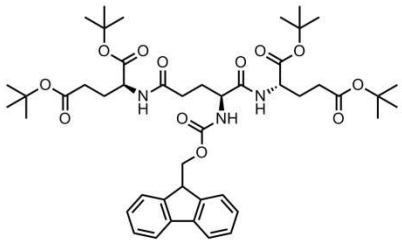

Reactions were carried out following a protocol similar to Fmoc-PG-OMe G0 synthesis (**5**) using the DCC/NHS (Yield: 96%), DIPC/NHS (Yield: 80%), EDC/HOBt (Yield: 55%) or CDI (Yield: 88-90%) as coupling agents. The glutamic acid di-*tert*-butyl ester hydrochloride was used as the branching unit for generation growth. The product was obtained as a white solid. Alternatively, the reaction was carried out in benzene for the CDI coupling (Yield: 85%).

Rf 0.7 in ethyl acetate:methanol (95:5 v/v)

$^1$H NMR ($CDCl_3$, 400MHz, 300K) δ(ppm): 8.07 (d, 1H, NH), 7.68 (d, 2H, Fmoc CH), 7.59 (d, 3H, Fmoc CH + NH), 7.33 (t, 2H, Fmoc CH), 7.21 (t, 2H, Fmoc, CH), 5.28 (d,

1H, NH), 4.55-4.28 (m, 6H, 3xαC, Fmoc $CH_2$, Fmoc CH), 2.5-1.9 (m, 12H, $CH_2$), 1.36-1.30 (m, 36H, Ester $CH_3$)

$^{13}C$ NMR ($CDCl_3$, 400MHz, 300K) δ(ppm): 172.65 (CO) 171.79 (CO) 169.70 (CO) 143.82 (CO), 141.24 (CO), 127.75 (CO), 126.89 (R-CH2-O-CO), 125.30 (ArC), 120.02 (ArC), 83.10 (ArC), 80.77 (ArC), 52.19 (R-CH2), 51.80 (CH), 47.28 (R-CH), 33.79 (CH), 32.19 (CH), 31.82 ($CH_2$), 31.60 ($CH_2$), 28.0 ($CHCH_3$) 27.04 ($CH_2$), 25.69 ($CH_2$), 25.48 ($CH_2$), 24.84 ($CH_2$)

**Fmoc-PG-OH G0 (7);**

**IUPAC: (2S, 2'S)-2,2'(((S)-2-((((9H-fluoren-9-yl)methoxy) carbonyl)amino) pentanedioyl)bis(azanediyl)dipentanedioic acid**

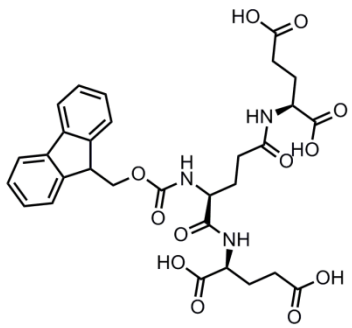

**(A) Acid hydrolysis of ethyl and methyl esters:** Fmoc-PG-OEt G0 (**4**) or Fmoc-PG-OMe G0 (**5**) was refluxed with HCl, TFA or $H_2SO_4$ (10 eq. per ester) aqueous solutions in minimum acetone or ethanol for 8-16 hours. The reaction was followed by TLC with the disappearance of the precursor spot to give a new UV spot (bromocresol active: yellow) at the origin (ethyl acetate:methanol 95:5 v/v). The solution was then cooled down and the compounds were extracted with ethyl acetate or DCM from the acidic aqueous layer to yield on average 40% of the expected mass.

**(B) Acid hydrolysis of *tert*-butyl esters:** De-protection of Fmoc-PG-OtBu G0 (**6**) was carried out with 4-10 eq. of TFA per ester in TFA:DCM (1:1 v/v) or TFA:DMF (1:1 v/v) ice-bath and reacted for 8-24 hours (the reaction slowly became pale yellow). The reaction was followed by TLC for the disappearance of the precursor dendrimer spot but no eluent was found to differentiate partial hydrolysis of the esters. The reaction mixture was concentrated by repeated co-distillation with DCM and ethyl acetate or toluene to give a viscous yellow oil with white crystalline solid (TFA salt form) (quantitative yield).

When necessary further purification was carried out by re-dissolution of the product in a mixture of ethyl acetate:water (1:1 v/v) and addition of sodium hydrogen carbonate or HCl with vigorous stirring following by recovery with ethyl acetate. The organic phase was then dried with $MgSO_4$ and the solvent removed under vacuum. A dense oil was recovered (Yield: 56%).

Rf 0.5 in 100% ethyl acetate when protonated, and at origin when deprotonated.

$^{1}$H NMR ($CD_3COD$, 400MHz, 300K) δ(ppm): 7.70 (d, 2H, Fmoc), 7.66 (t, 2H, Fmoc), 7.38 (t, 2H Fmoc), 72.93 (t, 2H, Fmoc), 4.52-4.22 (m, 6H, Fmoc $CH_2$, CH and 3xαC), 1.91-2.39 (m, 12H, $CH_2$).

$^{13}$C NMR ($CD_3COD$, 400MHz, 300K) δ(ppm): 172.59 (CO), 172.57 (CO), 171.93 (CO), 143.92 (CO), 141.42 (CO), 127.58 (CO), 126.99 (R-CH2-O-CO), 125.15 (ArC), 119.96 (ArC), 62.26 (ArC), 60.71 (ArC), 51.77 (ArC), 51.70 (ArC) 47.08 (R-$CH_2$), 32.10 (CH), 30.68 (CH), 30.36 (CH), 29.43 (CH), 26.80 ($CH_2$), 26.63 ($CH_2$), 14.17 ($CH_2$). 14.11 ($CH_2$), 14.03 ($CH_2$)

$C_{30}H_{33}N_3O_{12}$ requires 627.59 g.mol$^{-1}$; found $M^+H$ 628 g.mol$^{-1}$ + $M^+Na^+$ 650.3 g.mol$^{-1}$

**N-Boc-PG-OMe G0 (8);**

**IUPAC: (2S, 2'S)-tetramethyl 2,2'-(((S)-2-((*tert*-butoxycarbonyl)amino) pentanedioyl)bis(azanediyl)dipentanedioate**

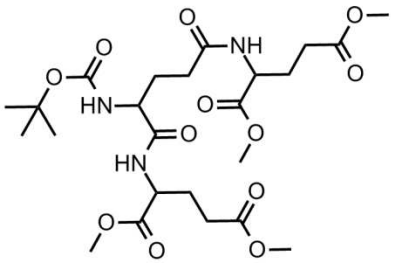

**(A)** N-Boc-Glutamic acid was used as the core and a similar method to the synthesis of Fmoc-PG-OMe G0 (**5**) using HBTU/HOBt/DIPEA or HOAT/HBTU/DIPEA in DMF was employed. For both coupling reagent systems the reaction was carried out for 12 hours after which the solvent was evaporated and the product was re-dissolved in ethyl acetate and washed with cold 10% citric acid (TLC showed no degradation of N-Boc), water, $NaHCO_3$ and brine. The organic layer was then dried over $MgSO_4$ and the solvent evaporated to give a crystalline white solid (Yield: 86-88% (for HBTU) and 84-99% (for HOAT).

**(B)** The N-Boc-Glutamic acid was coupled with glutamic acid di-methyl ester hydrochloride by CDI coupling in a similar methodology for the Fmoc-PG-OMe G0 (**5**) to afford a crystalline white solid (Yield: 86-88%)

Rf 0.5 (chloroform), 0.7 (chloroforom:methanol 90:10 v/v), 0.7 (ethyl acetate), 0.8 (ethyl acetate:hexane 1:1 v/v)

$^{1}$H NMR ($CD_3COD$, 400MHz, 300K) δ(ppm): 7.72 (br, 1H, NH), 5.0 (br, 1H, NH), 4.69 (m, 1H, αC), 4.60 (m, 1H, αC), 3.91 (br, 1H, αC), 3.70-3.61 (s, 12H, Ester $CH_3$), 1.79-2.40 (m, 12H, $CH_2$), 1.36 (s, 9H, N-boc $CH_3$)

**N-Boc-PG-OH G0 (9);**

**IUPAC: (2S, 2'S)-2,2-(((S)-2-((*tert*-butoxycarbonyl)amino)pentanedioyl) bis(azanediyl)dipentanedioic acid**

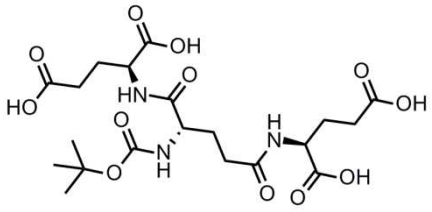

**(A) Basic ester hydrolysis with NaOH:** N-Boc-PG-OMe G0 (**8**) (0.01M) was refluxed with NaOH (10 eq. per ester) in methanol or THF at RT or at 50$^{o}$C for 6-12 hours[26]. The solution was then cooled down t room temperature, neutralized with HOAc and concentrated under vacuum. Alternatively, methanol was removed under vacuum and acidified with ice-cold 5% HCl or 10% citric acid to pH 3 and extracted to ethyl acetate followed by evaporation to dryness to obtain a sticky yellow oil (Yield: 70-80%).

**(B) Basic ester hydrolysis with LiOH:** Alternatively, hydrolysis of N-Boc-PG-OMe G0 (**8**) was carried out with LiOH-$H_2O$ (2-10 eq. per ester) in THF:Ethanol (1:5) or water:THF (1:1) for 12-48 hours at room temperature. The aqueous layer was then acidified with 10% citric acid or 5% HCl or acetic acid to pH 3-5, diluted in brine and extracted with ethyl acetate or DCM[70]. The organic layer was then dried over $MgSO_4$ or $Na_2SO_4$ and evaporated under vacuum to give a sticky yellow oil (Yield: 65-86%).

$^1$H NMR ($CD_3COD$, 400MHz, 300K) δ(ppm): 4.44-4.53 (m, 2H, 2x αC), 3.99 (t, 1H, αC), 2.44-1.95 (m, 12H, $CH_2$), 1.43 (s, 9H, N-boc $CH_3$).

$C_{20}H_{31}N_3O_{12}$ requires 505.47 g/mol; MS found $M^+$ 505.25 g/mol

**$NH_2$-PG-OEt G0 (10);**

**IUPAC: (2S, 2'S)-tetraethyl 2,2'(((S)-2-aminopentanedioyl) bis(azanediyl)) dipentanedioate;**

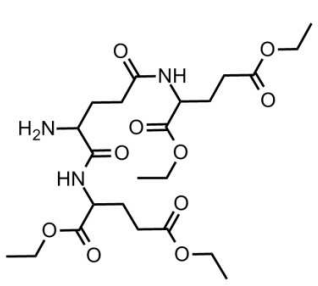

Fmoc-PG-OEt G0 (**4**) was dissolved in either DMF or DCM with varied amounts of piperidine (20-50% v/v; 5-10 eq). The reaction was followed by UV and TLC and was completed after 2 hours. The solvent was then evaporated to afford a yellow oil with white solid precipitated in it. The oil was re-dissolved in ethyl acetate and washed with saturated $NaHCO_3$ and brine. The organic layer was then evaporated and the residue was suspended in cold methanol or acetonitrile to remove most of the precipitate (Fmoc-piperidine) for several cycles.

When necessary column chromatography was carried out using ethyl acetate:methanol (95:5 or 80:20 v/v) or ethyl acetate:hexane (3:1 v/v) in the presence of trimethylamine (Yield 50-66%). Alternatively, the purification of the product was carried out by dissolving it in DMF and vigorous stir with n-hexane. Once phases separated, the DMF layer was washed 2x with n-hexane and evaporated under vacuum (Yield: 78%).

Rf 0.5 (dendrimer) in ethyl acetate:methanol (95:5 v/v) that was active to ninhydrin (purple color) and bromocresol (blue color). Other TLC spot was found at 0.9 (Fmoc-piperidine). Similar TLC spots were found with chloroform:methanol (92:8). Rf 0.2 (dendrimer) in ethyl acetate:hexane (95:5).

$^{1}$H NMR ($CD_3COD$, 400MHz, 300K) δ(ppm): 4.72-4.62 (m, 2H, 2x αC), 4.22-4.05 (m, 9H, Ester $CH_2$ + 1x αC), 2.54-1.83 (m, 14H, $CH_2$ + $NH_2$), 1.27 (m, 12H, Ester $CH_3$)

$^{13}$C NMR ($CD_3COD$, 400MHz, 300K) δ(ppm): 174.30, 173.31, 170.12, 65.54, 61.75, 55.17, 53.18, 34.85, 32.26, 31.27, 30.87, 27.48, 26.69, 26.09, 14.53

**$NH_2$-PG-OMe G0 (11);**

**IUPAC: (2S, 2'S)-tetramethyl 2,2'(((S)-2-aminopentanedioyl)bis(azanediyl)) dipentanedioate**

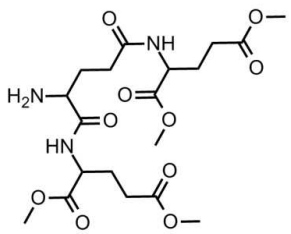

**(A) Fmoc removal with piperidine:** Fmoc-PG-OMe G0 (**5**) was reacted with piperidine in a similar protocol used for $NH_2$-PG-OEt G0 (**10**) to generate a yellow oil that was chromatographed with 5% methanol in ethyl acetate spiked with or without triethylamine (Yield: 40-68%).

**(B) N-Boc removal with TFA:** N-Boc-PG-OMe G0 (**8**) was dissolved in cold DCM (Alternatively DCM:methanol 10:1). TFA (10 eq) in equal volume to DCM was added at 0$^{o}$C dropwise over a period of 30 min. The reaction was then allowed to warm up to room temperature and stirred for 8-12 hours where the reaction mixture turned pale yellow. The solvent was then removed under vacuum in co-distillation with ethyl acetate, THF or toluene for several cycles. For further purification the residue was stirred vigorously with ethyl acetate or DCM and saturated $NaHCO_3$ (alternatively ice cold NaOH aqueous solution[61]). Once phase separation the organic layer was washed with brine, dried over $MgSO_4$ and concentrated under vacuum to afford a yellow oil (Yield: 80-91%).

Rf 0.5 (dendrimer) in ethyl acetate:methanol (95:5 v/v) that was active to ninhydrin (purple color) and bromocresol (blue color); and 0.9 (Fmoc-piperidine).

$^1$H NMR ($CD_3COD$, 400MHz, 300K) δ(ppm): 4.61 (m, 1H, αC), 4.49 (m, 1H, αC), 3.99 (t, 1H, αC), 3.78-3.71 (s, 12H, $CH_3$), 2.58-2.02 (m, 14H, $CH_2$ + $NH_2$)

**$NH_2$-PG-OtBu G0 (12);**

**IUPAC name (2S, 2'S)-tetra-*tert*-butyl 2,2'(((S)-2-aminopentanedioyl)bis (azanediyl))dipentanedioate**

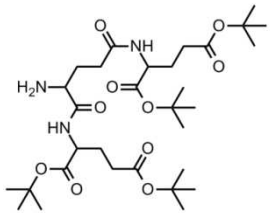

Using Fmoc-PG-tBu G0 (**6**), the Fmoc removal was carried out by following the standard protocol used for $NH_2$-PG-OEt G0 (**10**) using piperidine (4 eq) as base. The purification was carried out by diluting the oil in DMF and extracting the impurities with n-hexane or c-hexane following by evaporation of DMF. The product was then further washed with petroleum ether which did not solubilize the product but removed further impurities to afford a yellow oil (Yield: 65-79%)

Rf 0.6 (dendrimer) in ethyl acetate:methanol (95:5 v/v) that was active to ninhydrin (purple color) and bromocresol (blue color) and rf 0.9 (Fmoc-piperidine).

$^1$H NMR ($CD_3COD$, 400MHz, 300K) δ(ppm): 4.46 (q, 1H, αC), 4.38 (q, 1H, αC), 3.16 (t, 1H, αC), 1.72-2.50 (m, 14H, $CH_2$ + $NH_2$), 1.49 (m, 36H, Ester $CH_3$)

**Fmoc-PG-OEt G1 (13);**

**IUPAC: (3S,8S,11S,16S,21S)-tetraethyl 11-((((9H-fluoren-9-yl)methoxy) carbonyl)amino)8,16-bis(((S)-1,5-diethoxy-1,5-dioxopentan-2-yl)carbamoyl)-5,10,14,19-tetraoxo-4,9,15,20-tetraazatricosane-1,3,21,23-tetracarboxylate**

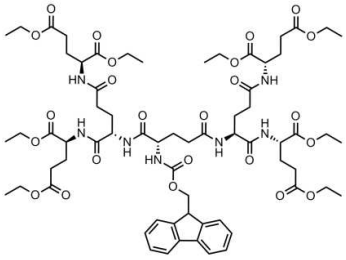

**(A) Convergent synthesis:** Similar to the synthesis of Fmoc-PG-OEt G0 (**4**), Fmoc-glutamic acid was pre-activated with DCC/NHS/DMAP for 30 min followed by the addition of $NH_2$-PG-OEt (**10**) (2.5 eq) with equimolar amounts of TEA. The reaction was carried out for 80 hours. The precipitate was filtered out and acetic acid was added for 1 hour to react with unreacted DCC. The remaining urea was filtered out and the reaction mixture was washed with HCl 0.1M, water, 5% $NaHCO_3$ and brine. The organic solvent was then reduced under vacuum and the product was purified by silica column chromatography using chloroform:methanol (92:8) to give a white plastic solid (Yield: 44%).

**(B) Divergent synthesis:** Fmoc-PG-OH G0 (**7**) was pre-activated with DCC (6 eq.)/NHS (6 eq.)/DMAP(cat.) for 4 hours in a similar protocol to Fmoc-PG-OEt G0 (**4**), followed by addition of glutamic acid diethyl ester hydrochloride (10 eq.) with equimolar amounts of TEA. The reaction was stirred for 80 hours and standard purification was carried out to yield a white plastic solid. Further purification was carried out by silica column chromatography using hexane:ethyl acetate (7:3 v/v) (Yield: 73-88%).

Rf 0.8 in ethyl acetate:methanol (95:5 v/v), acetone and hexane:ethyl acetate (7:3 v/v) and rf 0.7 in ethyl acetate

$^1$H NMR ($CDCl_3$, 400MHz, 300K) δ(ppm): 7.67 (d, 2H, Fmoc CH), 7.63 (d, 2H, Fmoc CH), 7.50 (d, 1H, 2x NH), 7.30 (t, 2H, Fmoc CH), 7.25 (t, 2H, Fmoc CH), 6.70 (d, 2H, NH), 6.55 (d, 2H, NH), 6.24 (d, 2H, NH) 4.47 (m, 3H, 3x αC), 4.13-3.94 (m, 23H, Fmoc $CHCH_2$, Ester $CH_2$ + 4x αC), 2.43-2.04 (br, 28H, CH2), 1.19 (m, 24, Ester $CH_3$)

**Fmoc-PG-OMe G1 (14);**

**IUPAC: IUPAC: (3S,8S,11S,16S,21S)-tetramethyl 11-((((9H-fluoren-9-yl)methoxy)carbonyl)amino)8,16-bis(((S)-1,5-dimethoxy-1,5-dioxopentan-2-yl)carbamoyl)-5,10,14,19-tetraoxo-4,9,15,20-tetraazatricosane-1,3,21,23-tetracarboxylate**

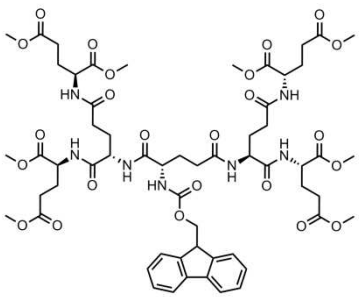

The Fmoc-G0-OH (**7**) was activated with HATU/HOBt/DIPEA (4.2-5 eq) followed by addition of 5-8 eq. of glutamic acid di-methyl ester formed *in situ* with DIPEA. The product was purified by washing the recovered organic phase with citric acid, water, $NaHCO_3$ and brine.

$^1$H NMR ($CDCl_3$, 400MHz, 300K) δ(ppm):The NMR showed a complex mixture composed of Fmoc-PG-OMe G1 (14), Fmoc- de-protected PG-OMe G1 as well as the presence of the fulvene

**Fmoc-PG-tBu G1 (15);**

**IUPAC: IUPAC: (3S,8S,11S,16S,21S)-tetra-*tert*-butyl 11-((((9H-fluoren-9-yl)methoxy)carbonyl)amino)8,16-bis(((S)-1,5-di-*tert*-butoxy-1,5-dioxopentan-2-yl)carbamoyl)-5,10,14,19-tetraoxo-4,9,15,20-tetraazatricosane-1,3,21,23-tetracarboxylate**

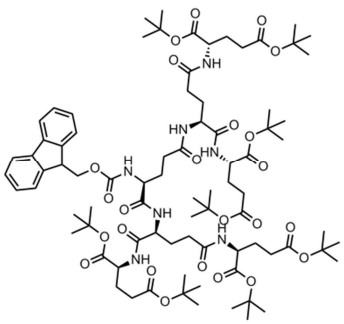

**(A)** The Fmoc-PG-OH (**7**) was pre-activated with DCC/NHS/DMAP (similarly to Fmoc-PG-OEt (**13**)). Glutamic acid di-*tert*-butyl ester hydrochloride (2.05-2.1 eq.) with equimolar amount of DIPEA was then added. The product was purified by washing the organic phase with citric acid, water, $NaHCO_3$ and brine and dried over $MgSO_4$. (Yield: 85%).

**(B)** Alternatively, Fmoc-PG-OH (**7**) was pre-activated with CDI for 4 hours followed by addition of glutamic acid di-*tert*-butyl ester hydrochloride (4.05-5 eq.) and the reaction was carried out for 72 hours at room temperature. The solvent was removed and the product re-dissolved in ethyl acetate and washed with 10% citric acid, water, 5% $NaHCO_3$ and brine and dried over $MgSO_4$. The organic phase was then removed and cold chloroform was added to filter impurities leaving a white solid (Yield: 62-80%)

When necessary the product was further purified by preparative TLC (ethyl acetate:methanol 95:5 v/v)

Rf 0.85 in ethyl acetate:methanol (95:5 v/v), acetone, rf 0.6 hexane:ethyl acetate (7:3 v/v) and rf 0.7 on ethyl acetate

$^1$H NMR ($CDCl_3$, 400MHz, 300K) δ(ppm): 8.28-8.23 (d, 2H, 2x NH), 7.83 (d, 1H, NH), 7.63 (d, 4H, Fmoc CH), 7.53 (d, 1H, NH), 7.42 (m, 1H, NH), 7.30 (t, 2H, Fmoc CH), 7.24(t, 2H, Fmoc CH), 5.19 (d, 1H, NH), 4.67 (m, 2H, 2x αC), 4.5 (m, 2H, 2x αC), 4.36 (t, 1H, Fmoc CH), 4.18 (m, 3H, Fmoc $CH_2$ + αC), 3.99 (m, 1H, αC), 3.79 (m, 1H, αC), 1.57-2.48 (m, 28H, $CH_2$), 1.39-1.20 (m, 72H, Ester $CH_3$)

**Fmoc-PG-OH G1 (16);**

**IUPAC: (3S,8S,11S,16S,21S)-11-((((9H-fluoren-9-y)methoxy(carbonyl)amino)-8,16-bis(((S)-1,3-dicarboxypropyl)carbomoyl)-5,10,14,19-tetraoxo-4,9,15,20-tetraazatricosane-1,3,21,23-tetracarboxylic acid**

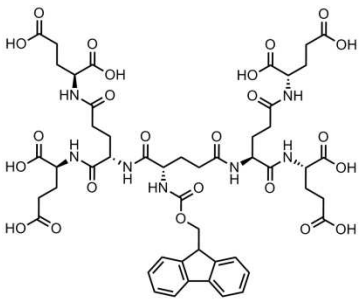

Fmoc-PG-tBu G1 (**15**) was dissolved in ice-cold DCM, and cold TFA (10 eq. per ester) was slowly added and the reaction was carried out for 12h. The organic solvent was then co-distilled with ethyl acetate multiple times and the obtained product was recovered as a dense orange oil. When necessary the product was further purified by re-dissolution in water and acidification to pH 2-3 and extraction to ethyl acetate. (Yield: 56-72%).

Rf at origin in ethyl acetate:methanol (5:95 v/v) that was active to PMA and bromocresol (yellow)

$^1$H NMR ($CDCl_3$, 400MHz, 300K) δ(ppm): 7.80 (d, 2H, Fmoc CH), 7.70 (d, 2H, Fmoc CH), 7.39 (t, 2H, Fmoc CH), 7.33 (t, 2H, Fmoc CH), 4.63-4.25 (m, 9H, Fmoc CH and $CH_2$ + 6 αC), 3.45 (m, 1H, αC), 2.45-1.93 (m, 28H, $CH_2$).

$C_{50}H_{61}N_7O_{24}$ requires 1144.05 g/mol and MS found $M^+$ 1144.40 g/mol

**Fmoc-PG-OtBu G2 (17);**

**IUPAC: (3S,8S,13S,16S,21S,26S,31S)-tetra-*tert*-butyl 11-((((9H-fluoren-9-yl13,21-bis(((6S,9S,14S)-6,14-bis(methoxycarbonyl)-3,8,12,17-tetraoxo-2,18-dioxa-7,13-diazanonadecan-9-yl)carbamoyl)-8,26-bis(((S)-1,5-di-*tert*-buthoxy-1,5 dioxopentan-2-yl)carbamoyl)-5,10,15,19,24,29-hexaoxo-4,9,14,20,25,30-hexaazatritriacontane-1,3,31,33-tetracarboxylate**

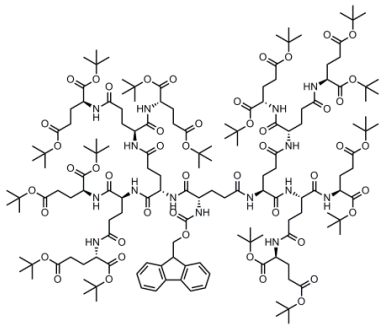

Fmoc-PG-OH G1 (**16**) was pre-activated with CDI (10 eq.) for 24 hours followed by addition of glutamic acid *tert*-butyl ester hydrochloride (12 eq.) and the reaction was allowed to stir for 7 days. The purification was carried out similarly to Fmoc-PG-OtBu G1 (**15**) and the product was obtained as a sticky white plastic (Yield: 5%).

$^1$H NMR ($CDCl_3$, 400MHz, 300K) δ(ppm): 7.635 (br, 1H, Fmoc), 7.50 (br, 1H, Fmoc), 7.28 (br, 1H, Fmoc), 7.19 (br, 1H, Fmoc), 6.62 (d, 4H Fmoc), 4.42-4.10 (m, 9H, Fmoc CH + $CH_2$, 6x αC), 3.67-3.41 (m, 9H, 9x αC), 2.40-1.58 (m, 56H, $CH_2$), 1.374 (m, 144H, Ester $CH_3$).

**Fmoc-PG-OH G2 (18);**

**IUPAC: (3S,8S,13S,16S,21S,26S,31S)-16-((((9H-fluoren-9-yl)methoxy) carbonyl)amino)-13,21-bis(((S)-1,5-bis(((S)-1,3-dicarboxypropyl)amino)-1,5-dioxopentan-2-yl)carbamoyl)-8,26-bis(((S)-1,3-dicarboxypropyl)carbamoyl)-5,10,15,19,24,29-hexaoxo-4,9,14,20,25,30-hexaazatritriacontane-1,3,31,33-tetracarboxylic acid**

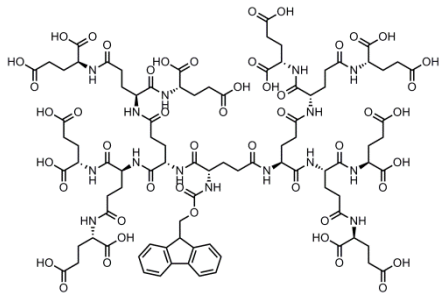

The hydrolysis of *tert*-butyl esters of Fmoc-PG-OtBu G2 **(17)** was carried out in a similar manner to that of Fmoc-PG-OH G1 (**16**) using TFA (20 eq). The solvent was then removed in co-distillation and no further purification was carried out.

$^1$H NMR ($CD_3COD$, 400MHz, 300K) δ(ppm):7.69 (d, 2H, Fmoc), 7.58 (br, 2H, Fmoc), 7.27 (t, 2H, Fmoc), 7.23 (t, 2H, Fmoc), 4.38-3.86 (m, 18H, Fmoc $CH_2$,CH and 15x αC), 2.29-1.052 (m, 64H, $CH_2$).

**Fmoc-PG-OtBu G3 (19);**

**IUPAC:** Not shown for clarity

**Structure:** Not shown for clarity; The structure is composed of Fmoc linked to a central GLU as the core and 2, 4, 8 GLU for each layer followed by 16 GLU-OtBu as terminal groups (Fmoc-GLU-$GLU^2$-$GLU^4$-$GLU^8$-$GLU^{16}$-OtBu)

The synthesis of Fmoc-PG-tBu G3 **(19)** was carried out similarly to the synthesis of Fmoc-PG-OtBu G2 (**17**). However after washing the organic phase a very small amount of product was recovered.

$^1$H NMR ($CD_3COD$, 400MHz, 300K) δ(ppm): too complex to directly assign the correct peaks or to characterize the ratio between different peaks.

**N-Boc-PG-OMe G1 (20);**

**IUPAC: (3S,8S,11S,16S,21S)-tetramethyl 11-((*tert*-butoxycarbonyl)amino)-8-16-bis(((S)-1,5-dimethoxy-1,5-dioxopentan-2-yl)carbamoyl)-5,10,14,19-tetraoxo-4,9,15,20-tetraazatricosane-1,3,21,23-tetracarboxylate**

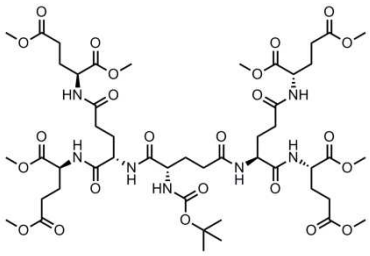

Synthesis was carried out similarly to N-Boc-PG-OMe G0 (**5**) using CDI as the coupling agent. The product was washed with water and 5% $NaHCO_3$ and then purified on a short silica gel column with cyclohexane/AcOET (8:2) to obtain a yellow oil (Yield: 50%).

$^1$H NMR ($CDCl_3$, 400MHz, 300K) δ(ppm): 4.87-4.78 (m, 4H, αC), 4.14-4.09 (br, 2H, αC), 3.70-3.56 (s, 24H, Ester $CH_3$), 2.40-1.90 (m, 28H, $CH_2$), 1.32 (s, 9H, N-Boc $CH_3$)

**N-Boc-PG-OH G1 (21);**

**IUPAC: (3S,8S,11S,16S,21S)-11-((*tert*-butoxycarbonyl)amino)-8-16-bis(((S)-1,3-dicarboxypropyl)carbamoyl)-5,10,15,20-tetraazatricosane-1,3,21,23-tetracarboxylic acid**

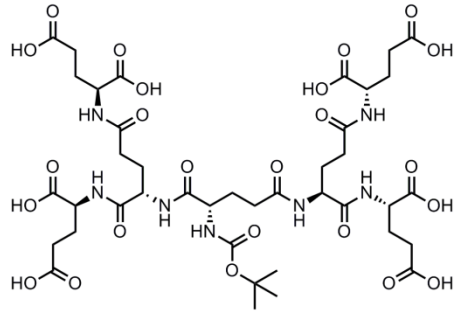

N-Boc-PG-OMe G1 (**20**) was hydrolyzed with LiOH (10 eq. per ester) in a mixture of water:THF 1:1 for 24 hours at room temperature. The aqueous layer was then acidified with 10% citric acid to pH 3, diluted in brine and extracted with ethyl acetate or ether to yield a yellow oil (recovered mass: 38%)

MS confirmed the presence of the product in small amounts and the $^1$H NMR showed the majority corresponded to loss of the N-Boc (data now shown).

**$NH_2$-PG-OEt G1 (22);**

**IUPAC: (3S,8S,11S,16S,21S)-tetraethyl 11-amino-8,16-bis(((S)-1,5-diethoxy-1,5-dioxopentan-2-yl)carbamoyl)-5,10,14,19-tetraoxo-4,9,15,20-tetraazatricosane-1,3,21,23-tetracarboxylate**

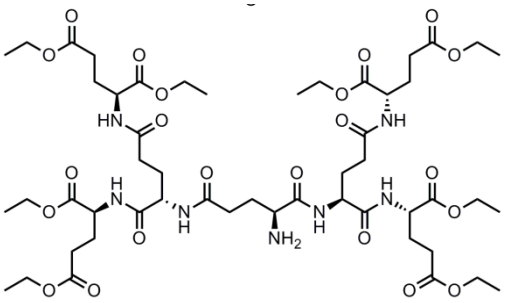

Fmoc-PG-OEt G1 **(13)** was mixed with 50% piperidine in DMF and stirred for 8 hours. The solvent was evaporated and the product was then dissolved in minimum methanol, mixed with silica and dried followed by purification by flash chromatography from a dry loading using ethyl acetate as eluent (Yield: 34%).

$^1$H NMR ($CD_3COD$, 400MHz, 300K) δ(ppm): 4.52-4.45 (m, 4H, αC), 4.22-4.12 (m, 16, Ester $CH_2$), 4.05 (t, 1H, αC), 3.75 (m, 1H, αC), 2.43-1.86 (m, 28H, $CH_2$), 1.26 (m, 24H, Ester $CH_3$).

**$NH_2$-PG-OMe G1 (23);**

**IUPAC: (3S,8S,11S,16S,21S)-tetramethyl 11-amino-8,16-bis(((S)-1,5-dimethoxy-1,5-dioxopentan-2-yl)carbamoyl)-5,10,14,19-tetraoxo-4,9,15,20-tetraazatricosane-1,3,21,23-tetracarboxylate**

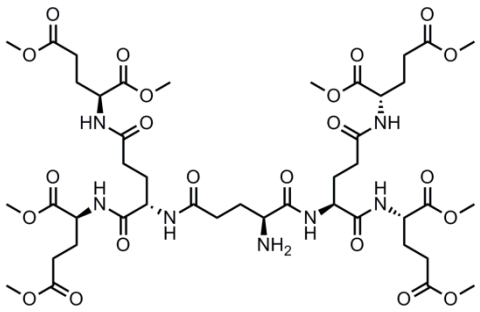

**(A) Fmoc-removal:** Fmoc-PG-OMe G1 **(14)** was reacted with 50% piperidine in DMF for 12 hours. The solvent was evaporated and the product was then purified through a preparative TLC with methanol:ethyl acetate (5:95 v/v). The product was re-dissolved in ethyl acetate and washed with saturated $NaHCO_3$ and brine, and the organic phase was evaporated to yield a yellow gel (Yield: 65-78%). Alternatively, the DMF phase was washed with n-hexane or cyclohexane and the DMF was then evaporated.

**(B) N-Boc removal:** The N-Boc-PG-OMe G1 **(20)** was dissolved in cold DCM, and TFA (10 eq.) were slowly added under inert atmosphere. The reaction was stirred for 12 hours and the DCM was co-distilled multiple times with ethyl acetate and THF.

Rf 0.6 in methanol:ethyl acetate (5:95 v/v) with 1% TEA.

$^1$H NMR ($CD_3COD$, 400MHz, 300K) δ(ppm): 4.23-4.12 (m, 4H, αC), 3.47 (t, 1H, αC), 3.30 (m, 1H, αC), 2.96-2.85 (m, 24, Ester $CH_3$), 1.92-1.43 (m, 28H, $CH_2$), 1.26 (m, 24H, Ester $CH_3$).

**N-Boc-PG-OMe G2 (24);**

**IUPAC: (3S,8S,13S,16S,21S,26S,31S)-tetramethyl 13,21-bis(((6S,9S,14S)-6,14-bis(methoxycarbonyl)-3,8,12,17-tetraoxo-2,18-dioxa-7,13-diazanonadecan-9-yl)carbamoyl)-16-((tert-butoxycarbonyl)amino)-8,26-bis(((S)-1,5-dimethoxy-1,5-dioxopentan-2-yl)carbamoyl)-5,10,15,19,24,29-hexaoxo-4,9,14,20,25,30-hexaazatritriacontane-1,3,31,33-tetracarboxylate**

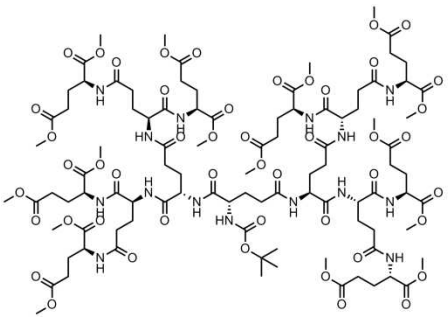

N-Boc-PG-OH G1 (**21**) was pre-activated with HBTU/HOBt/DIPEA (8.5 eq.) for 24 hours before adding glutamic acid di-methyl ester (10 eq.) formed *in situ* with DIPEA. The reaction was stirred for 10 days. The product was then recovered by washing the product with 10% citric acid, water and brine and the organic phase was evaporated to obtain the product as a yellow oil (Yield 45%).

Rf 0.6 on THF/n-hexane.

$^1$H NMR of the product recovered did not match the desired product but a possible partial degraded dendrimer.

**NBD-GLU-OEt (25);**

**IUPAC: (S)-diethyl-2-((7-nitrobenzo[c][1,2,5]oxadiazol-4-yl)amino)pentanedioate**

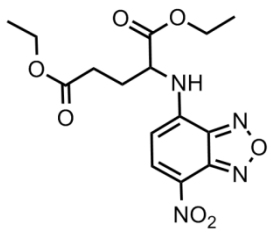

L-glutamic acid diethyl ester hydrochloride (0.2M-0.6M) was dissolved in dry dichloromethane, chloroform:methanol (1:1 v/v), DMF or acetonitrile in a presence of a base (1-4 eq. of TEA, DIPEA, $Na_2CO_3$, $K_2CO_3$ or $Cs_2CO_3$). The mixture was stirred for 30 min at room temperature and then mixed with NBD-Cl dissolved in the same solvent. The reaction mixture was then stirred for 2-12 hours protected from light at room temperature, 60$^o$C (for DMF) or 80$^o$C ( for ACN) after which the reaction turned into a dark brown color. The solvent was then evaporated and the product re-dissolved with ethyl acetate and washed with HCl 0.1M, water and dried over $MgSO_4$. The solvent was then removed by rotary evaporation the and crude product was obtained as a dark solid.

Rf 0.7 in chloroform:methanol (7:3 v/v) colored orange/brown

$^1$H NMR ($CDCl_3$, 400MHz, 300K) δ(ppm): 8.40 (d, 1H, NBD), 7.59 (d, 1H, NBD), 7.02 (br, 0.5H, αC) 6.19 (d, 1H, NH), 4.47 (br, 0.5H, αC), 4.27-4.03 (m, 4H, Ester $CH_2$), 2.58-2.28 (m, 4H, $CH_2$), 1.24-1.14 (m, 6H, Ester $CH_3$).

$C_{20}H_{23}NO_4$ requires 357.2 g.mol$^{-1}$; MS found $M^+H^+$ 358.2 g.mol$^{-1}$ and $M^+Na^+$ 380.2 g.mol$^{-1}$.

**NBD-GLU-OMe (26);**

**IUPAC: (S)-dimethyl 2-((7-nitrobenzo[c][1,2,5]oxadiazol-4-yl)amino)pentanedioate**

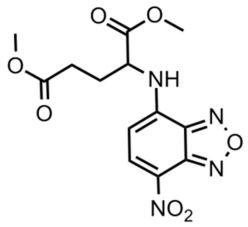

L-Glutamic acid di-methyl ester hydrochloride was coupled to NBD-Cl similarly to the NBD-GLU-OEt (**25**). The reaction was tested in different solvents including DCM, DMF, THF, MeOH and acetonitrile. Different bases (TEA, DIPEA, $Na_2CO_3$, $K_2CO_3$ or $Cs_2CO_3$) with different ratios and different temperatures (0$^o$C, 25$^o$C and 40$^o$C) were also tested. Alternatively the NBD-Cl was added at 0$^o$C and then refluxed at 48$^o$C (acetonitrile) or 80$^o$C (DMF). The reaction turned from a light orange to a dark brown colour.

$^1$H NMR ($CDCl_3$, 400MHz, 300K) δ(ppm): 8.50 (d, 2H, NBD), 7.67 (d, 2H, NBD), 6.28 (d, 2H, NH), 4.14 (t, 1H, αC), 3.72-3.87 (s, 6H, Ester $CH_3$), 2.70-2.22 (m, 4H, $CH_2$)

$C_{13}H_{14}N_4O_7$ requires 338.09 g.mol$^{-1}$; MS found $M^+$ 338.01 g.mol$^{-1}$

**NBD-GLU-OtBu (27);**

**IUPAC: (S)-di-*tert*-butyl 2-((7-nitrobenzo[c][1,2,5]oxadiazol-4-yl)amino) pentanedioate**

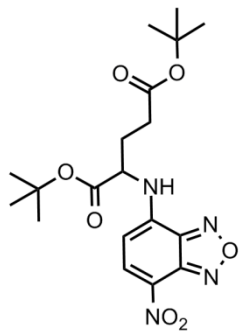

L-glutamic acid di-*tert*-butyl ester was coupled to NBD-Cl similarly to the NBD-GLU-OEt (**25**) and NBD-GLU-OMe (**26**) using DCM or acetonitrile as solvents and using DIPEA or $Cs_2CO_3$ as base at room temperature.

$^1$H NMR ($CDCl_3$, 400MHz, 300K) δ(ppm): 8.40 (d, 1H, NBD), 6.1 (d, 1H, NBD), 4.36 (b, 1H, αC), 2.41 (m, 2H, $CH_2$) 2.21 (m, 2H, $CH_2$), 1.47-1.28 (s, 18H, Ester $CH_3$)

$^{13}$C NMR ($CD_3COD$) δ: 171.24, 168.46, 143.38, 142.78, 141.79, 135.09, 142.08, 82.71, 80.52, 79.95, 55.26, 29.80, 27.21, 25.63.

$C_{19}H_{26}N_4O_7$ requires 422.43 g.mol$^{-1}$; MS found M$^+$H 423.00 g.mol$^{-1}$

**NBD-GLU-OH (28);**

**IUPAC: (S)-2-((7-nitrobenzo[c][1,2,5]oxadiazol-4-yl)amino)pentanedioic acid**

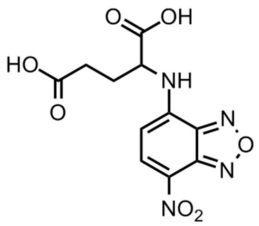

**(A) Direct coupling:** L-Glutamic acid was reacted with NBD-Cl in acetonitrile using TEA or DIPEA as base similar the synthesis of NBD-GLU-OEt (**25**). The solvent was then evaporated and re-dissolved in an aqueous solution of HCl and extracted to ethyl acetate. The organic phase was reduced under vacuum to obtain a dark colored oil (Yield: 54%).

**(B) From basic hydrolysis:** NBD-GLU-OEt (**25**) or NBD-GLU-OMe (**26**) were hydrolyzed using LiOH (10 eq./ester)/THF/Water. The reaction was stirred for 8 hours and then washed with ethyl acetate. The aqueous solution was then acidified with HCl 0.1M and extracted to ethyl acetate. The organic phase was then dried over $MgSO_4$ and evaporated under vacuum to obtain a dark colored oil (yield: 30%)

**(C) From acidic hydrolysis:** NBD-GLU-OtBu was mixed with TFA (10 eq./ester) in DCM. The reaction was stirred for 8 hours and then extracted with ethyl acetate. The organic phase was then dried over $MgSO_4$ and evaporated under vacuum to obtain a dark colored oil (Yield: 78%).

$^1$H NMR ($CD_3COD$, 400MHz, 300K) δ(ppm):8.49 (d, 1H, NBD), 6.65 (d, 1H, NBD), 4.00 (q, 1H, αC), 1.89 (t, 2H, CH2) 1.12 (q, 2H, $CH_2$)

**NBD-PG-OEt G0 (29);**

**IUPAC: (2S,2'S)-tetraethyl 2,2'-(((S)-2-((7-nitrobenzo[c][1,2,5]oxadiazol-4-yl) amino)pentanedioyl)bis(azanediyl))dipentanedioate**

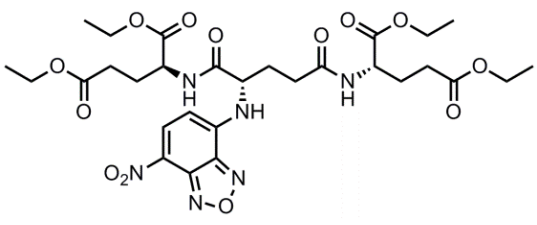

The $NH_2$-PG-OEt G0 **(10)** was mixed with different bases (NaHCO3, K2CO3, TEA, DIPEA) in different solvents (DMF, ACN, MeOH, EtOH) and reacted for 4-12h at room temperature or at 40-70$^o$C. The

solvent was then reduced under vacuum and re-dissolved in ethyl acetate and washed with HCl 0.1M, $NaHCO_3$, water and brine. The organic phase was then dried with $MgSO_4$ and evaporated under vacuum to obtain a dark colored solid (Yield: 60-65%).

$^1$H NMR ($CD_3COD$, 400MHz, 300K) δ(ppm): 8.40 (d, 1H, NBD), 8.34 (d, 1H, NH), 6.79 (d, 1H, NH), 6.23 (d, 1H, NBD), 4.76 (m, 1H, αC), 4.56 (m, 1H, αC), 4.19-4.01 (m, 13H, Ester $CH_2$ + αC), 2.46-1.91 (m, 12H, $CH_2$), 1.28-1.18 (m, 12H, $CH_3$)

$C_{29}H_{40}N_6O_{13}$ requires 680.66 g.mol$^{-1}$; MS found $M^+H$ 681.45 g.mol$^{-1}$

**NBD-PG-OMe G0 (30);**

**IUPAC: (2S,2'S)-tetramethyl 2,2'-(((S)-2-((7-nitrobenzo[c][1,2,5]oxadiazol-4-yl) amino)pentanedioyl)bis(azanediyl))dipentanedioate**

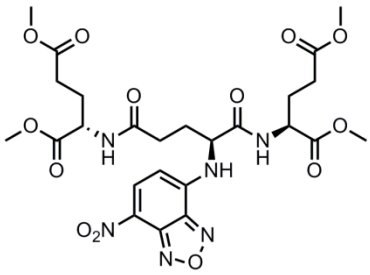

The $NH_2$-PG-OMe G0 **(11)** was reacted with NBD-Cl similarly to NBD-PG-OEt G0 (**29**) to obtain a dark colored solid after purification (Yield: 68%).

$^1$H NMR ($CD_3COD$, 400MHz, 300K) δ(ppm): 8.40 (d, 1H, NBD), 6.18 (d, 1H, NBD), 5.78 (m, 1H, NH), 4.51 (m, 1H, αC), 4.37 (m, 1H, αC), 3.67-3.55 (s, 12H, Ester $CH_3$), 2.78-2.46 (m, 12H, $CH_2$), 1.28-1.18 (m, 12H, $CH_3$)

**NBD-PG-OH G0 (31);**

**IUPAC: (2S,2'S)-2,2'-(((S)-2-((7-nitrobenzo[c][1,2,5]oxadiazol-4-yl)amino) pentanedioyl)bis(azanediyl))dipentanedioic acid**

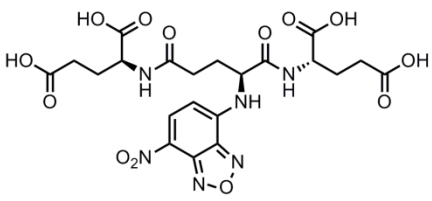

NBD-PG-OMe G0 **(30)** was hydrolyzed with LiOH/THF/MeOH for 12 hours. The product was then acidified and extracted to ethyl acetate to obtain a dark colored oil (yield: 53%).

$^1$H NMR ($CD_3COD$, 400MHz, 300K) δ(ppm):8.63 (d, 1H, NBD), 6.76 (d, 1H, NBD), 4.24-4.13 (d, 3H, αC), 2.02-1.65 (m, 12H, $CH_2$)

**NBD-PG-OtBu G0 (32);**

**IUPAC: (2S,2S')-tetra-*tert*-butyl 2,2'-(((S)-2-((7-nitrobenzo[c][1,2,5]oxadiazol-4-yl)amino)pentanedioyl)bis(azanediyl))dipentanedioate**

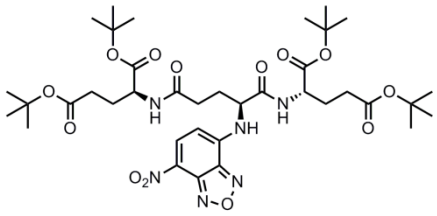

NBD-GLU-OH (**28**) was pre-activated with CDI for 30 min before adding glutamic acid di-*tert*-butyl ester (2.05-2.2 eq). The solvent was evaporated and the product was purified by preparative TLC using ethyl acetate as eluent (Yield: 44-67%).

$^1$H NMR ($CDCl_3$, 400MHz, 300K) δ(ppm): 8.58-8.34 (d, 1H, NBD), 6.15 (d, 1H, NBD), 4.9 (d, 1H,NH) 4.35-4.22 (br, 2H, αC), 4.04 (q, 1H, αC), 2.93-2.08 (m, 12H, $CH_2$), 1.44-1.26 (m, 36H, Ester $CH_3$)

$C_{37}H_{56}N_6O_{13}$ requires 792.39 g.mol$^{-1}$; MS found $M^+$ 792.66 g.mol$^{-1}$

**NBD-PG-OtBu G1 (33);**

**IUPAC: (3S,8S,11S,16S,21S)-tetra-*tert*-butyl 8,16-bis(((S)-1,5-di-tert-butoxy-1,5-dioxopentan-2-yl)carbamoyl)-11-((7-nitrobenzo[c][1,2,5]oxadiazol-4-yl)amino)-5,10,14,19-tetraoxo-4,9,15,20-tetraazatricosane-1,3,21,23-tetracarboxylate**

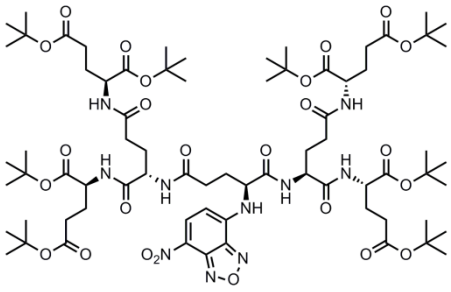

NBD-PG-OH G0 **(31)** was pre-activated with HBTU/HOBt/DIPEA in DMF for 2 hours. Glutamic acid di-*tert*-butyl ester (6 eq) was then added to the reaction mixture and stirred for 72 hours. The solvent was evaporated and the product was re-dissolved in ethyl acetate and washed with citric acid, water, NaHCO3 and brine. The organic phase was then evaporated to obtain a dark colored plastic solid (Yield: 55%).

$^1$H NMR ($CDCl_3$, 400MHz, 300K) δ(ppm): 8.41 (d, 2H, NBD), 6.17 (d, 2H, NBD), 4.98 (d, 1H, NH), 4.39-4.22 (m, 2H, αC), 1.85-2.88 (m, 28H, $CH_2$), 1.28-1.41 (m, 72H, Ester $CH_3$)

**NBD-PG-OtBu G3 (34);**

**IUPAC:** Not shown for clarity

**Structure:** Not shown for clarity; the core is composed of NBD linked to GLU, followed by 2, 4 and 8 GLU for each layer and 16 GLU-OtBu as terminal monomers (NBD-GLU-$GLU^{2}$-$GLU^{4}$-$GLU^{8}$-$GLU^{16}$-OtBu)

Fmoc-PG-OtBu **(19)** was mixed with piperidine in DMF and the reaction was carried out at room temperature for 7 days after which NBD was added and reacted for another 7 days. The product was then isolated from a preparative TLC to obtain the color spot that did not match the same Rf as NBD-Cl or NBD-OH (Yield: not determined due to small amounts)

$^{1}$H NMR showed that even after preparative TLC the product is impure and it was too complex to assign correctly the peaks and integration. Two duplet at 7.65 and 6.60 suggests the presence of NBD (possibly complexed) and it was in an integration ratio compatible with a possible PG-OBtu G3.

**N-Boc-NBD-GLU-OH (35);**

**IUPAC: (S)-2-((tert-butoxycarbonyl)(7-nitrobenzo[c][1,2,5]oxadizol-4-yl)amino) pentanedioic acid**

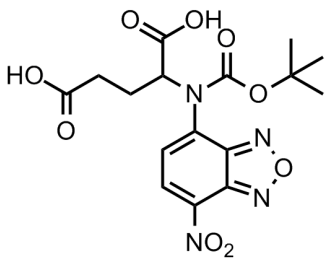


N-Boc glutamic acid was mixed with DMAP in THF. NBD-Cl was then added to the previous solution and stirred for 24 hours. The solvent was evaporated and the product was then re-dissolved in citric acid and extracted to ethyl acetate (Yield: 33%).

$^{1}$H NMR: complex NMR with multiple products (multiple NBD species). Peak at 5.96 (d, 1H) indicates the presence of NBD attach to glutamic acid with a ratio of ~1:9 to a singlet at 1.35 (possibly n-Boc); 2.29 ppm (m, 2H, $CH_2$), 1,9-1.7 (m, 2H, $CH_2$).

**N-alkyl-GLU-OMe (36);**

**IUPAC: (S)-dimethyl 2-(methylamino)pentanedioate**

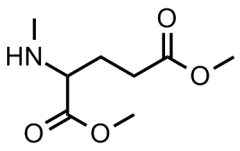

**(A)** Glutamic acid di-ethyl ester hydrochloride (0.2 M) was dissolved in DMF or acetonitrile with $Cs_2CO_3$ and MeI at room temperature or 90$^oC$[81–83]. The reaction was carried out with vigorous stirring for 24 hours. The solvent was then evaporated and the product re-dissolved in ethyl acetate and washed with water and brine. The organic solvent was then removed under vacuum to obtain a yellow oil.

**(B)** L-Glutamic acid di-methyl ester (0.1M) was dissolved in THF and treated by slow addition of LDA (1.1-2 eq) at -78$^oC$ for 2 hour followed by addition of methyl iodide (10 eq). The reaction was allowed to warm to room temperature and was stirred for 24 hours under argon. The reaction mixture was then diluted in DCM and washed with water.

**(C)** L-Glutamic acid di-methyl ester hydrochloride (0.1M) was added dropwise to a suspension of a sodium hydride (0.4 M 60 wt% dispersion in mineral oil or alternatively washed with hexanes) in DMF at 0$^oC$ under inert atmosphere. Methyl iodide (10 eq.) was then added and stirred for 4 hours. Once the reaction was completed (as indicated by TLC), the mixture was stirred at room temperature for 30 min[84,85]. The reaction was quenched by addition of ice and the resulting mixture was diluted with ethyl acetate and washed with hexane followed by washing with brine and dried over MgSO4. The organic phase was then evaporated under vacuum.

$^1$H NMR ($CD_3COD$, 400MHz, 300K) δ(ppm): 5.98 (q, 1H, αC), 4.77-4.62 (s, 6H, Ester $CH_3$), 4.26 (t, 2H, $CH_2$), 3.98 (m, 1H, $CH_2$), 3.73 (m, 1H, $CH_2$), 3.14 (s, 3H, N-$CH_3$).

**N-alkyl-GLU-OH (37) ;**

**IUPAC: (S)-dimethyl 2-(methylamino)pentanedioate**

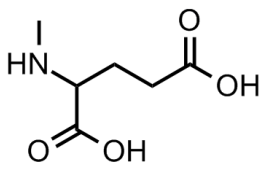

Sodium hydride was slowly added to a round bottom flask containing L-glutamic acid and MeI in ice cold THF. The reaction was then allowed to warm up to room temperature, and stirred for 12 hours. Ethyl acetate was then added, and the organic phase was washed with $NaHCO_3$ (sat). Yield: 34%

$^1$H NMR ($CD_3COD$, 400MHz, 300K) δ(ppm): 5.74 (m, 1H, αC), 3.53 (s, 3H, N-$CH_3$), 2.36-2.05 (m, 4H, $CH_2$)

**N-Boc-alkyl-GLU (38);**

**IUPAC: dimethyl 2-((*tert*-butoxycarbonyl)(methyl)amino)pentanedioate**

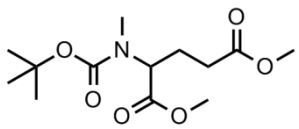

N-Boc glutamic acid was mixed with MeI (10 eq) in ice cold THF. Sodium hydride was slowly added and the reaction was allowed to warm to room temperature and stirred for 24 hours. Ethyl acetate was added and the organic phase was washed with 10% citric acid, water and brine.

$^1$H NMR ($CD_3COD$, 400MHz, 300K) δ(ppm): 4.96 (br, 1H, CH), 3.72-3.60 (s, 6H, $CH_3$), 3.22 (t, 2H, $CH_2$), 2.95 (m, 1H, $CH_2$), 2.71 (m, 1H, $CH_2$), 2.65 (s, 9H, N-Boc $CH_3$), 2.10 (s, 3H, $CH_3$), 1.70 (m, 1H, NH)

**N-alkyl-NBD-GLU-OMe (39);**

**IUPAC: (S)-dimethyl 2-(methyl(7-nitrobenzo[c][1,2,5]oxadiazol-4-yl)amino) pentanedioate**

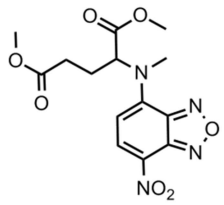

N-alkyl-Glu-OMe (36) was reacted with NBD-Cl (1.5 eq) using DIPEA (1.5 eq) or Cs2CO3 (1.5 eq) as base in DCM. The reaction was carried out at room temperature for 18 hours. The solvent was then evaporated and the product was purified by preparative TLC using methanol:ethyl acetate (5:95) as eluent.

Rf 0.8 in methanol:ethyl acetate (5:95)

$^1$H NMR ($CD_3COD$, 400MHz, 300K) δ(ppm): 8.4 (d, 1H, NBD), 6.20 (d, 1H, NBD), 4.53 (q, 1H, CH), 3.76 (s, 3H, $CH_3$), 3.67 (s, 3H, $CH_3$), 2.50 (m, 2H, $CH_2$), 2.24 (m, 2H, $CH_2$), 1.46 (s, 3H, $CH_3$)

**N-alkyl-NBD-GLU-OtBu (40);**

**IUPAC: (S)-di-*tert*-butyl 2-(methyl(7-nitrobenzo[c][1,2,5]oxadiazol-4-yl)amino) pentanedioate**

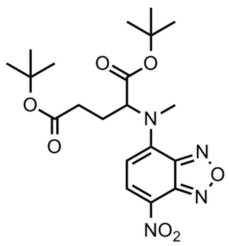

NBD-GLU-OtBu **(27)** was reacted with MeI and DIPEA in THF for 12 hours at room temperature or with $Cs_2CO_3$ in DCM or DMF. Ethyl acetate was then added and the reaction was washed with water, $NaHCO_3$ (sat) and brine. The organic phase was then evaporated and the product was purified by preparative TLC

using methanol:ethyl acetate (5:95) as eluent.

$^1$H NMR ($CD_3COD$, 400MHz, 300K) δ(ppm): 8.40 (d, 1H, NBD), 6.19 (d, 1H, NBD), 4.37 (br, 1H, CH), 2.38 (m, 2H, $CH_2$), 2.19 (m, 2H, $CH_2$), 1.45-1.34 (s, 21H, Ester $CH_3$ + N-$CH_3$).

**N-alkyl-NBD-GLU-OH (41);**

**IUPAC: (S)-2-(methyl(7-nitrobenzo[c][1,2,5]oxadiazol-4-yl)amino)pentanedioic acid**

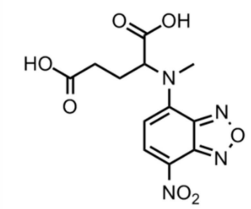

TFA (10 eq.) was slowly added to N-alkyl-NBD-GLU-OtBu (40) in dry ice cold DCM. The reaction was allowed to warm up to room temperature and was stirred for 8 hours. The solvent was then co-distilled with ethyl acetate and THF to obtain a yellow oil (Yield: 98%).

$^1$H NMR ($CD_3COD$, 400MHz, 300K) δ(ppm): 8.40 (d, 1H, NBD), 6.32 (d, 1H, NBD), 4.26 (t, 1H, CH), 2.38-2.00 (m, 4H, $CH_2$), 1.88 (s, 3H, N-$CH_3$).

**NBD-proline-OMe (42);**

**IUPAC: (S)-methyl 1-(7-nitrobenzo[c][1,2,5]oxadiazol-4-yl)pyrrolidine-2-carboxylate**

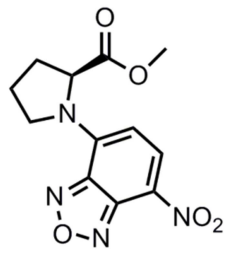

L-proline was mixed with DIPEA or $Cs_2CO_3$ in acetonitrile or THF, and NBD-Cl was then added in equimolar amounts at room temperature. The solvent was removed, and the product was re-dissolved in ethyl acetate and washed with water and brine and dried over $MgSO_4$. The organic phase was then evaporated under vacuum to obtain a dark orange plastic. (Yield: 59% (DIPEA), 37% ($Cs_2CO_3$))

$^1$H NMR ($CD_3COD$, 400MHz, 300K) δ(ppm): 8.39 (d, 1H, NBD), 6.04 (br, 1H, NBD), 3.69 (s, 3H, $CH_3$), 2.37 (m, 3H, $CH_2$), 2.15 (m, 3H, $CH_2$), 1.47 (br, 1H, CH)

**N-sulfonamide-GLU-OMe (43);**

**IUPAC: (S)-dimethyl 2-(methylsulfonamido)pentanedioate**

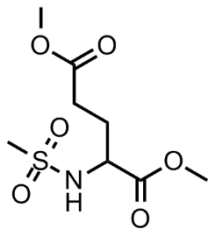

L-glutamic acid di-ethyl ester was mixed with sulfonyl chloride (1.02 eq) in THF at room temperature (or alternatively at 40$^{o}$C). DIPEA (2.1 eq) or NaH was slowly added over a period of 20 min and the reaction was stirred for 12 hours. The solvent was then evaporated under vacuum and re-dissolved in ethyl acetate and washed with 10% citric acid, water and brine (Yield: 13%).

$^{1}$H NMR ($CD_3COD$, 400MHz, 300K) δ(ppm): 4.98 (d, 1H, NH), 4.11 (m, 1H, CH), 3.73 (s, 3H, Ester $CH_3$), 3.62 (s, 3H, Ester), 2.88 (s, 3H, $SO_2CH_3$), 2.44 (m, 2H, $CH_2$), 2.16 (m, 1H, $CH_2$), 1.89 (m, 1H, $CH_2$)

**N-Boc-GLU-(Fmoc)$_2$ (44);**

**IUPAC: (S)-*tert*-butyl-(1,19-di(9H-fluoren-9-yl)-3,8,12,17-tetraoxo-2,18-dioxa-4,7,13,16-tetraazanonadecan-9-yl)carbamate**

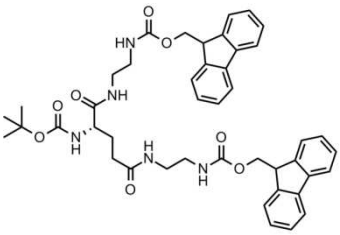

N-Boc-glutamic acid was pre-activated with CDI (2.05 eq.) in THF for 30 min. Fmoc-Ethylenediamine hydrochloride was then added (2.05 eq.) and the reaction was stirred for 12 hours at room temperature. The precipitated product was then filtered and washed with water and 10% citric acid to obtain a white solid (yield: 97%).

$^{1}$H NMR ($CD_3COD$, 400MHz, 300K) δ(ppm): 7.88 (d, 4H, Fmoc), 7.83 (br, 2H, NH), 7.69 (d, 4H, Fmoc), 7.42 (t, 4H, Fmoc), 7.32 (t, 4H, Fmoc), 7.27 (br, 2H, NH), 6.78 (d, 1H, NH), 4.28-4.21 (m, 6H, Fmoc $CH_2$ + CH), 3.05 (m, 8H, N-$CH_2$), 2.09 (t, 2H, $CH_2$), 1.84-1.70 (m, 2H, $CH_2$), 1.37 (s, 9H, $CH_3$)

**$NH_2$-GLU-(Fmoc)$_2$ (45);**

**IUPAC: (S)-bis-((9H-fluoren-9-yl)methyl) (((2-aminopentanedioyl) bis(azanediyl))bis(ethane-2,1-diyl))dicarbamate**

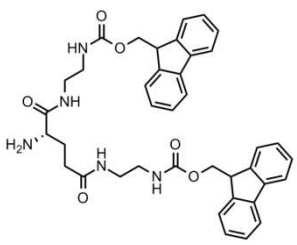

N-Boc-GLU-(Fmoc)$_2$ **(44)** was mixed with TFA (10 eq.) in ice cold DCM and stirred for 8 hours. The solvent was co-distilled with ethyl acetate to yield a white solid (quantitative yield).

$^1$H NMR ($CD_3COD$, 400MHz, 300K) δ(ppm): 8.42 (t, 1H, NH), 8.11 (br, 3H, NH), 7.91 (t, 1H, NH), 7.82 (d, 4H, Fmoc), 7.61 (d, 4H, Fmoc), 7.36 (t, 4H, Fmoc), 7.23 (t, 5H, Fmoc + NH), 4.21-4.11 (m, 6H, Fmoc $CH_2$+CH), 3.64 (br, 1H, CH), 3.15-2.93 (m, 8H, N-$CH_2$), 2.10 (t, 2H, $CH_2$), 1.85 (m, 2H, $CH_2$).

**Fmoc-GLU-(phenylalanine)$_2$ (46);**

**IUPAC: (2S,2'S)-dimethyl 2,2'-(((S)-2-((((9H-fluoren-9-yl)methoxy)carbonyl)amino) pentanedioyl)bis(azanediyl))bis(3-phenylpropanoate)**

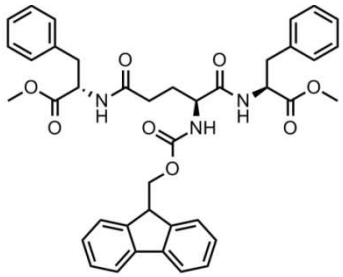

Fmoc-glutamic acid was pre-activated with CDI (2.05 eq) in THF for 30 min. L-phenylalanine methyl ester hydrochloride (2.1 eq) was then added and the reaction was stirred for 12 hours at room temperature. The precipitated residue was filtered and washed with water and brine to obtain a white solid (yield: 98%).

$^1$H NMR ($CD_3COD$, 400MHz, 300K) δ(ppm): 7.68 (d, 3H, Fmoc + NH), 7.50 (d, 2H, Fmoc), 7.31 (t, 2H, Fmoc), 7.22-7.13 (12H, Fmoc + Aromatics), 5.29 (d, 1H, NH), 4.80 (br, 2H, CH), 4.26-4.10 (br, 4H, Fmoc $CH_2$ + CH, CH), 3.69 (s, 6H, Ester $CH_3$), 2.99-2.82 (m, 4H, $CH_2$), 2.20-2.07 (m, 3H, $CH_2$), 1.80 (m, 1H, $CH_2$)

**Fmoc-GLU-(phenylalanine)$_2$ (47);**

**IUPAC: (2S,2'S)-dimethyl 2,2'-(((S)-2-aminopentanedioyl)bis(azanediyl))bis(3-phenylpropanoate)**

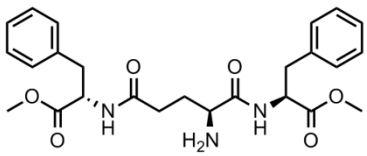

Fmoc-GLU-(phenylalanine)$_2$ **(46)** was mixed with piperidine (2 eq) in DMF at room temperature and stirred for 8 hours. The solvent was then evaporated under vacuum, and the product was purified by preparative TLC using ethyl acetate as eluent to obtain a white solid (yield: 69%)

Rf 0.8 in ethyl acetate

$^1$H NMR ($CD_3COD$, 400MHz, 300K) δ(ppm): 7.29-7.12 (m, 10H, Aromatics), 6.39 (d, NH), 4.76 (m, 1H, CH), 3.97 (t, 1H, CH), 3.81 (t, 1H, CH), 3.16-2.94 (m, 4H, $CH_2$), 2.50 (s, 6H, $CH_3$), 2.06-1.93 (m, 3H, $CH_2$)

**N-Boc-GLU(OtBu)-ethylamine (48);**

**IUPAC: (S)-*tert*-butyl 5-((2-aminoethyl)amino-4-((tert-butoxycarbonyl)amino)-5-oxopentanoate**

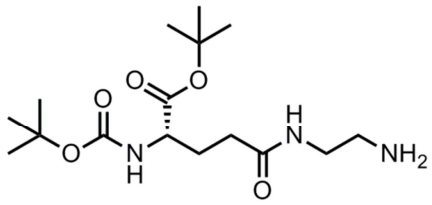

The synthesis was performed similarly to a previous published method[69]. Briefly, to a vigorously stirred solution of ethane-1,3-diamine (10 eq) in DCM at room temperature was added a solution of N-Boc-Glu(OtBu)(OH) previously activated with CDI (1 eq.) in DCM over a period of 5 hours. The resulting solution was stirred for 24h at room temperature and then concentrated in vacuum. The obtained oil was then partitioned between DCM and $Na_2CO_3$ and concentrated under vacuum to obtain an yellow oil.

$^1$H NMR ($CD_3COD$, 400MHz, 300K) δ(ppm): 4.33 (t, 2H, $CH_2$), 3.97 (br, CH), 2.47 (t, 2H, $CH_2$), 2.35-2.23 (m, $CH_2$), 2.06 (m, $CH_2$), 1.86 (m, $CH_2$), 1.45-1.40 (s, $CH_3$)

## 3.4. Conclusions

This chapter describes the attempts of synthesizing the PG dendrimers candidates provided by molecular modelling. Different coupling reagents commonly employed in the synthesis of peptides were used for the synthesis of these dendrimers. Despite reactions carried out with DCC afforded the desired products in high synthetic yields for low generation, the side product urea that was formed was difficult to remove for higher generations. In fact, it was not possible to determine whether the urea was complexed or directly attached to the structure backbone for dendrimers higher than G1. Alternatively, other coupling agents were tested and, similar to DCC, showed high yields for low generations dendrimers and low yields for the higher generations. Moreover, some reagents such as uranium salts showed to be incompatible with certain derivatives of GLU. Furthermore, it was observed that the interplay between the core protecting group and the protecting groups of the branching monomers was important to carry these reactions. In fact, reagents that would not de-protect the protecting groups of the core at low generations resulted in de-protection at higher generations attributed to the increased reaction times. As a result, different core derivatives of GLU with different amine protecting groups were tested. Finally, the CDI coupling reagents provided a suitable alternative as coupling reagents. This reagent was able to afford the desired products in high yields and was easy to remove.

However, the synthesis of dendrimers of generation beyond G2 was not viable due to a combination of attached impurities and low yields. The overall trend of the results indicates that the side-chain of GLU may be too short and crowding effects may create severe steric hindrance. This is further supported by the literature. Therefore, alternative methods should be explored in the future such as the use of SPPS or other potent and selective coupling agents together with other glutamic acid derivatives. Alternatively, new modelling structures could benefit from the limited reactivity observed in this work and new branching alternatives could be tested that facilitated the synthesis and minimize the crowding effects. Nevertheless, the optimized reactions used for PG dendrimers successfully translated to the synthesis of the terminal groups. However, issues related with the physicochemical properties (too lipophilic) of the monomers issues resulted in limited solubility which would be incompatible with dendrimer growth. Therefore, new alternatives for protecting groups should be tested.

Alternatively, this chapter described the coupling of NBD to the core. The attachment of NBD to the GLU was successful under various conditions but not for PG dendrimers. This effect was attributed to steric effects. Therefore alternative modifications to the NBD-GLU core were tested to prevent the secondary amine from further react when growing the PG dendrimers. Both alkylation and sulfonamide showed promising results and should be further explored in the future. However, even though selective alkylation was achieved it was obtained in low yield and further optimization is required. Nevertheless, the use of these modified cores could be used to further grow the dendrimers and would allow better tracking of the desired product as well as provide information regarding the surrounding environments during reaction by measuring the fluorescence properties of NBD. Overall, the results herein described open opportunities to improve the design of future PG dendrimers.

# REFERENCES


(1) Sadler, K.; Tam, J. P. Peptide Dendrimers: Applications and Synthesis. *Rev. Mol. Biotechnol.* **2002**, *90*, 195–229.

(2) Gao, C.; Yan, D. Hyperbranched Polymers: From Synthesis to Applications. *Prog. Polym. Sci.* **2004**, *29*, 183–275.

(3) Chow, H.-F.; Mong, T. K. .; Nongrum, M. F.; Wan, C.-W. 1998 – The Synthesis and Properties of Novel Functional Dendritic Molecules.Pdf. *Tetrahedron* **1998**, *54*, 8543–8660.

(4) Lee, J. W.; Kim, B.; Jin, S. Convergent Synthesis of Triazole Dendrimers via Click Chemistry Using Tripodal Core. *Bull. Korean Chem Soc.* **2005**, *26*, 833–836.

(5) Maciejewski, M. Concepts of Trapping Topologically by Shell Molecules. *J. Macromol. Sci. Part A - Chem.* **1982**, *17*, 689–703.

(6) Denkewalter, R. G.; Kolc, J.; Lukasavage, W. J. Preparation of Lysine Based Macromolecular Highly Branched Homogeneous Compound. 4,360,646, 1982.

(7) Gennes, P. G. De; Hervet, H. Statistic of << Starburst >> Polymers. **1983**, *44*, 351–360.

(8) Tomalia, D. a. Birth of a New Macromolecular Architecture: Dendrimers as Quantized Building Blocks for Nanoscale Synthetic Polymer Chemistry. *Prog. Polym. Sci.* **2005**, *30*, 294–324.

(9) Lim, J.; Kostiainen, M.; Maly, J.; da Costa, V. C. P.; Annunziata, O.; Pavan, G. M.; Simanek, E. E. Synthesis of Large Dendrimers with the Dimensions of Small Viruses. *J. Am. Chem. Soc.* **2013**, *135*, 4660–4663.

(10) Montalbetti, C. A. G. N.; Falque, V.; Park, M.; Ox, A. Amide Bond Formation and Peptide Coupling. *Tetrahedron* **2005**, *61*, 10827–10852.

(11) Zeng, X.; Pan, S.; Li, J.; Wang, C.; Wen, Y. A Novel Dendrimer Based on Poly ( L -Glutamic Acid ) Derivatives as an Efficient and Biocompatible Gene Delivery Vector. *Nanotechnology* **2011**, *22*, 375102.

(12) Uehara, T.; Ishii, D.; Uemura, T.; Suzuki, H.; Kanei, T.; Takagi, K.; Takama, M.; Murakami, M.; Akizawa, H.; Arano, Y. Gamma-Glutamyl PAMAM Dendrimer as

Versatile Precursor for Dendrimer-Based Targeting Devices. *Bioconjug. Chem.* **2010**, *21*, 175–181.

(13) Yuan, H.; Luo, K.; Lai, Y.; Pu, Y.; He, B.; Wang, G.; Wu, Y.; Gu, Z. A Novel Poly ( L -Glutamic Acid ) Dendrimer Based Drug Delivery System with Both PH-Sensitive and Targeting Functions. *Mol. Pharm.* **2010**, *7*, 953–962.

(14) Pu, Y.; Chang, S.; Yuan, H.; Wang, G.; He, B.; Gu, Z. The Anti-Tumor Efficiency of Poly ( L-Glutamic Acid ) Dendrimers with Polyhedral Oligomeric Silsesquioxane Cores. *Biomaterials* **2013**, *34*, 3658–3666.

(15) Twyman, L.; Beezer, A. .; Mitchell, J. . The Synthesis of Chiral Dendritic Molecules Based on the Repeat Unit L-Glutamic Acid. *Tetrahedron Lett.* **1994**, *35*, 4423–4424.

(16) Rewatkar, P. V; Parekh, H. S.; Parat, M. Molecular Determinants of the Cellular Entry of Asymmetric Peptide Dendrimers and Role of Caveolae. *PLoS One* **2016**, *11*, 1–15.

(17) Rewatkar, P. V; Sester, D. P.; Parekh, H. S.; Parat, M. Express in Vitro Plasmid Transfection Achieved with 16 + Asymmetric Peptide Dendrimers. *ACS Biomater. Sci. Eng* **2016**, *2*, 438–445.

(18) Maryanoff, B. E.; Greco, M. N.; Zhang, H.; Andrade-gordon, P.; Kauffman, J. A.; Liu, K. C. N. A.; Brungs, P. H.; Jolla, L. Macrocyclic Peptide Inhibitors of Serine Proteases. Convergent Total Synthesis of Cyclotheonamides A and B via a Late-Stage Primary Amine Intermediate. Study of Thrombin Inhibition under Diverse Conditions. *J. Am. Chem. Soc* **1995**, *117*, 1225–1239.

(19) Newkome, G. R.; Young, J. K.; Baker, G. R.; Potter, R. L.; Audoly, L.; Cooper, D.; Weislc, C. D.; Morris, K.; Johnson, C. S.; Hill, C.; *et al.* Cascade Polymers.1 PH Dependence of Hydrodynamic Radii of Acid Terminated Dendrimers. *Macromolecules* **1993**, *26*, 2394–2396.

(20) Ranganathan, D.; Karle, I. L. Self-Assembling Bis-Dendritic Peptides: Design, Synthesis and Characterization of Oxalyl-Linked Bis-Glutamyl Peptides [Glun(CO2Me)N+1-CO-]2; N=1,3,7. *J. Pept. Res* **1998**, 297–302.

(21) Morpurgo, M.; Bayer, E. A.; Wilchek, M. N-Hydroxysuccinimide Carbonates and Carbamates Are Useful Reactive Reagents for Coupling Ligands to Lysines on Proteins. *J. Biochem. Biophys. Methods* **1999**, *38*, 17–28.

(22) Lin, X.; Weis, C. D.; Newkome, G. R. Polytryptophane Terminated Dendritic Macromolecules *. *Tetrahedron: Asymmetry* **1991**, *2*, 957–960.

(23) Sheenan, J. C.; Hess, G. P. A New Method of Forming Peptide Bonds. *J. Am. Chem. Soc* **1955**, *77*, 1067–1068.

(24) Mathews, B. T.; Beezer, A. E.; Snowden, M. J.; Hardy, M. J.; Mitchell, J. C.; B, U. K. M. E. The Synthesis of Immobilised Chiral Dendrimers. *New. J. Chem* **2001**, *25*, 807–818.

(25) Woodman, E. K.; Chaffey, J. G. K.; Hopes, P. A.; Hose, D. R. J.; Gilday, J. P. N , N ′ -Carbonyldiimidazole-Mediated Amide Coupling : Significant Rate Enhancement Achieved by Acid Catalysis with Imidazole · HCl Abstract : *Org. Process Res. Dev.* **2009**, *13*, 106–113.

(26) Li, Y.; Wang, T.; Liu, M. Ultrasound Induced Formation of Organogel from a Glutamic Dendron. *Tetrahedron* **2007**, *63*, 7468–7473.

(27) Ranganathan, D.; Kurur, S.; Madhusudanan, K. P.; Roy, R.; Karle, I. L. Self-Assembling Bis-Dendritic Peptides: Design, Synthesis and Characterization of Oxalyl-Linked Bis-Glutamyl Peptides [Glu(n)(CO2Me)n + 1-CO-]2; n = 1,3,7. *J. Pept. Res.* **1998**, *51*, 297–302.

(28) Vinogradov, S. A.; Lo, L.; Wilson, D. F. Dendritic Polyglutamic Porphyrins : Probing Porphyrin Protection by Oxygen-Dependent Quenching of Phosphorescence. *Chem. Eur. J.* **1999**, *5*, 1338–1347.

(29) Ranganathan, D.; Kurur, S. Synthesis of Totally Chiral, Multiple Armed, Poly Glu and Poly Asp Scaffoldings on Bifunctional Adamantane Core. *Tetrahedron Lett.* **1997**, *38*, 1265–1268.

(30) Ranganathan, D.; Kurur, S.; Gilardi, R.; Karle, I. L. Design and Synthesis of AB3-Type (A = 1,3,5-Benzenetricarbonyl Unit; B = Glu DiOMe or GLU7 Octa OMe) Peptide Dendrimers: Crystal Structure of the First Generation*. *Biopolymers* **2000**, *54*, 289–295.

(31) Hartwig, S.; Nguyen, M. M.; Hecht, S. Exponential Growth of Functional Poly(Glutamic Acid) Dendrimers with Variable Stereochemistry. *Polym. Chem.* **2010**, *1*, 69.

(32) Tansey, W.; Ke, S.; Cao, X.; Pasuelo, M. J.; Wallace, S.; Li, C. Synthesis and

Characterization of Branched Poly ( L -Glutamic Acid ) as a Biodegradable Drug Carrier. *J. Control. release* **2004**, *94*, 39–51.

(33) Xie, L.; Wang, L.; Jia, X.; Kuang, G. Effects of Glutamic Acid Shelled PAMAM Dendrimers on the Crystallization of Calcium Phosphate in Diffusion Systems. *Polym. Bull* **2011**, *66*, 119–132.

(34) Higashi, N.; Koga, T.; Niwa, M. Enantioselective Binding and Stable Encapsulation of a -Amino Acids in a Helical Poly (L-Glutamic Acid)-Shelled Dendrimer in Aqueous Solutions. *ChemBioChem* **2002**, *3*, 448–454.

(35) Duan, P.; Qin, L.; Zhu, X.; Liu, M. Hierarchical Self-Assembly of Amphiphilic Peptide Dendrons : Evolution of Diverse Chiral Nanostructures Through Hydrogel Formation Over a Wide PH Range. *Chem. Eur. J.* **2011**, *17*, 6389–6395.

(36) Qin, L.; Duan, P.; Xie, F.; Zhang, L.; Liu, M. A Metal Ion Triggered Shrinkable Supramolecular Hydrogel and Controlled Release by an Amphiphilic Peptide Dendron. *Chem. Commun.* **2013**, *49*, 10823–10825.

(37) Qin, L.; Xie, F.; Duan, P.; Liu, M. A Peptide Dendron-Based Shrinkable Metallo-Hydrogel for Charged Species Separation and Stepwise Release of Drugs. *Chem. Eur. J.* **2014**, *20*, 15419–15425.

(38) Ghosh, P. B.; Whitehouse, M. W. 7-Chloro-4-Nitrobenzo-2-Oxa-1,3-Diazole: A New Fluorigenic Regaent for Amino Acids and Other Amines. *Biochem. J.* **1968**, *108*, 155–156.

(39) Fager, R.; Kutina, C.; Abrahamson, E. The Use of NBD Chloride (7 Chloro-4-Nitrobenzo-2-Oxa-1,3-Diazole) in Detecting Amino Acids and as an N-Terminal Reagent. *Anal. Biochem.* **1973**, *53*, 290–294.

(40) Bem, M.; Badea, F.; Draghici, C.; Caproiu, M. T.; Vasilescu, M.; Voicescu, M.; Beteringhe, A.; Caragheorgheopol, A.; Maganu, M.; Constantinescu, T.; *et al.* Synthesis and Fluorescent Properties of New Derivatives of 4-Amino-7-Nitrobenzofurazan. *ARKIVOC* **2007**, 87–104.

(41) Paprica, P. A.; Baird, N. C.; Petersen, N. O. Theoretical and Experimental Analyses of Optical Transitions of Nitrobenzoxadiazole (NBD) Derivatives. *Journal of Photochemistry and Photobiology, A: Chemistry*, 1993, *70*, 51–57.

(42) ElBashir, A., Suliman, F. and Aboul-Enein, H. The Application of 7-Chloro-4-Nitrobenzoxadiazole and 4-Fluoro-7-Nitro-2, 1, 3-Benzoxadiazole for The Analysis of Amines and Amino Acids Using High-Performance. *Gazi Univ. J. Sci.* **2011**, *24*, 679–697.

(43) Pound, G. J.; Pletnev, A. A.; Fang, X.; Pletneva, E. V. A Small Fluorophore Reporter of Protein Conformation and Redox State. *Chem. Commun.* **2011**, 1–16.

(44) Jung, M. E.; Dong, T. A.; Cai, X. Improved Synthesis of 4-Amino-7-Nitrobenz-2 , 1 , 3-Oxadiazoles Using NBD Fluoride ( NBD-F ). *Tetrahedron Lett.* **2011**, *52*, 2533–2535.

(45) Bragg, P. D.; Hou, C. Effect of NBD Chloride ( 4-Chloro-7-Nitrobenzo-2-Oxa-1 , 3-Diazole ) on the Pyridine Nucleotide Transhydrogenase of Escherichia Coli. *Biochim. Biophys. Acta* **1999**, *1413*, 159–171.

(46) Benzofuroxans, T. N.; Ghosh, P. B.; Whitehouse, W. Potential Antileukemic and Immunosuppressive Drugs. 11. Further Studies with Benzo-2,1,3-Oxadiazoles (Benzofurazans) and Their N-Oxides (Benzofuroxans). **1969**, *1151*, 9–11.

(47) Crampton, M. R.; Delaney, J.; Rabbitt, L. C. The Reaction of 4-Nitrobenzofuroxan with Amines in DMSO; Kinetic and Equilibrium Studies. *J. Chem. Soc., Perkin Trans.* **1999**, *2*, 2473–2480.

(48) Verma, R. P.; Shandilya, A.; Haridas, V. Peptide Dendrimers with Designer Core for Directed Self-Assembly. *Tetrahedron* **2015**, *71*, 8758–8765.

(49) Fields, G. B. CHAPTER 2 Methods for Removing the Fmoc Group. In *Methods in Molecular Biology*; 1994; Vol. 35, pp. 17–27.

(50) Takahashi, D. Method for Selective Removal of Dibenzofulvene Derivative, 2010.

(51) Dayal, B.; Salen, G.; Toome, B.; Tint, G. S.; Shefer, S.; Padia, J. Lithium Hydroxide / Aqueous Methanol : Mild Reagent for the Hydrolysis of Bile Acid Methyl Esters. *Steroids* **1990**, *55*, 233–237.

(52) Li, S.; Yao, H.; Xu, J.; Jiang, S. Synthetic Routes and Biological Evaluation of Largazole and Its Analogues as Potent Histone Deacetylase Inhibitors. *Molecules* **2011**, *16*, 4681–4694.

(53) Pascal, R.; Sola, R. Preservation of the Fmoc Protective Group under Alkaline Conditions by Using CaC12 . Applications in Peptide Synthesis. *Tetrahedron Lett.* **1998**, *39*, 0–3.

(54) Lin, L. S.; Jr, T. L.; Laszlo, S. E. De; Truong, Q.; Kamenecka, T.; Hagmann, W. K. Deprotection of N - Tert -Butoxycarbonyl ( Boc ) Groups in the Presence of Tert -Butyl Esters. *Tetrahedron Lett.* **2000**, *41*, 7013–7016.

(55) Rivero-buceta, E.; Doyagüez, E. G.; Colomer, I.; Quesada, E.; María-jesús, P. Tryptophan Dendrimers That Inhibit HIV Replication , Prevent Virus Entry and Bind to the HIV Envelope Glycoproteins Gp120 and Gp41. *Eur. J. Med. Chem.* **2015**, *106*, 34–43.

(56) Hanessian, S.; Margarita, R.; Hall, A.; Johnstone, S.; Tremblay, M.; Parlanti, L. Total Synthesis and Structural Confirmation of the Marine Natural Product Dysinosin A : A Novel Inhibitor of Thrombin and Factor VIIa. *J. Am. Chem. Soc* **2002**, *124*, 13342–13343.

(57) Hartwig, S.; Nguyen, M. M.; Hecht, S. Exponential Growth of Functional Poly(Glutamic Acid) Dendrimers with Varying Stereochemistry. *Polym. Chem.* **2010**, 69–71.

(58) Khattab, S. N.; Mansour, E. M. E.; E-rahman, M. M. A. Coupling of Iminodiacetic Acid with Amino Acid Derivatives in Solution and Solid Phase. *Lett. Pept. Sci.* **2001**, *7*, 331–345.

(59) Viault, G.; Poupart, S.; Mourlevat, S.; Lagaraine, C.; Devavry, S.; Lefoulon, F.; Bozon, V.; Dufourny, L.; Delagrange, P.; Guillaumet, G.; *et al.* Design, Synthesis and Biological Evaluation of Fluorescent Ligands for MT1 and/or MT2 Melatonin Receptors. *RSC Adv.* **2016**, *6*, 62508–62521.

(60) Guminski, Y.; Grousseaud, M.; Cugnasse, S.; Brel, V.; Annereau, J.; Vispé, S.; Guilbaud, N.; Barret, J.; Bailly, C.; Imbert, T. Synthesis of Conjugated Spermine Derivatives with 7-Nitrobenzoxadiazole ( NBD ), Rhodamine and Bodipy as New Fluorescent Probes for the Polyamine Transport System. *Bioorg. Med. Chem. Lett.* **2009**, *19*, 2474–2477.

(61) Jiang, W.; Fu, Q.; Wang, W. An NBD Fluorophore-Based Sensitive and Selective Fluorescent Probe for Zinc Ion {. *Chem. Commun.* **2008**, *0*, 259–261.

(62) Perotti, J. P.; Grau, R. J. A.; Vaillard, S. E. Method for the Synthesis of N-Alkyl-

O-Alkyl Carbamates. *RSC Adv.* **2014**, *4*, 13012–13017.

(63) Jarowicki, K.; Kocienski, P. Protecting Groups. *J. Chem. Soc* **2001**, *1*, 2109–2135.

(64) Kawabata, T.; Wirth, T.; Suzuki, H.; Fuji, K. Direct Asymmetric A-Alkylation of Phenylalanine Derivatives Using No External Chiral Sources. *J. Am. Chem. Soc* **1994**, *116*, 10809–10810.

(65) Cisneros-pérez, P. A.; Frontana-uribe, B. A.; Martínez-otero, D.; Cuevas-yáñez, E. Synthesis of Bis-3 , 4-Dialkoxythiophenes Linked by a m -Xylene Bridge. *Tetrahedron Lett.* **2016**, *57*, 5089–5093.

(66) Sommer, H. Z.; Jackson, L. Alkylation of Amines. A New Method for the Synthesis of Quarternary Ammonium Compounds from Primary and Secondary Amines. *J. Org. Chem.* **1970**, *55*, 1558–1562.

(67) Salvatore, R. N.; Yoon, H.; Woon, K. Synthesis of Secondary Amines. *Tetrahedron* **2001**, *57*, 7785–7811.

(68) Koza, G.; Theunissen, C.; Dulayymi, R. Al; Baird, M. S. The Synthesis of Single Enantiomers of Mycobacterial Ketomycolic Acids Containing Cis - Cyclopropanes. *Tetrahedron* **2009**, *65*, 1–16.

(69) Landi, F.; Johansson, C. M.; Campopiano, D. J.; Hulme, A. N. Synthesis and Application of a New Cleavable Linker for “Click”-Based Affinity Chromatography. *Org. Biomol. Chem.* **2010**, *8*, 56–59.

(70) Eggert, U.; Diestel, R.; Sasse, F.; Jansen, R.; Kunze, B.; Kalesse, M. Chondramide C : Synthesis , Configurational Assignment , and Structure – Activity Relationship Studies **. *Angew Chem Int Ed Engl.* **2008**, *47*, 6478–6482.

(71) Hanessian, S.; Margarita, R. 1, 3-Asymmetric Induction in Dianionic Allylation _ Reactions of Amino Acid Derivatives-Synthesis of Functionally Useful Enantiopure Glutamates , Pipecolates. *Tetrahedron Lett.* **1998**, *39*, 5887–5890.

(72) Malkov, A. V; Vrankov, K.; Cern, M.; Ko, P.; Chemistry, O. On the Selective N - Methylation of BOC-Protected Amino Acids. *J. Org. Chem* **2009**, *74*, 8425–8427.

(73) Englund, E. A.; Gopi, H. N.; Appella, D. H. An Efficient Synthesis of a Probe for Protein Function : 2 , 3-Diaminopropionic Acid with Orthogonal Protecting Groups. *Org. Lett.* **2004**, *6*, 213–215.

(74) Sankar, U.; Raju, C.; Uma, R. Cesium Carbonate Mediated Exclusive Dialkylation of Active Methylene Compounds. *Curr. Chem. Lett.* **2012**, *1*, 123–132.

(75) Shimamoto, K.; Ishida, M.; Ohfune, Y. Synthesis of Four Diastereomeric L-2-(Carboxycyclopropyl)Glycines. Conformationally Constrained L-Glutamate Analogs. *J. Org. Chem* **1991**, *56*, 4167–4176.

(76) Fauber, B.; Rene, O. WO 2013/092941 A1 Benzyl Sulfonamide Derivatives as RORc Modulators, 2013.

(77) Scozzafava, A.; Carta, F.; Supuran, C. T. Secondary and Tertiary Sulfonamides : A Patent Review ( 2008 – 2012 ). *Expert Opin.* **2013**, *23*, 203–213.

(78) Rajeev, S.; Menon, S. Catalyst-Controlled Divergence in Cycloisomerisation Reactions of N -Propargyl- N - Vinyl Sulfonamides : Gold-Catalysed Synthesis Of. *Chem. Commun.* **2015**, *51*, 13748–13751.

(79) Bae, Y.; Lee, S.; Green, E. S.; Park, J. H.; Ko, K. S.; Han, J.; Choi, J. S. Characterization of Basic Amino Acids-Conjugated PAMAM Dendrimers as Gene Carriers for Human Adipose-Derived Mesenchymal Stem Cells. *Int. J. Pharm.* **2016**, *501*, 76–86.

(80) Baldassarre, L.; Baldassarre, L.; Pinnen, F.; Cornacchia, C.; Fornasari, E.; Cellini, L.; Baffoni, M.; Cacciatore, I. Synthesis of Short Cationic Antimicrobial Peptidomimetics Containing Arginine Analogues Synthesis of Short Cationic Antimicrobial Peptidomimetics Containing Arginine Analogues. *J. Pept. Sci.* **2012**, *18*, 567–578.

(81) Mitronova, G. Y.; Belov, V. N.; Bossi, M. L.; Wurm, C. A.; Meyer, L.; Medda, R.; Moneron, G.; Bretschneider, S.; Eggeling, C.; Jakobs, S.; *et al.* New Fluorinated Rhodamines for Optical Microscopy and Nanoscopy. *Chem. Eur. J.* **2010**, *0*, 1–13.

(82) Kotubo, T.; Sassa, S.; Kaiser, E. T. Flavohemoglobin: A Semisynthetic Hydroxylase Acting in the Absence of Reductase. *J. Am. Chem. Soc* **1987**, *109*, 606–607.

(83) Vedejs, E.; Kongkittingam, C. Solution-Phase Synthesis of a Hindered N -Methylated Tetrapeptide Using Bts-Protected Amino Acid Chlorides : Efficient Coupling and Methylation Steps Allow Purification by Extraction. *J. Org. Chem*

**2000**, *65*, 2309–2318.

(84) Yan, B.; Nguyen, N.; Liu, L.; Holland, G.; Raju, B. Kinetic Comparison of Trifluoroacetic Acid Cleavage Reactions of Resin-Bound Carbamates , Ureas , Secondary Amides , and Sulfonamides from Benzyl-, Benzhydryl-, and Indole-Based Linkers. *J Comb Chem* **2000**, *2*, 66–74.

(85) Nagamoto, M.; Yanagi, T.; Nishimura, T.; Yorimitsu, H. Asymmetric Cyclization of N-Sulfonyl Alkenyl Amides Catalyzed by Iridium/Chiral Diene Complexes. *Org. Lett.* **2016**, *18*, 4474–4477.

# CHAPTER IV

# EFFECT ON CISPLATIN AND ITS CATIONIC ANALOGUES IN THE BIOPHYSICAL PHASE BEHAVIOR AND INTEGRITY OF MODEL LIPID BILAYERS

# Chapter IV - Effect of cisplatin and its cationic analogue in the biophysical phase behavior and integrity of model lipid bilayers

The introduction of this chapter is presented as an unpublished review manuscript that originated from this work and is relevant for the discussion of this chapter (ready for submission).

## PAPER 4 (Review) – Cisplatin-membrane interactions and their influence on platinum complexes activity and toxicity

**Authors: Nuno Martinho, Tânia Santos, Liana C. Silva**

**Outline**

1. Introduction
2. General considerations on the physicochemical properties of cisplatin and analogues
3. Brief overview on cellular uptake and resistance mechanisms
4. Cisplatin interaction with lipid membranes

4.1. Mechanistic interaction of cisplatin with lipids

4.2. Cell signaling modulation by cisplatin interaction with cell membrane

4.3. Resistance to cisplatin induced by changes on membrane biophysical properties and sphingolipid metabolism

5. Innovative cisplatin-based therapeutic strategies
6. Conclusions

## Abstract

Cisplatin and other platinum(II) analogues are widely used in clinical practice as anti-cancer drugs for a wide range of tumours. The primary mechanism by which they exert their action is through the formation of adducts with genomic DNA. However, multiple cellular targets by platinum(II) complexes have been described. In addition, the early events occurring at the plasma membrane, i.e., platinum-membrane interactions, seem to be involved in the uptake, cytotoxicity and cell-resistance to cisplatin. In fact, plasma membrane influences signalling events and perturbation of membrane organization and fluidity by cisplatin has shown to promote apoptotic pathways. This review discusses the sequence of events caused by lipid-platinum interactions, with emphasis on the mechanisms that lead to changes in the biophysical properties of the membranes (e.g. fluidity and permeability), and how these correlate with sensitivity and resistance phenotypes of cells to platinum(II) complexes.

## 1. Introduction

Cisplatin (cis-diamminedichloridoplatinum(II)) is a widely used chemotherapeutic drug to treat various types of cancers, including testicular, bladder, ovarian, breast, head and neck, and small and non-small cell lung cancers. Despite its effectiveness, cisplatin still displays significant side effects and mechanisms of resistance by cancer cells are widely reported. Therefore, combination therapies and innovative cisplatin-based therapies have been pursued to improve its clinical use. These range from the development of more effective and less toxic cisplatin analogues, to the use of drug carriers that deliver cisplatin in a more controlled way[1]. Progress in this area is, however, dependent on the understanding of the mechanisms underlying cisplatin and other platinum(II) complexes action, toxicity and induced resistance. The primary target of cisplatin is the genomic DNA. Once inside the cell, cisplatin becomes activated and forms adducts with DNA, preventing further DNA replication that culminates in cell death[2]. Nonetheless, other mechanisms not dependent of DNA replication have been implicated in cisplatin cytotoxicity, including oxidative stress, modulation of calcium signaling and activation of various stress signaling cascades (reviewed in[2]).

Besides its effects at the intracellular level, it is now recognized that cisplatin-induced cytotoxic events might start at the level of the plasma membrane (PM), where it directly interacts with proteins and lipids, causing alterations in membrane structure and biophysical properties[3,4]. Such alterations are likely to impact cell signaling events that result in cancer cell death. However, it may also have implications in the activation of mechanisms that lead to cancer cell resistance or those associated with side effects. In this review, we summarize the current knowledge on cisplatin-membrane interactions obtained from studies performed both in artificial membrane systems and living cells, and critically address how these interactions influence cell response to cisplatin.

## 2. General considerations on the physicochemical properties of cisplatin and analogues

Several platinum(II) complexes have been explored for their antitumor activity, commonly attributed to platination of nucleic acids. Among them, cisplatin has been the most studied but suffers from severe limiting side effects that have prompted second generation platinum(II) complexes. Cisplatin is a squared planar platinum(II) complex composed by a central metal atom coordinated with two chlorides and two ammonia molecules in a *cis* configuration (Figure 1). Even though the amines are relatively inert, the two chlorides are relatively labile ligands that are prone to nucleophilic substitution.

In fact, cisplatin in solution exists as an equilibrium of different neutral or positively charged "aquated" species (Figure 2)[5,6]. The equilibrium of these species is dependent on the pH, temperature and chloride concentration. It is generally accepted that in the blood, where a relatively high concentration of chloride is present, the equilibrium minimizes the formation of positively charged species. However, inside cells, where the chloride concentration is much lower, these forms are promoted. Cisplatin aquated form is much more reactive at forming coordinated intra- and inter-strand cross-links with DNA that cancerous cells cannot repair[6]. Despite the higher reactivity, the low chloride concentration inside the cells is however not the limiting factor to cisplatin cytotoxicity or resistance behavior since platinum accumulation and DNA platination was found to be similar in different cells lines with varied concentrations of chloride[7].

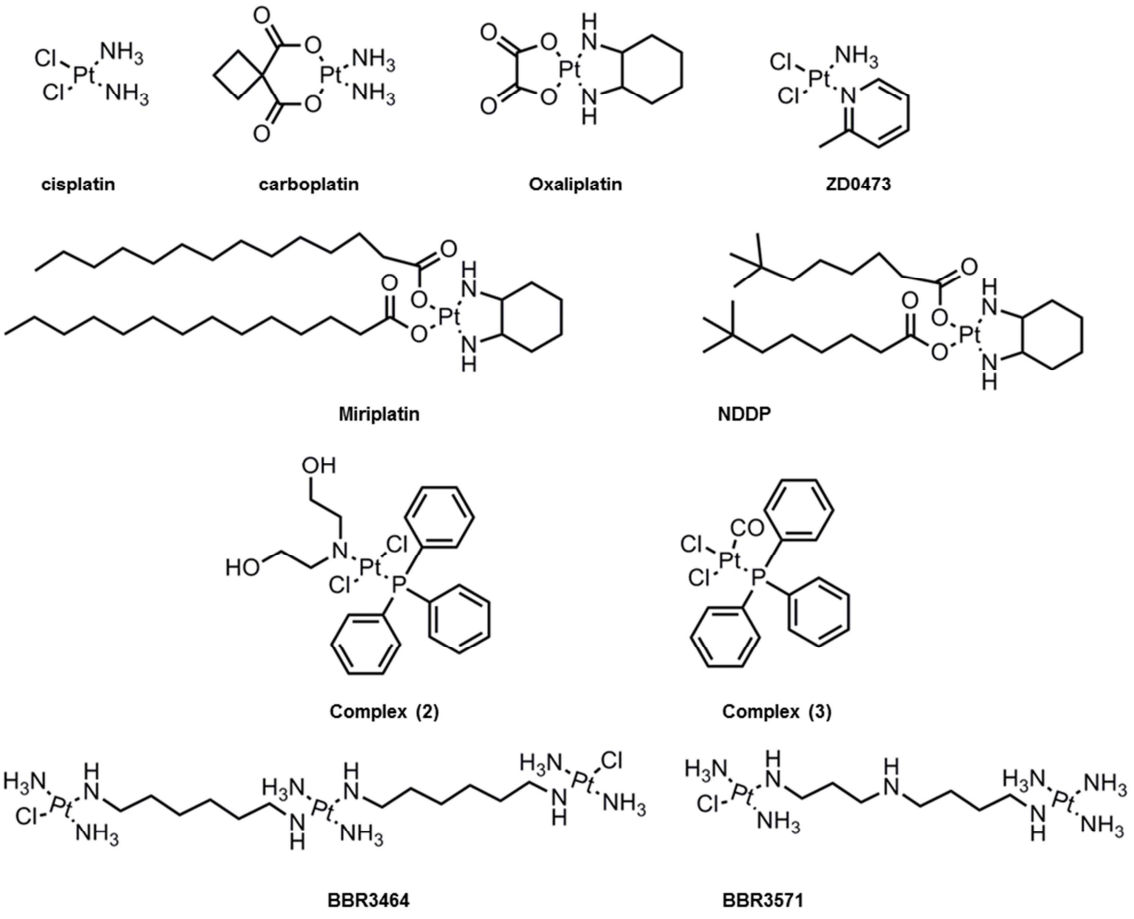


**Figure 1 – Molecular chemical structure of several platinum(II) compounds studied for interaction with lipid membranes**

Due to the inherent cytotoxicity problems associated with cisplatin, several analogues have been synthesized[8] and have been tested for clinical use based on the balance between binding to nucleic acids, stability, water solubility, acceptable levels of toxicity and increased spectrum of activity. These modifications have been generally carried by

chelation with anionic groups (e.g. carboplatin and oxaliplatin) or alterations to the amine (e.g oxaliplatin) as can be observed in figure 1. Furthermore, other substantial modifications to platinum(II) complexes have been tested including the addition of aliphatic chains (e.g. miriplatin)[9] or using a *trans*-configuration and positive charge as in the case of BBR3464 and BBR3571[10,11]. These changes in platinum(II) complexes ultimately result in variations in size and spatial configurations that affect their permeation, hydrolysis and reactivity rate, as well as, impact on cells-resistance mechanisms[12]. Moreover, the different analogues form adducts with the DNA that are different from one another. For example, the formed adducts can be more hydrophobic or bulkier (e.g. oxaliplatin) and thus contribute to increased DNA synthesis inhibition. Overall these factors result in clinical differences as exemplified by carboplatin, which has shown lower kidney and nervous system toxicity compared to cisplatin[13].

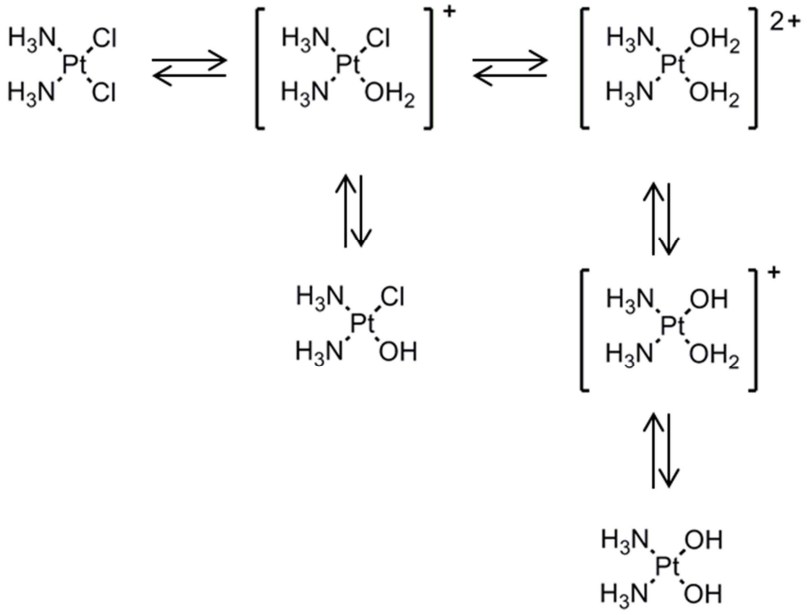

**Figure 2 – Cisplatin equilibrium in aqueous medium where it exchanges chloride with hydroxyls and water to form the so called aquated species**

Besides DNA as their primary target, cisplatin and its analogues have shown to have multiple off targeting interactions. Off target effects were early evidenced in patients where cisplatin caused hemolysis[14], and the mechanisms of resistance that arise after prolonged exposure. It has been proposed that the labile chemistry of platinum(II) complexes is responsible for the associated off target effects, where chemical transformations lead to a dynamic cascade of cellular events . In particular, cisplatin has high affinity for N and S donors. Thus, covalent Pt-S complexes with proteins are relatively stable and can only be reverted by other strong nucleophiles or otherwise render an irreversible bond[15]. Therefore, even before cisplatin reaches the cells

membranes it encounters many obstacles. This is clearly observed by its high protein binding (>95%) and biological terminal half-life (60-90 hours)[16].

Upon reaching the cell, cisplatin and its analogues can also interact with a variety of biomolecules including membrane proteins, small molecules harbored at the surface of the bilayer as well as lipids. This interaction will affect its cellular uptake and efflux, and ultimately its bioactivity and toxicity. Hence, it is of uppermost importance to understand the fundamental interactions of platinum(II) complexes at biological interfaces, so that the mechanisms of toxicity can be understood and novel complexes can be designed. In particular, there has been an effort to understand the mechanisms by which cisplatin enters cells since its uptake is not fully understood[15]. Moreover, understanding the mechanisms leading to drug efflux and/or decreased intracellular accumulation is pivotal, since they determine drug efficacy and are associated to drug resistance mechanisms. Below we present a brief summary of the mechanisms involved in cisplatin uptake and efflux and the importance of cellular membranes for them.

## 3. Brief overview on cellular uptake and resistance mechanisms

The entry of cisplatin in cells is a complex process[6]. Upon contact with the PM, cisplatin and its analogues need to cross the phospholipid bilayer to reach its primary intracellular target. In this regard, evidence suggests that the major mechanisms involved in cisplatin uptake are through passive diffusion and through facilitated transporters in particular organic cation transporters, such as, copper transporters (Ctr1)[17]. Transmembrane passive diffusion is a process that depends on both the size and hydrophilic/hydrophobic nature of the molecule. Cisplatin has a small size and no net charge and thus it is expected to enter via passive diffusion, even if low due to its hydrophilic nature. Indeed, studies in model membranes confirm the ability of cisplatin to cross the bilayer through passive diffusion[18–20]. Studies in cells also showed that cisplatin can be taken up by passive diffusion mechanisms since its accumulation by concentration gradient up to its saturation point was not the rate limiting factor[18–20]. Moreover, cisplatin structural analogues did not inhibit platinum accumulation inside cells. In addition, when cell transporters were inhibited (e.g. by temperature) there was still intracellular platinum accumulation to a certain extent[21]. Evidence further showed that cisplatin diffusion in DOPC membranes was much slower at low chloride concentrations[22], further highlighting the importance of neutral charge of cisplatin in its diffusion. Finally, other platinum(II) complexes have showed higher diffusion rate due to their more hydrophobic nature[23].

The permeation of drugs through the membrane also depends on its composition. Biological membranes are commonly perceived as entities displaying lateral organization into compositionally and functionally distinct domains. The biophysical properties of these domains are different and affect the interaction of drugs with membranes. It is thus not surprising that drug affinity for those domains can be different due to the packing density and free volume within those domains. The membrane fluidity has therefore a critical role in drug diffusion since the larger interior volume of membranes in the liquid-crystalline phase is more prone to accommodate molecules. On the other hand, the insertion of molecules into the lipid bilayer or the existence of specific interactions with lipids may cause changes in membrane structure and lateral organization. This can affect protein insertion and/or conformation within the membrane, which can be translated into changes in cell signaling and other membrane-associated cellular processes. Moreover, a variety of external factors (e.g. pH, concentration of ions) can influence membrane composition and fluidity that might result in a higher or lower uptake of platinum(II) complexes. In fact, several studies have shown that cisplatin accumulation and passive permeation into the cells could be modulated by a number of different factors including pH, osmolality, temperature, $Na^+K^+$ ATPase, docosohexaenoic acid, digitonin, genistein, halenaquinone and ouabain[18,24–26]. Furthermore, the different platinum(II) complexes are expected to have different metabolisms, and the resultant metabolites will interact differently with the lipid bilayer. As an example, the metabolism of oxaliplatin results in the formation of products that have shown greater cellular uptake while being more toxic than the precursor[27–29].

There is also several resistance mechanisms associated with treatment of cisplatin that result in reduced binding of the drug to the DNA. These include the ability of cells to repair cisplatin-induced damage, as well as increase of pro-survival events that detoxify the platinum (e.g. increase production of molecules with sulfhydryl groups such proteins, glutathione or metallothionins)[30–32]. Recently, the reduced intracellular accumulation of cisplatin has also been suggested to be a major factor for resistance. Cisplatin can trigger degradation of its transporter at the membrane interface resulting in lower influx rate[33,34]. Moreover, increased expression of MRP1 and MRP4 transporters results in reduced accumulation of cisplatin and oxaplatin[35]. Similarly TMEM205 protein was found to be overexpressed in resistant cells and when transfected into sensitive KB-3-1 cells it conferred resistance to cisplatin by approximately 2.5 fold[36]. In addition, other studies have suggested that the lipid membrane composition may also play a crucial role in the intracellular accumulation of

cisplatin and thus contribute to lower platinum accumulation. It was shown that the overall membrane permeability of resistant cells is lower compared to sensitive cells[25], thus resulting in a reduced intracellular cisplatin accumulation. However, whether this effect is due to changes in lipid composition is not fully understood[37].

In summary, the composition and biophysical properties of cellular membranes significantly affects cisplatin uptake. In addition, several intrinsic and extrinsic factors may modulate the features of biological membranes and thus influence cisplatin-membrane interactions. Therefore, it is highly desirable to understand how these interactions occur prior to binding to nucleic acid so that new improvements can be carried in future platinum(II) analogues and/or delivery systems.

## 4. Cisplatin interaction with lipid membranes

### 4.1. Mechanistic interaction of cisplatin with lipids

Despite the binding of cisplatin to phospholipids is in order of magnitude lower compared to proteins, it has been shown to still be relevant in cells[15]. In this regard, both the type of lipids in the membrane and the surrounding aqueous environment influence cisplatin-membrane interactions. This is supported by studies showing that binding of cisplatin to large unilamellar vesicles (LUV) composed of neutral lipids (DOPC, DOPE, SM) was negligible but significant in the presence of anionic charged lipids, such as, DOPA, DOPS, DOPG, phosphatidylinositol and cardiolipin[5]. The binding to these lipids was also found to be stronger in chloride free buffers. This suggests that the formation of aquated species of opposing charge is the factor determining the binding to anionic lipids[38]. On the other hand, direct observation of erythrocytes exposed to cisplatin showed evident changes in their shape suggesting that cisplatin affect the erythrocyte membrane structure[39]. Cisplatin was also directly observed by electron microscopy to be aggregated at the surface with extensions across the cell membrane of ovarian carcinoma cell line[40]. In addition, studies performed in rat human cell membranes suggested binding of cisplatin to cell membranes[26] and lipid-cisplatin specific interactions, particularly in the lipid chain, were also detected in cells using Raman-spectroscopy [41–43]. Altogether, these results indicate that cisplatin interacts with membrane lipids and may contribute to its action. Therefore, mechanistic studies that aim to understand the interactions that result from binding (charge-charge interactions) or coordination to the head groups and whether these can lead to alterations in the features of the membranes is of uppermost importance.

Several studies have been carried out to provide further insights into this issue, particularly, studies that take advantage of artificial membranes, where specific interactions can be more clearly investigated. Since model membranes correlate well with what is observed in cells, the specific molecular interactions with lipids can be used to correlate with cellular data. In this regard, NMR studies on platinum-lipid interactions have shown that cisplatin lowered the motion of lipids attributed to lipid-protein interactions[43,44]. Upon interaction with DPPC LUV, cisplatin altered the pre-transition of gel phase to ripple phase but not the main transition temperature of the gel to the fluid phase. This was attributed to rearrangement of the head groups with complexation of cisplatin to two phosphate headgroups, that did not cause alterations on the lipid chains (Figure 3)[45]. Similar results were observed for the cationic aquated species of cisplatin in DPPC LUV, where strong alterations in the headgroups consistent with *gauche* to *trans* transformation in the glycerol moiety were observed[15,46]. Additionally, these changes recovered slowly, in a process that started from the headgroups and extended to the interior of the membrane[15,43]. Despite the conformational changes on the lipid bilayer, no significant changes in the fluidity of the membrane were observed as measured by changes in fluorescence anisotropy of DPH and generalized polarization (GP) values for Laurdan in DMPC LUV[39]. However, this effect may be related to membrane composition. Indeed, evidence of phase alterations in the pig lipid extract bilayer were observed, consistent with the co-existence of at least 3 lipid phases, including a non-lamellar hexagonal II phase[43,44]. However, these alterations were not observed in model LUV composed of a mixture of phosphatidylcholine/cholesterol/PEG-DSPE (51:44:5) [47], showing the specificity of membrane lipid composition in cisplatin-mediated effects.

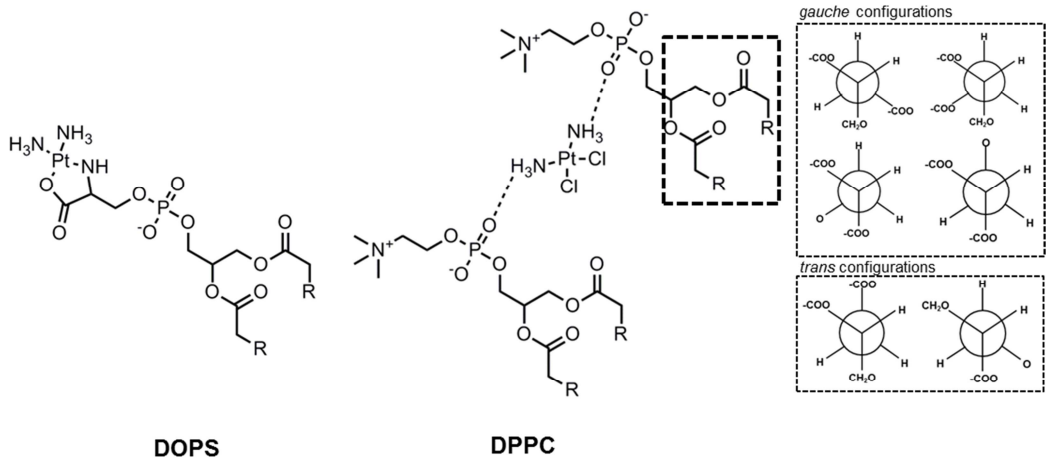


**Figure 3 – Interaction of cisplatin with DOPS and with two DPPC lipids. In the DPPC interaction it was observed further changes in the glycerol group changing the common *gauche* configurations to a *trans* configuration.**

Cisplatin interaction with the serine group of phospholipids (e.g. phosphatidylserine (PS)) has also been extensively studied. It was observed that cisplatin inserted into the inner monolayer of human erythrocytes and induced stomatocytic shape changes[39], most likely due to the formation of cisplatin-PS complex[39,48]. PS is a negatively charged phospholipid that is mostly located in the inner leaflet of the PM of non-cancer cells. This lipid is crucial in many cellular events as it interacts with proteins anchoring them to the inner monolayer of the PM[49]. However, cancer cells present an increased level of PS in their external leaflet of the PM[50,51]. Thus, an increased level of this lipid on the external leaflet of the PM could promote changes on its surface charge and lipid packing, changing membrane biophysical properties and consequently its functioning and response to chemotherapy. In addition, PS influences the activity of enzymes including the $Na^+/K^+$-ATPase[52] a transporter that has been reported to be involved in the uptake of cisplatin[18,53].

NMR studies suggest that cationic aquated cisplatin establishes an electrostatic interaction with PS, causing its reorganization[54]. This results in changes in the lipid bilayer, including the formation several lamellar phases[54]. Other studies showed that cisplatin induces structural perturbations in model membranes containing DAPS, but not in those composed of zwitterionic lipids[39]. Moreover, contrary to cisplatin-DPPC interaction, it was observed that the phosphate group was not responsible for platinum coordination to POPS but rather it formed a complex with both the carboxyl and amine group of the serine head group (Figure 2) that was stabilized by the phosphate group[38]. Together this evidence shows that lipid headgroup structure has a major role determining cisplatin-membrane interaction.

In fact, the headgroups of lipids determine the hydrophilic/hydrophobic balance at the surface of the bilayer and have major influence on the conformation, transition from gel to liquid crystalline phase, hydration levels, as well as, penetration of water, ions and small molecules[55,56]. Even small alterations in the headgroup of phospholipids, such as, addition of an extra methyl in the glycerol moiety results in conformational changes of lipid bilayers[57]. Thus, coordination of cisplatin to serine groups of phospholipids is expected to result in changes to accommodate the platinum complex. It should however be stressed that platinum-PS complex formation is not always observed. In fact, the platinum-PS complex has not been detected in some cancer cells and in intact erythrocytes[48,58]. This has been attributed to the fact that cisplatin can react with other cellular components and not be available to coordinate with PS. Moreover, the membrane permeability was shown to be an important factor for the formation of platinum-PS complex. Indeed, in aged erythrocytes and in cells exposed to digitonin

where the membrane permeability was increased, the platinum-PS complex was detected[48].

Further insight into the interactions of platinum(II) compounds with lipid bilayers was obtained from other cisplatin analogues (Figure 1). As expected, the positively charged BBR3464 and BBR3571 exhibited higher levels of cellular uptake compared to cisplatin due to their enhanced hydrophobic nature. In addition, they were shown to interact not only with the phosphate groups but also with the core of the bilayer[26]. These analogues were shown to coordinate with DPPG, DPPA and DPPS and cause changes in the pre-transition temperature of these lipids, but not of DPPE and DPPC. These interactions occurred rapidly within 20 minutes likely due to electrostatic and hydrogen interactions, followed by slower formation of platinum-lipid complexes as observed by $^{31}$P NMR[26]. Other analogues (Figure 1, complex (2) and complex (3)) were shown to cause phase changes consistent with hexagonal phase formation upon interaction with DMPC membranes[59]. The effect of structural modifications of the platinum complexes on their interactions with lipid membranes was further explored by comparing complex (2) and (3) with cisplatin. While cisplatin induced significant ordering of the alkyl chains with decrease in the area per lipid molecule and membrane elasticity, complex (2) only showed a small effect in the ordering[59]. Moreover, both complex (2) and (3) partitioned to the interior of the membrane whereas cisplatin accumulated at the surface[59]. It can therefore be concluded that the mechanisms underlying cisplatin and analogues-membrane interactions depend both on the platinum(II) complex structure particularly, hydrophobic moieties, and membrane lipid composition. This interplay will influence the type of interactions (e.g electrostatic, covalent, etc.) and the depth at which these occur. Moreover, they will influence the organization, structure and properties of the membrane. Thus, it is fundamental that future studies integrate lipid interactions as a strategy to improve the toxicity profile of cisplatin.

The membrane fluidity is also determined by its lipid composition and the interactions established between lipids and proteins. In this regard, several platinum(II) complexes were shown to increase the transition temperatures of human erythrocytes membrane, resulting in 1.4-3.5% increase in lipid membranes order[15]. In ascites cancer cells the lateral diffusion of phospholipids was also lower after treatment with a platinum(II) complex[15], consistent with a cisplatin-induced decrease in membrane fluidity. The type and amount of aquated species, as well as, the anionic lipids appeared to be responsible for this effect. Indeed, platinum(II) complexes were able to increase the $T_m$ of anionic (DPPG) but not zwitterionic (DPPC) phospholipids, indicating that the charge of the lipid head group also influences the interaction and the resultant cisplatin-

induced effects. Such electrostatic interactions established between platinum(II) and phospholipids are likely to be responsible for the more rigid and less fluid membrane[5]. This is further supported by studies showing that the influence of ions in the aqueous environment (e.g. $Ca^{2+}$, $Mn^{2+}$, $Mg^{2+}$. $Cu^{2+}$, $Zn^{2}$) altered the fluidity of the membrane by interacting with phosphates (e.g. electrostatic complexation) which in turn resulted in higher encapsulation of cisplatin into LUV (since the permeation was slower)[60,61]. These results seem to indicate a connection between the ability of platinum (II) complexes to establish electrostatic interactions in model membranes and decreased membrane fluidity induced by complexation with the headgroups. However, in biological membranes this interaction becomes much more complex, as it will be discussed in the next section.

Besides changes in membrane fluidity it was also reported that cisplatin might create small conducting defects in the inner hydrocarbon core. Such defects increase ion passage, as shown by ion conducting studies in a phospholipid mix of egg yolk in presence of cisplatin[6]. These results also correlated well with *in vitro* studies in epithelial cells where a drop of 89% on the TEER was observed 24h upon addition of cisplatin[62].

Overall literature data highlight that cisplatin interacts with lipid bilayers but its effect are complex and dependent on a variety of extrinsic factors including pH and chloride concentration, as well as, membrane composition and other unknown factors[61,63–65]. In fact, the importance of the physical state of membranes for the mechanisms of cisplatin and other platinum(II) complexes interaction remains to be determined. It is likely that differences in membrane composition can lead to structural differences that in turn affect the permeability of cisplatin. Ultimately, understanding how drug-membrane interactions occur creates new opportunities to develop novel innovative drug development strategies. In particular tacking issues related to the bypass of mechanisms of drug resistance originated by efflux or the repair mechanism can further guide the development of newly improved platinum(II) complexes or DDS.

### 4.2. Cell signaling modulation by cisplatin interaction with cell membrane

Cell signaling events are often dependent on membrane organization and structure. For instance, activation of apoptotic cascades has been related to changes on membrane biophysical properties fundamental for receptor clustering[66]. Since cisplatin is able to induce alterations in the fluidity of the membrane it is not unlikely that this drug might modulate signaling events upon its interaction with the membrane. In fact, relevant therapeutic concentration of cisplatin was shown to cause a transient increase

in membrane fluidity that persisted for 4h[4]. These changes on membrane fluidity were accompanied by the formation of large CD95 aggregates and the redistribution of CD95, together with the DISC-forming molecules FADD and procaspase-8 into PM lipid rafts[4,67]. The CD95 aggregates were found to be promoted by a rapid and transient activation of acid sphingomyelinase (aSMase)[4], which occurred in response to a decrease in intracellular pH mediated by cisplatin via inhibition of NHE1 ($Na^+/H^+$ membrane exchanger-1)[67,68]. Interestingly, the activation of this signaling pathway correlated with the formation of ceramides that occur at the external leaflet of the PM due to aSMase-mediated sphingomyelin hydrolysis[4,67,69]. This is supported by previous studies showing that ceramide domains are important for the clustering of CD95 at the cell surface and subsequent amplification of CD95 signaling[4,66,67,70]. Increased aSMase activity with concomitant upregulation of FAS was also recently described[71] in ovarian carcinoma A2780 cell line suggesting a common mode of action for cisplatin when used in the treatment of different cancer cells. It should however be stressed that the observed increase in membrane fluidity induced by cisplatin is biophysically not compatible with the formation of ceramide enriched domains since these are expected to be highly ordered[72,73] and therefore cause a decrease in membrane fluidity, as already reported for live cells[73]. Therefore, changes in membrane fluidity observed in these cells upon treatment with cisplatin might derive from other factors, not related to ceramide formation.

Other studies also suggested that cisplatin-induced membrane fluidification was implicated in activation of Fas death receptor pathway that in turn resulted in rapid and transient re-organization of F-actin microfilaments[74]. This is in agreement with the observation that cisplatin-induced damage to F-actin in proximal tubular cells occurred prior to changes in nuclear morphology[75]. Furthermore, F-actin damage may cause an increased monolayer permeability[76]. These observations are also in accordance with a work showing that cisplatin is able to induce permeabilization of the PM of T24 cells[5,38,77]. The importance of cisplatin interaction with actin was further shown in human ovarian cancer cells where F-actin was indeed considerably remodeled by cisplatin, causing changes in cellular nano-mechanics and increasing cell stiffness[78]. This is of major importance since the polymerization of actin monomer (G-actin) and depolymerization of filamentous actin (F-actin) represent fundamental molecular processes critically involved in cell motility, morphology, transport, cytokinesis and intracellular signalling[79,80]. Therefore, cisplatin interference with actin might impair these activities increasing the toxic effects induced at the PM level.

However, literature data is controversial regarding the mechanisms by which cisplatin modulates cellular structural features. In accordance, it was shown that cisplatin induces changes in PS120 fibroblasts membrane morphologic features with the appearance of noticeable villosities and long protrusions but no changes were observed in cell stiffness or actin cytoskeleton structure[81]. This suggests that cisplatin has a direct effect on the bilayer and not on actin. It should however be stressed that different studies use different cell lines[75,78,81], different cisplatin concentrations[75,81] and different methods of analysis[75,81] that might all contribute to the observed differences. In fact, it was already shown that the time required for cisplatin-induced cytoskeleton remodeling and loss of F-actin was concentration dependent[75].

Altogether, these studies suggest that cisplatin-induced changes on membrane biophysical properties and cytoskeleton structure might underlie the clustering of death receptors and activation of apoptotic cascades. These events occur upstream of platinum-DNA adduct formation and are likely to be the early steps contributing to cisplatin cytotoxicity.

### 4.3. Resistance to cisplatin induced by changes on membrane biophysical properties and sphingolipid metabolism

A large fraction of human malignancies rapidly becomes (or intrinsically is) insensitive to the cytotoxic effects of cisplatin[30,31]. Many studies have tried to elucidate the process responsible for the resistance to cisplatin treatment to overcome it and improve the success of the therapeutic regimen [30,31]. The complexity of the multiple factors involved is however a major obstacle for the development of an effective strategy to overcome resistance. Besides, all the proposed targets are non-specific for cancer cells which further increase this challenge.

Conversely, PM biophysical properties of cancer cells are known to be different from the ones of their non-cancerous counterpart[82,83]. Since cisplatin cytotoxicity starts at the PM level as discussed above, cancer cells PM could represent a good target not only for developing a specific and directed therapy but also for improvement of cisplatin mode of action. To this end, it is important to understand the differences between sensitive and resistant cells to cisplatin.

Cisplatin-resistant ovarian cancer cell lines present a significantly higher cell stiffness compared to their cisplatin-sensitive counterparts[78,84]. Furthermore, an increase in sensitive cells stiffness was observed after cisplatin treatment whereas no alterations

were observed for resistant cells[78]. This is also in agreement with the studies showing that cisplatin-induced changes in the transition temperature of the membranes were directly correlated with the degree of cisplatin resistance. Indeed, no significant changes were observed when resistant cells were treated with cisplatin compared to cisplatin-sensitive cells or cells with intermediate sensitivity to cisplatin[61,85,86]. Furthermore, modulating the fluidity of the membrane also resulted in different response to cisplatin. In models of cells of intermediary sensitivity to cisplatin, increasing its fluidity of the membrane with isopropanol resulted in an additive effect of increased fluidity upon addition of cisplatin. On the contrary, decreasing the fluidity of these cells with menthol, canceled the effect of increased fluidity by addition of cisplatin[85]. This result also correlated with the toxicity of cisplatin on those cells. When isopropanol was added to those cells, cisplatin treatment resulted in more cell death compared to cisplatin treatment alone. On the contrary, adding menthol to those cells resulted in lower toxicity by cisplatin[85].

However, literature evidence is controversial regarding the overall effect of membrane fluidity as a mechanism of resistance to cisplatin. Despite similar lipid composition, human lung adenocarcinoma $A_{549}$ cisplatin-resistance cells showed to have more fluid membranes compared to sensitive cells but the latter became even more sensitive after increasing the fluidity of the membrane with heptadecanoic acid[37,61]. On the contrary, A549 sensitive cells showed to have more fluid membranes and significant altered lipid composition compared to A549/DDP cisplatin-resistance cells[61,86] which could be attributed to shorter unsaturated fatty acids which are known to decrease lipid packing and alter lateral diffusion[87,88]. Cisplatin itself also affected the membrane fluidity of these cells over time by increasing membrane fluidity and membrane microviscosity in sensitive and resistant cells, respectively[89].Similarly, cisplatin-resistant breast cancer MCF-7/S cells had an increased content of cholesterol and SM suggesting a decrease in membrane fluidity compared to cisplatin-sensitive MCF-7/CP cells[90].

In addition, cisplatin resistant ovarian cancer cells were shown to present a highly organized actin architecture with a more robust actin cytoskeleton and stress fibers compared to cisplatin sensitive cells[78,84]. A highly dense F-actin network could thus create a barrier preventing cisplatin uptake and conferring resistance or inefficacy of the drug, for instance by influencing cell membrane biophysical properties, including membrane fluidity[78,84]. Moreover, the membrane potential of human epidermal KCP-20 carcinoma cells resistant to cisplatin was found to be hyperpolarized compared to the

low level resistant KB-CP.5 and sensitive KB-3-1 cell line from where they were originated, due to an increased expression of $K^+$ channels on their PM[37].

Finally, as mentioned above, it has been described that cisplatin cytotoxic mechanism comprises the activation of aSMase[4,67,71]. However, the activation of this pathway also seems to be dependent on cell sensitivity to cisplatin[71]. Accordingly, while aSMase pathway is activated in ovarian carcinoma A2780 cell line the same is not observed for the cisplatin-resistant counterpart A2780/C30 cell line[71]. Even 24h after treatment no alterations were observed in the levels of FAS, FASL, BCL2, CASPASE-3 and -9 transcripts corroborating the resistant state of the cells to cisplatin[71]. These results evidence the importance of aSMase activation and consequent changes on PM biophysical properties in the mechanism underlying cisplatin-induced cell death. Moreover, it also highlights that a dysregulation of sphingolipids metabolism on resistant cancer cells can be implicated in the development of such resistance, as already describe for other therapeutic regimens[91].

In fact, sphingolipids are ubiquitous components of eukaryotic cell membranes known to be involved in a variety of cellular processes including proliferation, growth, differentiation, apoptosis and membrane structure[92–94]. Dysregulation of their metabolism is evident in various pathological conditions including cancer[91,95–97]. Formation of ceramide in response to a variety of stimuli is typically a hallmark for the activation of cell death pathways[98,99]. Accordingly, it is not surprising that cells treated with cisplatin show elevation in ceramide levels. Indeed, elevation in C16-, C18- and C-20 ceramide species was observed in BKM sensitive cells to cisplatin[100]. However, no changes in ceramide levels were observed in DKO cisplatin-resistant cells[100], suggesting that these cells developed mechanisms to prevent ceramide-induced cell death. In addition to changes in the ceramide pathway, cisplatin-resistant cells tend to overexpress glucosylceramide synthase[101,102], and have higher levels of glycosphingolipids with longer carbohydrate chains and α-hydroxy fatty acids[103]. The distribution of the α-hydroxy groups of fatty acids in the hydrogen bonding region of the lipid bilayer, will influence membrane structure and interaction with intrinsic proteins[103]. These changes might contribute to impairment in signaling cascades including those leading to cell death. Such observations placed sphingolipid metabolism in the spotlight, as one of the target pathways for the development of therapeutic strategies to treat cancer disease. Accordingly, studies using different cancer cell lines have already shown that modulating the level of certain SLs and specific enzymes from sphingolipid metabolism is a good strategy to increase cells sensitivity to cisplatin[19,97,101,104,105], but also to other anticancer drugs[106–109].

As suggested above, the observed differences on membrane biophysical properties and actin structure of cisplatin-resistant cells could be the direct cause of resistance due to changes on membrane structure and consequent impairment of receptors clustering and intracellular signaling that could lead to a decreased apoptotic response to cisplatin in resistant cells. The passive diffusion and intracellular accumulation of cisplatin could also be reduced by an increase in lipid membrane packing, limiting its cytotoxic effect as observed for the confluence-dependent resistance phenomenon[88].

However, these differences could also have an indirect contribution by promoting changes on the structure and/or function of transmembrane proteins, impairing their functioning and, altering their binding and/or response to cisplatin. For instance, it is known that P-glycoprotein has greater affinity to substrates when the lipid bilayer is in the gel phase than in the fluid phase[110]. Moreover, protein kinase C migrates to PM when activated by cisplatin[111]. Alterations on the membrane composition and properties could alter protein kinase C binding to the PM and hence its activity and cell sensitivity to cisplatin action. Finally, cisplatin destabilizes membrane anchoring of actin filaments, leading to rearrangement of filamentous actin network and overall loss of cellular processes[69].

Overall, the evidence presented herein suggests that sphingolipid metabolism and membrane biophysical properties are two interconnected factors that determine cisplatin-induced cell death and/or development of cisplatin-resistance mechanisms.

## 5. Innovative cisplatin-based therapeutic strategies

There has been a tremendous effort in designing new platinum(II) based drugs or to develop and improve new delivery strategies to target tumors. Because platinum(II) complex have inherent clinical problems, it has been extensively studied the use of drug delivery systems to modulate their toxicity. There have been several types of drug delivery systems tested but, generally, they are used to circumvent solubility problems, modulate release rates, avoid resistance mechanism and avoid non-tumor tissues[112,113]. These types of drug delivery have been extensively tested and are outside of the scope of this review. However, honorable mentions have to be given to liposomes since they provide interesting information regarding platinum(II) complexes interaction with lipids. Liposomes have been commonly used for platinum formulations such as SPI-077 and Lipoplatin for cisplatin and Lipoxal for oxaliplatin[114]. These lipidic nanoparticles protect cisplatin from the outside biomolecules that would normally react with platinum(II) complexes and then fuse with cells releasing its contents. Interestingly, cisplatin in a lipid suspension of MLVs with equimolar amounts of

dioleoyl-phosphatidylserine (PS) and dioleoyl-phosphatidylcholine (PC) showed to be more cytotoxic than cisplatin or cisplatin mixed with the lipids[115].

Another interesting case from the use of liposomes has been the combination with NDDP (Bis-neodecanoato-1,2-diaminocyclohexaneplatinum(II)) and miriplatin (Figure 1.1). In particular, miriplatin is a phospholipid dicarboxylic acid platinum complex that has been developed for the hepatocellular carcinoma. Both these complexes are highly insoluble and thus liposomes offer an alternative for their use. However, in the case of NDDP the lipid composition of the liposome was shown to determine its biological activity and toxicity. In fact, using liposomes composed of DMPC, DMPG:DMPC (7:3 and 3:7) as well as DMPG, it was observed that the presence of DMPG was essential for NDDP activity. These studies demonstrated that NDDP was inactive, and the reaction intermediate between DMPG and NDDP was the active product[9,116–118]. Interestingly, even though miriplatin has similar structure to NDDP, it is active on its own and not requiring DMPG. Nevertheless, the loading capacity of different liposomes to miriplatin was shown to be higher for DMPC, DMPG and DPPC in comparison to HSPC, DPPG and DSPG[9].

Also worth mentioning are the delivery system that take advantage of sphingolipids[119–123] or modulate sphingolipid metabolism[124], as a synergistic strategy to enhance cisplatin-induced cell death. Examples of such strategies include reports of drug delivery systems that combine both the effect of the encapsulated anti-cancer drug with the effects of sphingomyelin or ceramide to increase the intracellular levels of ceramide and enhance the apoptosis, even in resistance cell lines. In general, the use of liposomes in this strategy has shown significant transport of the drug across the plasma membranes with enhanced accumulation of ceramide levels that lead to increased sensitivity to the cytotoxic effects of the drug[119–123]. However, to the best of our knowledge, the combination with SL-based drug delivery systems has not been studied for platinum(II) based drugs and thus further research is needed.

## 6. Conclusions

The clinical use of platinum(II) complexes and in particular cisplatin has been limited due to side effects and resistance mechanisms that arise on continuous treatment. These effects are not limited to changes in the primary target of cisplatin, such as, enhanced DNA repair mechanisms but rather due to a multitude of other molecular targets, such as, lipids. Platinum(II) complexes interact directly with lipids and induce phase changes that are dependent on plasma membrane lipid composition and other external factors. However, these interactions are complex and not fully understood.

The design of novel platinum(II) chemotherapeutics should therefore account for these interactions and its consequences on platinum accumulation and efficacy in cells. Therefore, new modifications in the platinum(II) complexes should not only confer stability to reaction with other cell components (e.g. steric hindrance on the ZD0473) but also focus on permeation through resistant cells. The increased knowledge regarding cisplatin-lipid interaction should therefore contribute to a better understanding of the anti-tumor activity and how to overcome the mechanisms that determine resistance.

## References


(1) Johnstone, T. C.; Suntharalingam, K.; Lippard, S. J. The Next Generation of Platinum Drugs: Targeted Pt(II) Agents, Nanoparticle Delivery, and Pt(IV) Prodrugs. *Chem Rev.* **2016**, *116*, 3436–3486.

(2) Dasari, S.; Tchounwou, P. B. Cisplatin in Cancer Therapy : Molecular Mechanisms of Action. *Eur J Pharmacol* **2014**, *0*, 364–378.

(3) Huang, C.; Jin, Z.; Dong, L.; Tong, X.; Yue, S. U. N. Cisplatin Augments FAS-Mediated Apoptosis through Lipid Rafts. *Anticancer Res.* **2010**, *30*, 2065–2072.

(4) Lacour, S.; Hammann, A.; Lagadic-gossmann, D.; Athias, A.; Sergent, O.; Laurent, G.; Gambert, P.; Solary, E. Cisplatin-Induced CD95 Redistribution into Membrane Lipid Rafts of HT29 Human Colon Cancer Cells. *Cancer Res.* **2004**, *64*, 3593–3598.

(5) Speelmans, G.; Sips, W. H. H. .; Grisel, R. J. H.; Staffhorst, R. W. H. M.; Fichtinger-Schepman, A. M. J.; Reedijk, J.; Kruijff, B. de. The Interaction of the Anti-Cancer Drug Cisplatin with Phospholipids Is Specific for Negatively Charged Phospholipids and Takes Place at Low Chloride Ion Concentration. *Biochim. Biophys. Acta* **1996**, *1283*, 60–66.

(6) Maheswari, K. U.; Ramachandran, T.; Rajaji, D. Interaction of Cisplatin with Planar Model Membranes - Dose Dependent Change in Electrical Characteristics. *Biochim. Biophys. Acta* **2000**, *1463*, 230–240.

(7) Jennerwein, M.; Andrews, P. A. Effect of Intracellular Chloride on the Cellular Pharmacodynamics of Cis-Diamminedichloroplatinum(II). *Drug Metab. Dispos.* **1995**, *23*, 178–184.

(8) Montaña, Á. M.; Batalla, C. The Rational Design of Anticancer Platinum Complexes : The Importance of the Structure-Activity Relationship. *Curr. Med. Chem.* **2009**, *16*, 2235–2260.

(9) Liu, S.; Li, Y.; Wang, X.; Ma, J.; Zhang, L.; Xia, G. Preparation , Characterization , and Antitumor Activities of Miriplatin-Loaded Liposomes. *J. Pharm. Sci.* **2016**,

*105*, 78–87.

(10) Billecke, C.; Finniss, S.; Tahash, L.; Miller, C.; Mikkelsen, T.; Farrell, N. P.; Bögler, O. Polynuclear Platinum Anticancer Drugs Are More Potent than Cisplatin and Induce Cell Cycle Arrest in Glioma1. *Neuro. Oncol.* **2006**, *8*, 215–226.

(11) Liu, Q.; Qu, Y.; Antwerpen, R. Van; Farrell, N.; Commonwealth, V.; Uni, V.; December, R. V; Re, V.; Recei, M.; February, V. Mechanism of the Membrane Interaction of Polynuclear Platinum Anticancer Agents . Implications for Cellular Uptake. *Biochemistry* **2006**, *45*, 4248–4256.

(12) Abu-Surrah, A.; Kettunen, M. Platinum Group Antitumor Chemistry: Design and Development of New Anticancer Drugs Complementary to Cisplatin. *Curr. Med. Chem.* **2006**, *13*, 1337–1357.

(13) Kelland, L. R. New Platinum Antitumor Complexes. *Crit. Rev. Oncol. Hematol.* **1993**, *15*, 191–219.

(14) Getaz, E. P.; Beckley, S.; Fitzpatrick, J.; Dozier, A. Cisplatin-Induced Hemolysis. *N Engl J Med* **180AD**, *302*, 334–335.

(15) Wang, K.; Lu, J.; Li, R. The Events That Occur When Cisplatin Encounters Cells. *Coord. Chem. Rev.* **1996**, *151*, 53–88.

(16) Deconti, R. C.; Toftness, B. R.; Lange, R. C.; Creasey, W. A. Clinical and Pharmacological Studies with Cis-Diamminedichloroplatinum( II ). *Cancer Res.* **1973**, *33*, 1310–1315.

(17) Ishida, S.; Lee, J.; Thiele, D. J.; Herskowitz, I. Uptake of the Anticancer Drug Cisplatin Mediated by the Copper Transporter Ctr1 in Yeast and Mammals. *Proc. Natl. Acad. Sci.* **2002**, *99*, 14298–14302.

(18) Gately, D. P.; Howell, S. B. Cellular Accumulation of the Anticancer Agent Cisplatin : A Review. *Br. J. Cancer* **1993**, *67*, 1171–1176.

(19) Min, J.; Mesika, A.; Sivaguru, M.; Veldhoven, P. P. Van; Alexander, H.; Futerman, A. H.; Alexander, S. (Dihydro)Ceramide Synthase 1 – Regulated Sensitivity to Cisplatin Is Associated with the Activation of P38 Mitogen-Activated Protein Kinase and Is Abrogated by Sphingosine Kinase 1. *Mol Cancer Res* **2007**, *5*, 801–813.

(20) Hromas, R.; North, J.; Burns, C. Decreased Cisplatin Uptake by Resistant L1210 Leukemia Cells. *Cancer Lett.* **1987**, *36*, 197–201.

(21) Gale, G. R.; Morris, C. R.; Atkins, L. M.; Smith, A. B. Binding of an Antitumor Platinum Compound to Cells as Influenced by Physical Factors and Pharmacologically Active. *Cancer Res* **1973**, *33*, 813–818.

(22) Eljack, N. D.; Ma, H. M.; Drucker, J.; Shen, C.; Hambley, T. W.; New, E. J.;

Clarke, R. J. Mechanisms of Cell Uptake and Toxicity of the Anticancer Drug Cisplatin. *Metallomics* **2014**, 2126–2133.

(23) Ghezzi, A.; Maurizio, A.; Cassino, C.; Gabano, E.; Osella, D. Uptake of Antitumor Platinum(II)-Complexes by Cancer Cells, Assayed by Inductively Coupled Plasma Mass Spectrometry (ICP-MS). *J. Inorg. Biochem.* **2004**, *98*, 73–78.

(24) Loh, S. Y.; Mistry, P.; Kelland, L. R.; Abel, G.; Harrap, K. R. Reduced Drug Accumulation as a Major Mechanism of Acquired Resistance to Cisplatin in a Human Ovarian Carcinoma Cell Line : Circumvention Studies Using Novel Platinum ( II ) and ( IV ) Ammine / Amine Complexes. *Br. J. Cancer* **1992**, 1109–1115.

(25) Marverti, G.; Andrews, A. Stimulation Modulation Response of Cis-Diamminedichloroplatinum ( II ) of Passive Permeability with Genistein : In Accumulation-Defective Resistant Accumulation An Altered By. *Clin. Cancer Res.* **1996**, *2*, 991–999.

(26) Baowei, C.; Kui, W. Interaction of Cisplatin with Membranes of Rat Ehrlich Ascites Tumor Cell. *Chinese J. Cancer Res.* **1995**, *7*, 1–4.

(27) Graham, M.; Lockwood, G.; Greenslade, D.; Brienza, S.; Bayssas, M.; Gamelin, E. Clinical Pharmacokinetics of Oxaliplatin: A Critical Review. *Clin. Cancer Res.* **2000**, *6*, 1205–1218.

(28) Luo, F.; Wyrick, S.; Chaney, S. Cytotoxicity, Cellular Uptake, and Cellular Biotransformations of Oxaliplatin in Human Colon Carcinoma Cells. *Oncol Res* **1998**, *10*, 595–603.

(29) Luo, F.; Wyrick, S.; Chaney, S. Comparative Neurotoxicity of Oxaliplatin, Ormaplatin, and Their Biotransformation Products Utilizing a Rat Dorsal Root Ganglia in Vitro Explant Culture Model. *Cancer Chemother Pharmacol* **1999**, *44*, 29–38.

(30) Galluzzi, L.; Vitale, I.; Michels, J.; Brenner, C.; Szabadkai, G.; Harel-Bellan, A.; Castedo, M.; Kroemer, G. Systems Biology of Cisplatin Resistance: Past, Present and Future. *Cell Death Dis.* **2014**, *5*, e1257.

(31) Siddik, Z. H. Cisplatin : Mode of Cytotoxic Action and Molecular Basis of Resistance. *Oncogene* **2003**, *22*, 7265–7279.

(32) Amable, L. Cisplatin Resistance and Opportunities for Precision Medicine. *Pharmacol. Res.* **2016**, *106*, 27–36.

(33) Lin, X.; Okuda, T.; Holzer, A.; Howell, S. B. The Copper Transporter CTR1 Regulates Cisplatin Uptake in Saccharomyces Cerevisiae. *Mol. Pharmacol.* **2002**, *62*, 1154–1159.

(34) Holzer, A. K.; Manorek, G. H.; Howell, S. B. Contribution of the Major Copper Influx Transporter CTR1 to the Cellular Accumulation of Cisplatin, Carboplatin, and Oxaliplatin. *Mol. Pharmacol.* **2006**, *70*, 1390–1394.

(35) Beretta, G. L.; Benedetti, V.; Cossa, G.; Assaraf, Y. G. A.; Bram, E.; Gatti, L.; Corna, E.; Carenini, N.; Colangelo, D.; Howell, S. B.; *et al.* Increased Levels and Defective Glycosylation of MRPs in Ovarian Carcinoma Cells Resistant to Oxaliplatin. *Biochem. Pharmacol.* **2010**, *79*, 1108–1117.

(36) Shen, D.-W.; Ma, J.; Okabe, M.; Zhang, G.; Xia, D.; Gottesman, M. M. Elevated Expression of TMEM205, a Hypothetical Membrane Protein, Is Associated with Cisplatin Resistance. *J. Cell. Physiol.* **2010**, *225*, 822–828.

(37) Liang, X.; Yin, J.; Zhou, J.; Wang, P. C.; Taylor, B.; Cardarelli, C.; Kozar, M.; Forte, R.; Aszalos, A.; Gottesman, M. M. Changes in Biophysical Parameters of Plasma Membranes Influence Cisplatin Resistance of Sensitive and Resistant Epidermal Carcinoma Cells. *Exp. Cell Res.* **2004**, *293*, 283–291.

(38) Speelmans, G.; Staffhorst, R. W. H. M.; Versluis, K.; Reedijk, J.; Kruijff, B. De. Cisplatin Complexes with Phosphatidylserine in Membranes. *Biochemistry* **1997**, *36*, 10545–10550.

(39) Suwalsky, M.; Hernández, P.; Villenab, F.; Sotomayorc, C. P. The Anticancer Drug Cisplatin Interacts with the Human Erythrocyte Membrane. *Z Naturforsch C.* **2000**, *55*, 461–466.

(40) Beretta, G. L.; Righetti, S. C.; Lombardi, L. Electron MicroscopyAnalysis of Early Localization of Cisplatin in Ovarian Carcinoma Cells. *Ultrastruct. Pathol.* **2002**, *26*, 331–335.

(41) Carvalho, A. L. M. B. De; Pilling, M.; Gardner, P.; Doherty, J. Chemotherapeutic Response to Cisplatin- like Drugs in Human Breast Cancer Cells Probed by Vibrational Microspectroscopy. *Faraday Discuss.* **2016**, *187*, 273–298.

(42) Marques, M. P. .; Batista de Carvalho, A. L. M.; Garcia Sakai, V.; Hatter, L.; Batista de Carvalho, L. A. E. Intracellular Water - an Overlooked Drug Target? Cisplatin Impact in Cancer Cells Probed By. *Phys. Chem. Chem. Phys.* **2017**, *19*, 2702–2713.

(43) Lu, J.-F.; Xia, W.-S.; Wang, K.; Zhai, C.; Liu, Q.-L. A Study of Interaction of Cisplatin and Its Analogues WithPhospholipid of Erythrocyte Membrane. *J. Chinese Pharm. Sci.* **1995**, *4*, 136–143.

(44) Fang, A.; Wang, S.-H.; Zou, J.; Chen, B. The Kinetic Studies of Across-Erythrocyte Membrane Transport of 1,2-Cyclohexanediamine Platinum(Ⅱ) Complexes. *Chinese J. Inorg. Chem.* **2000**, *4*, 680–682.

(45) Shen, Z.-W.; Sun, Z.-P.; Zhao, N.-M. Study of the Effects of the Antitumor Drug

Cis-DPP on the Phase Behavior of DPPC Liposomes and Molecular Mechanism of the Interaction. *Chinese Sci. Bull.* **1991**, *36*, 149–153.

(46) Wang, K.; Liu, D.; Zhuo, Z. C. A NMR Study of the Reaction Between Cis-Diaquodiammine-Platinum(Ⅱ) and Biomembranic Phospholipids. *Chem. J. Chinese Univ.* **1991**, *12*, 1382–1385.

(47) Peleg-shulman, T.; Gibson, D.; Cohen, R.; Abra, R. Characterization of Sterically Stabilized Cisplatin Liposomes by Nuclear Magnetic Resonance. *Biochim. Biophys. Acta* **2001**, *1510*, 278–291.

(48) Burger, K. N. J.; Sta, R. W. H. M.; Kruij, B. De. Interaction of the Anti-Cancer Drug Cisplatin with Phosphatidylserine in Intact and Semi-Intact Cells. *Biochim. Biophys. Acta* **1999**, *1419*, 43–54.

(49) Buckland, A. G.; Wilton, D. C. Anionic Phospholipids, Interfacial Binding and the Regulation of Cell Functions. *Biochim. Biophys. Acta* **2000**, *1483*, 199–216.

(50) Manjarika; Ghosh, S.; Sen, T.; Shadab, M.; Banerjee, I.; Basu, S.; Ali, N. A Novel Therapeutic Strategy for Cancer Using Phosphatidylserine Targeting Stearylamine-Bearing Cationic Liposomes. *Mol. Ther. - Nucleic Acids* **2018**, *10*, 9–27.

(51) Sharma, B.; Kanwar, S. S. Phosphatidylserine: A Cancer Cell Targeting Biomarker. *Semin. Cancer Biol.* **2017**.

(52) Schuurmans Stekhoven, FM Tesser, G.; Ramsteyn, G.; Swarts, H.; De Pont, J. Binding of Ethylenediamine to Phosphatidylserine Is Inhibitory to Na+/K(+)-ATPase. *Biochim Biophys Acta* **1992**, *1109*, 17–32.

(53) Andrews, P. A.; Mann, S. C.; Huynh, H. H.; Albright, K. D. Role of the Na + , K + -Adenosine Triphosphatase in the Accumulation of Cis-Diamminedichloroplatinum ( II ) in Human Ovarian Carcinoma Cells ’. *Cancer Res.* **1991**, 3677–3682.

(54) Jensen, M.; Bjerring, Æ. M.; Chr, N.; Willy, N. Æ.; Á, C. Á. M. N. M. R. Cisplatin Interaction with Phosphatidylserine Bilayer Studied by Solid-State NMR Spectroscopy. *J Biol Inorg Chem* **2010**, *15*, 213–223.

(55) Scherer, J. R. On the Position of the Hydrophobic / Hydrophilic Boundary in Lipid Bilayers. *Biophys J.* **1989**, *55*, 957–964.

(56) Serrallach, E.; Dijkman, R.; de Haas, G.; GG, S. Structure and Thermotropic Properties of 1,3-Dipalmitoyl-Glycero-2-Phosphocholine. *J Mol Biol* **1983**, *170*, 155–174.

(57) Lewis, E.; Bittman, R.; IW, L. Methyl Group Substitution at C(1), C(2) or C(3) of the Glycerol Backbone of a Diether Phosphocholine: A Comparative Study of Bilayer Chain Disorder in the Gel and Liquid-Crystalline Phases. *Biochim*

*Biophys Acta* **1986**, *861*, 44–52.

(58) Shirazi, F. H.; Wong, P. T. T.; Goel, R. Interaction of Cisplatin with Cellular Macromolecules : A Fourier Transform Infrared Spectroscopy Study. *Iran. J. Pharm. Res.* **2003**, 11–15.

(59) Nierzwicki, L.; Wieczor, M.; Censi, V.; Baginski, M.; Calucci, L.; Samaritani, S. Interaction of Cisplatin and Two Potential Antitumoral Platinum ( II ) Complexes with a Model Lipid Membrane : A Combined NMR and MD Study. *Phys. Chem. Chem. Phys.* **2014**, *17*, 1458–1468.

(60) Liu, H.; Zhang, Y.; Han, Y.; Zhao, S.; Wang, L.; Zhang, Z.; Wang, J.; Cheng, J. Characterization and Cytotoxicity Studies of DPPC : M 2 + Novel Delivery System for Cisplatin Thermosensitivity Liposome with Improving Loading Efficiency. *Colloids Surfaces B Biointerfaces* **2015**, *131*, 12–20.

(61) Liang, X.; Huang, Y. Physical State Changes of Membrane Lipids in Human Lung Adenocarcinoma A 549 Cells and Their Resistance to Cisplatin. *Int. J. Biochem. Cell Biol.* **2002**, *34*, 1248–1255.

(62) Ekle, M. I. G.; Chwerdt, G. E. S. Nephrotoxicity of Platinum Complexes Is Related to Basolateral Organic Cation Transport. *Kidney Int.* **2004**, *66*, 196–202.

(63) Jensen, M.; Nerdal, W. Anticancer Cisplatin Interactions with Bilayers of Total Lipid Extract from Pig Brain : A 13 C , 31 P and 15 N Solid-State NMR Study ☆. *Eur. J. Pharm. Sci.* **2008**, *34*, 140–148.

(64) Mann, S. C.; Andrews, P. A.; Howell, S. B. Short-Term Cis-Diamminedichloroplatinum ( II ) Accumulation in Sensitive and Resistant Human Ovarian Carcinoma Cells *. *Cancer Chemother Pharmacol* **1990**, 236–240.

(65) Lu, J.-F.; Wang, K.; Sun, X.-Z.; Xing, F.; An, P.-D.; Yang, Z.-H.; Yin, J.-J. Effects of Cisplatin and Its Analogues on the Permability of Humam Membrane Erythrocyte Membrane. *Met. Based Drugs* **1995**, *2*, 73–80.

(66) Grassme, H.; Jekle, A.; Riehle, A.; Schwarz, H.; Berger, J.; Sandhoff, K.; Kolesnick, R.; Gulbins, E. CD95 Signaling via Ceramide-Rich Membrane Rafts. *J. Biol. Chem.* **2001**, *276*, 20589–20596.

(67) Rebillard, A.; Tekpli, X.; Meurette, O.; Sergent, O.; Vernhet, L.; Gorria, M.; Chevanne, M.; Christmann, M.; Kaina, B.; Counillon, L.; *et al.* Cisplatin-Induced Apoptosis Involves Membrane Fluidification via Inhibition of NHE1 in Human Colon Cancer Cells. *Cancer Res* **2007**, *67*, 7865–7874.

(68) Shirmanova, M. V.; Druzhkova, I. N.; Lukina, M. M.; Dudenkova, V. V.; Ignatova, N. I.; Snopova, L. B.; Shcheslavskiy, V. I.; Belousov, V. V.; Zagaynova, E. V. Chemotherapy with Cisplatin: Insights into Intracellular PH and Metabolic

Landscape of Cancer Cells in Vitro and in Vivo. *Sci. Rep.* **2017**, *7*, 8911.

(69) Zeidan, Y. H.; Jenkins, R. W.; Hannun, Y. A. Remodeling of Cellular Cytoskeleton by the Acid Sphingomyelinase/Ceramide Pathway. *J. Cell Biol.* **2008**, *181*, 335–350.

(70) Grassmé, H.; Schwarz, H.; Gulbins, E. Molecular Mechanisms of Ceramide-Mediated CD95 Clustering. *Biochem. Biophys. Res. Commun.* **2001**, *284*, 1016–1030.

(71) Maurmann, L.; Belkacemi, L.; Adams, N. R.; Majmudar, P. M.; Moghaddas, S.; Bose, R. N. A Novel Cisplatin Mediated Apoptosis Pathway Is Associated with Acid Sphingomyelinase and FAS Proapoptotic Protein Activation in Ovarian Cancer. *Apoptosis* **2015**, *20*, 960–974.

(72) Castro, B. M.; Prieto, M.; Silva, L. C. Ceramide: A Simple Sphingolipid with Unique Biophysical Properties. *Prog. Lipid Res.* **2014**, *54*, 53–67.

(73) Pinto, S. N.; Laviad, E. L.; Stiban, J.; Kelly, S. L.; Merrill, A. H.; Prieto, M.; Futerman, A. H.; Silva, L. C. Changes in Membrane Biophysical Properties Induced by Sphingomyelinase Depend on the Sphingolipid N-Acyl Chain. *J. Lipid Res.* **2014**, *55*, 53–61.

(74) Rebillard, A.; Jouan-Lanhouet, S.; Jouan, E.; Legembre, P.; Pizon, M.; Sergent, O.; Gilot, D.; Tekpli, X.; Lagadic-Gossmann, D.; Dimanche-Boitrel, M.-T. Cisplatin-Induced Apoptosis Involves a Fas-ROCK-Ezrin-Dependent Actin Remodelling in Human Colon Cancer Cells. *Eur. J. Cancer* **2010**, *46*, 1445–1455.

(75) Kruidering, M.; van de Water, B.; Zhan, Y.; Baelde, J. J.; Heer, E.; Mulder, G. J.; Stevens, J. L.; Nagelkerke, J. F. Cisplatin Effects on F-Actin and Matrix Proteins Precede Renal Tubular Cell Detachment and Apoptosis in Vitro. *Cell Death Differ.* **1998**, *5*, 601–614.

(76) Kroshian, V. M.; Sheridan, A. M.; Lieberthal, W. Functional and Cytoskeletal Changes Induced by Sublethal Injury in Proximal Tubular Epithelial Cells. *Am. J. Physiol.* **1994**, *266*, F21-30.

(77) Zhang, M.-N.; Ding, Z.; Long, Y.-T. Sensing Cisplatin-Induced Permeation of Single Live Human Bladder Cancer Cells by Scanning Electrochemical Microscopy. *Analyst* **2015**, *140*, 6054–6060.

(78) Sharma, S.; Santiskulvong, C.; Bentolila, L. A.; Rao, J.; Dorigo, O.; Gimzewski, J. K. Correlative Nanomechanical Profiling with Super-Resolution F-Actin Imaging Reveals Novel Insights into Mechanisms of Cisplatin Resistance in Ovarian Cancer Cells. *Nanomedicine* **2012**, *8*, 757–766.

(79) Khaitlina, S. Y. Intracellular Transport Based on Actin Polymerization. *Biochem.*

**2014**, *79*, 917–927.

(80) Rajakylä, E. K.; Vartiainen, M. K. Rho, Nuclear Actin, and Actin-Binding Proteins in the Regulation of Transcription and Gene Expression. *Small GTPases* **2014**, *5*, e27539.

(81) Milosavljevic, N.; Duranton, C.; Djerbi, N.; Puech, P. H.; Gounon, P.; Lagadic-Gossmann, D.; Dimanche-Boitrel, M. T.; Rauch, C.; Tauc, M.; Counillon, L.; *et al.* Nongenomic Effects of Cisplatin: Acute Inhibition of Mechanosensitive Transporters and Channels without Actin Remodeling. *Cancer Res.* **2010**, *70*, 7514–7522.

(82) Zoellner, H.; Paknejad, N.; Manova, K.; Moore, M. A. S. A Novel Cell-Stiffness-Fingerprinting Analysis by Scanning Atomic Force Microscopy: Comparison of Fibroblasts and Diverse Cancer Cell Lines. *Histochem. Cell Biol.* **2015**, *144*, 533–542.

(83) Deliconstantinos, G. Physiological Aspects of Membrane Lipid Fluidity in Malignancy. *Anticancer Res.* **1987**, *7*, 1011–1021.

(84) Sharma, S.; Santiskulvong, C.; Rao, J.; Gimzewski, J. K.; Dorigo, O. The Role of Rho GTPase in Cell Stiffness and Cisplatin Resistance in Ovarian Cancer Cells. *Integr. Biol. (Camb).* **2014**, *6*, 611–617.

(85) Raghunathan, K.; Ahsan, A.; Ray, D.; Nyati, M. K. Membrane Transition Temperature Determines Cisplatin Response. *PLoS One* **2015**, 1–15.

(86) Liang, X.; Huang, Y. Alteration of Membrane Lipid Biophysical Properties and Resistance of Human Lung Adenocarcinoma A549 Cells to Cisplatin. *Sci. China Ser. C Life Sci.* **2001**, *44*, 25–32.

(87) Pinto, S. N.; Silva, L. C.; Futerman, A. H.; Prieto, M. Effect of Ceramide Structure on Membrane Biophysical Properties: The Role of Acyl Chain Length and Unsaturation. *Biochim. Biophys. Acta - Biomembr.* **2011**, *1808*, 2753–2760.

(88) Dimanche-Boitrel, M. T.; Pelletier, H.; Genne, P.; Petit, J. M.; Le Grimellec, C.; Canal, P.; Ardiet, C.; Bastian, G.; Chauffert, B. Confluence-Dependent Resistance in Human Colon Cancer Cells: Role of Reduced Drug Accumulation and Low Intrinsic Chemosensitivity of Resting Cells. *Int. J. cancer* **1992**, *50*, 677–682.

(89) Huang, Z.; Tong, Y.; Wang, J.; Huang, Y. NMR Studies of the Relationship between the Changes of Membrane Lipids and the Cisplatin-Resistance of A549/DDP Cells. *Cancer Cell Int.* **2003**, *8*, 1–8.

(90) Todor, I. N.; Lukyanova, N. Y.; Chekhun, V. F. The Lipid Content of Cisplatin- and Doxorubicin-Resistant MCF-7 Human Breast Cancer Cells. *Exp. Oncol.* **2012**, *34*, 97–100.

(91) Giussani, P.; Tringali, C.; Riboni, L.; Viani, P.; Venerando, B. Sphingolipids: Key Regulators of Apoptosis and Pivotal Players in Cancer Drug Resistance. *Int. J. Mol. Sci.* **2014**, *15*, 4356–4392.

(92) Carreira, A. C.; Ventura, A. E.; Varela, A. R. P.; Silva, L. C. Tackling the Biophysical Properties of Sphingolipids to Decipher Their Biological Roles. *Biol. Chem.* **2015**, *396*, 597–609.

(93) Lahiri, S.; Futerman, A. H. The Metabolism and Function of Sphingolipids and Glycosphingolipids. *Cell. Mol. Life Sci.* **2007**, *64*, 2270–2284.

(94) Futerman, A. H.; Hannun, Y. A. The Complex Life of Simple Sphingolipids. *EMBO Rep.* **2004**, *5*, 777–782.

(95) Gulbins, E.; Petrache, I. *Sphingolipids in Disease*; Springer, 2013.

(96) Don, A.; Lim, X.; Couttas, T. Re-Configuration of Sphingolipid Metabolism by Oncogenic Transformation. *Biomolecules* **2014**, *4*, 315–353.

(97) Roh, J.-L. L.; Park, J. Y.; Kim, E. H.; Jang, H. J. Targeting Acid Ceramidase Sensitises Head and Neck Cancer to Cisplatin. *Eur. J. Cancer* **2016**, *52*, 163–172.

(98) Saddoughi, S. A.; Ogretmen, B. Diverse Functions of Ceramide in Cancer Cell Death and Proliferation. *Adv. Cancer Res.* **2013**, *117*, 37–58.

(99) Hannun, Y. A.; Obeid, L. M. Principles of Bioactive Lipid Signalling: Lessons from Sphingolipids. *Nat. Rev. Mol. Cell Biol.* **2008**, *9*, 139–150.

(100) Siskind, L. J.; Mullen, T. D.; Romero Rosales, K.; Clarke, C. J.; Hernandez-Corbacho, M. J.; Edinger, A. L.; Obeid, L. M. The BCL-2 Protein BAK Is Required for Long-Chain Ceramide Generation during Apoptosis. *J. Biol. Chem.* **2010**, *285*, 11818–11826.

(101) Roh, J.-L.; Kim, E. H.; Park, J. Y.; Kim, J. W. Inhibition of Glucosylceramide Synthase Sensitizes Head and Neck Cancer to Cisplatin. *Mol. Cancer Ther.* **2015**, *14*, 1907–1915.

(102) Tyler, A.; Johansson, A.; Karlsson, T.; Gudey, S. K.; Brännström, T.; Grankvist, K.; Behnam-Motlagh, P. Targeting Glucosylceramide Synthase Induction of Cell Surface Globotriaosylceramide (Gb3) in Acquired Cisplatin-Resistance of Lung Cancer and Malignant Pleural Mesothelioma Cells. *Exp. Cell Res.* **2015**, *336*, 23–32.

(103) Kiguchi, K.; Iwamori, Y.; Suzuki, N.; Kobayashi, Y.; Ishizuka, B.; Ishiwata, I.; Kita, T.; Kikuchi, Y.; Iwamori, M. Characteristic Expression of Globotriaosyl Ceramide in Human Ovarian Carcinoma-Derived Cells with Anticancer Drug Resistance. *Cancer Sci.* **2006**, *97*, 1321–1326.

(104) Min, J.; Van Veldhoven, P. P.; Zhang, L.; Hanigan, M. H.; Alexander, H.;

Alexander, S. Sphingosine-1-Phosphate Lyase Regulates Sensitivity of Human Cells to Select Chemotherapy Drugs in a P38-Dependent Manner. *Mol. Cancer Res.* **2005**, *3*, 287–296.

(105) Sassa, T.; Suto, S.; Okayasu, Y.; Kihara, A. A Shift in Sphingolipid Composition from C24 to C16 Increases Susceptibility to Apoptosis in HeLa Cells. *Biochim. Biophys. Acta - Mol. Cell Biol. Lipids* **2012**, *1821*, 1031–1037.

(106) Chalfant, C. E.; Rathman, K.; Pinkerman, R. L.; Wood, R. E.; Obeid, L. M.; Ogretmen, B.; Hannun, Y. A. De Novo Ceramide Regulates the Alternative Splicing of Caspase 9 and Bcl-x in A549 Lung Adenocarcinoma Cells. Dependence on Protein Phosphatase-1. *J. Biol. Chem.* **2002**, *277*, 12587–12595.

(107) Martínez, R.; Navarro, R.; Lacort, M.; Ruiz-Sanz, J. I.; Ruiz-Larrea, M. B. Doxorubicin Induces Ceramide and Diacylglycerol Accumulation in Rat Hepatocytes through Independent Routes. *Toxicol. Lett.* **2009**, *190*, 86–90.

(108) Charles, A. G.; Han, T. Y.; Liu, Y. Y.; Hansen, N.; Giuliano, A. E.; Cabot, M. C. Taxol-Induced Ceramide Generation and Apoptosis in Human Breast Cancer Cells. *Cancer Chemother. Pharmacol.* **2001**, *47*, 444–450.

(109) Dumitru, C. A.; Sandalcioglu, I. E.; Wagner, M.; Weller, M.; Gulbins, E. Lysosomal Ceramide Mediates Gemcitabine-Induced Death of Glioma Cells. *J. Mol. Med. (Berl).* **2009**, *87*, 1123–1132.

(110) Clay, A. T.; Sharom, F. J. Lipid Bilayer Properties Control Membrane Partitioning, Binding, and Transport of p-Glycoprotein Substrates. *Biochemistry* **2013**, *52*, 343–354.

(111) Muscella, A.; Vetrugno, C.; Antonaci, G.; Cossa, L. G.; Marsigliante, S. PKC-δ/PKC-α Activity Balance Regulates the Lethal Effects of Cisplatin. *Biochem. Pharmacol.* **2015**, *98*, 29–40.

(112) Kim, J.; Yoon, H.; Kim, S.; Wang, K.; Ishii, T.; Kim, Y. Polymer – Metal Complex Micelles for the Combination of Sustained Drug Releasing and Photodynamic Therapy †. *J. Mater. Chem.* **2009**, *19*, 4627–4631.

(113) Howell, A. B. A.; Fan, D. Poly (Amidoamine) Dendrimer-Supported Organoplatinum Antitumor Agents. *Proc. R. Soc. A* **2010**, *466*, 1515–1526.

(114) Hamelers, I. H. L.; Loenen, E. Van; Staffhorst, R. W. H. M.; Kruijff, B. De; Kroon, A. I. P. M. De. Carboplatin Nanocapsules : A Highly Cytotoxic , Phospholipid-Based Formulation of Carboplatin. *Mol Cancer Ther* **2006**, *5*, 2007–2013.

(115) Burger, K. N. J.; Staffhorst, R. W. H. M.; De Vijder, H. C.; Velinova, M. J.; Bomans, P. H.; Frederik, P. M.; De Kruijff, B. Nanocapsules : Lipid-Coated Aggregates of Cisplatin with High Cytotoxicity. *Nat. Med.* **2002**, *8*, 81–85.

(116) Perez-Soler, R.; Siddik, Z. H.; Vadiei, K.; Krakoff, I. H.; Khokhar, A. R. *Platinum and Other Metal Coordination Compounds in Cancer Chemotherapy - Chapter: Pharmacological Studies with New Lipsome-Entrapped Cislatin Derivatives*; Stephen B. Howell, Ed.; Springer, Boston, MA, 1991.

(117) Perez-soler, R.; Khokhar, A. R. Lipophilic Cisplatin Analogues Entrapped in Liposomes: Role of Intraliposomal Drug Activation in Biological Activity1. *Cancer Res* **1992**, *52*, 6341–6347.

(118) Orena, J.; Andrews, K. M.; Torchia, A. J.; Karla, L.; Millar, L. J.; Mcpherson, R. K.; Bernice, H.; Genereux, P. E.; Conway, L.; Lali, L. Chemical and Biological Studies on a Series of Lipid-Soluble (Trans-(R,R)- and -( S,S)-1,2-Diaminocyclohexane)Platinum(II) Complexes Incorporated in Liposomes Abdul. *J. Med. Chem.* **1991**, *34*, 325–329.

(119) Shabbits, J. A.; Mayer, L. D. Intracellular Delivery of Ceramide Lipids via Liposomes Enhances Apoptosis in Vitro. *Biochim. Biophys. Acta* **2003**, *1612*, 98–106.

(120) Semple, S. C.; Leone, R.; Wang, J.; Leng, E. C.; Klimuk, S. K.; Eisenhardt, M. L.; Yuan, Z.; Edwards, K.; Maurer, N.; Hope, M. J.; *et al.* Optimization and Characterization of a Sphingomyelin / Cholesterol Liposome Formulation of Vinorelbine with Promising Antitumor Activity. *J. Pharm. Sci.* **2005**, *94*, 1024–1038.

(121) Webb, M. S.; Harasym, T. O.; Masin, D.; Bally, M. B.; Mayer, L. D. Sphingomyelin-Cholesterol Liposomes Significantly Enhance the Pharmacokinetic and Therapeutic Properties of Vincristine in Murine and Human Tumour Models. *Br. J. Cancer* **1995**, *72*, 896–904.

(122) Wang, M.; Xie, F.; Wen, X.; CHen, H.; Zhang, H.; Liu, J.; Zhang, H.; Zou, H.; Gao, J.; Jiang, B.; *et al.* Therapeutic PEG-Ceramide Nanomicelles Synergize with Salinomycin to Target Both Liver Cancer Cells and Cancer Stem Cells. *Nanomedicine (Lond).* **2017**, *12*, 1025–1042.

(123) Mehta, S.; Blackinton, D.; Omar, I.; Kouttab, N.; Myrick, D.; Mehta, S.; Myrick, D.; Klostergaard, J.; Wanebo, H. Combined Cytotoxic Action of Paclitaxel and Ceramide against the Human Tu138 Head and Neck Squamous Carcinoma Cell Line. *Cancer Chemother. Pharmacol.* **2000**, *46*, 85–92.

(124) Lucci, A.; Han, T. Y.; Liu, Y. Y.; Giuliano, A. E.; Cabot, M. C. Modification of Ceramide Metabolism Increases Cancer Cell Sensitivity to Cytotoxics. *Int. J. Oncol.* **1999**, *15*, 541–546.

The results of this chapter are presented as an unpublished original manuscript ready for submission.

## PAPER 5 (Results) - Effect of cisplatin and its cationic analogue in the phase behavior and integrity of model lipid bilayers


### Abstract

Increasing evidence suggests a critical role of lipids in both the mechanisms of toxicity and resistance of cells to platinum(II) complexes. In particular, cisplatin and other analogues were shown to interact with lipids and transiently promote lipid phase changes both in the bulk membranes and in specific membrane domains, such as, the lipid rafts. However, these processes are complex and not fully understood. In this work, cisplatin and its cationic species formed at pH 7 in low chloride concentrations were tested for their ability to induce phase changes in model membranes with different lipid composition. To this end, fluorescent probes that partition to different lipid phases were used to report on the fluidity of the membrane and a leakage assay was performed to evaluate the integrity of these vesicles. The results showed that platinum(II) complexes induced only small decrease in membrane fluidity at high infestation concentrations, preferentially in membranes containing gel phase, such as, DPPC and ceramide-enriched membranes. Moreover, at high concentration platinum(II) complexes were prone to compromise the permeability of the membranes without inducing its collapse or aggregation.



**Keywords**: cisplatin, aquated cisplatin, membrane fluidity, membrane permeability, gel phase

## 1. Introduction

Cisplatin (*cis*-diaminedichloroplatinum(II)) is a widely used anti-cancer drug in clinical practice in a variety of tumors[1]. Inside cells, genomic DNA is the primary cellular target of cisplatin and other platinum(II) complexes with which they form cross-linked adducts[2]. However, growing evidence suggests that other non-DNA targets have an important role in cisplatin's cytotoxic action[3]. In fact, one of the major limitations associated with platinum(II) complexes are the mechanisms of resistance in cells that are not dependent on DNA adduct formation and includes reduction of platinum accumulation inside the cell[4–6]. These resistance mechanisms are multifactorial and still largely unknown.

In this regard, membrane lipids were shown to be involved in both the mechanisms of cytotoxicity and resistance. Before reaching its primary target, cisplatin needs to cross the plasma membrane, which can occur via passive diffusion and receptor-mediated uptake (e.g. organic cation transporters)[3,7]. The passive diffusion depends on the surrounding environment, including chloride concentration and pH, which influences the formation of "aquated" platinum species (AqCis). These have different physicochemical properties and thus interact differently with lipids and lipid membranes[8]. Furthermore, the membrane lipid composition and permeability were linked to the resistance mechanisms of cells to platinum(II) compounds[4–6], and membrane modulators, such as digitonin, were shown to increase the absorption of platinum complexes into cells[9]. Cisplatin is also able to directly interact with phospholipids headgroups and further induce lipid phase changes, including non-lamellar phases (e.g. hexagonal II phase[10]). The binding of platinum complexes to the head group of lipids was also shown to induce structural changes at deeper sites of the lipid membrane[7,11], but these effects were transient and recoverable within a few hours[7,12]. On the other hand, whether complexation is relevant for cisplatin mode of action is still not fully understood[12].

Finally, the molecular response regarding lipid metabolism was also linked to the toxicity of cisplatin in cells via activation of apoptotic pathways. Evidence suggests that activation of death signaling pathways might involve the lipid raft domains[13]. Indeed, cisplatin was shown to induce ceramide (Cer) formation in lipid rafts via acid sphingomyelinase (aSMase) activation. This resulted in the clustering of Fas receptor and activation of apoptosis[14], with a concomitant increase in membrane fluidity. However, membrane enrichment in Cer commonly results in increased membrane order[15,16], suggesting that mechanisms other than Cer formation might be responsible for the observed increased fluidity. Furthermore, other studies showed that cisplatin i) reduces the fluidity of erythrocytes and model membranes[7], ii) elevates the transition temperature and order of the aliphatic chains, and iii) increases the thickness of the bilayer[17]. Therefore, contradictory data are present in the literature regarding how cisplatin affects the biophysical properties of the membranes, and whether these effects may be linked to its mechanisms of action.

To gain further insight into this subject, the impact of cisplatin and AqCis in the fluidity of lipid model bilayers containing different lipid composition, and thus different biophysical properties, was evaluated, as well as its contribution to the permeability of these membranes. A better understanding on these factors should provide context regarding the lipid membrane interactions that lead to apoptosis and the potential mechanisms of resistance by changes in cell lipid composition.

## 2. Materials and methods

### 2.1. Materials

POPC (1-palmitoyl-2-oleoyl-*sn*-glycero-3-phosphocholine), DPPC (1,2-dipalmitoyl-*sn*-glycero-3-phosphocholine), C16Cer (C16 ceramide, N-palmitoyl-D-erythro-sphingosine), C24:1Cer (C24:1 Ceramide, N-nervonoyl-D-erythro-sphingosine), SM (sphingomyelin, from egg, chicken), POPS (1-palmitoyl-2-oleoyl-*sn*-glycero-3-phospho-

L-serine) were obtained from Avanti Polar Lipids, Inc, (Alabaster, AL, U.S.A.). DPH (1,6-diphenyl-1,3,4-hexatriene), TMA-DPH (1-(4-(trimethylamino)phenyl)-6-phenylhexa-1,3,5-triene), t-PnA (*trans-parinaric acid) and CF (5(6)-carboxyfluorescein)* were obtained from Molecular Probes/Invitrogen (Eugene). Chol (Cholesterol) and Triton X-100 (TX-100) were obtained from Sigma-Aldrich (St. Louis, MO, U.S.A.). All other chemicals were analytical grade from Merck and Fluka (St Louis, MO, U.S.A.) and were used without further purification.

The concentration of lipids stock solutions as well as lipids recovered from Sephadex G-25 gel filtration column were confirmed by established colorimetric assay of phosphorus analysis using $Na_2HPO_4$ as a standard and ammonium molibdate as reagent[18,19]. Chol stock solution concentration was determined gravimetrically with a high precision balance (Mettler Toledo UMT2, Columbus, OH). Probe concentrations were determined spectrophotometrically using ε for (i) t-PnA, set at 299.4 nm in ethanol as $89x10^3$ $M^{-1}$ $cm^{-1}$; (ii) DPH, set at 355 nm in chloroform as $80.6x10^3$ $M^{-1}$ $cm^{-1}$; and (iii) TMA-DPH set at 355 nm in methanol as $74.1x10^3$ $M^{-1}$ $cm^{-1}$. All solutions were kept at -20ºC protected from light.

### 2.2. Large unilamellar vesicles (LUV) preparation

Multilamellar lipid vesicles (MLV) were first prepared by a thin-film hydration freeze-thawing method. To this, different aliquots of the desired lipid or lipid mixture (POPC, DPPC, POPC:DPPC (1:1), POPC:POPS (7:3), POPC:Chol (7:3), POPC:C24:1Cer (7:3), POPC:C16Cer (8:2), POPC:SM:Chol (1:1:1)) in chloroform were evaporated to dryness under a nitrogen stream with or without probes (DPH, TMA-DPH, CF). Residual chloroform was further removed overnight under vacuum. The resultant lipid film was then hydrated with the appropriate buffer ((A) PBS: 10 mM $NaHPO_4$ with 150 mM of NaCl, pH 7.4; (B) PBS: 10 mM $NaHPO_4$ with 150 mM of $Na_2SO_3$, pH 7.4; (C) 10 mM HEPES with 150 mM NaCl, pH 7.4; (D) 10 mM HEPES with 150 mM $Na_2SO_3$, pH

7.4;) and vigorously shaken with a vortex mixer. The MLV suspension was then freeze-thawed for 6 cycles and the resulting suspension was extruded 22 times through polycarbonate filters of 100 nm pore size (nucleopore, Pleasanton CA, USA) maintained at proper temperature (25-70$^{o}$C) above the transition temperature of lipids being used. The dead volume was reduced during extrusion by pre-wetting the extruder with the same buffer being used. In lipid models with t-PnA, the probe was added to the LUV only after extrusion.

### 2.3. Dynamic light scattering (DLS) and electrophoretic measurements

The average size (Z-average and number size) and zeta-potential of LUV were measured on ZetaSizer Nano ZS equipment (Malvern Instruments). The DLS measurements were carried using a 90$^{o}$C scattering optics at 25$^{o}$C with parameters set for a viscosity of 0.890 cP and refractive index of 1.330, equilibration time of 1 min, and each sample was measured for 3 successive runs. All measurements were carried using LUV at concentrations between 0.1-1 mM.

The zeta-potential (ζ) was determined from the electrophoretic mobility of LUV with and without incorporation of cisplatin by means of the Helmholtz-Smoluchowski correlation. Measurements were carried using a disposable zeta cell at a concentration range of 0.1-0.5 mM and the sample was maintained at 25$^{o}$C.

### 2.4. Fluorescence spectroscopy

Fluorescence anisotropy of DPH (lipid:probe (l:p) ratio of 1:200), TMA-DPH (l:p ratio of 1:200) and t-PnA (l:p ratio of 1:500) in the different LUV (total lipid concentration of 1 mM) was measured in a SLM Aminco 8100 series 2 spectrofluorimeter. Measurements were carried in a thermostat cell holder maintained at 25$^{o}$C by a Julabo F25 circulated water bath. Samples were placed in a 0.5 cm x 0.5 cm quartz cuvette under magnetic stirring and fluorescence anisotropy was obtained by using 5-7 scans. The slit bandwidth was 8 nm for both excitation and emission beams for DPH and TMA-DPH,

and 16 nm for t-PnA. The excitation ($\lambda_{exc}$)/emission ($\lambda_{em}$) wavelengths were set up to 358 nm/430 nm for DPH and TMA-DPH, and to 305 nm/405 nm for t-PnA. Background noise was tested by measuring the fluorescence in the same buffer and lipid concentration without probe. Platinum(II) complexes were then added in small aliquots to a final concentration of 15, 35, 100 and 300 μM. The steady-state fluorescence anisotropy was calculated through the expression in equation 1:

$$r = \frac{I_{VV} - I_{VH}}{I_{VV} + 2I_{VH}} \quad \text{(eq. 1)}$$

In which the different intensities are the steady-state when both excitation and emission polarization are vertical (VV) and when emission is aligned horizontally ($VH$). Time-resolved fluorescence of t-PnA ($\lambda_{exc}$/ $\lambda_{em}$ of 295/405) and DPH ($\lambda_{exc}$/ $\lambda_{em}$ of 360/430) were obtained by laser pulse excitation as previously described[19]. The fitting on the experimental decays were analyzed using TRFA software (Scientific Software Technologies Center, Minsk, Belarus) by nonlinear least squares iterative reconvolution method. The mean fluorescence lifetime was described as a sum of exponentials as follows:

$$\langle \tau \rangle = \frac{\sum_i \alpha_i \tau_i^2}{\sum_i \alpha_i \tau_i} \quad \text{(eq. 2)}$$

Where α is the normalized exponentials (amplitude) and τ is the lifetime of decay component i.

### 2.5. UV spectroscopy

The UV spectra of DPH, TMA-DPH and t-PnA in LUV composed of different lipids were measured at different time points (0, 30 min, 4h, 12h, 24h, 48h, 72h) in Hitachi Model U-2000 instrument in the 250-550 nm range using quartz cells with a 0.5 cm path length and temperature of 25$^{o}$C. The derivative spectra were calculated using the Savitzky-Golay method in which a second-order polynomial convolution of 13 points was employed[20].

### 2.6. LUV leakage studies

LUV at a lipid concentration of 2 mM were prepared as described above with 40 mM of CF in 10 mM HEPES buffer at pH 7.4. The suspension containing LUV and non-encapsulated CF was then centrifuged (Ultracentrifuge Hitachi CP80NX with P70AT rotor) at 41000 rpm for 2 hours. The supernatant was removed and the pellet was re-suspended in 1 mL of 50 mM HEPES buffer (pH 7.4) and filtered through a Sephadex G-25 gel filtration column with the same buffer. The vesicles containing CF were mainly obtained in fraction 3 and 4 (0.5 mL each) as verified by DLS and UV-spectrophotometry. The recovered LUV suspension was then diluted in a 96-well plate to a final lipid concentration of 0.17-0.25 mM (total volume of 0.250 mL) in order to get an optimal magnitude of the fluorescence signal over the required experimental time. Cisplatin and AqCis were then added to each well and the fluorescence intensity was read in a microplate reader SpectraMAX GeminiEM every 2 min at 25$^{o}$C for 14 hours ($\lambda_{exc}$/ $\lambda_{em}$ of 492/530 with a cutoff at 515 nm). After this time, 10 µL of TX-100 were added to each well to disrupt the vesicles, and 10 intensity reads were performed for each well after approximately 30 minutes. The extent of CF release was determined as follows:

$$CF\ \%\ release = \frac{F_t - F_0}{F_{Tx100} - F_0} x\ 100 \qquad \text{(eq. 3)}$$

Where $F_t$ represents the fluorescence intensity at time t, $F_0$ represents the fluorescence intensity at first measurement and $F_{Tx100}$ represents the fluorescence intensity after addition of TX-100.

## 3. Results

### 3.1. Characterization of LUV by DLS

Cisplatin in aqueous solutions exists as an equilibrium of multiple neutral and charged species, commonly named “aquated” species, which depends on both pH and

concentration of chloride. At high chloride concentrations, cisplatin remains neutral whereas at low chloride concentration if forms positively charged species. Therefore, the cationic AqCis were formed in chloride-free buffers at pH 7, which according to previous reports[21], should represent a mixture of 70% neutral species and 30% positively charged species. The formation of these charged species was verified by measuring the zeta potential of POPC:POPS (7:3) LUV containing the negatively charged POPS lipid (Figure 1A). As it can be observed, increased amounts of AqCis increased the zeta potential of these vesicles, which was attributed to charge neutralization at the surface. This was supported by the addition of cisplatin at the same concentrations, which did not significantly alter the zeta potential (-22.66 ± 0.98 mV and -23.16 ± 2.11 mV for 35 μM and 300 μM respectively). On the other hand, the zeta potential of POPC:POPS (7:3) prepared in buffer A (high chloride) in the presence of AqCis was similar to the control after 24 hours, indicating a transient effect possibly due to reversal of AqCis back to cisplatin. Finally, in zwitterionic models of POPC, POPC:DPPC (1:1), DPPC and POPC:Chol (7:3) LUV, the presence of both cisplatin and AqCis did not significantly alter the zeta potential (Figure 1B).

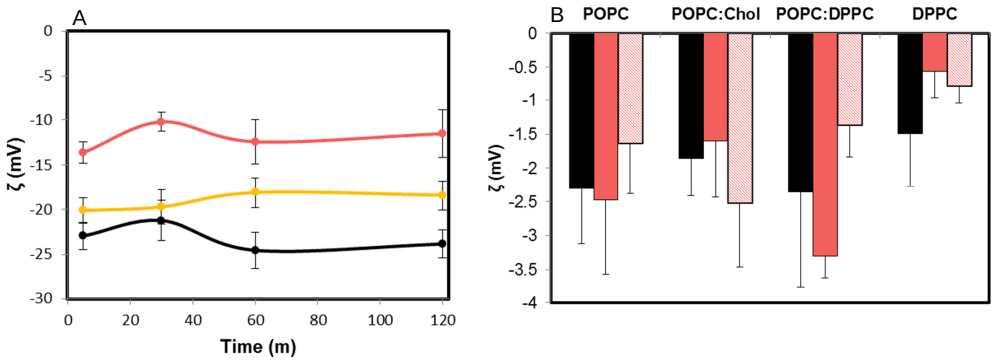


**Figure 1 – Effect of cisplatin and AqCis on the Zeta potential of LUV with different lipid composition.** A) variation of the zeta potential of POPC:POPS (7:3) LUV in the absence (black line) and in the presence of AqCis at concentrations of 35 μM (orange line) and 300 μM (red line). B) The effect of 300 μM of Cisplatin (red solid bars) and AqCis (red grid bars) on the zeta potential of LUV containing zwitterionic lipids (each control displayed as black bars) over a period of 24 hours.

The stability of the different LUV (POPC, POPC:DPPC, DPPC, POPC:POPS and POPC:Chol) in the presence of cisplatin or AqCis was also evaluated by measuring their average size after 24 and 48 hours. No significant changes in size were observed in the presence of cisplatin or AqCis up to concentrations of 600 μM, with $Z_{average}$ sizes ranging from 88 to 150 nm. Therefore, since no alterations in size were found and the size of both cisplatin and AqCis are very small in comparison, the curvature effect of the LUV surface on the interaction can be disregarded. Moreover, these results further indicate that interaction of AqCis and cisplatin with the LUV do not induce aggregation and/or fusion of the vesicles.

### 3.2. Effect of platinum complexes in the phase behavior of different phospholipid mixtures

The fluidity of lipid membranes upon addition of platinum complexes was evaluated by measuring the fluorescence anisotropy of three different probes (DPH, TMA-DPH and t-PnA). The fluorescence anisotropy of these probes provides information regarding the fluidity of the membranes. These probes were selected because they have different partition coefficients towards fluid or gel phases and, in addition, are located at different depths of the hydrophobic region, thus reporting the behavior of the lipid acyl chains at different depths of the bilayer[22,23]. In this regard, both DPH and TMA-DPH partition equally between gel and fluid phases[16]. However, DPH is located in the center of the bilayer whereas TMA-DPH is anchored at the surface and is more sensitive to hydration[24]. On the other hand, t-PnA has a higher partition and quantum yield in the gel phase compared to liquid ordered and disordered phases[16].

Figure 2A shows the distribution of fluorescence anisotropy of DPH in POPC LUV measured every 5 minutes for 30 minutes upon addition of cisplatin and AqCis at different concentrations (15, 35, 100 and 300 μM). A normal distribution around the initial control values (<r> of 0.1020 ± 0.0035) was observed for all concentrations

tested, except for the lowest concentration of cisplatin (15μM) where a slightly lower average anisotropy was obtained (<r> of 0.1000 ± 0.0014), and the anisotropy profile distribution was shifted towards lower values. On the other hand, between 60-100 minutes a very small concentration-dependent effect that resulted in increased anisotropy of DPH was observed, particularly for the highest cisplatin concentration (Figure 2B-F). At this time range a small shift in the DPH anisotropy profile towards higher values was observed, compared to the first 30 min for the different concentrations tested (Figure 2B-D). In this regard, DPH anisotropy profile revealed the presence of two populations with anisotropy values centered at 0.1010 and 0.1050 and the contribution of the population with higher anisotropy increased overtime for all cisplatin concentrations studied (Figure 2C- F). These results suggest that cisplatin induces a very small increase in the packing of the lipid acyl chains, likely due to a slow penetration of the molecules to the interior of the bilayer. This effect was however transient and the distribution of anisotropy values were similar to the control throughout the rest of the measurements, as shown for the highest cisplatin concentration after 72 hours upon addition to the vesicles (Figure 3).

Contrary to cisplatin, the addition of increasing concentrations of AqCis to POPC LUV did not result in significant differences in DPH fluorescence anisotropy up to 24 hours even for the highest concentration (Figure 3). No further measurements were however carried after this time point since the high concentration of chloride in solution is likely to reverse the AqCis equilibrium back to cisplatin. Furthermore, no differences were observed in the UV spectra of POPC LUV at different time points upon addition of both cisplatin and AqCis (data not shown), which further evidenced the low influence of the platinum complexes on the biophysical properties of POPC bilayers.

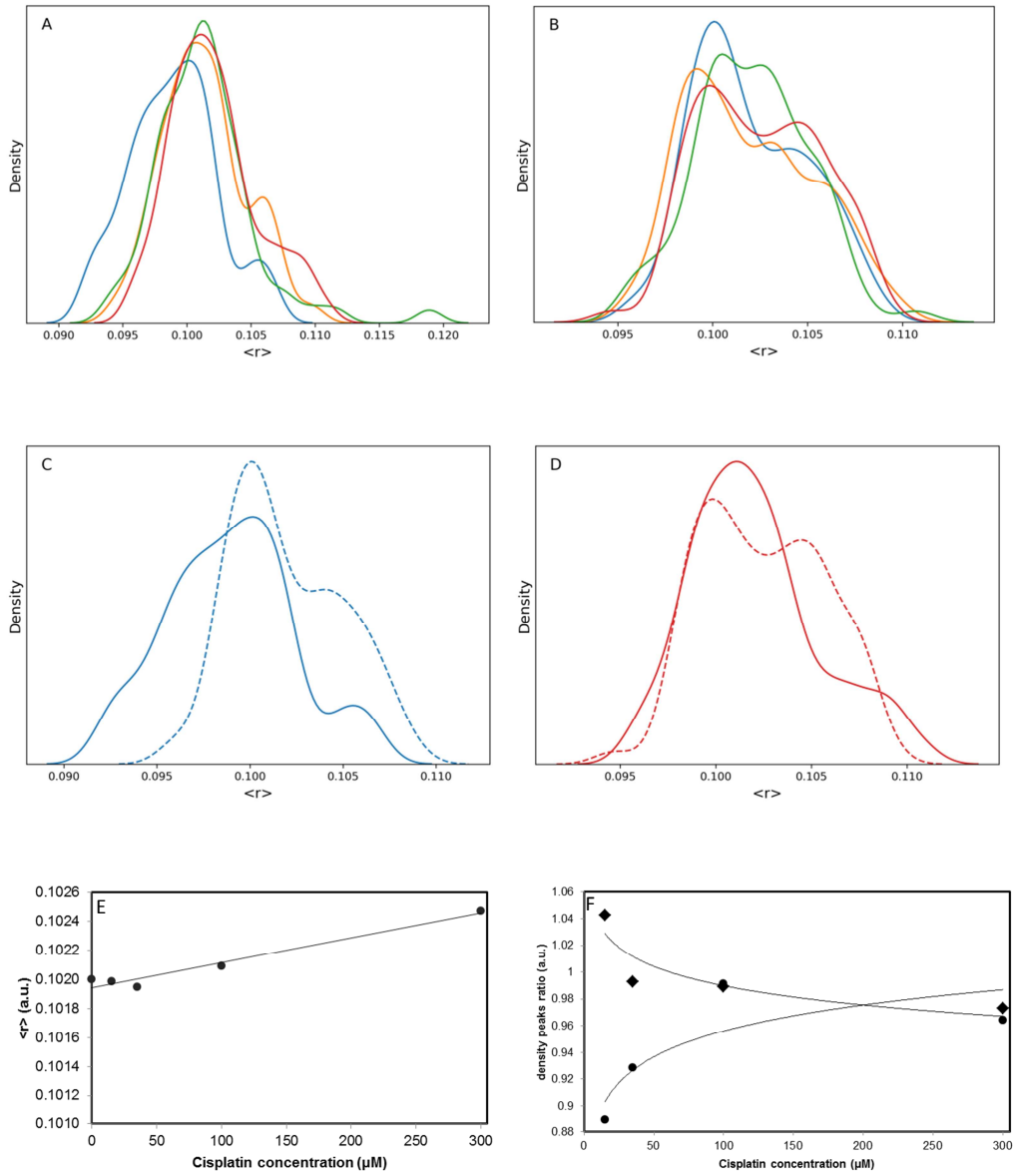


**Figure 2 – Density distribution of anisotropy values of DPH in POPC with different concentrations of cisplatin.** Fluorescence anisotropy distribution of DPH between (A) 5-30 minutes (t1) and (B) 60-100 minutes (t2) after adding 15 (blue), 35 (orange), 100 (green) and 300 μM (red) of cisplatin. Comparison between t1 (solid line) and t2 (dashed line) for POPC LUV in presence of (C) 15 μM and (D) 300 μM of cisplatin showed an increase in the contribution of a second peak of higher anisotropy at t2. (E) DPH anisotropy as a function of cisplatin concentration at t2. (F) ratio between DPH anisotropy at the secondary peak over the primary peak (●). This ratio increased at the same time that the ratio between the primary peaks at t1/t2 decreased (♦). The average fluorescence anisotropy of POPC LUV prior to cisplatin addition was determined to be 0.1020 ± 0.0035.

Similarly to POPC, the effects of cisplatin and AqCis in a variety of LUV with different lipid composition (POPC:Chol (7:3), POPC:POPS (7:3) and POPC:DPPC (1:1)) also showed no significant differences in DPH anisotropy up to 3 hours upon addition of

both cisplatin and AqCis at different concentrations (Figure 3). Moreover, extending the interaction of cisplatin with these LUV for 72 did not show any significant alteration in fluorescence anisotropy as well as in the UV spectra (data not shown), suggesting that the effects of the platinum complexes in the fluidity of these membranes are negligible.

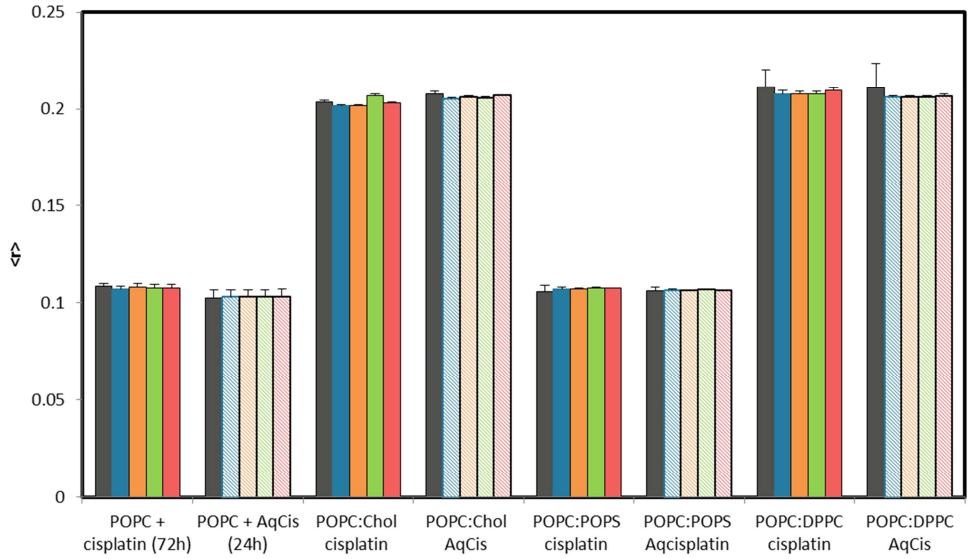


**Figure 3 – Fluorescence anisotropy of DPH in LUV with different composition after addition of cisplatin and AqCis.** Results show that DPH anisotropy recovered to control values 72 hours after addition of cisplatin to POPC. In contrast, AqCis did not induce any changes in DPH anisotropy over a period of 24h. Moreover, the average anisotropy between 30 min and 3 hours after addition of both cisplatin and AqCis to LUV of different composition showed no differences compared to control. Solid bars: cisplatin; dash bars: AqCis; Grey: control; Blue: 15 μM platinum; Orange: 35 μM platinum; Green: 100 μM platinum; Red: 300 μM platinum;

The interaction of cisplatin and AqCis with POPS and its possible changes in the membrane fluidity were further characterized with t-PnA and TMA-DPH probes in POPC:POPS (7:3) LUV. No significant differences in t-PnA anisotropy were observed up to 24 hours after addition of cisplatin (0.1426 ± 0.0049, for 300 μM) and AqCis (0.1414 ± 0.0075, for 300 μM) in buffer A (high chloride) compared to control (0.1399 ± 0.0063). Furthermore, no differences in the mean fluorescence lifetime of t-PnA was observed between control samples and 24 hours after addition of 35 μM of cisplatin or AqCis to POPC:POPS LUV. However, marked differences were observed for the long lifetime component of the fluorescence intensity decay of t-PnA, where a significant

shorter component was measured in the presence of cisplatin (8.84 ns) compared to control samples (16.47ns) and samples containing 35μM of AqCis (15.51 ns). In order to maintain the AqCis equilibrium and promote charge-charge interactions, measurements of the anisotropy of DPH and TMA-DPH in POPC:POPS (7:3) LUV were also carried in buffer B (low chloride) to an extended period of 120 hours. However, no differences in the fluorescence anisotropy of both probes were observed for both platinum(II) complexes at different concentrations tested (Figure 4 showcases a typical result for the highest concentration of 300 μM). These results suggest that both cisplatin and AqCis did not change the fluidity of this model membrane at different depths of the membrane.

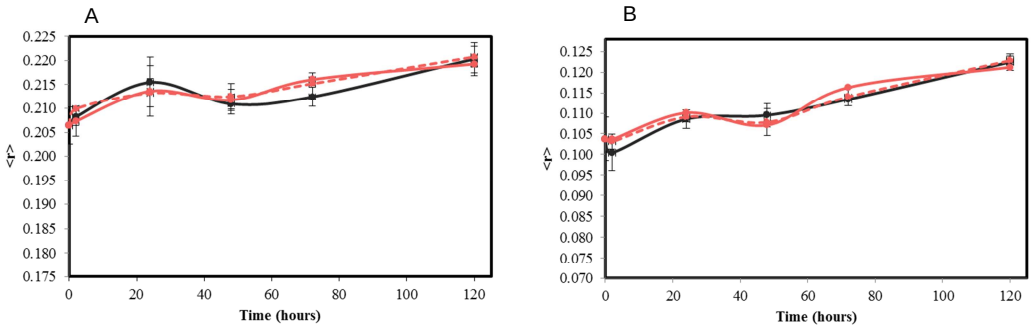


**Figure 4 – Effect of charged AqCis in the fluidity of POPC:POPS (7:3).** Fluorescence anisotropy of (A) TMA-DPH and (B) DPH in POPC:POPS (7:3) LUV in buffer B (low chloride) in the absence (black) and presence of 300 μM of cisplatin (red solid lines) and AqCis (red dash lines).

To further evaluate if cisplatin effects were dependent on membrane phase properties, the interaction of both complexes was studied in gel-phase DPPC vesicles (Figure 5). Contrary to the other lipid models, both cisplatin and AqCis induced significant decrease in membrane fluidity as observed by the increase of DPH anisotropy, particularly at higher concentrations. Furthermore, contrary to POPC LUV, this concentration-dependent effect was sustained and was observed even 72 hours after addition of cisplatin (Figure 5C and supplementary S1)

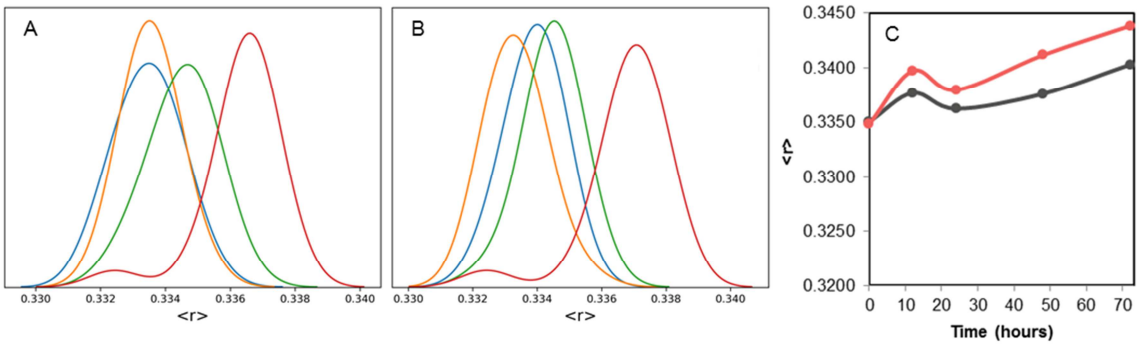


**Figure 5 – Effects of cisplatin and AqCis on the biophysical properties of gel phase DPPC model membranes.** Fluorescence anisotropy distribution of DPH in DPPC LUV between 5 min and 3 hours after addition of 15 (blue), 35 (orange), 100 (green) and 300 (red) μM of (A) cisplatin and (B) AqCis. The effects on increased anisotropy were observed throughout 72 hours (C) after addition of 300 μM of cisplatin (red line) compared to the control (grey).

### 3.3. Influence of cisplatin and AqCis on the phase behavior of sphingolipid mixtures

The probe t-PnA was used to study changes in the fluidity of lipid-raft model upon addition of platinum(II) complexes by using POPC:SM:Chol (1:1:1) LUV. Preliminary results for both cisplatin and AqCis suggested no significant changes in the fluorescence anisotropy of t-PnA up to 3 hours (Figure 6A). Similarly, no significant changes in the long lifetime component and mean fluorescence lifetime of t-PnA were observed 24 hours after addition of 35 μM cisplatin or AqCis to the LUV (supplementary Table 1).

In a similar manner, Cer models were used to study the effects of platinum(II) complexes on ceramide-enriched platforms. No differences in t-PnA fluorescence anisotropy were observed in POPC:C16Cer (8:2) LUV model, with an average anisotropy over the period of 3 hours of 0.2659 ± 0.0018 for control, 0.2662 ± 0.0037 and 0.2654 ± 0.0031 for 300 μM of cisplatin and AqCis, respectively (Figure 6A). On the contrary, in POPC:C24:1Cer (7:3) LUV it was observed a small but noticeable transient increase in t-PnA fluorescence anisotropy 30 min after addition of the highest

concentration of cisplatin, which disappeared after one hour (Figure 6C). This effect was however not observed when AqCis was added to this model membrane (Figure 6B). Furthermore, using the Savitzky-Golay method to smooth the UV spectra data, a small concentration-dependent effect was observed at 312 nm, 30 minutes after addition of cisplatin (Figure 6D). However, similar to the results in POPC, the effect of cisplatin was transient and no differences in t-PnA anisotropy were found after 3 hours (<r> of 0.2454 ± 0.0136, 0.2484 ± 0.0016 and 0.2453 ± 0.0029 for control and 300 μM of cisplatin and AqCis, respectively). Interestingly, analysis of the fluorescence intensity decay of t-PnA in POPC:C24:1Cer vesicles 24 hours after treatment with 35 μM of AqCis showed a longer mean fluorescence lifetime and long lifetime component compared to control samples and samples containing 35 μM of cisplatin (Supplementary Table 1). On the other hand, the amplitude of the decay components (αi) increased for both cisplatin and AqCis suggesting increase in the fraction of the gel phase[25]. Together these results suggest that cisplatin has an initial and transient effect in the packing of the lipid chains in bilayers containing C24:1Cer, while AqCis effects occur at longer times upon addition of the platinum complex to the membrane. Moreover, AqCis effects are likely to occur primarily in gel phase regions of the membrane, since changes in the photophysical parameters of t-PnA are mainly observed at the level of the long lifetime component of the fluorescence intensity decay, which is commonly associated to the t-PnA molecules emitting from the ordered gel phase[16,23].

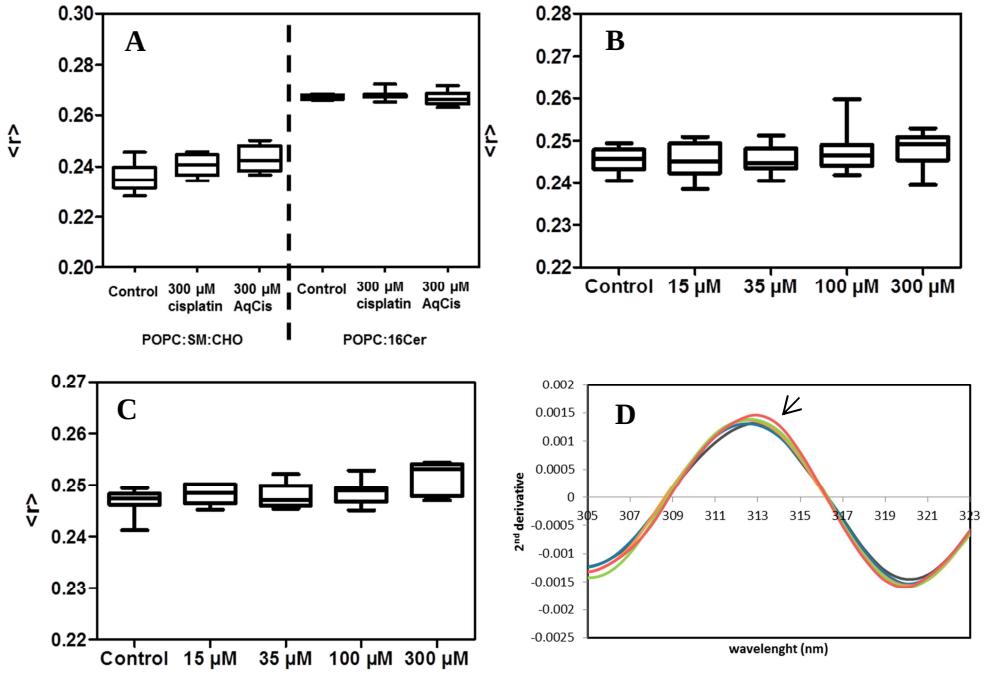


**Figure 6 – Effect of cisplatin and AqCis on the biophysical properties of sphingolipid mixtures.** Fluorescence anisotropy of t-PnA in (A) POPC:SM:Chol and POPC:C16Cer over 3 hours after addition of 300 µM of cisplatin and AqCis; Fluorescence anisotropy of t-PnA in POPC:C24:1 (B) over 3 hours after addition of increasing concentrations of AqCis and (C) 30 minutes after addition of increasing concentrations of cisplatin. At the latter time point, a small increase in t-PnA anisotropy was observed at higher concentrations of cisplatin.(D) 2$^{nd}$ derivative of the UV spectra of t-PnA in POPC:C24:1Cer LUV in the absence (grey) and 30 min after addition 15 (blue), 35 (orange), 100 (green) and 300 (red) µM of cisplatin where a small concentration-dependent effect was observed.

### 3.4. Leakage assay to study membrane permeability

Membrane integrity was evaluated using a leakage assay on different LUV (POPC, POPC:Chol, POPC:POPS, POPC:DPPC, DPPC). The CF leakage assay from LUV is an established method to evaluate the membrane permeability in the presence of various molecules[26–28]. The influence of platinum complexes on the permeability of model membranes can be determined by the increase in the fluorescence intensity of CF that results from the release of the probe from the interior of the vesicles. This is because at high local concentration CF fluorescence intensity is lower due to self-quenching. However, upon release from the vesicles, the fluorescence intensity

increases as a consequence of decreased local concentration, and therefore of CF self-quenching Figure 7A-B shows that at 35 μM both cisplatin and AqCis did not induce significant effects on the release of CF from POPC vesicles. However, at concentrations of 300 μM both platinum(II) complexes induced increase in the release of CF from these vesicles. In particular, AqCis showed a very prominent release with up to 80% of total CF (Figure 7B).

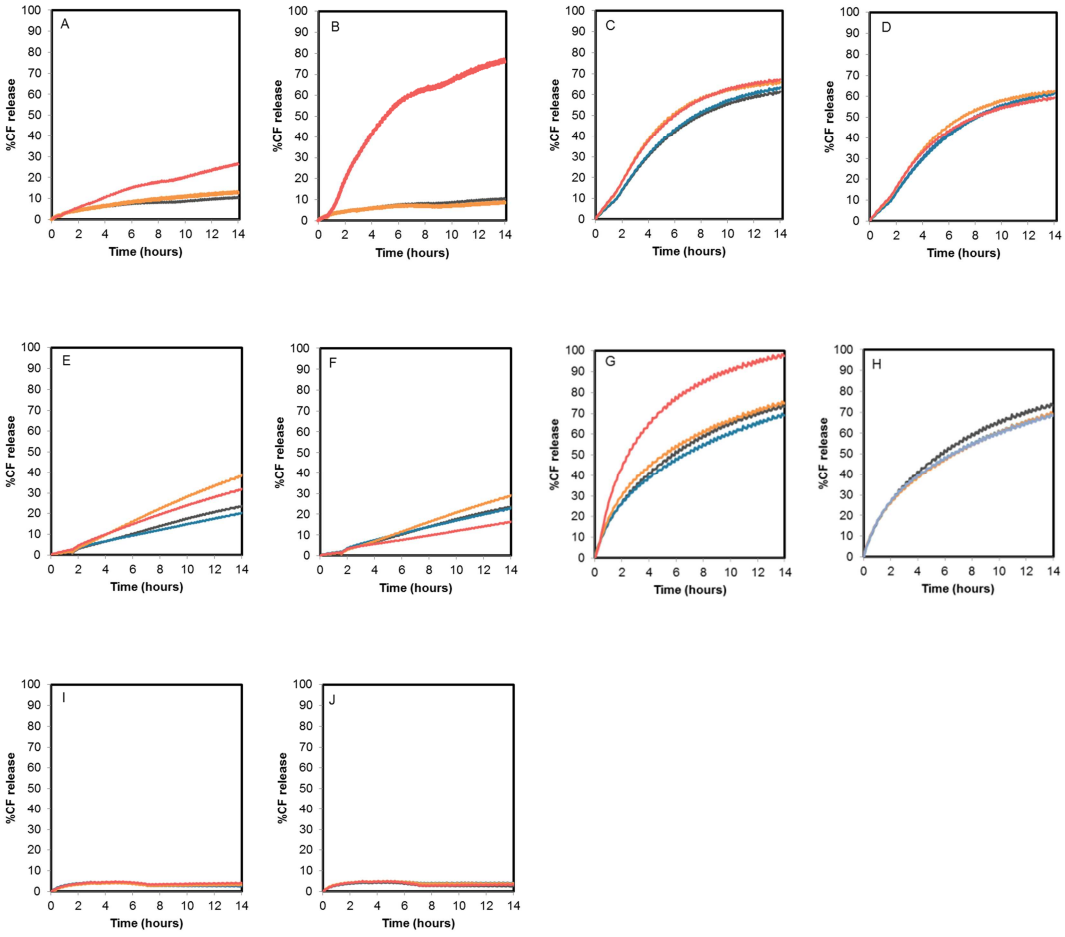


**Figure 7 – CF release from LUV with different lipid composition after addition of different concentrations of cisplatin and AqCis.** Release of CF was measured from (A-B) POPC, (C-D) POPC:Chol; (E-F) POPC:POPS; (G-H) POPC:DPPC; and (I-J) DPPC LUV in the presence of (A,C,E,G, I) cisplatin and (B,D,F,H,J) AqCis respectively for each pair of graphs. Grey: Control; Blue: 15 μM platinum; Orange: 35 μM platinum; Red: 300 μM platinum.

POPC:Chol vesicles displayed an intrinsic higher permeability to CF compared to POPC, which did not significantly changed upon addition of AqCis (Figure 7C-D).

However, cisplatin at 35 μM and 300 μM had a small faster rate (<10%) of CF release that converged to an extent of CF release similar to the control at the end point (Figure 7C). On the other hand, cisplatin and AqCis induced release of CF from POPC:POPS (7:3) LUV in a non-linear concentration-dependent manner (Figure 7E-F). At the lower concentration of 15 μM no differences in the release of CF were observed compared to the control. On the other hand, at increased concentrations of 35 μM both cisplatin and AqCis increased the CF release, with a significant higher release in vesicles treated with cisplatin (Figure 7E). However, at higher concentrations of 300 μM, both cisplatin and AqCis showed lower CF released compared to the 35 μM concentration. In particular, AqCis showed to reduce the release of CF compared to control (Figure 7F). This interplay between cisplatin and AqCis at different concentrations suggests the involvement of the serine headgroup particularly due to charge-charge interactions.

Finally, in model membranes containing gel phase, i.e. POPC:DPPC (1:1) (Figure 7G-H) and DPPC (Figure 7I-J) LUV no significant differences were observed for both platinum complexes except for the highest concentration of cisplatin in the POPC:DPPC (1:1) LUV, which showed to completely release the CF within the time tested (Figure 7G). On the other hand, in the gel phase DPPC membranes almost no release of CF was observed, with only 4-5% of CF released after 14 hours for both control and platinum complexes (Figure 7I-J).

## 4. Discussion

### 4.1. Effects of cisplatin and AqCis on fluid and gel phase phospholipid model membranes

Drug-lipid interactions are complex and a variety of factors such as lipid type, lipid chain length and saturation, hydrophobic character of both the drug and the lipid headgroup can have a significant contribution. Moreover, cell plasma membranes are dynamic and heterogeneous which can change the response to drug interactions. In

addition, drugs can interact with specific types of lipids and induce structural and biophysical changes in the membrane. In this regard, the plasma membrane fluidity has been shown to be involved in many cellular events including protein clustering at the surface and play a significant role in drug diffusion. In the case of platinum(II) compounds, these have shown to induce lipid phase changes, as well as mixing of plasma membrane components, and modulate the lipid metabolism and membrane composition[29–32]. These events are however complex and not fully understood.

To further elucidate the interactions of platinum(II) complexes with lipid membranes, the fluidity, surface charge and integrity of lipid models with different lipid composition and phase properties were studied. Previous studies in DMPC LUV showed that cisplatin accumulated at the headgroup region of the membrane and induced ordering of the acyl chains with decrease in area per lipid molecule and membrane elasticity[17]. However, other study using DPH and Laurdan as probes on DMPC LUV showed no significant differences in the anisotropy and general polarization, respectively, up to 10 mM of cisplatin[33]. This is in line with the results obtained for cisplatin and AqCis on the different models tested in the present study. The results suggest that in fluid phase model membranes both cisplatin and AqCis have very minor influence on the fluidity measured at the interior of the membrane, even at “infestation” concentrations. However, at these high concentrations significant alterations in the permeability of POPC and POPC:DPPC membranes were observed. These effects cannot be attributed to the collapse of the membrane since the size of LUV as measured by DLS in presence of both platinum complexes at this concentration did not change. For POPC this effect was higher for AqCis, which suggests the involvement of the zwitterionic headgroups in the interaction established with this positively-charged platinum complex. In contrast, in POPC:DPPC increased membrane permeability was only observed for cisplatin, which suggests that this effect may be related to an increase in membrane packing defects due to cisplatin incorporation at the interface

between the fluid and gel phases. In the latter, the cationic species may be not favored for interaction at this interface due to the hydrophobic characteristics created by height mismatch between lipids. Previous studies have already reported that several platinum complexes, including cisplatin and AqCis, were able to increase the permeability of erythrocyte membrane to small molecules[34]. Similar observations were made in planar model membranes of hen's egg yolk (mostly composed of phospholipids of PC and PE), where the increase in membrane permeability by platinum complexes was attributed to the creation of small holes[35]. Our results suggest that indeed the permeability of the membrane is increased without major alterations of the lipid phase properties and thus further studies should be carried in these membranes to understand if this is due to the creation of small holes, or small packing defects that are formed upon interaction of the platinum complexes with the membrane.

. Chol is an important component of the plasma membrane, which due to its planar rigid structure intercalates within the hydrocarbon chain and increases the order of the fluid phase and reduces the formation of gel phase[36–38]. It was previous shown that digitonin, a compound that interacts with cholesterol, increases the permeability of the membrane[9] and consequently increases cisplatin uptake[9,12]. In our POPC:Chol model system, where both the liquid disordered (ld) and liquid ordered (lo) phases coexist[39,40], the overall rate of intrinsic membrane permeability was considerably higher in comparison to POPC. Under these experimental conditions, it is therefore difficult to evaluate the effects that cisplatin and AqCis have in the permeability of these membranes in comparison to POPC. Indeed, it was observed a small faster release (<10%) of CF for 35 and 300 μM of cisplatin but not AqCis, but it converged to similar values of control. It should however be stressed that, in contrast to the observed in POPC membranes, cisplatin was unable to induce transient changes in the fluidity of POPC:Chol membranes, which might suggest that Chol might prevent the transient and modest ordering effect that cisplatin might have in the lipid hydrophobic chains.

Regarding platinum(II) complexes interactions with gel phase phospholipid membranes, previous studies suggested that cisplatin interacts with the headgroup of DPPC forming a 2:1 lipid-platinum complex with the phosphate groups and causes rearrangements that result in lower mobility of the headgroup[41]. This effect resulted in alteration of the pre-transition temperature but not the main transition temperature. Similarly, AqCis was shown to strongly interact with the DPPC lipid headgroup consistent with binding to the headgroup, and induce structural alterations of the glycerol moiety[7,11]. The results obtained with cisplatin and AqCis in DPPC LUV by measuring the fluorescence anisotropy of DPH showed that both complexes were able to induce small but significant concentration-dependent increase in the order of DPPC membranes. This effect was noticeable within the first minutes and was maintained throughout 72 hours. Since formation of Pt-O-P complexes seems to be transient occurring only after 2.5 hours and disappearing after 12 hours[10], these results suggest that the formation of the complex may not be necessary for the observed changes in DPPC membrane fluidity. The increase in the packing of the DPPC acyl chains might indeed be a result of the incorporation of platinum complexes within the membrane, which occurs without strong perturbations of the structure of the membrane, as shown by the lack of changes in the permeability of the membrane in the presence of platinum complexes.

### 4.2. Platinum(II) complexes interactions with POPS.

Phosphatidylserines are anionic phospholipids mostly located in the inner leaflet of the plasma membrane of non-cancer cells and have a crucial role in many cellular events including activity of proteins[4,42–44]. However, in some cancer cells this type of lipid is increased in the outer leaflet of the plasma membrane[45,46]. This shift in membrane lipid composition can promote changes on membrane surface charge and lipid packing, and influence its interactions with drugs and response to chemotherapy. In particular, platinum(II) complexes have shown to specifically interact with anionic lipids including

POPS, and AqCis charge may be the determining factor for the binding[7,17,21,47,48]. Indeed, literature reports have shown that AqCis was able to increase the main transition temperature of anionic DPPG lipid but not of the zwitterionic DPPC, which was attributed to the electrostatic interactions that lead to a more rigid and less fluid membrane[21]. Platinum complexes are also able to coordinate with the serine group of phospholipids. Contrary to DPPC, it was not the phosphate group but rather the carboxyl and amine group of the serine headgroup stabilized by the phosphate that complexed with platinum(II) complexes[49]. However, at room temperature this process is very slow with half-life of formation around 70h[49].

The obtained results suggest that the interaction between AqCis was rapidly established in POPC membranes containing the anionic lipid POPS, strongly suggesting that the electrostatic forces drove direct binding to the surface resulting in charge neutralization. Calculating the partition coefficient from zeta potential[50,51] suggests that these charged species accounted for approximately 40% and 51% of POPS neutralized by 35 and 300 μM of AqCis respectively. From a biological perspective, this surface charge neutralization can have important consequences in cells since this potentially changes the overall surface charge of the membrane, affecting its interaction with proteins and other membrane-associated cellular events. The results further suggest that if the coordination complex was formed, it is reversed by increased chloride concentration, since the zeta potential returned to values similar to the control sample. Furthermore, charge neutralization has been regarded as the mechanism by which platinum compounds rigidify the membrane, similarly to effects observed for charged ions, such as, $Mg^{2+}$ and $Ca^{2+}$ cations[21,52]. Moreover, charge neutralization might also increase gel-to-fluid transition temperatures[21,53], likely due to decreased electrostatic repulsion between the lipid headgroups, and consequent increase in the lipid packing. However, using different fluorescent probes no differences in the fluidity in the POPC:POPS model membranes was observed by

addition of both cisplatin and AqCis, even for an extended period of time. These results suggest that both the charge neutralization or/and the platination of the serine headgroup did not have a significant influence in the phase properties of this model membrane. However, a complex behavior in the permeability properties of these vesicles was observed within the first 14 hours, suggesting that both cisplatin and AqCis are able to specifically interact with POPS. As to why increasing amounts of both cisplatin and AqCis resulted in lower release of CF and in particular for the highest concentration of AqCis is yet to be determined. It is possible that the coordination to the serine groups promotes aggregation of CF at the surface and thus induces self-quenching effects.

This complex behavior was further evidenced by the fluorescence decay of t-PnA where the long lifetime component 24 hours after addition of 35 μM of cisplatin was half of that measured for the control and for 35 μM of AqCis. This suggests that cisplatin induced a more disordered membrane[16] and in comparison to AqCis induced a higher release of CF, which could be attributed by increased defects in the membrane core that do not involve phase change.

### 4.3. Effect of platinum complexes on sphingolipid mixtures

Lipid rafts are fundamental for many cell signaling pathways. In particular, lipid raft integrity was shown to be required for cisplatin-induced apoptosis in cells[13,54,55] and is also involved in mechanisms of cisplatin-resistance[56]. These domains are the primary site for aSMase action and in response to stress stimulus, such as cisplatin, this enzyme converts SM to Cer leading to ceramide-enriched domains formation and clustering of receptors at these lipid platforms[13,15,55,57]. In particular, in HT29 human colon carcinoma cells, cisplatin-induced aSMase activation (via NHE1-dependent intracellular acidification) was concomitant with an induced transient increase in membrane fluidity for both bulk membrane and lipid rafts that led to reorganization of

the lipid domains and clustering of CD95 receptors and subsequent apoptosis[55]. However, these observations contrast with the expected alterations in membrane properties upon Cer generation. Indeed, Cer is highly hydrophobic and prone to form tightly packed gel phase domains, which cause a decrease in the overall fluidity both of model and biological membranes[15,16,58–61]. Such evidence suggests that other factors besides Cer formation, might be responsible for the observed cisplatin-induced increase of membrane fluidity. To gain further insight into cisplatin and AqCis interactions with lipid raft- and Cer platform-like domains, three representative mimetic systems (POPC:SM:Chol, POPC:16Cer and POPC:24:1Cer) were studied.

Interestingly, platinum complexes had a transient effect on the properties of membranes containing C24:1Cer, causing a further decrease in its fluidity. This was due to an increase in the fraction of the gel phase observed upon interaction both with cisplatin and AqCis, and due to an increase in the packing of the C24:1Cer-enriched gel domains promoted by AqCis. No changes in the fluidity of the other lipid systems were observed. Many factors might contribute to these observations. First the gel phase formed by C24:1Cer is less rigid than the one formed by C16Cer. This might facilitate the incorporation of the platinum molecules within the membrane. Moreover, the presence of an unsaturation at the membrane interior might cause packing defects that might further increase the partition of cisplatin and AqCis to the membrane. Furthermore, the chain mismatch in C24:1Cer determines its ability to form interdigitated gel phases[22,59]. The interaction of platinum complexes with this partially interdigitated phase, could promote a reorganization of the hydrophobic chains, or even a transition to another more rigid gel phase. On the other hand, cisplatin and AqCis might also be able to partition to membranes enriched in C16Cer gel domains. However, because these are already highly ordered, further decrease in membrane fluidity might not be noticeable. It should however be stressed that such interaction do not induce a decrease in the fluidity of the membranes, suggesting that these platinum

complexes do not compromise the overall packing of C16Cer gel phase. Therefore, other factors may contribute to the observed increase in fluidity at lipid rafts in HT29 cells[13]. In particular, cisplatin is known to easily exchange its chlorides with other biomolecules with particular high affinity for thiols[3,7], and therefore these could potentially interact differently with lipid bilayers.

## 5. Conclusions

This work indicates that the interaction of platinum(II) complexes with lipid membranes is complex and a multitude of factors contribute to this interaction. These effects result from combination of membrane lipid composition, fluidity and surface charge of the lipid membrane, as well as, the type of platinum(II) complex. Overall, both cisplatin and AqCis did not induce a substantial increase in membrane fluidity. On the contrary, these complex seem to promote further ordering of gel phases, particularly in membranes composed of DPPC and POPC:C24:1Cer. However, the interaction of these complexes with the membrane resulted in changes in membrane permeability to an extent that depends on the concentration and type of the platinum complex, as well as, on the lipid composition and properties of the membranes. These results thus suggest that the molecular mechanism underlying cisplatin interaction with biological membranes is not straightforward and generalization of the effects of cisplatin in the properties of biological membrane should be made with caution.

## References

(1) Dasari, S.; Tchounwou, P. B. Cisplatin in Cancer Therapy : Molecular Mechanisms of Action. *Eur J Pharmacol* **2014**, *0*, 364–378.

(2) Abu-Surrah, A.; Kettunen, M. Platinum Group Antitumor Chemistry: Design and Development of New Anticancer Drugs Complementary to Cisplatin. *Curr. Med. Chem.* **2006**, *13*, 1337–1357.

(3) Mezencev, R. Interactions of Cisplatin with Non-DNA Targets and Their Influence on Anticancer Activity and Drug Toxicity: The Complex World of the Platinum Complex. *Curr. Cancer Drug Targets* **2015**, *14*, 794–816.

(4) Gately, D. P.; Howell, S. B. Cellular Accumulation of the Anticancer Agent Cisplatin : A Review. *Br. J. Cancer* **1993**, *67*, 1171–1176.

(5) Liang, X.; Huang, Y. Physical State Changes of Membrane Lipids in Human Lung Adenocarcinoma A 549 Cells and Their Resistance to Cisplatin. *Int. J. Biochem. Cell Biol.* **2002**, *34*, 1248–1255.

(6) Liang, X.; Yin, J.; Zhou, J.; Wang, P. C.; Taylor, B.; Cardarelli, C.; Kozar, M.; Forte, R.; Aszalos, A.; Gottesman, M. M. Changes in Biophysical Parameters of Plasma Membranes Influence Cisplatin Resistance of Sensitive and Resistant Epidermal Carcinoma Cells. *Exp. Cell Res.* **2004**, *293*, 283–291.

(7) Wang, K.; Lu, J.; Li, R. The Events That Occur When Cisplatin Encounters Cells. *Coord. Chem. Rev.* **1996**, *151*, 53–88.

(8) Binks, S. P.; Dobrota, M. Kinetics and Mechanism of Uptake of Platinum-Based Pharmaceuticals by the Rat Small Intestine. *Biochem. Pharmacol.* **1990**, *40*, 1329–1336.

(9) Jekunen, A. P.; Shalinsky, D. R.; Hom, D. K.; Albright, K. D.; Heath, D.; Howell, S. B. Modulation of Cisplatin Cytotoxicity by Permeabilization of the Plasma Membrane by Digitonin in Vitro. *Biochem. Pharmacol.* **1993**, *45*, 2079–2085.

(10) Lu, J.-F.; Xia, W.-S.; Wang, K.; Zhai, C.; Liu, Q.-L. A Study of Interaction of Cisplatin and Its Analogues WithPhospholipid of Erythrocyte Membrane. *J. Chinese Pharm. Sci.* **1995**, *4*, 136–143.

(11) Wang, K.; Liu, D.; Zhuo, Z. C. A NMR Study of the Reaction Between Cis-

Diaquodiammine-Platinum(Ⅱ) and Biomembranic Phospholipids. *Chem. J. Chinese Univ.* **1991**, *12*, 1382–1385.

(12) Burger, K. N. J.; Sta, R. W. H. M.; Kruij, B. De. Interaction of the Anti-Cancer Drug Cisplatin with Phosphatidylserine in Intact and Semi-Intact Cells. *Biochim. Biophys. Acta* **1999**, *1419*, 43–54.

(13) Lacour, S.; Hammann, A.; Lagadic-gossmann, D.; Athias, A.; Sergent, O.; Laurent, G.; Gambert, P.; Solary, E. Cisplatin-Induced CD95 Redistribution into Membrane Lipid Rafts of HT29 Human Colon Cancer Cells. *Cancer Res.* **2004**, *64*, 3593–3598.

(14) Noda, S.; Yoshimura, S. I.; Sawada, M.; Naganawa, T.; Iwama, T.; Nakashima, S.; Sakai, N. Role of Ceramide during Cisplatin-Induced Apoptosis in C6 Glioma Cells. *J. Neurooncol.* **2001**, *52*, 11–21.

(15) Castro, B. M.; Silva, L. C.; Fedorov, A.; Almeida, R. F. M. De; de Almeida, R. F. M.; Prieto, M. Cholesterol-Rich Fluid Membranes Solubilize Ceramide Domains: Implications for the Structure and Dynamics of Mammalian Intracellular and Plasma Membranes. *J. Biol. Chem.* **2009**, *284*, 22978–22987.

(16) Castro, B. M.; De Almeida, R. F. M.; Silva, L. C.; Fedorov, A.; Prieto, M. Formation of Ceramide/Sphingomyelin Gel Domains in the Presence of an Unsaturated Phospholipid: A Quantitative Multiprobe Approach. *Biophys. J.* **2007**, *93*, 1639–1650.

(17) Nierzwicki, L.; Wieczor, M.; Censi, V.; Baginski, M.; Calucci, L.; Samaritani, S. Interaction of Cisplatin and Two Potential Antitumoral Platinum ( II ) Complexes with a Model Lipid Membrane : A Combined NMR and MD Study. *Phys. Chem. Chem. Phys.* **2014**, *17*, 1458–1468.

(18) Carreira, A. C.; De Almeida, R. F. M.; Silva, L. C. Development of Lysosome-

Mimicking Vesicles to Study the Effect of Abnormal Accumulation of Sphingosine on Membrane Properties. *Sci. Rep.* **2017**, *7*, 1–16.

(19) Zupancic, E.; Carreira, A. C.; De Almeida, R. F. M.; Silva, L. C. Biophysical Implications of Sphingosine Accumulation in Membrane Properties at Neutral and Acidic PH. *J. Phys. Chem. B* **2014**, *118*, 4858–4866.

(20) Magalhães, L. M.; Nunes, C.; Lúcio, M.; Segundo, M. A.; Reis, S.; Lima, J. L. F. C. High-Throughput Microplate Assay for the Determination of Drug Partition Coefficients. *Nat. Protoc.* **2010**, *5*, 1823–1830.

(21) Speelmans, G.; Sips, W. H. H. .; Grisel, R. J. H.; Staffhorst, R. W. H. M.; Fichtinger-Schepman, A. M. J.; Reedijk, J.; Kruijff, B. de. The Interaction of the Anti-Cancer Drug Cisplatin with Phospholipids Is Specific for Negatively Charged Phospholipids and Takes Place at Low Chloride Ion Concentration. *Biochim. Biophys. Acta* **1996**, *1283*, 60–66.

(22) Pinto, S. N.; Silva, L. C.; De Almeida, R. F. M.; Prieto, M. Membrane Domain Formation, Interdigitation, and Morphological Alterations Induced by the Very Long Chain Asymmetric C24:1 Ceramide. *Biophys. J.* **2008**, *95*, 2867–2879.

(23) Pinto, S. N.; Laviad, E. L.; Stiban, J.; Kelly, S. L.; Merrill, A. H.; Prieto, M.; Futerman, A. H.; Silva, L. C. Changes in Membrane Biophysical Properties Induced by Sphingomyelinase Depend on the Sphingolipid N-Acyl Chain. *J. Lipid Res.* **2014**, *55*, 53–61.

(24) Duportail, G.; Klymchenko, A. S.; Baye, G. M.; Me, Y. Liquid Ordered and Gel Phases of Lipid Bilayers : Fluorescent Probes Reveal Close Fluidity but Different Hydration. *Biophys J.* **2008**, *95*, 1217–1225.

(25) Pinto, S. N.; Fernandes, F.; Fedorov, A.; Futerman, A. H.; Silva, L. C.; Prieto, M. A Combined Fluorescence Spectroscopy , Confocal and 2-Photon Microscopy

Approach to Re-Evaluate the Properties of Sphingolipid Domains. *Biochim. Biophys. Acta* **2013**, *1828*, 2099–2110.

(26) Engelke, M.; Bojarski, P.; Bloß, R.; Diehl, H. Tamoxifen Perturbs Lipid Bilayer Order and Permeability : Comparison of DSC , Fluorescence Anisotropy , Laurdan Generalized Polarization and Carboxyfluorescein Leakage Studies. *Biophys. Chem.* **2001**, *90*, 157–173.

(27) Au, S.; Weiner, N. D.; Schacht, J. Aminoglycoside Antibiotics Preferentially Increase Permeability in Phosphoinositide-Containing Membranes : A Study with Carboxyfluorescein in Liposomes. *Biochim. Biophys. Acta* **1987**, *902*, 80–86.

(28) Drori, S.; Eytan, G. D.; Assaraf, Y. G. Potentiation of Anticancer-Drug Cytotoxicity by Multidrug-Resistance Chemosensitizers Involves Alterations in Membrane Fluidity Leading to Increased Membrane Permeability. *Eur. J. Biochem* **1995**, *228*, 1020–1029.

(29) Mohammadi, A. S.; Li, X.; Ewing, A. G. Mass Spectrometry Imaging Suggests That Cisplatin Affects Exocytotic Release by Alteration of Cell Membrane Lipids Mass Spectrometry Imaging Suggests That Cisplatin Affects Exocytotic Release by Alteration of Cell Membrane Lipids. *Anal Chem* **2018**, *XXX*, 1–10.

(30) Raghunathan, K.; Ahsan, A.; Ray, D.; Nyati, M. K. Membrane Transition Temperature Determines Cisplatin Response. *PLoS One* **2015**, 1–15.

(31) Duarte, I. F.; Lamego, I.; Marques, J.; Marques, M. P.; Blaise, B. J.; Gil, A. M. Nuclear Magnetic Resonance (NMR) Study of the Effect of Cisplatin on the Metabolic Profile of MG-63 Osteosarcoma Cells. *J Proteome Res* **2010**, 5877–5886.

(32) Lamego, I.; Duarte, I. F.; Marques, M. P. M.; Gil, A. M. Metabolic Markers of MG-63 Osteosarcoma Cell Line Response to Doxorubicin and Methotrexate

Treatment: Comparison to Cisplatin. *J. Proteome Res.* **2014**, *13*, 6033–6045.

(33) Suwalsky, M.; Hernández, P.; Villenab, F.; Sotomayorc, C. P. The Anticancer Drug Cisplatin Interacts with the Human Erythrocyte Membrane. *Z Naturforsch C.* **2000**, *55*, 461–466.

(34) Lu, J.-F.; Wang, K.; Sun, X.-Z.; Xing, F.; An, P.-D.; Yang, Z.-H.; Yin, J.-J. Effects of Cisplatin and Its Analogues on the Permability of Humam Membrane Erythrocyte Membrane. *Met. Based Drugs* **1995**, *2*, 73–80.

(35) Maheswari, K. U.; Ramachandran, T.; Rajaji, D. Interaction of Cisplatin with Planar Model Membranes - Dose Dependent Change in Electrical Characteristics. *Biochim. Biophys. Acta* **2000**, *1463*, 230–240.

(36) Oldfield, E.; Chapman, D. Dynamics of Lipids in Membranes: Heterogeneity and the Role of Cholesterol. *FEBS Lett.* **1972**, *23*, 285–297.

(37) Crane, J. M.; Tamm, L. K. Role of Cholesterol in the Formation and Nature of Lipid Rafts in Planar and Spherical Model Membranes. *Biophys. J.* **2004**, *86*, 2965–2979.

(38) Lu, J.; Hao, Y.; Chen, J. Effect of Cholesterol on the in Lysophosphatidylcholine Formation of an Interdigitated Gel Phase and Phosphatidylcholine Binary. *j. Biochem* **2001**, *129*, 891–898.

(39) Almeida, R. F. M. De; Loura, L. M. S.; Prieto, M. Membrane Lipid Domains and Rafts : Current Applications of Fluorescence Lifetime Spectroscopy and Imaging. *Chem. Phy* **2009**, *157*, 61–77.

(40) Loura, M. S.; Prieto, M.; Watts, A.; Fedorov, A.; Almeida, R. F. M. De; Barrantes, F. J. Cholesterol Modulates the Organization of the YM4 Transmembrane Domain of the Muscle Nicotinic Acetylcholine Receptor. *Biophys. J.* **2004**, *86*, 2261–2272.

(41) Shen, Z.-W.; Sun, Z.-P.; Zhao, N.-M. Study of the Effects of the Antitumor Drug Cis-DPP on the Phase Behavior of DPPC Liposomes and Molecular Mechanism of the Interaction. *Chinese Sci. Bull.* **1991**, *36*, 149–153.

(42) Andrews, P. A.; Mann, S. C.; Huynh, H. H.; Albright, K. D. Role of the Na + , K + -Adenosine Triphosphatase in the Accumulation of Cis-Diamminedichloroplatinum ( II ) in Human Ovarian Carcinoma Cells '. *Cancer Res.* **1991**, 3677–3682.

(43) Schuurmans Stekhoven, FM Tesser, G.; Ramsteyn, G.; Swarts, H.; De Pont, J. Binding of Ethylenediamine to Phosphatidylserine Is Inhibitory to Na+/K(+)-ATPase. *Biochim Biophys Acta* **1992**, *1109*, 17–32.

(44) Buckland, A. G.; Wilton, D. C. Anionic Phospholipids, Interfacial Binding and the Regulation of Cell Functions. *Biochim. Biophys. Acta* **2000**, *1483*, 199–216.

(45) Manjarika; Ghosh, S.; Sen, T.; Shadab, M.; Banerjee, I.; Basu, S.; Ali, N. A Novel Therapeutic Strategy for Cancer Using Phosphatidylserine Targeting Stearylamine-Bearing Cationic Liposomes. *Mol. Ther. - Nucleic Acids* **2018**, *10*, 9–27.

(46) Sharma, B.; Kanwar, S. S. Phosphatidylserine: A Cancer Cell Targeting Biomarker. *Semin. Cancer Biol.* **2017**.

(47) Jensen, M.; Bjerring, Æ. M.; Chr, N.; Willy, N. Æ.; Á, C. Á. M. N. M. R. Cisplatin Interaction with Phosphatidylserine Bilayer Studied by Solid-State NMR Spectroscopy. *J Biol Inorg Chem* **2010**, *15*, 213–223.

(48) Taylor, K. D.; Goel, R.; Shirazi, F. H.; Molepo, M.; Popovic, P.; Stewart, D.; Wong, P. Pressure Tuning Infrared Spectroscopic Study of Cisplatin-Induced Structural Changes in Phosphatidylserine Model Membrane. *Br. J. Cancer* **1995**, *72*, 1400–1405.

(49) Speelmans, G.; Staffhorst, R. W. H. M.; Versluis, K.; Reedijk, J.; Kruijff, B. De. Cisplatin Complexes with Phosphatidylserine in Membranes. *Biochemistry* **1997**, *36*, 10545–10550.

(50) Matos, C.; De Castro, B.; Gameiro, P.; Lima, J. L. F. C.; Reis, S. Zeta-Potential Measurements as a Tool to Quantify the Effect of Charged Drugs on the Surface Potential of Egg Phosphatidylcholine Liposomes. *Langmuir* **2004**, *20*, 369–377.

(51) Sathappa, M.; Alder, N. N. Ionization Properties of Phospholipids Determined by Zeta Potential Measurements. *Bio Protoc* **2016**, *6*, 1–23.

(52) Träuble, H.; Eibl, H. Electrostatic Effects on Lipid Phase Transitions: Membrane Structure and Ionic Environment. *Proc. Natl. Acad. Sci. U. S. A.* **1974**, *71*, 214–219.

(53) Carvalho, A. L. M. B. De; Pilling, M.; Gardner, P.; Doherty, J. Chemotherapeutic Response to Cisplatin- like Drugs in Human Breast Cancer Cells Probed by Vibrational Microspectroscopy. *Faraday Discuss.* **2016**, *187*, 273–298.

(54) Huang, C.; Jin, Z.; Dong, L.; Tong, X.; Yue, S. U. N. Cisplatin Augments FAS-Mediated Apoptosis through Lipid Rafts. *Anticancer Res.* **2010**, *30*, 2065–2072.

(55) Rebillard, A.; Tekpli, X.; Meurette, O.; Sergent, O.; Vernhet, L.; Gorria, M.; Chevanne, M.; Christmann, M.; Kaina, B.; Counillon, L.; *et al.* Cisplatin-Induced Apoptosis Involves Membrane Fluidification via Inhibition of NHE1 in Human Colon Cancer Cells. *Cancer Res* **2007**, *67*, 7865–7874.

(56) Roh, J.-L. L.; Park, J. Y.; Kim, E. H.; Jang, H. J. Targeting Acid Ceramidase Sensitises Head and Neck Cancer to Cisplatin. *Eur. J. Cancer* **2016**, *52*, 163–172.

(57) Maurmann, L.; Belkacemi, L.; Adams, N. R.; Majmudar, P. M.; Moghaddas, S.; Bose, R. N. A Novel Cisplatin Mediated Apoptosis Pathway Is Associated with

Acid Sphingomyelinase and FAS Proapoptotic Protein Activation in Ovarian Cancer. *Apoptosis* **2015**, *20*, 960–974.

(58) Silva, L.; Almeida, R. F. M. D. E.; Fedorov, A.; Matos, N. I. O. P. A.; Prieto, M. Ceramide-Platform Formation and -Induced Biophysical Changes in a Fluid Phospholipid Membrane. *Mol. Membr. Biol.* **2006**, *23*, 137–150.

(59) Pinto, S. N.; Silva, L. C.; Futerman, A. H.; Prieto, M. Effect of Ceramide Structure on Membrane Biophysical Properties: The Role of Acyl Chain Length and Unsaturation. *Biochim. Biophys. Acta - Biomembr.* **2011**, *1808*, 2753–2760.

(60) Garcia-arribas, A. B.; Ahyayauch, H.; Sot, J.; Lopez-gonzalez, P. L.; Alonso, A.; Goni, F. M. Ceramide-Induced Lamellar Gel Phases in Fluid Cell Lipid Extracts Ceramide-Induced Lamellar Gel Phases in Fluid Cell Lipid Extracts. *Langmuir* **2016**, *32*, 9053–9063.

(61) Goñi, F. M.; Alonso, A. Effects of Ceramide and Other Simple Sphingolipids on Membrane Lateral Structure. *Biochim. Biophys. Acta* **2009**, *1788*, 169–177.

## SUPPLEMENTARY INFORMATION

**Supplementary table 1 – Fluorescence decay components of t-PnA 24 hours after addition of cisplatin or AqCis to sphingolipid mixtures**

| System | ⟨*τ*⟩ (ns) | Long life time component (ns) |
|---|---|---|
| POPC:SM:Chol (control) | 22.07 | 28.85 |
| POPC:SM:Chol + 35 μM cisplatin | 21.57 | 28.82 |
| POPC:SM:Chol +35 μM AqCis | 21.63 | 28.62 |
| POPC:24:1Cer (control) | 25.26 | 34.58 |
| POPC:24:1Cer + 35 μM cisplatin | 25.63 | 34.87 |
| POPC:24:1Cer + 35 μM AqCis | 30.86 | 40.83 |

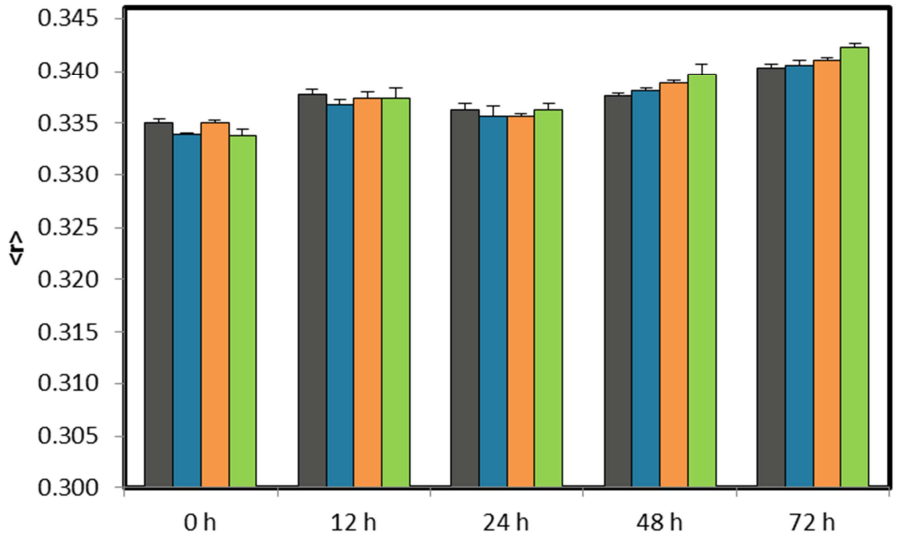


**Figure S1 – Effect of cisplatin on fluorescence anisotropy of DPH in DPPC LUV.** After 24 hours upon of addition of 15 μM (blue), 35 μM (orange) and 100 μM (green) cisplatin to DPPC LUV, a concentration-dependent effect of increased anisotropy was observed. Grey: control;

# CHAPTER V
# FINAL REMAKERS, ONGOING WORK AND FUTURE PERSPECTIVES

# Chapter V – Final remarks, ongoing work and future perspectives

Despite the tremendous amount of work in nanomedicine, it is still relatively difficult to design novel DDS. A fundamental problem is that there is a lack of knowledge on how these interact within the biological milieu and in particular at the cellular interfaces such at the lipid membranes. In this regard, dendrimers are suitable tools to study these interactions due to their versatility. Therefore, this thesis uses a multidisciplinary approach to design fluorescent dendrimers to be used as DDS. In summary this work describes: (i) computational methods developed to reliable build molecular models of different dendrimers; (ii) simulation of different PG dendrimers and evaluation of their ability to carry a fluorophore in their core protected from the external environment; (iii) the synthesis of PG dendrimers suggested by modeling studies and evaluation of the best synthetic route to incorporate the fluorophore; and (iv) evaluation of cisplatin effects on the biophysical properties of lipid membranes including phase behavior and permeability, to further guide the design of dendrimers.

Dendrimers are complex structures with still fairly unknown behavior. To this, molecular modeling and simulation methods provide useful tools to study dendrimers structure at the atomic level. However, building *in silico* models of different dendrimers is still not an easy task, particularly for higher generations. In this thesis, improved methods to reliable build different classes of dendrimers were developed in python language. These tools improved previously published protocols[1] and were able to quickly and reliably generate different dendrimers. These tools were then used to test different PG topologies and simulate these dendrimers with different terminal groups. Simulations allowed the characterization of PG dendrimers at the atomic level and the results suggested that at least generation 4 was necessary to incorporate a small fluorescent probe in the interior of these dendrimers. Moreover, the simulation of these dendrimers also showed that changes of the terminal groups strongly change the dynamics and the behavior of their surface.

Due to the versatility of these tools to readily create dendrimer topologies, these were currently used to model polyurea (PURE) dendrimers of generation 3 to 5 (Figure 5.1). These type of dendrimers were shown to have inherent fluorescent properties at higher generations and thus were useful to track their behavior *in vitro*[2,3]. Similar to PG dendrimers, these dendrimers were assembled using the same methods and are

currently being simulated to understand their structure and compare it to PG dendrimers.

One of the current problems with computational models of dendrimers is that there is no dedicated force field for this type of macromolecules. In the case of PG dendrimers, parameterizations were “borrowed” from the CHARMM force field designed for amino acids. Moreover, simulations were run surrounded by water molecules whereas reactions were carried in organic solvents. These have tremendous effects on the conformation of dendrimers scaffold and therefore could be the reason why limitations in the synthesis were observed. Therefore, development of dendrimers force field is an interesting approach to pursue. There has been increasing data on both crystal structure and supramolecular analysis of dendrimers and thus could be used for validation. Furthermore, despite the tool herein described performed well at creating models it still required significant knowledge on how to use it because it uses external software for the assembly. Therefore, future work should include further automatization and increased user friendly interfaces. Moreover, further development of a web application should be pursed so that this tool can be used for by other researchers with ease.

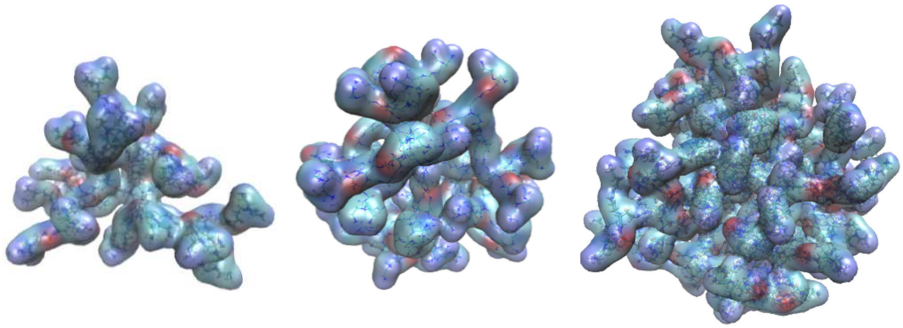

**Figure 5.1 – From left to right: 3D structure of PURE G3, G4 and G5.** Dendrimers were created using the same protocol for PG dendrimers in chapter 1. The topology files was carried using XPLOR-NIH and were modified with ParamChem parameters. Dendrimers were then loaded to Maestro and automatic attribution of atom types was carried.

The synthesis of PG G4 candidates from molecular modelling was then carried out using classical peptide coupling methods. Despite several optimized reaction conditions were successful at synthesizing small generations, these failed to generate the necessary generation 4. In general, the various coupling reagents tested resulted in: (i) defective dendrimers; (ii) dendrimers complexed with impurities; (iii) poor yields of recovery. Contrary to carbodiimide reagents, CDI and Uronium salts were shown to be viable alternatives as coupling reagents to grow the dendrimer since they were easier to purify. Nevertheless, due to the amount of reactions of coupling and de-protection

needed and the increasingly lower yields obtained till G2, the synthesis of PG G4 was shown to be unviable. These difficulties were attributed to the steric constraints due to the short side chain of glutamic acid. Therefore, new architectures of PG dendrimers should be explored based on the information obtained in this thesis.

On the other hand, the reactions used for PG dendrimers translated well into other types of monomers. In fact, the synthesis of different terminal groups using CDI showed good yields. However, these reactions also shown that the derivative of the monomer is of utmost importance when being selected since solubility problems were observed that would hinder their use. Finally, this thesis also describes the incorporation of a small fluorophore (NBD) into the core GLU. The results showed that the incorporation of the NBD should be carrier early on the synthetic route since the overall bulkiness even for small dendrimers resulted in steric effects and low yield of recovery. Moreover, new GLU derivatives were synthesized to further attach the NBD to GLU and prevent the core amine from further reaction when growing the dendrimer. Two successful candidates for the core were obtained and further work should be carried on using these.

Finally, in the last chapter of this thesis, cisplatin was used as a model anti-cancer drug to study its effects on the biophysical properties of the lipid membrane. The results showed that cisplatin had little influence in the properties of several lipid membranes, inducing a small decrease in membrane fluidity in gel phase model membranes. Despite the small effects in membrane fluidity, cisplatin was able to induce changes in the permeability of most of the membrane model systems studied. The rate and extent of membrane permeability was dependent on the lipid composition and cisplatin concentration. In particular, a higher release of CF was observed for POPC and POPC:DPPC (1:1) model vesicles when treated with high concentration of cisplatin . On the other hand a complex behavior was observed for POPS, which was attributed to the complexation of cisplatin at the lipid headgroup. Furthermore, a small but noticeable effect was observed for gel phase models of ceramide-enriched membranes where cisplatin induced ordering of the membrane. This is clear contrast to studies with cellular membranes where addition of cisplatin induced production of ceramide by conversion of SL at lipid rafts that resulted in increasing the membrane fluidity. Therefore, this suggests that the interaction of cisplatin with cells is complex and multiple factors contribute to the lipid phase change.

Currently, studies are being conducted using AFM to further characterize the cisplatin-lipid bilayer interactions. Preliminary results obtained on POPC:DPPC (1:1) model

membranes suggest that at high concentrations, cisplatin extended the defective pores observed at the fluid and gel phase interface (Figure 5.2), which might be the cause underlying the high leakage observed for these vesicles

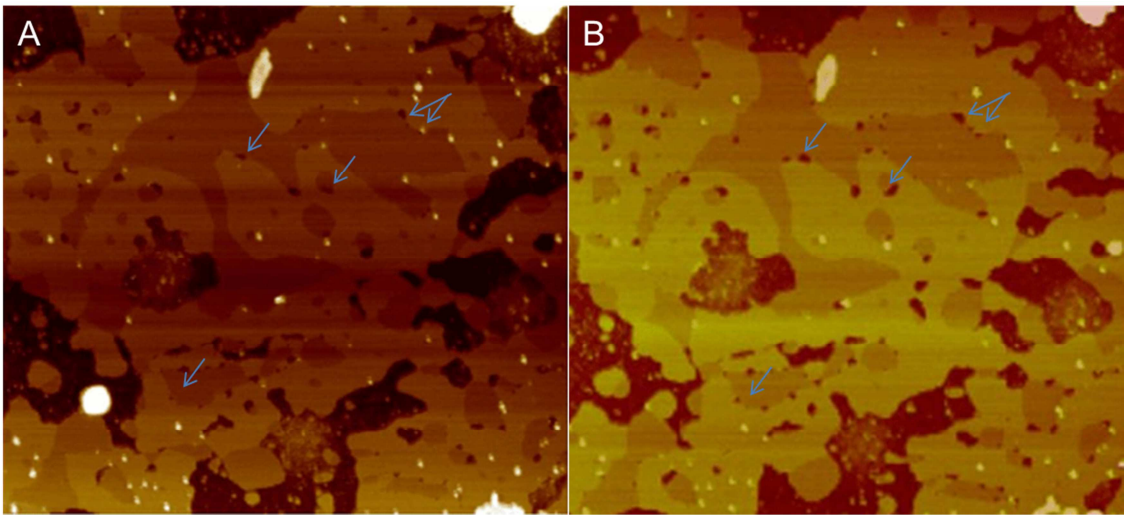


**Figure 5.2 – AFM of supported lipid bilayer composed of POPC:DPPC (1:1) .** Images were obtained (A) before and (B) after addition of 300 μM of cisplatin. Blue arrows point towards some examples where cisplatin expanded existing defects at the interface of fluid and gel phase. *In situ* tapping-mode imaging were performed at room temperature using a Multimode Nanoscope IIIa Microscope (Digital Instruments, Veeco) using a similar protocol previously established[4]. Scale: 5.5x5.5 μm

Finally, it should be mentioned that based on these results, an interesting approach to pursue in cisplatin delivery would be the combination with a synergistic molecule in the same DDS, such as a dendrimer scaffold. In fact, combining cisplatin and ceramide in a dendrimer could circumvent the resistance mechanisms associated with platinum accumulation and promote the induction of apoptosis. With this in mind, PURE dendrimers G3, G4 and G5 were kindly provided by Dr. Vasco Bonifácio to further evaluate their behavior with lipid membranes and their potential use for DDS. Preliminary results of all three generations showed that these dendrimers fluorescence intensity was pH- and generation-dependent (Figure 5.3). These properties are valuable to study since they can measure the pH differences inside cells and provide valuable information regarding their surroundings. Further studies with these dendrimers also showed that they were able to complex with carboxyfluorescein without changing their fluorescence spectrum. This property can be useful to further validate the molecular modeling studies by quantifying the amount of CF that complexes with these dendrimers both by computational and bench methods. Indeed, ongoing simulations are currently being undertaking to understand how CF binds to PURE dendrimers. The characterization of this property will also allow the study of

affinity of different drugs (including cisplatin) to these dendrimers by competitions assays.

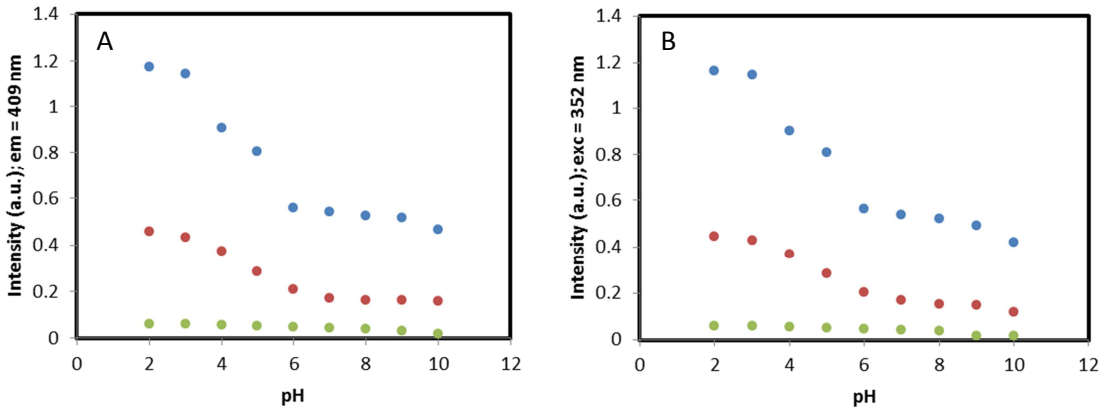


**Figure 5.3 – Fluorescence intensity of PURE G3 (green), G4 (red) and G5 (blue) dendrimers under the same experimental conditions (final concentration of 0.1 mM).** The fluorescence intensity of both emission (A) and excitation (B) increased with pH decrease and were dependent on the generation of PURE dendrimers.

Finally, PURE dendrimers were also tested on their effect to modulate the permeability of different model bilayers similarly to the methods used for cisplatin (Figure 4). Preliminary results showed that similar to the effects described above, CF strongly interacts with PURE dendrimers, making it difficult to clearly evaluate the effects of the dendrimers on the permeability of the lipid membranes. Nevertheless, for low concentrations of 1% mol dendrimer/lipid, where the effects of complexation are minimized it is possible to observed that both G4 and G5 (but not G3) significantly increased the permeability of POPC to CF. On the other hand, in POPC:POPS (7:3) model, all three concentrations increased the permeability of the membrane. On the contrary, for POPC:DPPC (1:1) all three concentrations reduced the release of CF compared to the control. It is unlikely that this effect can be explained by complexation of CF to PURE dendrimers. Instead, based on the results obtained for cisplatin, it is possible that PURE dendrimers intercalate at the interface between the fluid and gel phase and “cover” the defects, therefore preventing the release of CF. However, further studies are necessary, likely using different strategies to evaluate the permeability of model membranes by PURE, for instance, by encapsulating other fluorophores, such as the ANTS/DPX fluorophore/quencher pair.

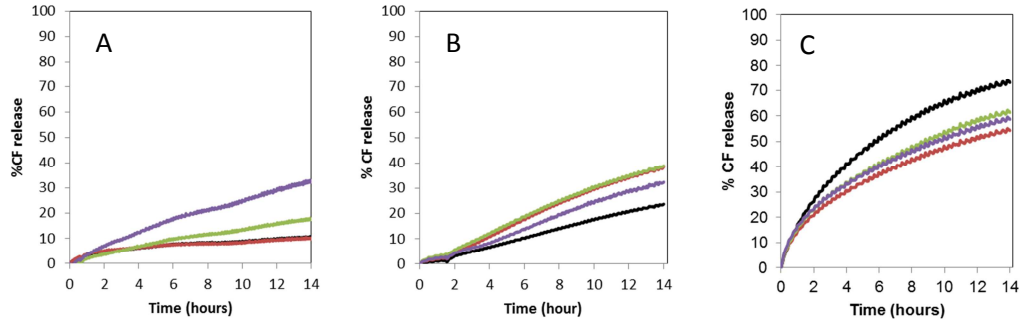


**Figure 5.4 – Release of CF from control (black) of (A) POPC; (B) POPC:POPS (7:3) and (C) POPC:DPPC (1:1) with 1 mol% of PURE dendrimers G3 (red), G4 (green), G5 (purple)**

Overall, this thesis provides a proof-of-concept methodology on how to approach the design of new DDS. The methods herein described allow a multidisciplinary approach from computational models to the understanding of the behavior of both the drug and carrier at the lipid interface. Results suggested that the effects of cisplatin at therapeutic concentrations are minimal on both the lipid phase changes and permeability of the membrane and that dendrimers could provide a good platform to increase the permeability of the membrane. Finally, the synthetic approach taken for PG dendrimers clearly demonstrated new avenues and possible alternatives that need to be taken for the design of PG dendrimers.

## References

(1) Barata, T. S.; Shaunak, S.; Teo, I.; Zloh, M.; Brocchini, S. Structural Studies of Biologically Active Glycosylated Polyamidoamine (PAMAM) Dendrimers. *J. Mol. Model.* **2011**, *17*, 2051–2060.

(2) Restani, R. B.; Morgado, P. I.; Ribeiro, M. P.; Correia, I. J.; Aguiar-, A.; Bonifµcio, V. D. B. Biocompatible Polyurea Dendrimers with PH-Dependent Fluorescence. *Angew. Chemie* **2012**, *124*, 1–5.

(3) Pires, R. F.; Martins, P.; Restani, R. B.; Fernandes, A. R.; Baptista, P. V; Bonif, V. D. B.; Aguiar-ricardo, A. POxylated Polyurea Dendrimers : Smart Core- Shell Vectors with IC 50 Lowering Capacity. *Macromol. Biosci.* **2015**, 1–6.

(4) Marquês, J. T.; Viana, A. S.; Almeida, R. F. M. De. Ethanol Effects on Binary and Ternary Supported Lipid Bilayers with Gel / Fl Uid Domains and Lipid Rafts. *Biochim. Biophys. Acta* **2011**, *1808*, 405–414.